Tampere University

NIRAJAN OJHA

Investigation of Upconversion Properties from Active Crystals in Oxyfluorophosphate Glasses

Tampere University Dissertations 317

Tampere University Dissertations 317

NIRAJAN OJHA

Investigation of Upconversion Properties from Active Crystals in Oxyfluorophosphate Glasses

ACADEMIC DISSERTATION
To be presented, with the permission of
the Faculty of Engineering and Natural Sciences
of Tampere University,
for public discussion in the auditorium TB109
of the Tietotalo building, Korkeakoulunkatu 1, Tampere,
on 6th of November 2020, at 12 pm.

ACADEMIC DISSERTATION
Tampere University, Faculty of Engineering and Natural Sciences
Finland

Responsible supervisor and Custos	Associate Professor Laeticia Petit Tampere University Finland	
Supervisor	Associate Professor Mikko Hokka Tampere University Finland	
Pre-examiners	Professor Dominik Dorosz AGH University of Science and Technology in Krakow Poland	Professor Rolindes Balda University of the Basque Country and Materials Physics Center CSIC-UPV/EHU Spain
Opponents	Professor Dominik Dorosz AGH University of Science and Technology in Krakow Poland	Professor Enrico Bernardo University of Padova Italy

The originality of this thesis has been checked using the Turnitin OriginalityCheck service.

Cover design: Roihu Inc.

ISBN 978-952-03-1715-7 (print)
ISBN 978-952-03-1716-4 (pdf)
ISSN 2489-9860 (print)
ISSN 2490-0028 (pdf)
http://urn.fi/URN:ISBN:978-952-03-1716-4

PunaMusta Oy – Yliopistopaino
Vantaa 2020

PREFACE

This thesis was carried out in Photonic Glasses group in the Photonics laboratory department of the faculty of engineering and natural science of Tampere University (Former Tampere University of Technology), Finland led and supervised by Associate Professor Dr. Laeticia Petit during 2017-2020 A.D. This thesis was co-supervised by Assoc. Professor Dr. Mikko Hokka from the materials science department of the same faculty. I would like to specially thank my supervisor Assoc. Prof. Dr Petit whose guidance have made this thesis successful. I am also fortunate to have my master's Thesis supervisor Assoc. Prof. Dr. Jonathan Massera and his group from the Biomedical Engineering Department of Tampere university for sharing his lab and useful knowledge on crystallization study.

I would also like this opportunity to thank the collaborators during this study. Specially Dr. Mika Lastusaari and his group from Turku University, Finland for providing me with the nanocrystals used in this study and for all the measurement of the spectroscopic properties of the materials. Special thanks go out to Dr. Catherine Boussard-Plédel of Université de Rennes, for helping with the difficult drawing of the phosphate glass fibers. I would also like to remember Dr. Antti Tukiainen for helping me with the luminescent measurements, Dr. Regina Gumenyuk for the fiber characterization, Dr. Turkka Salminen for the SEM/EDS measurements. It was great to work with the Photonic glasses group and I thank everyone in the group and the students I came across with for their tremendous help and support both in and off the lab.

Finally, I would especially like to thank my wife Srijana for pushing me for this PhD. son Savar and daughter Shravya for their cheerful smile after hard day's work. My family back home in Nepal were always there for my support.

Tampere, November 2020
Nirajan Ojha

ABSTRACT

Phosphate glasses have been of great interest for the fabrication of new lasing glasses. Indeed, as compared to other glass families, phosphate glasses can be prepared using low processing temperature and can incorporate a large amount of rare-earth (RE) ions, such as Er^{3+} ions. Er^{3+} ions have been of great interest as they can be used to convert Near InfraRed (NIR) radiation to shorter wavelengths due to the absorption of two or more photons by a process called upconversion. However, due to the high phonon energy of phosphate glasses, a large amount of Er^{3+} ions are usually required in phosphate glasses to exhibit upconversion.

Changing the site of the RE ions makes it possible to achieve upconversion while using lower amounts of Er^{3+} ions. The site of the RE ions can be modified by adjusting the glass composition and also by heat treating the glass to precipitate rare-earth doped crystals to obtain glass-ceramics. To be promising glass-ceramics for photonics applications, the glass-ceramics should be transparent with RE doped crystals dispersed evenly in their volume. However, it is crucial to control the nucleation and growth of the crystals when preparing the transparent glass-ceramics. As not all glasses can be heat treated into transparent glass-ceramics with volume precipitation of RE doped crystals, RE doped crystals with known chemistry and spectroscopic properties can be added in a glass matrix using the direct doping method. However, the crystals tend to decompose during the melting. Therefore, they should be added in the glass at lower temperature than the melting temperature to limit their decomposition during the glass preparation.

The main aim of this thesis was to develop new Er^{3+} doped phosphate glass-based materials for upconversion application. To improve their spectroscopic properties, the glasses were heat treated into transparent glass-ceramics. Due to the presence of Er^{3+} doped CaF_2 crystals in their volume, the glass-ceramics exhibit enhanced upconversion compared to their parent glasses. The nucleation and growth process of the glasses was investigated, and it was shown that it is possible to tailor the transparency and thermal properties of the glass-ceramic by modifying the glass composition without changing its nucleation and growth process. Additionally, the newly developed glasses were developed with large temperature difference between the onset of crystallization and the maximum nucleation temperature confirming that they are promising materials for the fabrication of upconverter glass-ceramics as it is then possible to control the

nucleation and growth of crystals in these glasses. Other glasses were also developed in this work; phosphate glasses were successfully prepared with $NaYF_4$: Er^{3+}, Yb^{3+} nanocrystals using the direct doping method. To limit the decomposition of the crystals during the glass preparation, the fundamental understanding of the direct doping method was advanced using persistent luminescent microparticles. Using optimized doping parameters, the $NaYF_4$: Er^{3+}, Yb^{3+} nanocrystals containing glass exhibit intense green upconversion confirming the presence of the nanocrystals in the glass. Finally, it was shown that a heat treatment of $NaYF_4$: Er^{3+}, Yb^{3+} nanocrystals containing glass to grow Ag nanoparticles, usually added in Er^{3+} doped glass to enhance the upconversion, led to a decrease in the intensity of the upconversion due to an increase of the inter defects in the $NaYF_4$: Er^{3+}, Yb^{3+} nanocrystals occurring during the heat treatment indicating that a heat treatment of the glass should be avoided after adding the $NaYF_4$: Er^{3+}, Yb^{3+} nanocrystals.

CONTENTS

List of Figures

List of Tables

ABBREVIATIONS AND SYMBOLS

2D	Two dimensional
3D	Three Dimensional
DTA	Differential Thermal Analyzer
EDS	Energy-dispersive X-ray spectroscopy
EPMA	Electron Probe Microanalyzer
FTIR	Fourier transform InfraRed spectroscopy
GCs	Glass-Ceramics
IR	InfraRed
JMA	Johnson–Mehl–Avrami
LIDAR	Light Detection and Ranging
MPs	Microparticles
Nc	Nanocrystals
NIR	Near InfraRed
NPs	Nanoparticles
PeL	Persistence Luminescence
PMT	Photomultiplier tube
RE	Rare-Earth
SEM	Scanning Electron microscope
UC	Upconversion
UV	Ultraviolet
Vis	Visible
WDX	Wavelength-dispersive X-ray spectrometer
XRD	X-ray Diffraction

σ	Absorption cross-section
at %	Atomic Percentage
$d\alpha_i$	Transformation rate at a temperature T_i
E_c	Activation energy for crystallization
I/I_o	Absorbance
L	Thickness in cm
mol %	Molar Percentage
N	Number of ions per cm^3
R	Gas constant
t	Dwell time
T_{doping}	Doping temperature
T_g	Glass transition temperature
$T_{n\ max}$	Maximum nucleation temperature
T_p	Crystallization peak temperature
T_x	Onset of crystallization temperature
T_m	Melting temperature
wgt %	Weight Precentage
α	Volume fraction of glass crystallized at a fixed temperature T
β	Heating rate
ΔT_{FWHM}	Full width at half maximum of the DTA peak
λ	Wavelength
λ_{exc}	Excitation wavelength
cm	centimeters
μm	micrometeres
nm	nanometers
μW	micro Watts

ORIGINAL PUBLICATIONS

Publication I N. Ojha, H. Nguyen, T. Laihinen, T. Salminen, M. Lastusaari, L. Petit, Decomposition of persistent luminescent microparticles in corrosive phosphate glass melt, Corr Sci, 135 (2018) 207-214, https://doi.org/10.1016/j.corsci.2018.02.050.

Publication II N. Ojha, T. Laihinen, T. Salminen, M. Lastusaari, L. Petit, Influence of the phosphate glass melt on the corrosion of functional particles occurring during the preparation of glass-ceramics, Ceram. Int., 44(10), (2018), 11807-11811, https://doi.org/10.1016/j.ceramint.2018.03.267.

Publication III N. Ojha, M. Tuomisto, M. Lastusaari, L. Petit, Upconversion from fluorophosphate glasses prepared with $NaYF_4$: Er^{3+}, Yb^{3+} nanocrystals, RSC Adv., 8 (2018), 19226, https://doi.org/10.1039/C8RA03298J

Publication IV N. Ojha, M. Bogdan, R. Galatus, L. Petit, Effect of heat treatment on the upconversion of $NaYF_4$:Yb^{3+}, Er^{3+} nanocrystals containing silver phosphate glass, J. Non. Cryst. Solids. 544 (2020) 120243. https://doi.org/10.1016/j.jnoncrysol.2020.120243

Publication V N. Ojha, A. Szczodra, N. G. Boetti, J. Massera, L. Petit, Nucleation and growth behavior of Er^{3+} doped oxyfluorophosphate glasses, RSC Adv., 10 (2020), 25703, https://doi.org/10.1039/D0RA04681G

AUTHOR'S CONTRIBUTION

Nirajan Ojha was the first author in all the publications. He planned the experiments along with his main supervisor, Assoc. Prof. Laeticia Petit, and conducted most of the research work. He analyzed the results and was in charge of the preparation of the manuscripts. All the co-authors in the publications discussed and analyzed the results and approved the final manuscript.

Publication I: General roles as discussed earlier. Additionally, Msc. H. Nguyen prepared the particle containing glasses which were analyzed by Nirajan Ojha. Under the supervision of Dr. T. Salminen, Nirajan Ojha did the SEM/EDS analysis. Dr. T. Laihinen did the spectroscopic measurement.

Publication II: Nirajan Ojha prepared and analyzed the particle containing glasses. Respective author roles as in publication I

Publication III: Nirajan Ojha and Dr. M. Tuomisto prepared and analyzed the nanocrystals containing glass. Therefore, Publication III is shared as main author by both Nirajan Ojha and Minnea Tuomisto. Minnea Tuomisto has also included Publication III in her doctoral Thesis. Respective author roles as in publication I

Publication IV: Nirajan Ojha prepared the Ag nanoparticles containing glass doped with nanocrystals. Under the supervision of Nirajan Ojha, Bsc. M. Bogdan was in charge in some of the spectroscopic measurements. Assoc. Prof R. Galatus co-ordinated the study.

Publication V: Apart from general roles of the author, Msc. A. Szczodra initiated the research which was continued by Nirajan Ojha. Prof. Massera took part in the investigation of the nucleation and growth process.

1 INTRODUCTION

Er^{3+} ions doped materials have been of great interest over the decades as they can be used to convert NIR radiation generally to shorter wavelengths as a result of the absorption of two or more photons. This process is known as upconversion (UC). These upconverter materials could find uses in various applications for instance solar cells, color displays, high resolution sensing, biomedical imaging and bio-label to name a few. Scientists around the world have been putting a lot of efforts on the development of new Er^{3+} doped materials with strong UC. It is well known that the host matrix and the amount of Er^{3+} ions have a significant impact on the UC efficiency as UC depends largely on the energy level structure of rare-earth (RE) ions.

Silica glass has been the mostly used glass for photonic applications. Indeed, silica glass possesses various excellent properties such as good optical transmission, good electrical performance and also good chemical durability and stability. However, due to its compact network, silica glass needs to be processed using high melting temperature limiting its use. Additionally, the solubility of rare-earth ions in the silica network is low clearly showing the need to develop new active glasses for photonic applications.

Phosphate glasses have been found to have numerous advantages over silica glass and other glasses such as silicate and germanate glasses for example, as they can be processed using low processing temperature. Additionally, they can incorporate a large amount of RE ions as quenching phenomenon occurs at very high concentrations of RE ions in phosphate glasses. However, phosphate glasses have a high phonon energy, which is disadvantageous to the UC emission. A large amount of Er^{3+} ions is then needed to achieve upconversion in such glasses. However, as the spectroscopic properties of the RE ions depend on their local environment, the intensity of the upconversion from an Er^{3+} doped phosphate glass could be increased by changing the site of the Er^{3+} ions.

The research presented in this thesis was focused on the development of new upconverter phosphate glasses and was performed at Tampere university (Finland) in collaboration with Prof. Dr. Mika Lastusaari from University of Turku (Finland), Dr. C. Boussard-Plédel from Rennes University (France), Dr. Nadia Giovanni Boetti from

Fondazione LINKS-Leading Innovation & Knowledge for Society (Italy) and Assoc. Prof. Ramona Galatus from Technical University of Cluj Napoca (Romania).

1.1 Aim of the work

The main aim of this thesis was to develop new Er^{3+} doped phosphate glass-based materials with higher intensity of upconversion compared to the parent glass without increasing the Er^{3+} concentration. The enhancement of the spectroscopic properties was obtained by changing the sites of the RE ions. Indeed, changes in the site of the RE ions can lead to an enhancement in the local crystals field and thus to an increase in the intensity of the emission. This could be achieved using Er^{3+} doped fluoride crystals as these crystals are known to be efficient upconverters of NIR to visible spectral range. These crystals could precipitate inside the glass matrix using a heat treatment or be added in the glass.

Materials which contain crystals after heat treatment of the glass are known as glass-ceramics. Glass-ceramics combine the mechanical and optical properties of the glass with the crystal-like environment for the rare-earth ions when located in the crystals. The presence of crystalline environment around the rare-earth ions can lead to a glass-ceramic with large absorption and emission cross-sections and long lifetime. To be promising glass-ceramics for photonics applications, the glass-ceramics need to be transparent and should contain RE doped crystals well dispersed in their volume. The glass should also be thermally stable to be processed into fibers or films. However, not all glasses are thermally stable nor can be processed into transparent glass-ceramics with volume precipitation of Er^{3+} doped crystals. To overcome this limitation, methods to introduce RE doped crystals of a known chemistry and spectroscopic properties directly in a glass matrix have been developed. The active crystals can be added in the glass batch prior to the melting but crystals tend to dissolve in the glass melt during the melting. Therefore, method such as the direct doping method has been developed to limit the dissolution of the crystals in the glass during the glass preparation. In this method, the crystals are added in the glass melt after the melting. To limit the dissolution of the crystals in the glass batch, the crystals should be added at a specific temperature which is lower than the melting temperature and should be in contact with the melt for a limited time before quenching the glass. Although crystallization and direct doping methods have been used to prepare various glasses, a deeper knowledge and understanding of the nucleation and growth mechanism and of the direct doping

process still remains necessary for the development of novel phosphate glasses with enhanced spectroscopic performances.

In this context, the main aim of this thesis was to develop new glass-based materials which contain Er^{3+} doped fluoride crystals using the nucleation and growth and the direct doping methods.

1.2 Research questions

The main research questions of this thesis are the following

- is it possible 1) to improve the thermal stability of a glass by modifying slightly its composition without modifying its nucleation and growth mechanism and 2) to tailor the transparency of the glass-ceramic using optimized heat treatment parameters? These questions will be answered by understanding the composition-structure-properties and also the nucleation and growth mechanism of newly developed glasses.
- how can the survival and dispersion of the crystals be balanced to prepare crystals containing glasses using the direct doping method? Is it possible to prepare $NaYF_4$: Er^{3+}, Yb^{3+} crystals containing glasses with strong upconversion using this method knowing that $NaYF_4$: Er^{3+}, Yb^{3+} crystals decompose at low temperature? Can Ag nanoparticles be used to enhance the upconversion properties from the $NaYF_4$: Er^{3+}, Yb^{3+} crystals containing glass? To answer these questions, it will be crucial to first determine a protocol to optimize the direct doping method to limit the decomposition of the crystals during the glass preparation.

These research questions are addressed in this thesis which is divided into 6 Chapters. The chapter 2 is a literature review of the relevant research, including the definition of glass and several types of glasses, a description of the structure and properties of phosphate-based glasses, the fundamentals of luminescence properties of the Er^{3+} ions. The nucleation and growth theory is also summarized and the work on the direct doping method reviewed. Chapter 3 describes the procedures used to prepare and characterize the newly developed glasses. These research questions are discussed and presented in Chapter 4. The first part of this chapter is focused on the processing and characterization of new glasses in the $NaPO_3$ - CaF_2 system. The nucleation and growth mechanism in these glasses are then investigated to show that it is possible to tailor the transparency of the glass-ceramics from these glasses. In the second part of

this chapter, it is explained how to optimize the direct doping process to successfully prepare $NaYF_4$: Er^{3+}, Yb^{3+} crystals containing phosphate glasses with strong upconversion. The impact of the corrosive behavior of various glass melts on crystals is studied. Finally, results related to the preparation and characterization of $NaYF_4$: Er^{3+}, Yb^{3+} crystals containing phosphate glass which also possess Ag nanoparticles are presented and discussed. The last chapter summarizes the main findings of this research and answers the research questions.

2 BACKGROUND

2.1 Glasses

A glass can be defined as an amorphous solid that lacks ordered distribution that can be found in crystalline solids and has a glass transition [1]. This definition implies that a glass is an amorphous solid having an atomic arrangement like that of a liquid. Glasses were traditionally formed by cooling a melt but other techniques to fabricate glasses have been developed such as vapor deposition, sol-gel and neutron irradiation of crystalline materials, just to cite a few [2].

Glasses are found in everyday life from windows, to mobile phones, to kitchenware, just to name a few examples of today uses of glasses. For example, electronics used vacuum tubes made of glass which led to the path of modern electronics and to computers and television. Since 1970's, glasses, especially silica glass, have allowed the development of low loss optical fibers to replace traditional copper wires and so to the development of relatively flawless and fast communication systems [3]. Although glasses have been developed worldwide, there is a clear need for new glasses for the development of new technologies offering huge commercial rewards worldwide.

2.1.1 Glass formation

The glass transition behavior of a melt forming a glass can be described using Figure 1. When the temperature of a liquid is decreased from high to low temperature, the temperature reaches the crystallization temperature (T_x).

- The liquid can crystallize leading to a drop in the enthalpy and also to noticeable changes in the volume.
- If the liquid does not crystallize, the liquid is then a supercooled liquid, the volume of which decreases progressively as the temperature is reduced.

As seen in Figure 1, the thermal properties of the glass, especially the glass transition temperature (T_g), depend on the cooling rate. Therefore, T_g is an important parameter to determine:

- at temperature below T_g, the glass is an amorphous material
- at around T_g, the glass acts as a viscoelastic solid

- at temperature higher than T_g, the glass acts as a viscous liquid

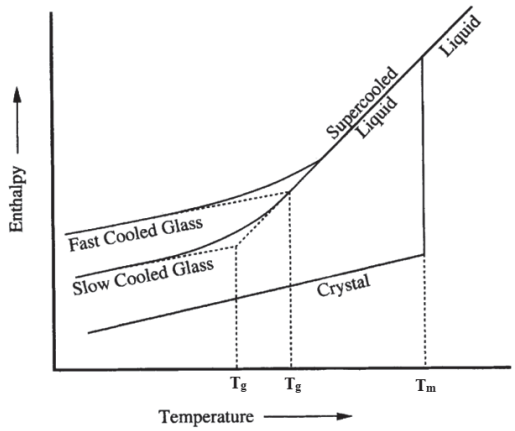

Figure 1. Enthalpy - Temperature relationship for a liquid forming either a crystalline solid or glass; picture modified from [2]

Another important characteristic of glass to consider when preparing a glass for photonics application is its thermal stability or also termed as glass processing window. The thermal stability of glass is an indicator of its ability to resist crystallization during hot processing, which is crucial when drawing the glass into a fiber or depositing the glass into a film for example. The thermal stability of a glass is usually estimated from the difference in temperature between the onset of crystallization (T_x) and T_g. Generally, a glass having $\Delta T = T_x - T_g$ greater than 90 °C is expected to be thermally stable against crystallization and so a good candidate for fiber drawing or film deposition [4].

The theories on the atomic arrangement in glasses were reported in 1931 by Zachariasen [5] who classified the three types of cations:

- **network formers** which form the interconnected backbone of the glass network. The most common network formers are boron, silicon, germanium, and phosphorus. They have a high valence state and will covalently bond with oxygen.
- **network modifiers** which are added to change the physical and chemical properties of the glasses by disrupting the strong bonds of the network formers. Most common modifiers are Na_2O, and CaO, just to cite a few
- **intermediates** which are strongly bonded to the glass network becoming their part and acting as stabilizer without causing any crystallization. They are not able to form a glass on their own. Oxides such as Al_2O_3 and TiO_2 are known to act as intermediates.

2.1.2 Fluorophosphate glass

Glasses in various glass systems have been under investigation due to their specific properties which depend on the glass composition. Among the glass families, the most studied glasses are silicate, phosphate, borate, chalcogenide and halide glasses. Phosphate glasses are based on P_2O_5. They have found uses in industrial applications such as clay processing and pigment manufacturing but also in more specialized applications, especially in photonics. These glasses are usually prepared using low melting temperature. They can be engineered with high thermal expansion coefficient., high transparency in UV-Vis-NIR region and relatively high refractive indices, depending on their composition [6–8]. When doped with rare-earth (RE) ions, they can also possess high absorption and emission cross-sections and long lifetime values [9–13]. Unlike silica glass which possesses a 3D network, phosphate glasses can dissolve considerable amounts of alkaline earth, transition metal and rare-earth ions due to their 2D network [14]. Effort has been focused on the development of oxyfluorophosphate glasses as these glasses combine the properties of both oxides and fluorides to possess good chemical durability, thermal stability, mechanical strength and high rare-earth ions solubility [15].

Phosphate based glasses are usually prepared using standard melting process. They can also be obtained using sol-gel technique with controlled morphology and composition [16,17]. The sol-gel method involves the formation of polymeric sols originating from the precursor's hydrolysis and condensation. The advantages of the sol-gel method are the low temperature use in this process and the homogenous mixing of the reactants during its synthesis. However, the long duration required for the glass synthesis is the major disadvantages of the sol-gel method.

Phosphate glass network is made up of PO_4 units, where at least one oxygen forms a non-bridging point with neighboring tetrahedra. Q^n units is generally used to represent the number of bridging oxygens per tetrahedron, where (n) is the number of bridging oxygensas shown in Figure 2.

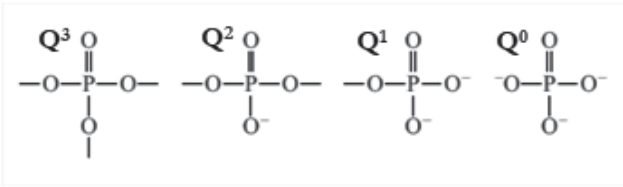

Figure 2. Representation of the different Q^n units forming phosphate network; picture modified from [18]

Depending on the [O]/[P] ratio of glass composition, phosphate glasses can be made with a range of structures, such as cross-linked network of Q^3 tetrahedra (vitreous

P_2O_5), polymer-like metaphosphate chains of Q^2 tetrahedra, invert glasses based on small pyro- (Q^1) and orthophosphate (Q^0) anions [19]. A more detailed study on the structure of phosphate glass can be found, for example in ref [19]

Due to their weak structure, some phosphate glasses possess low chemical durability. Thus, they are prone to absorb water, which could be detrimental especially when preparing RE doped glasses as hydroxyl ions can lead to drastic luminescence quenching [20]. Therefore, the low chemical durability of phosphate glasses when exposed to environmental moisture limits their use requiring researchers to develop new glasses with suitable thermal and optical properties while enhancing their chemical durability [21]. For example, the addition of MgO, TiO_2 or ZnO in the phosphate network was reported to improve the chemical durability of the glass as in ref [22,23].

2.2 Lasing glass

Lasing glasses are RE doped glasses with RE elements being in the lanthanide series, including also Scandium and Yttrium. RE doped glasses have been of great interest for a various applications in the field of telecommunications, light detection and ranging (LIDAR), solar panels, color sensing, biomedical diagnostics, just to name a few [24–26]. The discovery of Nd:YAG laser in 1960 led to the rapid growth in the use of RE doped glasses as lasers, amplifiers and other optical devices [27].

The different interactions of radiation with matter in a two-energy level system are absorption, spontaneous emission and stimulated emission as illustrated in Figure 3.

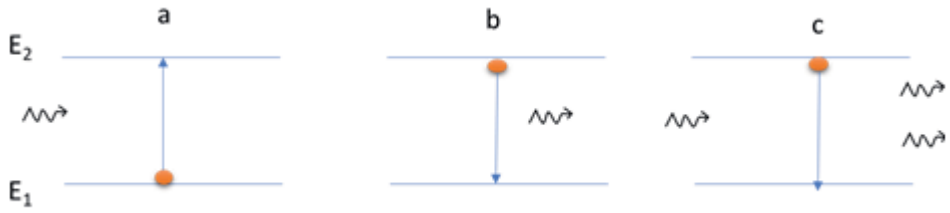

Figure 3. Schematic diagram showing interaction of radiation with matter: absorption a); spontaneous emission b); stimulated emission c). E_1 is the ground level and E_2 is the excited level

The **absorption process** occurs when light hits the matter raising the electron from E_1 ground state to E_2 energy level. This absorption process occurs only when the photon energy equals the $\Delta E = E_2 - E_1$. When on the E_2 level, the electron can decay to E_1 ground state emitting a photon with an energy equal to ΔE (**spontaneous radiative emission**). However, if the decay emits phonons instead, the process is then a non-

radiative emission. It is also possible to stimulate the emission using external radiation with an energy equal to ΔE. The matter will emit not only a spontaneous emission with photon having different energy, directing and polarization than the incoming photon but also **stimulated emission** with photon in phase with the incoming one

2.2.1 Er^{3+} ions

Among the different rare-earth ions, the use of Er^{3+} ions has been in the limelight due to their large number of energy levels (see Figure 4) and especially due to the transition from the $^4I_{13/2}$ to $^4I_{15/2}$ levels which corresponds to the emission centered at ~1530 nm that makes Er^{3+} doped glasses useful for application such as eye-safe laser and third optical window in telecommunication [28,29].

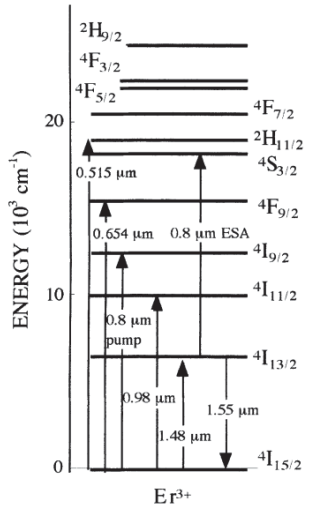

Figure 4. Schematic of energy diagram of Er^{3+} ions and relevant transitions for pumping and amplification; picture modified from [4]

The performance of the Er^{3+} ions luminescence can be degraded due to non-radiative phenomena such as

- **multiphonon relaxation** requires plenty of phonons to conduit the energy gap (ΔE) between the energy levels (Figure 5). This process depends on the glass matrix, especially on its phonon energy. More multiphonon relaxations occur in hosts with higher phonon energy compared to that of a material with lower phonon energy.

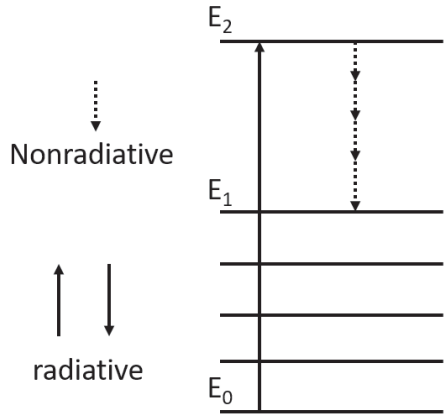

Figure 5. Schematic diagram showing multiphonon relaxation processes of RE ions [30].

- **non-radiative decay** occurs due to the absorption of water or impurities that act as quenching centers. The presence of OH group in the glass host leads to non-radiative decay processes as a result of the energy transfer from Er^{3+} ions to the –OH groups [31]. The absorption band of the –OH groups is between 2500 and 3600 cm^{-1} (2700 - 4000 nm) and overlaps with the Er^{3+} ions emission centered at 1.5 μm.
- **concentration quenching** occurs due to the interaction between two ions when using high concentration of RE ions. There can be cross relaxation and energy migration (Figure 6a, b). Another process is the upconversion process occurring between two excited ions, one ion giving its energy to the second one resulting in promotion to higher energy (Figure 6c).

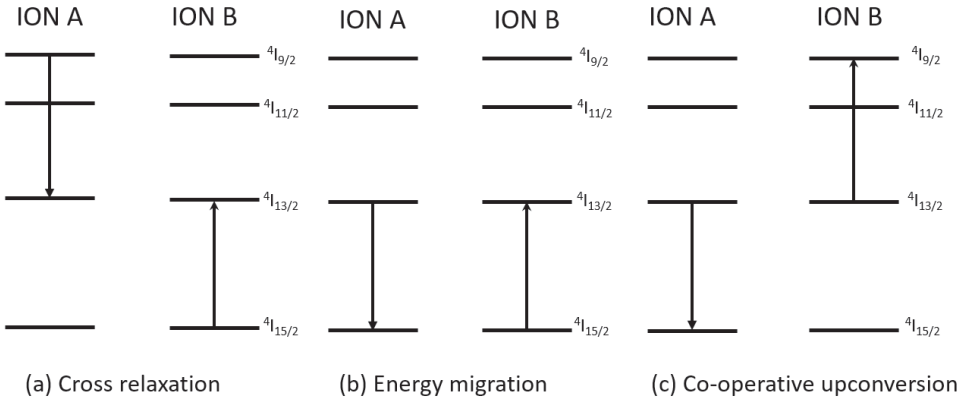

Figure 6. Schematic diagram showing upconversion processes: Cross relaxation a), Energy migration b) and co-operative upconversion c) processes between two adjacent Er^{3+} ions [27].

2.2.2 Upconversion process

Due to the absorption of two or more photons, the addition of Er^{3+} ions in glasses allows the conversion of NIR radiation to green and red emissions. As illustrated in Figure 7, the pumping at ~980 nm leads to the transition $^4I_{15/2} \rightarrow {}^4I_{11/2}$, followed by another transition $^4I_{11/2} \rightarrow {}^4F_{7/2}$ from which there is a non-radiative transition to the $^2H_{11/2}$, $^4S_{3/2}$ and $^4F_{9/2}$ levels leading to

- **green emission** between 520-535 and 535-575 nm ranges due to the radiative transitions from the $^2H_{11/2}$ and $^4S_{3/2}$ levels to the ground state, respectively
- **red emission** in the 640-700 nm range due to the transition from the $^4F_{9/2}$ level to the ground state.

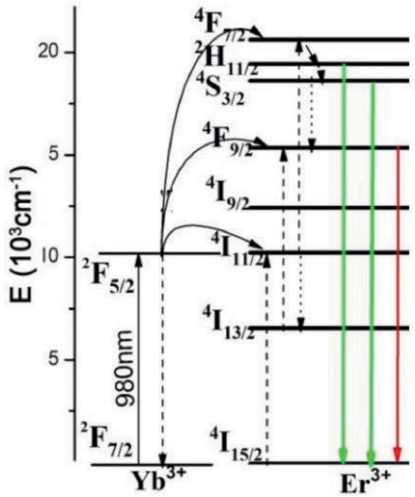

Figure 7. Schematic of the energy level diagram for the Er:Yb codoped system; picture modified form [32]

A suitable glass host should be carefully chosen when preparing a new upconverter glass. Glasses with low phonon energy are the most promising materials as they achieve highly efficient upconversion emission. Silicate, phosphate and borate glasses, for example, exhibit low upconversion due to their high phonon energy. Fluoride glasses, for example, are known to be glasses with low phonon energy and thus exhibit strong upconversion. However, the preparation of fluoride glasses is challenging due to the chemical reactivity of fluoride powders and melts. Fluorine is also known to be a volatile element [33]. Additionally, fluoride glasses have low chemical stability. Therefore, oxyfluoride glasses appear to be ideal candidates as upconverters as they possess the

low-phonon-energy of fluorine and the desirable chemical and mechanical properties of oxide glasses [34,35].

Yb^{3+} ions can be used to enhance the upconversion emission from Er^{3+} doped glass. Indeed, Yb^{3+} ions possess a high absorption cross-section at ~980 nm and also a broad absorption band between 850 and 1080 nm compared to Er^{3+} ions. When pumped at 980 nm, Yb^{3+} ions absorb the pump energy which is then transferred to the Er^{3+} ion [36] (See Figure 7).

Metallic nanoparticles (NPs) in RE doped glasses have received also considerable attention as a means for enhancing the spectroscopic properties of the glass. Enhancement of luminescence was observed when adding silver NPs in Pr^{3+}-doped lead–germanate glass by Naranjo et. al.[37] and also in Eu^{3+} doped tellurite glasses due to the presence of gold NPs by Almeida et. al. and Carmo et. al. [38,39]. An increase in the upconversion was also reported in Er^{3+}, Yb^{3+} co-doped bismuth-germanate-glasses which possess Ag NPs by Wu et. al.[40]. Similar results were reported in Er^{3+}, Yb^{3+} co-doped phosphate glasses containing Ag NPs by Eichelbaum et. al. [41]. The increase in the luminescence properties by Ag NPs is due to an enhanced local electric field around Er^{3+}. This electric field is induced by surface plasmon resonance (SPR) effect of silver NPs which exhibit strong plasmon absorption when larger than 5 nm [42], as illustrated in Figure 8. The enhancement is possible if the RE ions are located in proximity of the NPs [43]

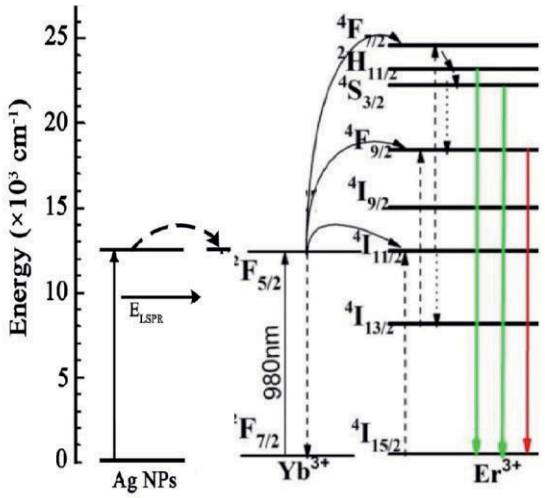

Figure 8. Schematic of the energy level diagram for the Ag NPs enhanced Er:Yb codoped system

However, the amount of Ag NPs needs to be optimized. Indeed, Soltani et al [41] reported a decrease in the intensity of the upconversion when using a large amount of Ag NPs due to an energy transfer from Er^{3+} and Yb^{3+} ions to silver NPs. Similar decrease in the intensity of the emission centered at 1.5 μm due to the presence of NPs in large amount in phosphate glass was also reported by Kuusela et al [44].

Several methods to grow metallic NPs inside glass matrices have been intensively investigated, such as sol-gel [45], heat treatment [38,46,47], direct metal-ion implantation [48], sonochemical method [49], SILAR (successive ionic layer adsorption and reaction) technique [50] just to cite a few, the heat treatment method being the most used due to its simplicity and cost effectiveness. Basically, in the heat treatment method, the formation of Ag NPs consists of two-steps: first the metal ions are added inside the glass matrix and secondly post heat treatment is performed to form metal clusters aided by nucleation and growth as described in refs [41,44] for example. Ag nanoparticles with spherical shape and various sizes can be obtained using different temperatures and durations of heat treatment as reported by Saad et. al. [51].

2.3 RE doped crystals in glass

A lasing material can exhibit larger absorption and emission cross-sections compared to their glassy counterparts when the RE ions are located in crystalline phases with desired nature and structure [52,53]. For example, an increase of the emission intensity of Er^{3+}/Yb^{3+} co-doped phosphate glass-ceramics compared to the as prepared glasses was reported by Yu et al due to the precipitation of Er^{3+} and Yb^{3+} ions doped $LiPO_3/TiP_2O_7$ crystals [54,55].

2.3.1 Glass-ceramic

Stookey discovered the first glass-ceramics (GCs) in 1960 where he defined them as special glasses that contain nucleating agent and controlled crystallization [56]. Since then, studies have been focused on the development of new glass-ceramic which shows promising spectroscopic properties especially for the photonic applications.

To be promising for photonics applications, the glass-ceramics should be transparent and should contain crystals homogeneously distributed in the volume of the glass matrix. These transparent GCs have most of the important features of glasses and ceramics, for instance high optical transparency, tailorable optical properties and good

mechanical stability. Thus, GCs are regarded as substitutes to glasses and crystalline materials for optical applications due to their easy processing into large plates and fibers possessing optical quality alike glass[57].

2.3.1.1 Nucleation and growth mechanism

The crystallization is typically defined by

- the activation energy for crystallization, which is related to the temperature dependence of the crystallization process
- the Johnson–Mehl–Avrami (JMA) exponent, which provides the information on the crystal growth dimensionality [58–60].

The growth rate of the crystals as a function of the heat treatment temperature should also be known in order to control the growth of the nuclei into crystals which is crucial when preparing transparent GCs.

The nucleation of a crystal is the formation of particles (called as nuclei) that are capable of spontaneously growing into larger crystals that are more stable solid phase within a glass. The process is then a heterogeneous nucleation if they form from solid particles or impurities already present in the system. Spontaneous generation of nuclei, also called homogeneous nucleation, can also occur.

In order to form such nuclei, the thermodynamic barrier and the kinetic barrier must be overcome (see Figure 9). Most of the crystallization occurs via the heterogeneous nucleation due to requirement of higher activation energy barrier for homogeneous nucleation [61].

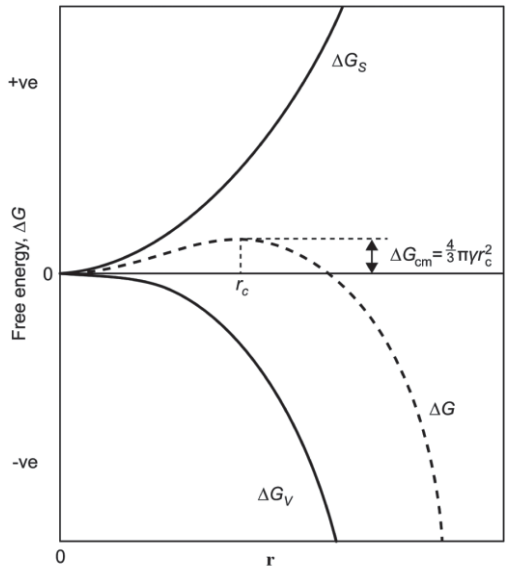

Figure 9. Free energy as a function of cluster radius showing ΔG as a minimum energy to form a nuclei with stable radius; picture modified from [62]

As illustrated in Figure 10, the GCs are usually fabricated using a three (3) step process: at first, a glass is obtained. Then, the glass is heat treated at a specific temperature called the nucleation temperature to form the nuclei, and finally heat treated at higher temperature in order to grow the nuclei into crystals. This process can result in a glass having crystals that are relatively uniform in size and dispersed homogeneously within the glassy matrix [63].

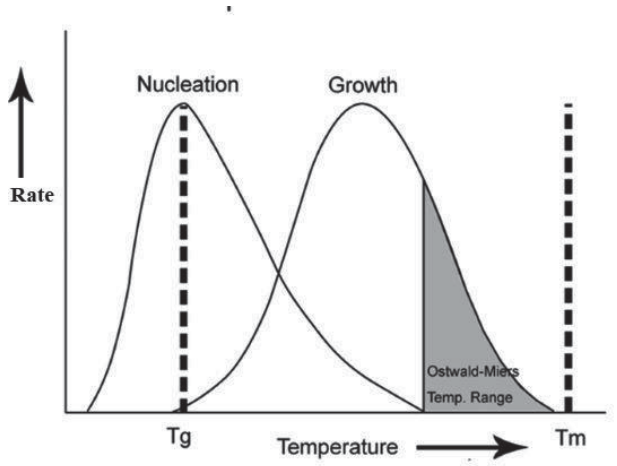

Figure 10. Nucleation and growth of crystals; picture modified from [61]

During heat treatment, crystallization may occur that can be either bulk or surface. However, bulk crystallization is more desirable when preparing a transparent glass-ceramic.

2.3.1.2 Transparent glass-ceramics

For the GCs to be transparent, the crystals need to be smaller than the incident light wavelength according to the Mie theory [64,65]. The Mie theory is used to describe the scattering when the size of the particle is on the order of wavelength. Using the Mie theory, it is possible to estimate the transmittance of a material as a function of crystal size and difference in refractive index between the crystals and the host as illustrated in Figure 11. Therefore, the size and size distribution of the crystals along with the refractive index difference between the crystals and the glass should be tailored in order to minimize light scattering.

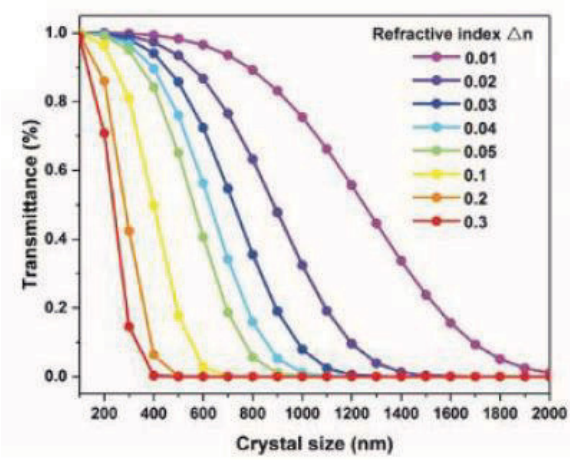

Figure 11. Transmittance as a function of crystal size for various refractive index, from [66]

One of the first transparent RE doped GCs was reported in 1993 by Wang et. al. [34]. Transparent Er^{3+}, Yb^{3+} codoped glass-ceramic with (Pb, Cd)F_2 crystalline phase was successfully prepared from fluoroaluminosilicate glass. Because of the presence of the RE doped fluoride crystals, this GC exhibits strong infrared to green or to red upconversion efficiency. Few years later, Tick et al [35] reported a study on transparent fluoro-aluminosilicate based GCs which contain nanocrystals with Cd–Pb-rich fluoride composition. This transparent GC contained 15–30 % by volume of praseodymium-doped nanocrystals of cadmium lead fluoride crystals, with sizes between 9–18 nm. The high transparency of the GCs was thought to be due to the nanocrystals being uniformly

dispersed, with comparable dimensions between interparticle spacing and the particle size. Although the number of studies on the development and characterization of new RE doped transparent GCs has grown significantly since these papers, the studies have been focused mainly on silicate glasses. Just to cite few examples, transparent Er^{3+} doped oxyfluoride aluminosilicate glass–ceramics have been reported with strong upconversion luminescence and near infrared luminescence due to the precipitation of CaF_2 crystals doped with Er^{3+}[67]. Yb^{3+} doped GCs in the SiO_2–Al_2O_3–Na_2O–CaF_2–PrF_3–YbF_3 have also been obtained with CaF_2 nanocrystals [68,69]. Recently, Pr^{3+}–Yb^{3+} co-doped oxyfluoride aluminosilicate GCs with LaF_3 nanocrystals were reported by Gorni et. al. [70]. GCs in other glass systems have been also investigated. The first transparent GCs in germanate and tellurite systems were reported in 1995 the germanate GC was prepared from the glass in the GeO_2–PbO–PbF_2–TmF_3 system and contained ~16 nm PbF_2:Tm^{3+} nanocrystals [71] while the first tellurite GC was obtained from the 70 TeO_2–15 Nb_2O_5–15 K_2O glass composition (mol %) with ~20–40 nm unidentified crystalline phases [72] Since these studies, the transparent GCs prepared have been reported from other germanate glasses as in ref [73–75] and tellurite glasses as in ref [71,72,76].

Surprisingly, only a few studies have been reported on RE doped transparent phosphate GCs. Recently, transparent undoped and Er^{3+} doped GCs with the composition (75 $NaPO_3$ - 25 CaF_2) (in mol %) were reported in ref [77,78]. A heat treatment of the Er^{3+} doped glass led to the volume precipitation of CaF_2 crystals doped with Er^{3+}increasing the intensity of the upconversion [79].

In this context, one part of the thesis was focused on determining the crystallization parameters of this promising glass with the composition (75 $NaPO_3$ - 25 CaF_2) (in mol %) and also on understanding the impact of the changes in the glass composition on these crystallization parameters in order to prepare new transparent GCs.

2.3.2 Direct doping method

As it is not possible to predict and control the precipitation of RE doped crystals with a specific crystalline phase in the volume of the glass using heat treatment, techniques such as direct doping method have been developed in order to prepare glasses with RE doped crystals with specific crystalline phase dispersed in their volume. The technique is illustrated in Figure 12. At first, the glass batch is melted. Then, the temperature is reduced to a specific temperature prior to adding the crystals in the glass melt. This temperature is called the doping temperature (T_{doping}). After a short time to

allow the homogeneous dispersion of the crystals in the glass melt, the melt is quenched and finally annealed. This doping parameter is called dwell time.

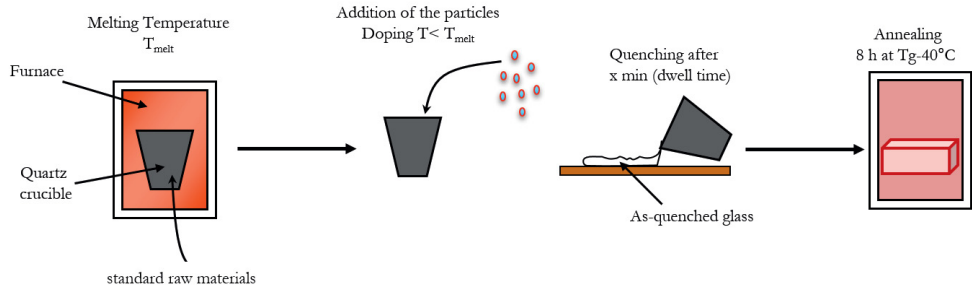

Figure 12. Schematic of the direct doping method

With this method, RE doped crystals are prepared separately and then added in the glass so the local environment of the RE ions can be controlled independently of the glass composition. However, to avoid the decomposition of the crystals while dispersing homogeneously the crystals in the glass during the glass melting, the doping parameters such as the doping temperature and the dwell time need to be optimized. Zhao et al.[80] successfully prepared lanthanide-containing upconversion nanocrystals in tellurite glasses using this direct doping method clearly showing the promises of this technique.

Strong enhancement of the upconversion luminescence intensity has been reported after heat treatment of an oxyfluoride glass within the system SiO_2–Al_2O_3–Na_2O–NaF–YF_3–ErF_3–YbF_3 by Liu et. al. and Gao et. al.[81,82] and the behavior has been related to the volume precipitation of $NaYF_4$: Er^{3+}, Yb^{3+} crystals occurring during the heat treatment. The $NaYF_4$: Er^{3+}, Yb^{3+} crystal is known to be one of the most efficient upconverter fluoride crystals due to its low phonon energies (<350 cm^{-1}) which reduces the energy losses at the intermediate states of lanthanide ions [83]. However, there is no known report of heat treatment leading to the precipitation of $NaYF_4$ nanocrystals in phosphate glasses. The direct doping method could then be used an alternative method to prepare $NaYF_4$: Er^{3+}, Yb^{3+} crystals containing phosphate glasses. However, one should remember that the evaporation of the particles and melting of NaF occur at 750 °C [78] indicating that the doping temperature should be lower than 750 °C to limit the decomposition of the crystals during the glass preparation. The first step in the preparation of such $NaYF_4$ nanocrystals containing phosphate glass is to identify a glass composition which melts at low temperature, so the doping temperature can be kept below 750 °C.

Therefore, the second part of the thesis was focused on the preparation and characterization of $NaYF_4$: Er^{3+}, Yb^{3+} crystals containing phosphate glasses using the direct doping method.

3 MATERIALS AND METHODS

This chapter described the techniques used to prepare the glass-based materials investigated in this study. The characterization techniques used to assess the different properties of the glass such as, physical, structural and optical properties of the samples are also presented.

3.1 Glass-based materials

3.1.1 Er^{3+} doped glasses and glass-ceramics

Oxyfluorophosphate glasses with the composition (100- x- 0.25) (75 $NaPO_3$ – 25 CaF_2) – x (TiO_2 /ZnO / MgO) (in mol %), doped with 0.25 mol % Er_2O_3, with x = 0 and 1.5 were prepared using standard melting procedure in air using platinum crucible. The glass with x = 0 is labelled as Ref and the glasses prepared with x = 1.5 and with TiO_2 as Ti glass, with ZnO as Zn glass and with MgO as Mg glass.
The chemicals used for the glass preparation were $NaPO_3$ (Alfa-Aesar, technical grade), CaF_2 (Honeywell-Fluka, 99 %), Er_2O_3 (Sigma-Aldrich, 99.9 %), MgO (Honeywell, ≥ 99 %), TiO_2 (Sigma-Aldrich, 99.8 %) and ZnO (Sigma-Aldrich, 99.99 %). The glasses were melted for 5 minutes between 900 and 1025 °C depending on the composition of the glass (see Table 1 for the melting temperature of each glass). After melting, the glasses were quenched and annealed for 6h at 40°C below their respective glass transition temperature to release the stress from the quench.

Code	Melting temperature (°C)
Ref	900
Ti	1025
Mg	900
Zn	1000

Table 1. Melting temperature of the Er^{3+} doped oxyfluoride glasses

After annealing, the glasses were polished and finally heat treated for 17h at 20°C above their respective glass transition temperature T_g to create the nuclei and then at higher temperature, near the crystallization temperature (T_p), for few minutes to few hours in order to grow the nuclei into crystals.

3.1.2 Crystals containing glasses

The crystals containing glasses were prepared using direct doping method by adding the crystals in the glass melt. The direct doping process was optimized using commercial persistent luminescent (PeL) particles such as $SrAl_2O_4$: Eu^{2+}, Dy^{3+} particles ((Realglow, China, PYG-6L)) and $Sr_4Al_{14}O_{25}$:Eu^{2+}, Dy^{3+} particles (Jinan G.L. New Materials, China, BG-01). Glasses with the following compositions were prepared with PeL particles:

- $50P_2O_5$ – 10 Na_2O – 40 CaO/SrO (mol %) (labelled as CaNaP and SrNaP, respectively)
- (90 $NaPO_3$ −(10 − x) Na_2O −x NaF) (mol %) (labeled as NaPF0 and NaPF10 respectively when x = 0 and 10)

The NaPF0 and NaPF10 glasses and glasses with the composition 83.25 $NaPO_3$ - 9.25 NaF – 5 ZnO - 2.5 Ag_2O (in mol %) (labeled as 2.5Ag) were also prepared using the same process by adding $NaYF_4$: Er^{3+}, Yb^{3+} crystals in the glass melt after the melting. The synthesis of the $NaYF_4$: Er^{3+}, Yb^{3+} can be found in ref [84].

Raw materials used for the glass preparation were $(NaPO_3)_6$ (Thermo Fisher Scientific, 99.0 %), Na_2CO_3 (Sigma Aldrich, > 99.5 %), NaF (Sigma Aldrich, 99.99 %), ZnO (Sigma-Aldrich, 99.50 %) and Ag_2SO_4 (Sigma Aldrich, 99.99 %). $Ca(PO_3)_2$ and $Sr(PO_3)_2$ were prepared from mixtures of $(NH_4)_2HPO_4$ and $CaCO_3$ (Thermo Fisher Scientific, 99.0 %) and $SrCO_3$ (Sigma Aldrich, 99.9 %), respectively heated slowly at a rate of 1 °C/min to 850 °C. Prior to the melting, the NaPF0 glass was treated at 300 °C for 15 min. This temperature was found to be high enough to decompose Na_2CO_3 and to evaporate CO_2. The glasses were melted in quartz crucibles. After melting, the temperature was reduced before adding the PeL particles. This temperature is called doping temperature (T_{doping}). The glasses were quenched a few min after adding the MPs. The time between adding the particles and quenching of the glass is called the dwell time (t). After quenching, the glasses were annealed at 40 °C below their respective glass transition temperature, for at least 4 h in air to release the stress induced from the quench. The doping parameters of the various particles containing glasses are summarized in Table 2.

Code	Melting temperature ($T_{melting}$)°C	Doping temperature (T_{doping}) °C	Dwell time t (min)
SrNaP	1050	975-1025	3-10
CaNaP	1100	1000-1050	3-10
NaPF0	750	525-575	3-5
NaPF10	750	525-575	3-5
2.5Ag	875	550	3

Table 2. Various doping parameters used to prepare particles containing glasses

3.1.3 Fiber drawing

The $NaYF_4$: Er^{3+}, Yb^{3+} crystals containing NaPF10 glass was prepared into a 10 cm long preform with a diameter of 1 cm as explained in section 3.1.2. Single core fiber with ~200 μm in diameter was drawn from this preform with a specially designed drawing tower in collaboration with Rennes University (France). The drawing temperature of 405 °C was used for fiber drawing with the feed rate of 1 mm/min and the drum speed of 6.18 m/min. 10 meters of uncoated fiber were drawn without any protective polymer layer to allow the characterization of the thermal, optical and structural properties of the fiber.

3.2 Physical properties

Archimedes principle was used to measure the density of the glasses. Polished samples, free from bubbles, were used for the measurement with ethanol as the immersion liquid at room temperature. The accuracy of the measurements is ±0.02 g/cm^3.

3.3 Thermal Properties

The glass transition temperature (T_g) as well as the onset of the crystallization (T_x) and the crystallization temperature (T_p) of the glasses were determined using a differential thermal analyzer (DTA) (NETZCH Jupiter F1, Selb, Germany). The measurement was performed at a heating rate of 10°C/min from samples crushed into

powder (30 mg). The samples were placed in a Pt crucible and were heat treated under a N_2 atmosphere with a flow below 50ml/min. The glass transition temperature was taken at the inflection point of the endotherm, as obtained by taking the minimum of the first derivative of the DTA curve. T_p was taken at the maximum of the exothermic peak and T_x at the onset of the crystallization peak. All measurements were performed with an accuracy of ± 3 °C.

3.4 Crystallization parameters

The crystallization is typically defined by the activation energy for crystallization, which is related to the temperature dependence of the crystallization process and by the Johnson–Mehl–Avrami (JMA) exponent, which provides the information on the crystal growth dimensionality (surface vs. bulk crystallization). It is also important to estimate the growth rate of the crystals as a function of the heat treatment temperature when preparing transparent GCs.

The activation energy for crystallization (E_c) was determined by measuring the T_p at different heating rates (5°, 10°, 15°, and 20 °C/min). The samples were crushed into powder of size 125-250 μm for the measurement. E_c was calculated using the Kissinger Equation [59]:

$$\ln\left(\frac{\beta}{{T_p}^2}\right) = -\frac{Ec}{RT_p} + Constant \qquad (1)$$

where β is the heating rate, T_p is the maximum of the crystallization peak measured with heating rates of 5°, 10°, 15°, and 20 °C/min, and R is the gas constant. The accuracy of the measurement was ±30 KJ/mol.

To verify the results obtained with the Kissinger Equation, the E_c was also determined using the Friedman method using the Equation [60]:

$$\ln\left(\frac{d\alpha_i}{dt}\right) = -\frac{E_{c\alpha}}{RT_i} + Constant \qquad (2)$$

where $d\alpha_i$ is the transformation rate at a temperature T_i.

The Johnson–Mehl–Avrami (JMA) exponent was determined using the equation proposed by Augis and Bennett [85]:

$$n = \frac{2.5}{\Delta T_{FWHM}} \frac{T_P^2}{\frac{E_c}{R}} \qquad (3)$$

where n is the JMA exponent, T_p is the crystallization temperature, ΔT_{FWHM} is the full

width at half maximum of the DTA peak, E_c is the activation energy for crystallization, and R is the gas constant. The accuracy of the measurement was found to be ±0.1.
n was also obtained by using the Ozawa method from the fraction of glass crystallized at various heating rates using the following equation at a constant temperature [58]:

$$\left[\frac{d(\ln(-\ln(1-\alpha)))}{d(\ln(\beta))}\right]_T = -n \qquad (4)$$

where β is the heating rate and α volume fraction of glass crystallized at a fixed temperature T. The plot of ln (-ln (1-α)) = f (ln (β)) based on this equation yields a straight line with a slope equal to -n. The accuracy of the measurement using this method was ±0.5.
The value of n corresponds to the different type of crystallization either surface, or bulk with different type shapes as shown in Table 3.

n	**Crystal growth Dimensionality**
1	Surface Crystallization
2	Bulk crystallization: needle like crystal
3	Bulk crystallization: crystal with 2D shape (Plate like)
4	Bulk crystallization: crystal with 3D shape (Sphere, cube etc.)

Table 3. Types of crystallization depending on n [86].

The temperature of maximum nucleation ($T_{n\ max}$) was determined from the nucleation-like curve using the method described by Marotta et al. [87]. In this method, the glass powder was subjected to an isothermal hold inside the DTA, at various temperatures T (between T_g and T_x) near the suspected temperature of the maximum nucleation ($T_{n\ max}$). The temperature was then reduced to 200 °C and finally increased to a temperature T, above the crystallization temperature. The nucleation like curve was obtained from the plot of $(1/T^o_p - 1/T_p) = f(T)$, (where T_p and T^o_p are the maximum of the exothermic peak with and without the nucleation thermal hold). The maximum of the obtained curve gives $T_{n\ max}$.

To estimate the crystal growth rate, polished glasses were heat treated at a temperature higher than the temperature of maximum nucleation for different durations. The crystal size was measured as a function of the heat treatment duration for each temperature in an optical microscope Olympus BH2-UMA. The crystal growth rate was then calculated from the slope of measured crystal size as a function of duration of heat treatment at different temperatures

3.5 XRD

The amorphous nature of the glass and crystal phases present in the glass-ceramics were analyzed using the Panalytical EMPYREAN multipurpose X-Ray Diffractometer with a Nickel filtered Copper K_α radiation (λ = 1.5406 Å). The spectra were obtained using the Bragg-Brentano geometry and by rotating the sample holder around the Phi-axis at a constant speed of 16 revolutions per minute. The spectra were collected from 2θ = 15°-80° with step width of 0.025° The glasses and glass-ceramics were crushed into powder and spread over a "zero-background holder" Si-plate for the measurement of the XRD spectra.

3.6 Structural Properties

3.6.1 FTIR

Fourier transformed Infrared spectroscopy (FTIR) in attenuated total reflectance (ATR) mode was used to analyse the structural properties of the glass with a PerkinElmer Spectrum One FTIR Spectrophotometer (Waltham, MA, USA). The spectra were recorded in the 600-1800cm^{-1} range. All spectra were obtained with a resolution of 2 cm^{-1} and accumulation of 8 scan.

3.6.2 Raman

The Raman spectra of the investigated glasses were measured at room temperature between 200 and 1400 cm^{-1} using a Thermo ScientificTM DXRTM 2xi Raman Imaging Microscope equipped with a 785 nm laser. The power incident on the sample was 600 μW with an exposure time of 30 seconds per pixel. All the glass samples were polished for the measurement.

3.7 Optical properties

The absorption spectra were measured using a UV-Vis-NIR spectrophotometer (UV-3600 Plus, Shimadzu) between the wavelength of 200 to 1800 nm with an interval of 0.5 nm. The thickness of the polished samples was measured using a digital caliper.

The accuracy of the measurement was ± 0.05 mm. The absorption cross-section σ (in cm^2) was calculated using the following Equation:

$$\sigma(\lambda) = \frac{2.303}{NL} log\left(\frac{I_o}{I}\right) \qquad (5)$$

where N is the number of ions per cm^3 absorbing at the specific wavelength (λ), I/I_o is the absorbance and L is the thickness of the sample (in cm). The accuracy of the measurement is ± 10 %.

3.8 Luminescent properties

The conventional luminescence spectra of the PeL particles containing glasses were measured at room temperature using a CCD camera (Avantes, AvaSpec–2048 × 14) using a 266 nm from Nd:YAG pulse laser (TII Lotis). For the measurement of the persistent luminescent (PeL) spectra, the PeL particles containing glasses were irradiated for 5 min at room temperature with a compact 254 nm UV lamp (UVGL-25, 4 W). The PeL spectra were recorded 1 min after ceasing the irradiation with a 4 s data collection time. The spectra were measured at room temperature using a Varian Cary Eclipse Fluorescence Spectrophotometer equipped with a Hamamatsu R928 photomultiplier (PMT). For both measurements, the PeL containing glasses were crushed into powder.

The emission spectra centered at 1.5 μm and the upconversion spectra of the Er^{3+} doped glasses and glass-ceramics were measured using a Spectro 320 optical spectrum analyzer (Instrument Systems Optische Messtechnik GmbH, Germany). The spectrum analyzer was equipped with a photomultiplier tube capable of measuring wavelengths between 350 nm and 850 nm. InGaAs detector was used for the measurement of the emission in the from 800 nm to 1700 nm range. The luminescence light was collected from the samples to the spectrum analyzer using a lens and a liquid light guide. The measurements were performed at room temperature. Samples were excited using a TEC-cooled fiber-coupled multimode laser (II-VI Laser Enterprise). The center emission wavelength of the laser was ~975 nm and its incident power at the sample surface was ~23.5 mW. To allow the comparison of the intensity of the emission, the samples were crushed into powder for the measurement.

The lifetime of the Er^{3+}:$^4I_{13/2}$ energy level was measured using a fiber pigtailed laser diode at 976 nm. A digital oscilloscope (Tektronix TDS350) was used to record the signal and the decay traces were fitted using single exponential. Thorlabs PDA10CS-

EC was used as the detector for this measurement. The accuracy of the measurement was ± 0.20 ms.

A FLS1000 Photoluminescence Spectrometer equipped with a xenon arc lamp and a PMT-900 detector were used to measure the visible emission spectrum of the 2.5Ag glass. The excitation was 320 nm.

3.9 Composition analysis

3.9.1 EPMA

The fluorine content in the glasses was measured by Electron Probe MicroAnalyzer (EPMA) (CAMECA, SX100) equipped with 5 wavelength dispersive x-ray analyzers (WDX). The accuracy of the measurement was ±0.1 at %. The EPMA was operated at 15 keV and 40 nA. Cameca QUANTITOOL analytical programme was used to perform the quantitative analyses, calibrated with ErF_3 reference standard and applying a PAP matrix correction. All the samples were polished for the measurement.

3.9.2 SEM/EDS

A SEM (Carl Zeiss Crossbeam 540) equipped with Oxford Instruments X-MaxN 80 EDS detector was used to image and analyse the composition of the crystals. The error of composition is ±1.5 mol %. The polished samples were coated with a thin carbon layer to prevent charging.

4 RESULTS AND DISCUSSION

The main objective of this work was the preparation and characterization of glass-based materials which contain rare-earth (RE) doped crystals in order to prepare new glass-based materials with enhanced spectroscopic properties as compared to the parent glass. The glass-based materials were prepared using heat treatment and also by adding RE doped crystals in the glass melt using the direct doping method. This chapter summarizes and discusses the main results which were published in 3 articles (2 additional publication being under review). Some unpublished results are also presented.

4.1 Transparent glass ceramics

Glasses with the composition (75 $NaPO_3$ - (25 - x) CaO – x CaF_2) (in mol %) were prepared and heat treated [77]. Depending on the glass composition, the glasses undergo surface to volume crystallization, the glass with x = 25 exhibiting bulk crystallization of CaF_2 crystals. Later it was shown that the addition of Er^{3+} ions does not change the crystallization process and that the CaF_2 crystals are doped with Er^{3+} leading to an increase in the intensity of the upconversion under 975 nm pumping [78,79]. However. the glass with x = 25 has a narrow thermal processing window, as evidenced by the small temperature difference between T_x and T_g, limiting its use. Thus, the goal of this study was 1) to study the nucleation and growth properties of the glass with x = 25 and 2) to develop new glasses in the similar $NaPO_3$ - CaF_2 system with better thermal stability while still exhibiting volume precipitation of Er^{3+} doped CaF_2 crystals.

4.1.1 Impact of the glass composition on various properties of the glass

By adding modifiers and/or intermediates, phosphate glasses are able to change their network, thus changing their chemical and thermal stabilities and other properties [88,89]. For example, TiO_2 is known to create Ti-O-P cross-linked bonds at the expense of P-O-P bonds [90] whereas ZnO can act as a modifier depolymerizing the glass

network[91]. In this study, new elements such as TiO_2, MgO and ZnO were added in the glass with x = 25. These elements were selected based on their covalency and their ability to change the structure of glass matrix. The purpose of this study was to understand their impact on the structural, optical and thermal properties of the glass and to investigate the nucleation and growth process of the newly developed glasses.

The thermal and physical properties of the glasses with composition (100- x- 0.25) (75 $NaPO_3$ – 25 CaF_2) – x (TiO_2 /ZnO / MgO) (in mol %), doped with 0.25 mol % Er_2O_3, with x = 0 and x = 1.5, are shown in Table 4. The changes in the glass composition slightly increased the density, T_g, T_x and T_p, the addition of TiO_2 being the most effective in these changes. As seen in Table 4, the increase in the melting temperature decreases the Fluorine at. % in the glass as quantified using EPMA in agreement with the previous study[79] . The increase in T_g may be related to the different Fluorine at % in the glasses and/or to an increase in the bond strength due to the changes in the glass composition as reported in [92]. The changes in the glass composition led also to a slight increase in ΔT ($\Delta T = T_x - T_g$) confirming that the addition Ti, Mg or Zn in this phosphate network can be used to increase the resistance of the glass towards crystallization.

Glass code	Quantification using EPMA/WDX		T_m (°C)	ρ ±0.02 (g/cm³)	T_g ±3 °C (°C)	T_x ±3 °C (°C)	T_p ±3 °C (°C)	ΔT ±6 °C (°C)
	Expected F at %	Measured F at % (± 0.1 at %)						
Ref	11.1	9.2	900	2.63	269	323	338	54
Ti	11.0	8.9	1025	2.65	286	350	370	64
Mg		9.4	900	2.66	279	345	365	66
Zn		9.1	1000	2.65	276	334	350	58

Table 4. Density, thermal properties and F quantification of the investigated glasses (Publication V)

The IR spectra of the new glasses are shown in Figure 13 and are similar to those reported in [78] where a detailed attribution of the bands can be found.

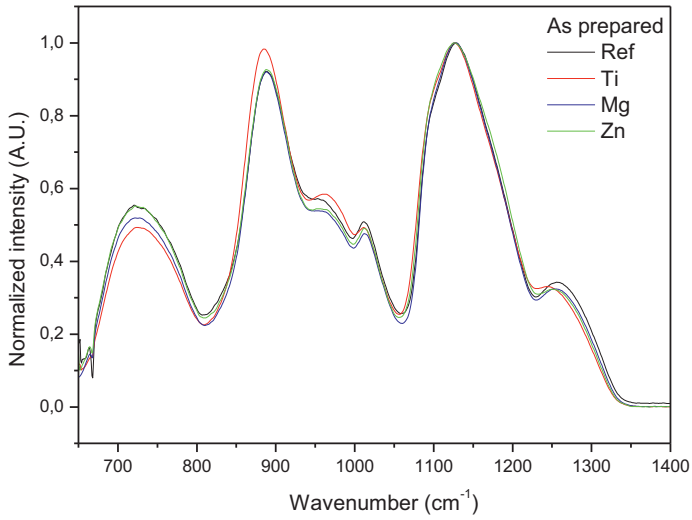

Figure 13. Normalized IR spectra of the investigated glasses (Publication V)

The addition of ZnO and MgO leads to a small decrease in intensity of the bands at about 700, 950, ~1000 and 1250 cm^{-1} and to a slight increase in the intensity of the shoulder at 1100 cm^{-1} as compared to the main band whereas the addition of TiO_2 increases the intensity of the bands at around 880 and 950 cm^{-1} and decreases the intensity of the band at 1250 cm^{-1}. The position of the bands at 880 and 1250 cm^{-1} shifts towards smaller wavenumbers when adding TiO_2 due to the strong field strength of the Ti ions. Due to the higher field strength of Mg compared to Zn [93], the changes in the IR spectra are more visible when adding MgO than ZnO in the network. The changes in the IR spectra when changing the glass composition can be related to a decrease in the Q^2 units and to an increase in Q^1 units [94]. In agreement with the results presented in [95], Mg, Ti and Zn are expected to cross-link the phosphate chains by creating P-O-Mg/Ti/Zn bonds at the expense of P-O-P bonds associated with a reduction in the number of Q^2 units[94,96]. Therefore, the addition of ZnO, MgO and TiO_2 is suspected to cause a distortion and compaction of the glass network which is in agreement with the increase in T_g seen in Table 4. Similar results were reported by Segawa et. al. [97].

The decrease in the glass connectivity was found to also shift the band gap to longer wavelengths (spectra can be found in Publication V). A large shift of the band gap to longer wavelength was seen when adding TiO_2 most probably due to the presence of Ti^{3+} as reported by Andrade et. al. [98]. Except their different optical band gap, the

glasses exhibit similar absorption and emission properties: similar absorption and emission bands, similar absorption coefficients and cross-sections at 975 and 1532 nm and similar intensity of the emission at 1.5 μm and in the visible after 975 nm pumping. Hence change in the glass composition has no noticeable impact on the site of the Er^{3+}; Ti, Mg and Zn are not suspected to participate in the second coordination shell around Er^{3+}.

4.1.2 Heat treatment of the glasses

As performed by Nomm et. al [78] and Szczodra et. al.[79], the glasses were heat treated at T_g + 20°C for 17h to create the nuclei and then at T_p for 1 to 6 h to grow the nuclei to crystals. The glasses were polished prior to the heat treatment and were heat treated in air on a Pt foil to avoid sample holder contamination. The glasses are less transparent after heat treatment confirming that crystallization occurred during the heat treatment (Figure 14). While the Ref and Zn glasses are still transparent after heat treatment, the Ti and Mg glasses became translucent.

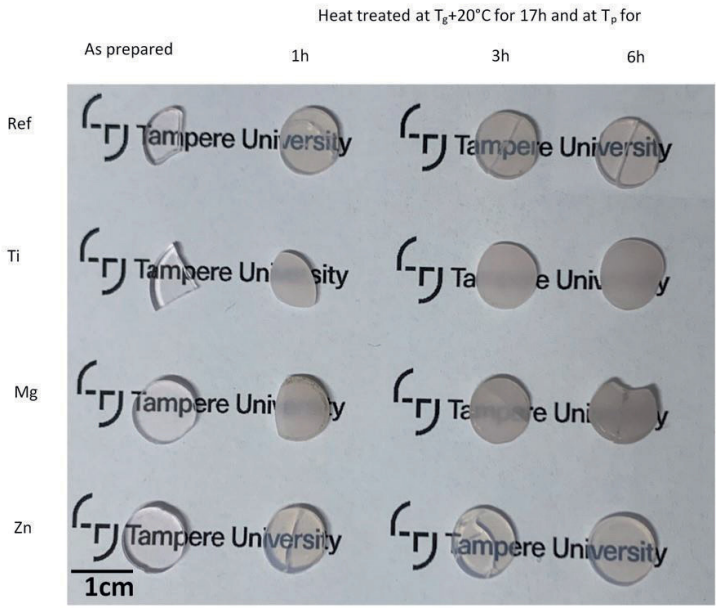

Figure 14. Pictures of the glasses heat treated at T_g+20°C for 17h and at T_p for 1, 3 and 6 hours (Publication V)

The XRD of the heat treated glasses can be found in Figure 15. They exhibit the same peaks which correspond to CaF_2 (ICDD PDF #00-035-0816) confirming that the change in the glass composition has no impact on the crystal phase precipitating in the glass.

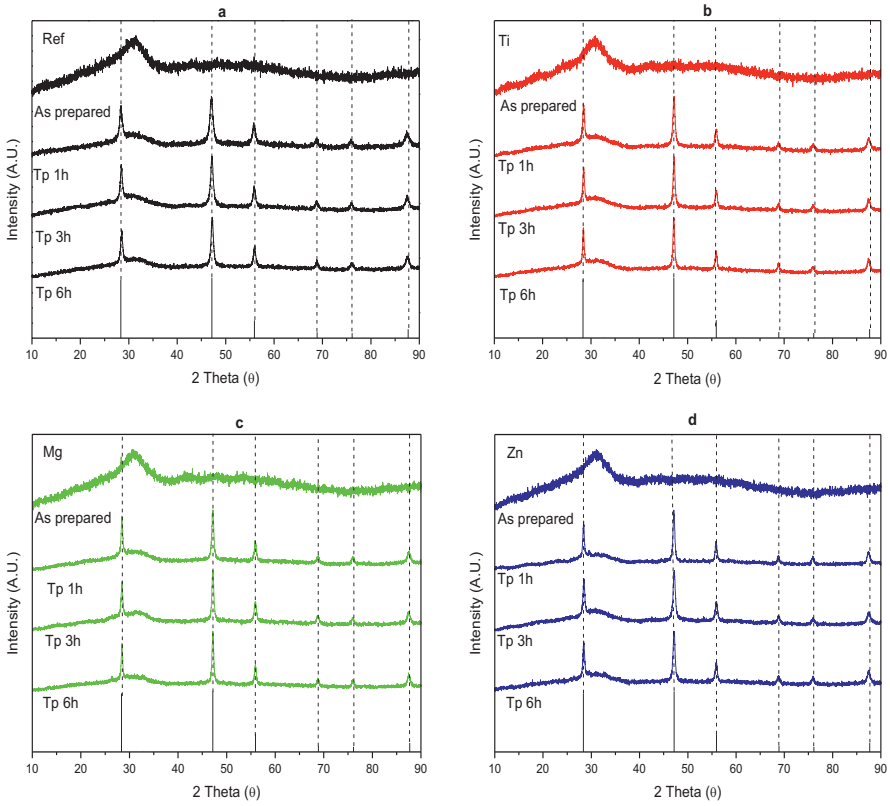

Figure 15. XRD patterns of the Ref a), Ti b), Mg c) and Zn d) glasses prior to and after heat treatment T_g+20°C for 17h and at T_p for 1, 3 and 6 hours (Publication V)

A decrease in the intensity of the emission centered at 1.5 μm, an increase in the intensity of the upconversion and an increase in the lifetime values of the Er^{3+}:$^4I_{13/2}$ level were observed after heat treatment confirming the precipitation of Er^{3+} doped CaF_2 crystals [79]. One should point out that the glass-ceramics, independently of their composition, exhibit similar intensity of the emission at 1.5 μm and in the visible after 975 nm pumping (within ± 10 %).

Although the investigated glass-ceramics possess the same Er^{3+} doped CaF_2 crystals and similar luminescence properties, the Ref and the Zn glass-ceramics are still

transparent while the Ti and Mg glasses become opaque after 6h at T_p (Figure 14). The transmittance spectra of the glasses are shown in Figure 16.

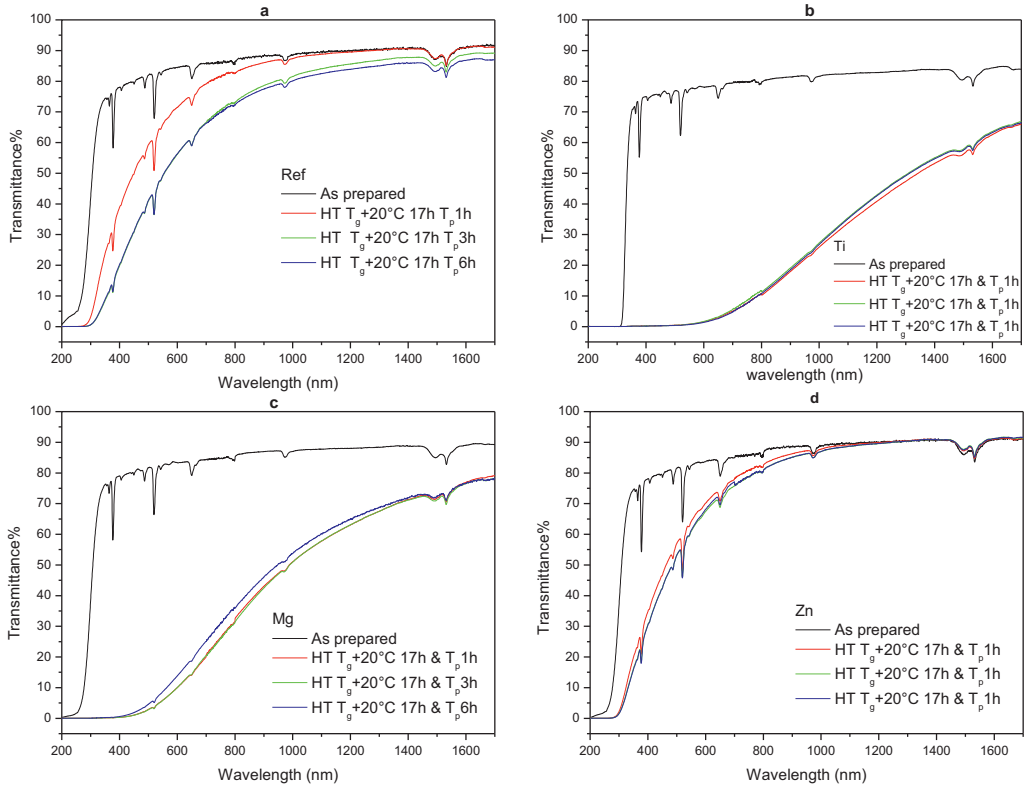

Figure 16. Transmittance spectra of the Ref a), Ti b), Mg c) and Zn d) glasses heat treated at T_g+20°C for 17h and at T_p for 1, 3 and 6 hours (Publication V)

The large decrease in the transmittance of the Ti and Mg glasses can be related to the presence of a large amount of crystals and/or large crystals inside these glass matrices leading to strong light scattering [57]

Thus, in order to better understand the different transparency of the glass-ceramics, the activation energy for crystallization (E_c), JMA exponent nucleation curve and crystal growth rate of the glasses were calculated.

The activation energy for crystallization of the glasses was calculated using two methods (Table 5).

Glass Code	Activation Energy (E_c)		JMA exponent (n)		Maximum nucleation temperature $T_{n\,max}$ (°C)	T_x - T_{nmax} (°C)
	Kissinger method ±30 kJ/mol	Friedman method kJ/mol	Augis Benett method (±0.1)	Ozawa Chen method		
Ref	190	182 ±10	2.1	2.0 ± 0.5	276 ± 5	47± 8
Ti	185	226 ±20	1.7	1.5 ±0.4	295 ± 5	55± 8
Mg	158	186 ±11	1.8	1.6 ±0.4	285 ± 15	60± 23
Zn	206	199 ±6	1.9	1.9 ± 0.5	280 ± 5	54± 8

Table 5. Activation energy for crystallization, maximum nucleation temperature and JMA exponent of the investigated glasses (Publication V)

The standard deviation of the E_c calculated using the Friedman method is less than 10 % indicating that only one crystallization mechanism is involved throughout the entire crystallization process. The low standard deviation also validates the Kissinger method which is often used to further calculate the JMA exponent. The similarity in E_c between glasses and the low standard deviation of E_c calculated using the Friedman technique tend to indicate that the crystallization process is nucleation and growth and the primary crystal field is similar in all glasses. [59,99].

The JMA exponent of the glasses was calculated using two methods (Augis-Bennett and Ozawa-Chen) and the n values can be found in Table 5. The n values from both techniques are in close agreement. The crystal growth dimensionality in the glasses is ~2 within the accuracy of the measurement indicating that the glasses, independently of their composition, have a dominant bulk crystallization with needle like crystals when subjected to heat treatment [86]. The needle like shape of the crystals was confirmed using SEM (SEM images of the crystals can be found in Publication V): the crystals have similar needle like shape as they grow preferentially in one direction. EDS was used also to confirm the CaF_2 chemical composition of those crystals.

The nucleation like curve was determined using the method proposed by Ray et al [100] and Marrota et al [87]. The maximum nucleation temperature ($T_{n\,max}$) was taken from the maximum of the nucleation-like curve. The maximum nucleation temperature varies between 276 °C to 295 °C depending on the glass composition (see Table 5). The Mg and Ti glasses exhibit similar nucleation like curve (spectra can be found in Publication V); their nucleation like curve is shifted to higher temperature and is broader than that of the Ref and Zn glasses.

Also shown in Table 5 is the temperature difference between the onset of crystallization (T_x) and $T_{n\ max}$ (ΔT) which is > 50 °C indicating that the nucleation and growth can be easily controlled in the investigated glasses which is crucial when preparing transparent glass-ceramics.

Finally, the crystal growth rate curves were calculated from the slope of crystal size as a function of the duration of heat treatment performed at different temperatures and are shown in Figure 17.

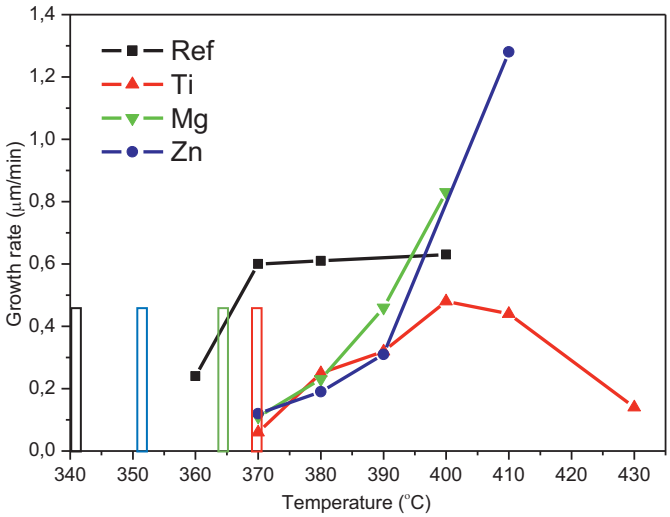

Figure 17. Crystal growth rate in the investigated glasses as a function of temperature (Modified from Publication V)

The maximum growth rate increases from (385±15)°C (Ref glass) to (400±10)°C when adding TiO_2 and to above 400°C when adding MgO and ZnO. It should be pointed out that the Mg and Zn glasses could not be heat treated above 410°C due to excessive viscous flow. The increase in the maximum growth rate when modifying the glass composition is probably due to the changes in the glass network as discussed earlier. The crystal growth rate curves are in agreement with the transparency of the glass-ceramic; according to Figure 17, the crystals are expected to be ~3, 4, 21 and 21 μm in the Ref, Zn, Mg and Ti glasses, respectively, after heat treatment at T_g + 20°C for 17h and then at T_p for 6 h confirming that larger crystals are present in the Mg and Ti glasses after heat treatment as suspected from the losses in the transparency of the Mg and Ti glasses reported in Figures 14 and 16.

4.1.3 MgO containing glasses

As the Mg glass exhibit the largest ΔT, glasses were prepared with different amount of MgO in order to check if it is possible to further increase ΔT without changing the crystallization process. As shown in Table 6, ΔT can be increased to ~ 90 °C when adding at least 3 mol % of MgO. However, a further increase in MgO content up to 6 mol % has no significant impact on ΔT.

Glass	**T_g ± 3 °C (°C)**	**T_x ± 3 °C (°C)**	**T_p ± 3 °C (°C)**	**ΔT ± 6 °C (°C)**
Ref	269	323	338	54
1.5MgO	279	345	365	66
3MgO	290	377	410-474	87
4.5MgO	297	381	410	84
6MgO	302	381	405-426	79

Table 6. Thermal properties of different concentration of Mg glass compared to Ref glass (unpublished data)

As shown in Figure 18, the addition of MgO leads to a progressive decrease in intensity of the IR bands at about 700, 950, ~1000 and 1250 cm^{-1} and to a slight increase in the intensity of the shoulder at 1100 cm^{-1} as compared to the main band confirming the progressive depolymerization of the glass network with the formation of P-O-Mg bonds at the expense of P-O-P bonds when adding MgO in the glass network. These changes in the glass structure are in agreement with the increase in T_g reported in Table 6.

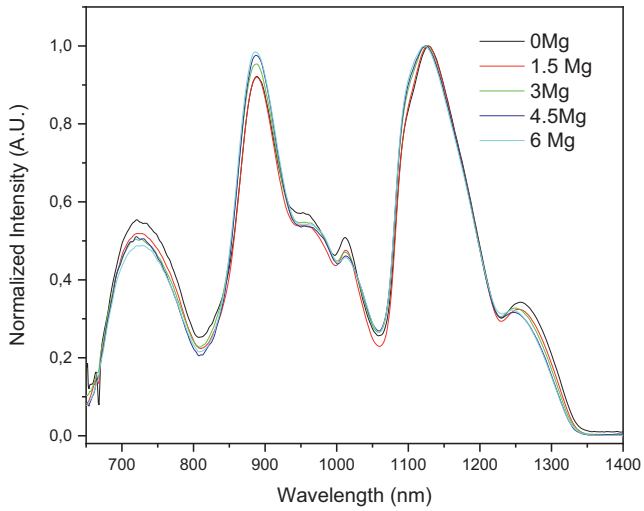

Figure 18. Normalized IR spectra of the investigated glasses (unpublished data)

Because of the changes in the glass structure, the increase in MgO was found to have also an impact on the crystallization tendency of the glass; it reduces the crystallization tendency of the glasses. The glasses were heat treated as in section 4.1.2 and their XRD patterns were measured. As shown in Figure 19, the pattern depicts peaks related to CaF_2 crystals. However, the XRD pattern of the glasses with MgO content larger than 3 mol % exhibit additional peaks which can be related to $NaPO_3$ (ICDD PDF#04-011-3120) and $Na_2Ca_2P_2O_7F_2$ (ICDD PDF#04-012-1844). An increase in the MgO content favors the precipitation of $NaPO_3$ and $Na_2Ca_2P_2O_7F_2$ at the expense of CaF_2.

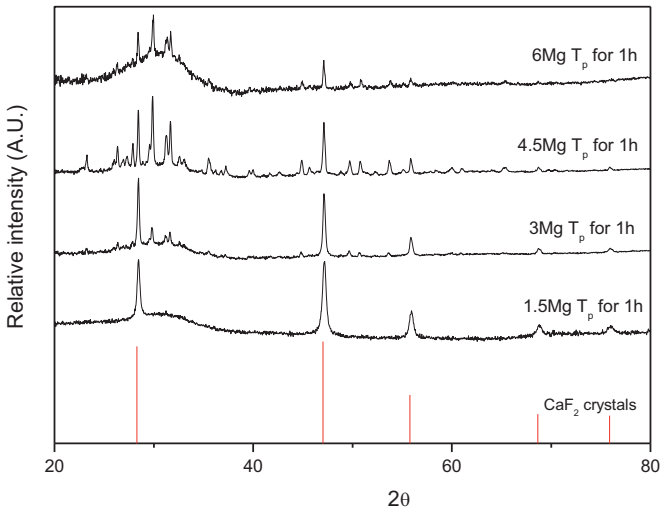

Figure 19. XRD patterns of the Mg glasses after heat treatment T_g+20°C for 17h and at T_p for 1 hour (unpublished data)

All glasses exhibit similar upconversion under 975 nm pumping, the intensity of which increases after heat treatment confirming the presence of Er^{3+} ions in the CaF_2 crystals in the glasses (not shown here). The glass with 3 mol % of MgO exhibits a stronger upconversion than the other MgO containing glasses which remains however slightly lower than that of the Mg free glass. Indeed, a lower amount of CaF_2 crystals are expected to precipitate when adding MgO in the glass network.

In summary, it was shown that the crystals growth rate can be tailored by modifying slightly the glass composition without changing the precipitation of Er^{3+} doped CaF_2 crystals in the volume of the glass during heat treatment. From the nucleation like curve of the investigated glasses, it can be concluded that the formation of nuclei occurs at higher temperature while being less dependent on the temperature when adding ions with strong field strength in the phosphate network such as Ti and Mg for example. It was clearly shown that the heat treatment of the newly developed glasses using tailored temperature and duration can be used for the fabrication of transparent GCs with small crystal size distribution. Due to their thermal stability against crystallization, the newly developed MgO glasses are promising materials to be drawn into glass-ceramic fibers.

4.2 Crystals containing glass

As it is not possible to predict and control the volume precipitation of RE doped crystals in a glass during heat treatment, RE doped crystals containing glasses were also prepared using the direct doping method. In this process, the RE doped crystals are added in the glass melt after the melting at a specific temperature (doping parameter labeled as doping temperature (T_{doping})). The glass is quenched few minutes after adding the crystals (doping parameter labeled as dwell time). As explained in [80], it is crucial to determine the best doping parameters to limit the decomposition of the crystals in the glass melt. Therefore, the first task was to define a protocol for the optimization of the direct doping process and to study the corrosive nature of the glass to limit the decomposition of the crystals occurring during the preparation of the glass. Then, it is explained how glasses can be prepared with $NaYF_4$: Er^{3+}, Yb^{3+}nanocrystals, known to be one of the best upconverter crystals [101]. Finally, as metallic Ag nanoparticles are known to enhance the upconversion properties of Er^{3+} doped glasses[40,41], glasses were prepared with Ag nanoparticles and $NaYF_4$: Er^{3+}, Yb^{3+} nanocrystals in order to prepare a glass with strong upconversion.

4.2.1 Optimization of the direct doping process

As explained in [80], it is crucial to optimize the T_{doping} and dwell time in order to minimize the decomposition of the crystals during the glass preparation. If the T_{doping} is too high and/or the dwell time too long, the decomposition of the crystals could occur. However, if the T_{doping} is too low, the viscosity of the glass melt would be too high limiting the dispersion of the crystals in the glass melt and thus leading to the formation of agglomerates of crystals. Poor dispersion of the crystals could also be observed when using a short well time. Due to their micrometer size and their visible persistent luminescence (PeL) after UV charging, commercial PeL microparticles were used for the optimization of the process.

The first step of the study was to define a protocol to use when optimizing the direct doping process. The $50P_2O_5$-$10Na_2O$-40SrO (mol %) glass (labeled as SrNaP) was chosen as it is a thermally stable glass [102]. This glass has been intensively studied in the Photonic Glasses group at Tampere University.

After melting the glass at 1050 °C, the temperature of the furnace was decreased to 975, 1000 and 1025 °C before adding 1 weight-% of Eu^{2+}, Dy^{3+}-doped $SrAl_2O_4$ microparticles (MPs) in the glass melt. The glasses were quenched 3 to 10 minutes after

adding the particles. After quenching, the glasses were annealed at 400 °C, which is about 40 °C below the glass transition temperature, for 4h in air. The samples are labeled as (T_{doping} – dwell time).
Figure 20 shows the picture of the glasses taken after stopping the UV irradiation.

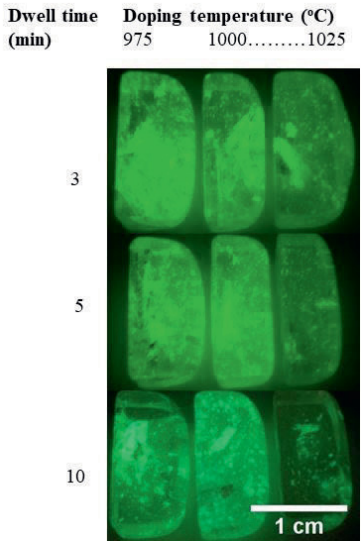

Figure 20. Pictures of the investigated SrNaP glasses after stopping the UV irradiation (Publication I)

All the investigated glasses exhibit green persistent luminescence after stopping the UV irradiation confirming the survival of the MPs in the glasses. A decrease in the intensity of the PeL with an increase in the T_{doping} and dwell time can be seen as result of the decomposition of the MPs occurred during the glass preparation. The changes of the PeL intensity as a function of the doping parameters were confirmed when measuring the PeL spectra of the glasses (spectra can be found in Publication I). Aggregated MPs can be seen in the glasses, the size and number of which increase with a decrease in the T_{doping} and dwell time.

A Java-based image processing program ImageJ was used to quantify and compare the standard deviation (StdDev) of the pixel intensity from the pictures of the glasses which could give an information about the dispersion of the MPs in the glasses (Figure 20); high StdDev indicates a large variation in the emission intensity within the glass and thus can be related to aggregated MPs. The data obtained are summarized in Table 7.

Melting condition		Sample code (T-t)	SdtDev
Dwell time (t)	T_{doping} (°C)		
3min	975	975-3	10
	1000	1000-3	11
	1025	1025-3	9
5min	975	975-5	10
	1000	1000-5	8
	1025	1025-5	6
10min	975	975-10	20
	1000	1000-10	12
	1025	1025-10	11

Table 7. Standard deviation of the pixel intensity of the glass pictures at different melting condition using ImageJ software (Publication I)

A smaller StdDev was measured in the glasses prepared with a 5 min dwell time indicating that the dispersion of the MPs is insufficient if the dwell time is too short (3 min) as suggested in ref [80]. However, a longer dwell time (>5 min) leads to the corrosion of the MPs as suspected from the light green emission of the glasses prepared using a 10 min dwell time (Figure 20).

The corrosion of MPs was confirmed by analyzing the morphology and composition of the MPs using SEM/EDS. The SEM image of a MP found at the surface of the different glasses are shown in Figure 21.

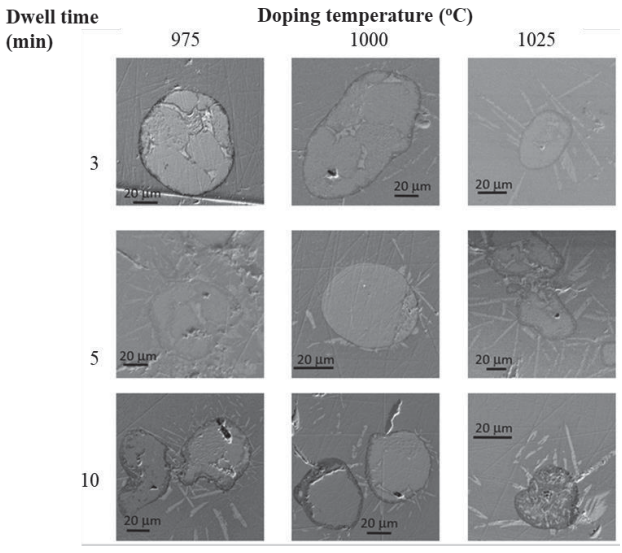

Figure 21. SEM picture of a MPs found on the surface of the glasses prepared using different T_{doping} and dwell time. (Publication I)

The average size of the particle was found to be between 50-150 μm. An increase in the T_{doping} and dwell time reduces the size the MPs which is a clear sign of corrosion. The corrosive behavior of this glass melt on the MPs was confirmed by tracking the reduction in the diameter of an alumina rod immersed in glass melts at different temperatures (see Publication I).

The morphology of the MPs in the (1025-10) glass also looks different compared to the morphology of the other MPs. Therefore, the composition of the MPs was analyzed using EDS. The SEM images and line profiles showing the elemental distribution along the diameter of a MP found at the surface of the 975-3, 1000-5 and 1025-10 glasses are shown in Figure 22.

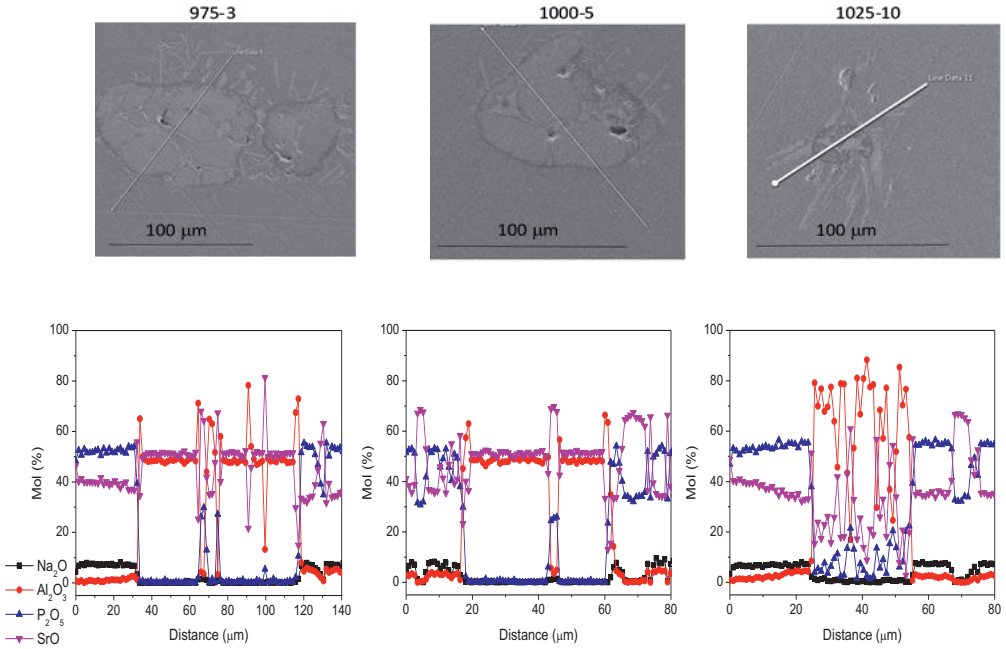

Figure 22. SEM/EDS line profiles giving the elemental distribution along the diameter of a microparticle in 975-3, 1000-5 and 1025-10 glasses (Publication I)

The composition of the glass matrix is in accordance with the theoretical one within the accuracy of the measurements (±1.5 mol %). As compared to the MP found at the surface of the 1025-10 glass, the composition of the MPs found in the (975-3) and (1000-5) glasses is $SrAl_2O_4$ indicating that the MPs embedded in these glasses maintain their compositional integrity in their center. One should point out that Al was detected in the glass at the glass - MP interface indicating that during the glass melting, elements from the MP diffuse in the glass confirming the decomposition of the MPs during the

glass preparation. It was clearly shown that SEM coupled with EDS can be used to check if decomposition of the MPs occurred during the glass preparation.

The decomposition of the MPs can also be tracked from the changes in the spectroscopic properties of the glasses. Figure 23 depicts the normalized conventional luminescence spectra of the glasses prepared using a 5 min dwell time and different T_{doping}.

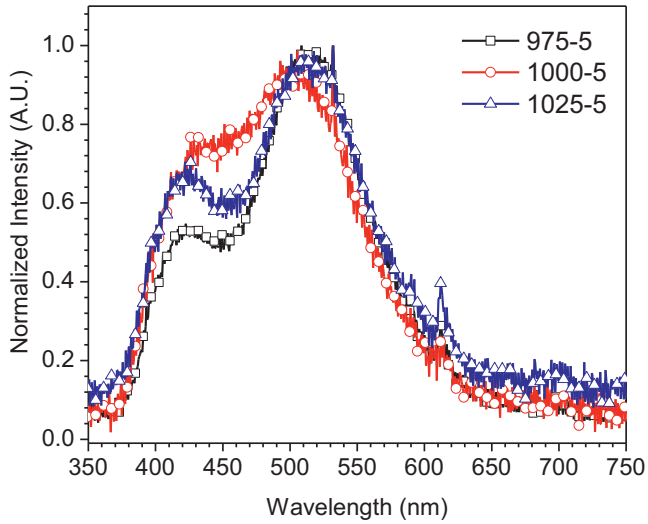

Figure 23. Normalized conventional luminescence (CL) spectra of the glasses prepared using (T_{doping}-5) parameters. The peak at 532 nm is a harmonic of the 266 nm excitation (Modified from Publication I)

The normalized CL spectra exhibit 2 bands at 410 and 490 nm which can be related to the emission from Eu^{2+} located in two different cation sites in the $SrAl_2O_4$ structure according to [103]. The intensity of the band at 410 nm increases as compared to the band at 490 nm when the T_{doping} increases. Same was observed when increasing the dwell time from 3 to 10 min (PeL and CL spectra can be found in Publication I). These changes in the CL spectra indicate changes in the Eu^{2+} environment due to the decomposition of the MP. Indeed, the structure of the corroded MPs is expected to change after embedding the MPs in the glass due to the diffusion of Al and Sr to the glass. As a consequence, the decomposition of the MPs leads to new sites for Eu^{2+} ions, thus changing the crystal field around Eu^{2+}[104].

Bands at 590, 610 and 680 nm can also be seen in the spectra and can be related to the emission from Eu^{3+} indicating that some Eu^{2+} ions oxidized to Eu^{3+} ions which is also a clear sign of the decomposition of the MPs. An increase in the dwell time and in the

T_{doping} temperature was found to increase the intensity of these emission bands confirming the oxidation of Eu^{2+} into Eu^{3+} in agreement with the decrease in the PeL seen in Figure 20.

With this study (Publication I), it was clearly shown that PeL MPs can be used to optimize the direct doping process as the decrease in the PeL can be related to the decomposition of the MPs. Therefore, the doping parameters were chosen by comparing the intensity of the PeL and also the homogeneous dispersion of the MPs in the glass. For example, particles containing SrNaP glass should be prepared using a 1000 °C doping temperature and 5 min dwell time to limit the decomposition of the MPs during the glass preparation.

The impact of various glass melts on the decomposition of the MPs occurring during the glass preparation was further investigated. Phosphate glasses with the following compositions were investigated

- 50 P_2O_5 - 10 Na_2O - 40 CaO/SrO (in mol %) (labeled as CaNaP and SrNaP),
- (90 $NaPO_3$ - (10 − x) Na_2O -x NaF) (in mol %) (labeled as NaPF0 (x = 0) and NaPF10 (x = 10))

The direct doping parameters were determined using 1 wgt % of the commercial $Sr_4Al_{14}O_{25}:Eu^{2+}$, Dy^{3+} microparticles (MPs) using the defined protocol and are listed in the table 8.

Glass	Melting temperature (°C)	Doping temperature (°C)	Dwell time (min)
CaNaP	1100	1025	5
SrNaP	1050	1000	5
NaPF0	750	550	3
NaPF10	750	550	3

Table 8. Direct doping parameters used for glass preparation (Publication II)

The pictures of the MPs-containing glasses after stopping UV irradiation are shown in Figure 24. All the glasses exhibit a blue-green PeL the intensity of which depends on the glass composition: intense PeL can be seen from the SrNaP and NaPF0 glasses while almost no PeL could be seen from the NaPF10 glass.

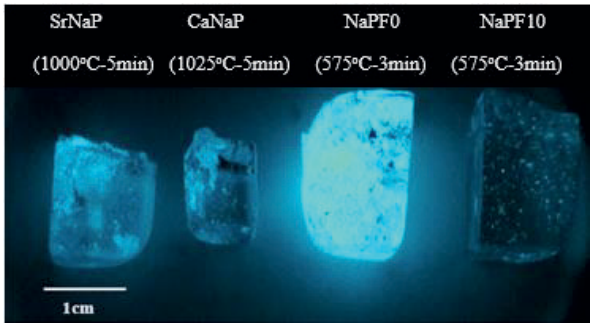

Figure 24. Pictures of the investigated PeL glass-ceramics with the different compositions, taken just after stopping the UV irradiation (Publication II)

Based on the intensity of the PeL from the glasses, the MPs are expected to be the most corroded in the NaFP10 glass and the least corroded in the NaPF0 showing that the decomposition of the MPs in the glass melt depends not only on the doping parameters but also on composition of the glass. Therefore, it was clearly shown that the direct doping method should be optimized when preparing new particles containing glasses.

4.2.2 $NaYF_4:Er^{3+}$, Yb^{3+} nanocrystals containing glass

As the evaporation of the $NaYF_4$: Er^{3+}, Yb^{3+} crystals and melting of NaF occur at 750 °C, the doping temperature should be lower than 750°C when adding these crystals in a glass melt [84]. Effort was focused on identifying a glass composition with a low melting temperature in order to successfully prepare $NaYF_4$: Er^{3+}, Yb^{3+} nanocrystals containing glass.

Due to their low melting and doping temperatures (see Table 8), the NaPF0 and NaPF10 glasses were chosen for the preparation of the $NaYF_4:Er^{3+}$, Yb^{3+} nanocrystals containing glasses. A complete characterization of the thermal, physical, optical and structural properties of glasses within the (90 $NaPO_3$ -(10 - x) Na_2O-x NaF) (mol %) system can be found in Publication III. The main important results are about the thermal properties of the glasses: a decrease in the thermal properties was noticed with the progressive replacement of Na_2O by NaF due to an increase in the network connectivity with the formation of the P-F bonds.

Due to the strong visible green emission from the $NaYF_4:Er^{3+}$, Yb^{3+} nanocrystals under 975 nm excitation, the direct doping process could be optimized as explained in section 4.2.1 using the $NaYF_4:Er^{3+}$, Yb^{3+} nanocrystals: the NaPF0 and NaPF10 glasses were prepared by adding 5 wgt % of $NaYF_4:Er^{3+}$, Yb^{3+} nanocrystals at T_{doping} varying

from 525 to 575 °C. The glasses were quenched after 3 and 5 min after adding the nanocrystals. The samples are labeled as (T_{doping} – dwell time).

The pictures of the glasses in daylight and under 975 nm excitation are presented in Figure 25.

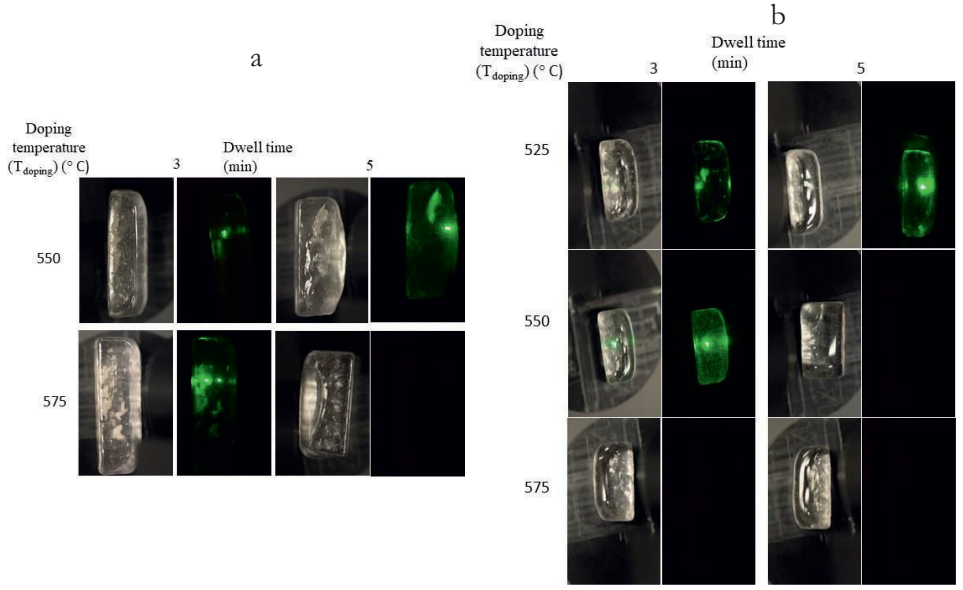

Figure 25. Pictures of the $NaYF_4:Er^{3+}$, Yb^{3+} nanocrystals-containing NaPF0 (a) and NaPF10 (b) glasses in daylight and under pumping at 975 nm. The glasses were prepared using different doping temperatures and dwell times (Publication III)

Depending on their doping parameters, some glasses exhibit green emission under 975 nm excitation confirming the survival of the $NaYF_4:Er^{3+}$, Yb^{3+} nanocrystals in the glasses. Even though green emission could be seen from the (575-3) NaPF0 glass, no green emission could be seen from the NaPF10 glass prepared using the same T_{doping} of 575 °C. T_{doping} was reduced to 550 °C in order to observe the green emission from the NaPF10 glass. The decrease in the T_{doping} from 575 to 550 °C when increasing the NaF content agrees with the different thermal properties of the glasses.

No agglomerates were seen with naked eyes in the (550-3) NaPF10 glass which exhibits strong and uniform upconversion. One should mention that we were not able to prepare NaFP0 glass with no agglomerate of the crystals.

The upconversion spectra of the investigated glasses are shown in Figure 26.

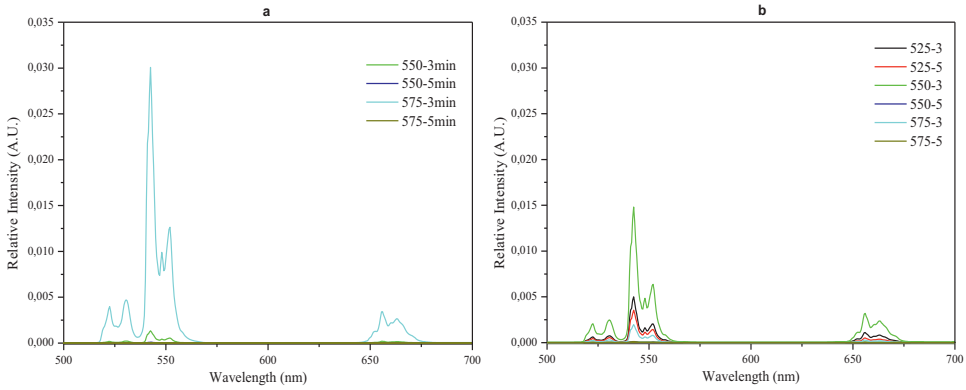

Figure 26. Upconversion spectra of the $NaYF_4:Er^{3+},Yb^{3+}$ nanocrystals in NaPF0 (a) and NaPF10 (b) glasses using a 975 nm excitation (modified from Publication III)

Green and red emissions are seen from the glasses and are due to the following transitions of Er^{3+} ions : $^2H_{11/2} - {}^4I_{15/2}$; $^4S_{3/2} - {}^4I_{15/2}$ and $^4F_{9/2} - {}^4I_{15/2}$ respectively as reported in ref [105]. Distinct fine structure can be also seen which is a characteristic of Er^{3+} ions coordinated in crystalline sites confirming the survival of $NaYF_4:Er^{3+},Yb^{3+}$ nanocrystals during the glass preparation. One should be careful when comparing the intensity of the emission as some glasses contain large agglomerate of the nanocrystals which leads to green and red emission with high intensity.

The intensity of the red emission decreases as compared to the green emission when the T_{doping} and dwell time were increased as depicted in Figure 27. As seen for the PeL MPs, changes in the spectroscopic properties of the nanocrystals might indicate changes in the site of the RE ions in the nanocrystals. Thus, the changes in the intensity of the red emission as compared to the green emission can be related to the decomposition of the nanocrystals during the glass melting with the diffusion of Er^{3+} from the nanocrystals to the glass and/or to an increase of the amount of the cubic phase.

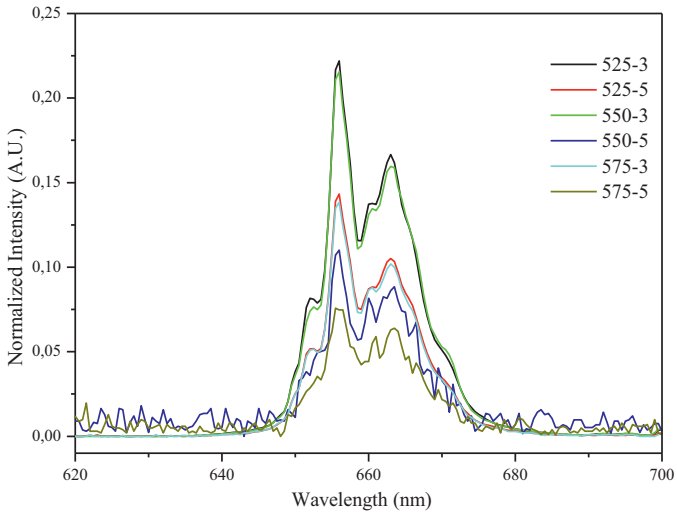

Figure 27. Red emission band when the upconversion spectra of the $NaYF_4:Er^{3+}$, Yb^{3+} nanocrystals-containing NaPF10 glasses are normalized to the green emission. The spectra were collected using a 975 nm excitation (Publication III)

One should mention that, due to the low amount of nanocrystals in the glass, no agglomerates of nanocrystals could be seen in the glasses with a SEM to confirm the decomposition of the nanocrystals nor peaks in the XRD pattern of the glass to confirm the changes in the crystalline phase. Nonetheless, the presence of the nanocrystals in the glasses was confirmed from the measurement of the emission centered at 1.5 μm under 975 nm excitation. As depicted in Figure 28, the spectra of the (975-3) NaFP0 and NaFP10 glasses exhibit an emission band of Er^{3+} ions which is due to the transition $^4I_{13/2}$- $^4I_{15/2}$. This band is different from the emission band of the nanocrystals indicating that the Er^{3+} ions are located in different sites after embedding the nanocrystals in the glass. The emission band is typical of the emission from Er^{3+} ions located in an amorphous network indicating that most of the Er^{3+} ions are located in the glass matrices. However, the emission band of the glasses also depicts a small peak at ~1510 nm which can be also seen in the emission band from the nanocrystals. Therefore, the emission band from the glasses is thought to be an overlay of the emission of Er^{3+} ions located in the nanocrystals and in the glass matrix.

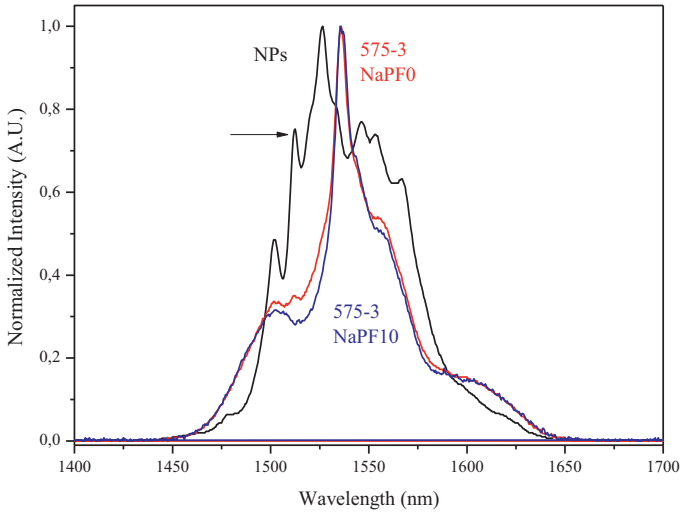

Figure 28. Normalized emission spectrum of the $NaYF_4:Er^{3+}$, Yb^{3+} nanocrystals compared to 575-3 NaPF0 and NaPF10 glasses(Publication III)

The promising (975-3) NaPF10 glass was drawn into an uncoated single core fiber with a diameter of ~200 μm in collaboration with Rennes University (France). The composition of the fiber was checked using SEM coupled with EDS and was found to be similar than that of the preform. A decrease in T_x and T_p was noticed after drawing probably due to a decrease in the network connectivity after the drawing process as evidenced from the changes in the IR spectra after drawing process (not shown here). A slight reduction in the number of Q^2 units and probably reorientation of the P-O-P bonds are expected to occur during the drawing process due to severe quenching occurring during the fiber drawing [106]. Similar changes in the thermal and structural properties of phosphate glasses after drawing were reported in [107]. As the glass is hygroscopic, the fiber degraded rapidly as shown in Figure 29a leading to a fragile fiber and so making the characterization of the fiber's spectroscopic properties difficult. Nonetheless, we have been able to measure the transmittance spectrum of a 1.2 cm long fiber which shows an absorption band at ~1 μm with low intensity (Figure 29b). Although the 1.2 cm long fiber exhibits a broad emission band due to the transition from $^4I_{13/2}$ to $^4I_{15/2}$ state of Er^{3+} ions (Figure 29c), no upconversion could be detected from the fiber. The absence of upconversion could be due to water absorption, inhomogeneous distribution of the nanocrystals in the fiber but also to the decomposition of the nanocrystals during the fiber drawing.

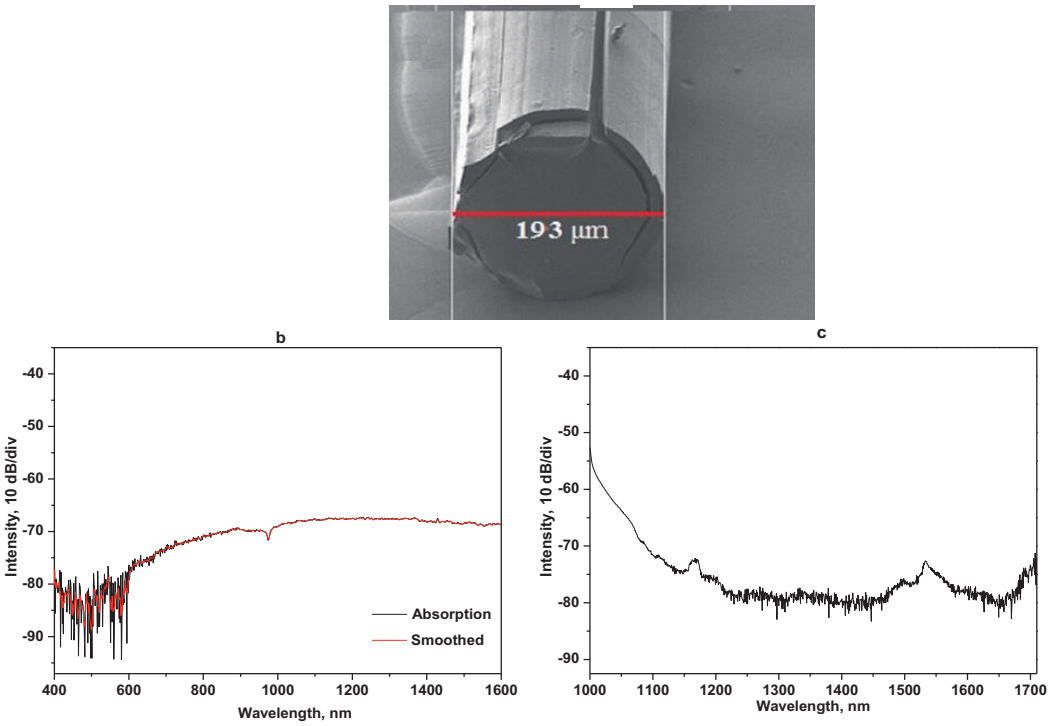

Figure 29. Figure: SEM image of the cross-section of the fiber (a). Transmittance (b) and emission (c) spectra of the fiber (1.2 cm long). The emission spectra were measured 975 nm excitation (unpublished data)

4.2.3 Ag nanoparticles in $NaYF_4:Er^{3+}$, Yb^{3+} nanocrystals containing glass

Effort was focused on developing new $NaYF_4:Er^{3+}$, Yb^{3+} nanocrystals containing glass with stronger upconversion in order to check if the nanocrystals survive the drawing process. It is well known that Ag nanoparticles (NPs) can be used to increase the intensity of the upconversion using 975 nm excitation [40]. In a recent study from the Photonic glasses group at Tampere University [44], ZnO and Ag_2SO_4, used as the precursor for the Ag NPs, were added the NaPF10 glass. Zn was found to depolymerize the glass network and thus to promote the clustering of silver ions during heat treatment at ~T_g for few hours.

Based on this promising result, $NaYF_4$: Er^{3+}, Yb^{3+} nanocrystals were added at 550 °C in the glass with the composition 83.25 $NaPO_3$ - 9.25 NaF – 5 ZnO - 2.5 Ag_2O (in mol %) (labeled as 2.5Ag) and the glass was quenched 3 min after adding the nanocrystals. As for the NaPF10 glass, no visible agglomerates of the nanocrystals could be seen in the glass and the 2.5Ag glass exhibits green and red emission when pumped at 975 nm as shown in Figure 30 confirming the survival of the $NaYF_4$: Er^{3+}, Yb^{3+} nanocrystals in this new glass.

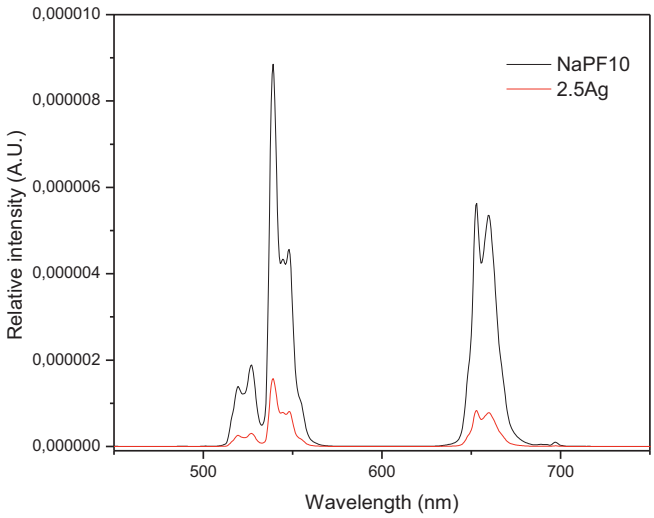

Figure 30. Upconversion spectra of NaPF10 and 2.5 Ag glasses (λ_{exc} = 975 nm) (Publication IV)

One should mention that the glass exhibits a yellowish color after quenching. Based on the absorption spectrum of the glass (Figure 31), the yellow color can be related to the presence of an absorption band at 430 nm which is thought to be the SPR band of silver nanoparticles [46]. The presence of the Ag nanoparticles was confirmed from the emission properties of the 2.5Ag glass. Upon 320 nm excitation, the glass exhibits a broad emission band which is an overlap of bands located at ~480 nm, ~540 nm and ~620 nm. These bands can be related to Ag^+ species, Ag^+ - Ag^+ species and Ag_3^{2+} species, respectively [108,109].

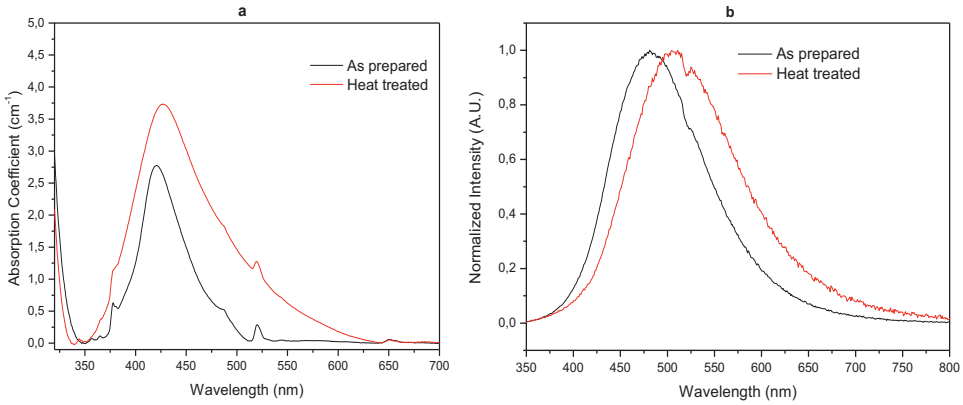

Figure 31. Absorption spectrum of the 2.5Ag glass a) and emission spectrum of the 2.5Ag glass prior to and after heat treatment at (T_g+10°C) for 4hours (λ_{exc} = 320 nm) b) (Publication IV)

One should point out that the nanocrystals free 2.5Ag glasses were melted /quenched at 875 °C and also melted at 875 °C /quenched at 550 °C to simulate the direct doping process. Both glasses are colorless indicating that the Ag NPs do not form in the crystals containing glass due to the low quenching temperature. As the precipitation of the Ag NPs is thought to be due to the nanocrystals, glasses were prepared with different amount of $NaYF_4$: Er^{3+}, Yb^{3+} nanocrystals. All the glasses exhibit similar yellow color and similar absorption band at 430 nm, the intensity of which increases with an increase in the amount of the nanocrystals. It is possible that it is the decomposition of the nanocrystals occurring during the glass melting which leads to the precipitation of the Ag NPs. Indeed, the elements from the nanocrystals (Na, Y, F, Er and Yb) are suspected to diffuse into the glass due to the decomposition of the nanocrystals as discussed earlier. These elements are expected to have a catalyst role on the formation of Ag nanoparticles as reported in [110–112]. The reduction of the Ag^+ ions can also be due to the presence of NBOs in the glass network as suggested by Pontuschka et. al. [113].

As depicted in Figure 30, the intensity of the upconversion from the 2.5Ag glass is lower than from the NaPF10 glass probably due to the energy transfer from the exited states of Er^{3+} to the silver NPs as reported in [44]. It is also possible that a lower amount of the $NaYF_4$: Er^{3+}, Yb^{3+} nanocrystals survive the melting process of the 2.5Ag glass due to the different corrosive behavior of the 2.5Ag glass melt on the nanocrystals.

As performed in [44,114], the 2.5Ag glass was heat treated for 4h at (T_g + 10 °C) in order to grow Ag NPs. After heat treatment, the number of Ag NPs increases and the NPs increase in size as evidenced by an increase in the intensity and in the bandwidth of the absorption band at 430 nm which also shifts to longer wavelength (Figure 31a)[115]. As shown in Figure 31b, the emission band shifts to longer wavelength after

heat treatment confirming the formation of molecule-like Ag nanoclusters (ML-Ag NCs) with large sizes after heat treatment. Migration of the Ag species to the surface forming a layer of Ag species of ~2 μm at the surface of the glass was found to also occur during the heat treatment (SEM images and concentration profile of Ag from surface to volume can be found in Publication IV).

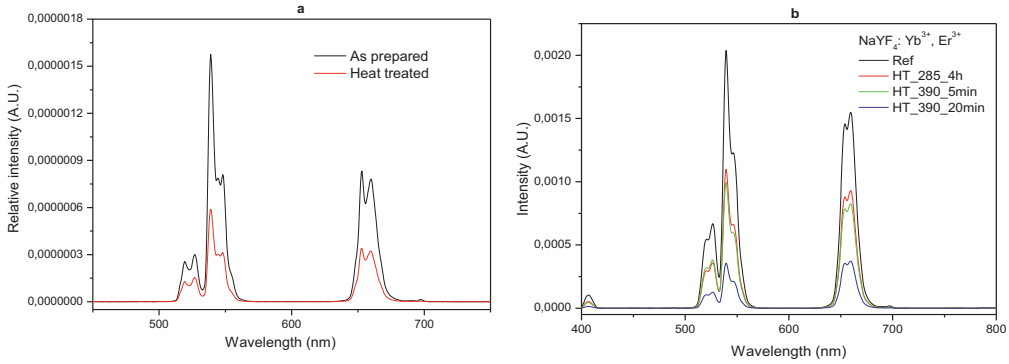

Figure 32. Upconversion spectra of the 2.5Ag glass prior to and after heat treatment at (T_g + 10 °C) for 4 hours.a) and of the nanocrystals alone prior to and after heat treatment at different temperatures and durations b) (λ_{exc} = 975 nm) (Publication IV)

As shown in Figure 32a, the heat treatment also leads to a decrease in the intensity of the upconversion probably due to the energy transfer from the exited states of Er^{3+} to the silver NPs as discussed earlier. The decrease of the upconversion intensity after heat treatment can also be related to the heat treatment itself as shown in Figure 32b: an increase in the temperature and duration of the heat treatment reduces the intensity of the upconversion of the nanocrystals alone due to the thermal activation of the deleterious thermal phonons from host lattice, internal/surface crystalline defects and surface chemical bonds as reported in [116].

In summary, NaPF10 glass was successfully prepared with strong and uniform upconversion by adding $NaYF_4$:Er^{3+}, Yb^{3+} nanocrystals in the glass melt at 550 °C. To ensure the survival and good dispersion of the nanocrystals in the glass, the glass should be quenched 3 minutes after adding the nanocrystals. The decomposition of the $NaYF_4$:Er^{3+}, Yb^{3+} nanocrystals during the glass preparation can be tracked from the changes in the red to green upconversion intensity, in the shape of the emission band centered at 1.5 μm and also in the transmittance properties of the glasses (spectra can be found in Publication III). $NaYF_4$: Er^{3+}, Yb^{3+} nanocrystals containing glass was also prepared with Ag NPs. However, no increase in the intensity of the upconversion was observed after heat treatment probably due to the energy transfer from the exited states of Er^{3+} to the silver NPs and also to an increase of the inter defects in the $NaYF_4$: Er^{3+},

Yb^{3+} nanocrystals occurring during the heat treatment. Glasses with lower amount of Ag_2O could be prepared to limit the energy transfer and so to possibly increase the intensity of the upconversion. With this study, it was clearly shown that a large variety of new glasses can be prepared by adding different nanocrystals with different chemical compositions using the direct doping method.

5 CONCLUSION

This thesis aimed at developing novel phosphate glass-based materials (glass-ceramics and crystals containing glass) with improved spectroscopic properties as compared to the parent glasses due to the presence of Er^{3+} doped crystals in the volume of these glass-based materials. With this work, the research questions are clearly answered as glass-ceramics were prepared using heat treatment and the crystals containing glasses using the direct doping method.

- ***Questions related to the topic on glass-ceramic:*** *is it possible 1) to improve the thermal stability of a glass by modifying slightly its composition without modifying its nucleation and growth mechanism and 2) to tailor the transparency of the glass-ceramic using optimized heat treatment parameters?*

New phosphate glasses in the $NaPO_3$ - CaF_2 system were prepared and heat treated in order to prepare transparent glass-ceramics. The impact of the changes in the glass composition on the physical, thermal, structural and optical properties was investigated as well as the nucleation and growth properties of these novel phosphate glasses. Their crystallization parameters, especially the crystal growth rate and maximum nucleation temperature, were determined.

It was demonstrated that it is possible to modify the glass composition to increase the thermal stability of the glass while maintaining the bulk precipitation of Er^{3+} doped CaF_2 crystals by adding a low amount (1.5 mol %) of TiO_2, ZnO or MgO. The addition of TiO_2, ZnO or MgO was found to increase slightly the thermal properties of the glasses while depolymerizing the network with the formation P-O-Ti/Mg/Zn bonds at the expense of P-O-P bonds. The activation energy for crystallization of these glasses were determined using two methods confirming that the crystallization process was a nucleation and growth process in all the glasses. All glasses possess similar JMA exponent measured at ~2 indicating bulk crystallization of needle like crystals as confirmed using SEM. From the large temperature difference between T_g and $T_{n\ max}$ of the glasses, it was demonstrated that the size and size distribution of the crystals can be controlled during heat treatment which is crucial for the preparation of transparent glass-ceramics. The MgO containing glass was found to be the most promising glass: a

glass was prepared with 3 mol % of MgO and exhibit a ΔT of ~90 °C and also the volume precipitation of Er doped CaF_2 crystals.

- ***Questions related to addition of crystals in glasses:*** *how can the survival and dispersion of the crystals be balanced to prepare crystals containing glasses using the direct doping method? Is it possible to prepare glasses containing $NaYF_4$: Er^{3+}, Yb^{3+} crystals with strong upconversion using this method knowing that $NaYF_4$: Er^{3+}, Yb^{3+} crystals decompose at 750°C? Can Ag nanoparticles be used to enhance the upconversion properties from the glasses containing $NaYF_4$: Er^{3+}, Yb^{3+} crystals?*

Glasses containing $NaYF_4$: Er^{3+}, Yb^{3+} nanocrystals were successfully prepared using the direct doping method. Due to the low decomposition temperature of the nanocrystals, effort was focused on developing new glasses with low melting temperature to ensure the survival of the nanocrystals when added in the glass melt. Glasses in the $NaPO_3$ - Na_2O / NaF system were found to be promising glasses due to their melting temperature at 750 °C. The protocol to optimize the direct doping process was defined using microparticles with persistent luminescence (PeL). Glasses were prepared using different doping parameters (T_{doping} and dwell time) and the losses in their PeL were related to the decomposition of the PeL microparticles which was confirmed from the spectroscopic properties of the glasses and also from the composition analysis of the microparticles found at the surface of the glasses. The corrosive behavior of the glass melt on nanocrystals was also confirmed by melting PeL phosphate glasses with different compositions. Using optimized doping parameters, $NaYF_4$: Er^{3+}, Yb^{3+} nanocrystals were successfully added in the phosphate glass with the composition 90 $NaPO_3$ – 10 NaF (in mol %). These glasses containing nanocrystals exhibits strong and homogeneous upconversion when pumped at 975 nm. Ag_2O was added in the glass to further enhance the intensity of the upconversion after heat treatment which is used for the precipitation of Ag nanoparticles. However, no increase in the intensity of the upconversion was observed after heat treatment probably due to energy transfer from the exited states of Er^{3+} to the silver NPs and also to an increase in the inter defects in the $NaYF_4$: Er^{3+}, Yb^{3+} nanocrystals occurring during the heat treatment.

Overall, this thesis led to a better understanding of the composition-structure-property relationships, nucleation and growth process and the direct doping method and so to the development of new glass-ceramics and crystals containing glasses with strong upconversion under 975 nm pumping. Results from this work were published in 5 publications (including 2 being under review).

One recommendation to continue the work is to draw fibers from these novel glass-based materials due to their excellent upconversion properties. Glass-ceramics fibers could be prepared from the MgO glass and the crystals containing fiber drawn from the $NaYF_4$: Er^{3+}, Yb^{3+} nanocrystals containing glass with the composition 90 $NaPO_3$ – 10 NaF. However, when preparing glass fibers which contain crystals, it will be crucial to work on the transparency of the fiber to minimize the light scattering. Consequently, the size of the crystals in the fiber should be controlled, the distance between the crystals should be comparable to their size and the distribution of the particle size distribution should be narrow. Additionally, the crystals should be also well dispersed in the glass without forming clusters. In the case of glass-ceramic fiber, the crystals could be precipitated in the glass before, after, or even during the fiber drawing step. However, one should keep in mind that the drawing process can lead to devitrification of the glass, transformation of the crystalline phases, and dissolution of the crystals. Therefore, it might easier to heat treat the glass after the heat treatment to better control the nucleation and growth of the crystals. It will be crucial to investigate the impact of the drawing process on the survival of the $NaYF_4$: Er^{3+}, Yb^{3+} crystals in the fibers.

REFERENCE

[1] C.B. Carter, M.G. Norton, Ceramic materials: Science and engineering, 2013. https://doi.org/10.1007/978-1-4614-3523-5.

[2] J.A. Wilder, J.E. Shelby, Property Variation in Alkali Alkaline-Earth Metaphosphate Glasses, J. Am. Ceram. Soc. 67 (1984) 438–444. https://doi.org/10.1111/j.1151-2916.1984.tb19732.x.

[3] D.B. Keck, R.D. Maurer, P.C. Schultz, On the ultimate lower limit of attenuation in glass optical waveguides, Appl. Phys. Lett. 22 (1973) 307–309. https://doi.org/10.1063/1.1654649.

[4] M. Yamane, Y. Asahara, Glasses for Photonics, Cambridge University Press: Cambridge, 2000.

[5] W.H. Zachariasen, The atomic arrangement in glass, J. Am. Chem. Soc. 54 (1932) 3841–3851. https://doi.org/10.1021/ja01349a006.

[6] D. Ehrt, W. Seeber, Glass for high performance optics and laser technology, J. Non. Cryst. Solids. 129 (1991) 19–30. https://doi.org/https://doi.org/10.1016/0022-3093(91)90076-I.

[7] T. Minamf, J.D. Mackenzie, Thermal Expansion and Chemical Durability of Phosphate Glasses, J. Am. Ceram. Soc. 60 (1977) 232–235. https://doi.org/10.1111/j.1151-2916.1977.tb14113.x.

[8] T. Töpfer, J. Hein, J. Philipps, D. Ehrt, R. Sauerbrey, Tailoring the nonlinear refractive index of fluoride-phosphate glasses for laser applications, Appl. Phys. B. 71 (2000) 203–206. https://doi.org/10.1007/s003400000240.

[9] J.H. Campbell, T.I. Suratwala, Nd-doped phosphate glasses for high-energy/high-peak-power lasers, J. Non. Cryst. Solids. 263–264 (2000) 318–341. https://doi.org/https://doi.org/10.1016/S0022-3093(99)00645-6.

[10] V.P. Gapontsev, S.M. Matitsin, A.A. Isineev, V.B. Kravchenko, Erbium glass lasers and their applications, Opt. Laser Technol. 14 (1982) 189–196. https://doi.org/https://doi.org/10.1016/0030-3992(82)90095-0.

[11] S. Jiang, M. Myers, N. Peyghambarian, Er^{3+} doped phosphate glasses and lasers, J. Non. Cryst. Solids. 239 (1998) 143–148. https://doi.org/https://doi.org/10.1016/S0022-3093(98)00757-1.

[12] D. Pugliese, N.G. Boetti, J. Lousteau, E. Ceci-Ginistrelli, E. Bertone, F. Geobaldo, D. Milanese, Concentration quenching in an Er-doped phosphate glass for compact optical lasers and amplifiers, J. Alloys Compd. 657 (2016) 678–683. https://doi.org/https://doi.org/10.1016/j.jallcom.2015.10.126.

[13] N.G. Boetti, D. Pugliese, E. Ceci-Ginistrelli, J. Lousteau, D. Janner, D. Milanese, Highly Doped Phosphate Glass Fibers for Compact Lasers and Amplifiers: A Review, Appl. Sci. 7 (2017). https://doi.org/10.3390/app7121295.

[14] R.J. Amjad, M.R. Sahar, S.K. Ghoshal, M.R. Dousti, S. Riaz, B.A. Tahir, Enhanced infrared to visible upconversion emission in Er^{3+} doped phosphate glass: Role of silver nanoparticles, J. Lumin. 132 (2012) 2714–2718. https://doi.org/https://doi.org/10.1016/j.jlumin.2012.05.008.

[15] S.E. Stokowski, W.E. Martin, S.M. Yarema, Optical and lasing properties of fluorophosphate glass, J. Non. Cryst. Solids. 40 (1980) 481–487. https://doi.org/https://doi.org/10.1016/0022-3093(80)90123-4.

[16] D. Carta, D.M. Pickup, J.C. Knowles, I. Ahmed, M.E. Smith, R.J. Newport, A structural study of sol–gel and melt-quenched phosphate-based glasses, J. Non. Cryst. Solids. 353 (2007) 1759–1765. https://doi.org/https://doi.org/10.1016/j.jnoncrysol.2007.02.008.

[17] D. Carta, D.M. Pickup, J.C. Knowles, M.E. Smith, R.J. Newport, Sol–gel synthesis of the P_2O_5–CaO–Na_2O–SiO_2 system as a novel bioresorbable glass, J. Mater. Chem. 15 (2005) 2134–2140. https://doi.org/10.1039/B414885A.

[18] J.D. Musgraves, J. Hu, L. Calvez, eds., Phosphate Glasses, in: Springer Handb. Glas., Springer International Publishing, Cham, 2019: pp. 553–594. https://doi.org/10.1007/978-3-319-93728-1_16.

[19] R.K. Brow, Review: the structure of simple phosphate glasses, J. Non. Cryst. Solids. 263–264 (2000) 1–28. https://doi.org/https://doi.org/10.1016/S0022-3093(99)00620-1.

[20] P.R. Ehrmann, K. Carlson, J.H. Campbell, C.A. Click, R.K. Brow, Neodymium fluorescence quenching by hydroxyl groups in phosphate laser glasses, J. Non. Cryst. Solids. 349 (2004) 105–114. https://doi.org/https://doi.org/10.1016/j.jnoncrysol.2004.08.216.

[21] A.E. Marino, S.R. Arrasmith, L.L. Gregg, S.D. Jacobs, G. Chen, Y. Duc, Durable phosphate glasses with lower transition temperatures, J. Non. Cryst. Solids. 289 (2001) 37–41. https://doi.org/https://doi.org/10.1016/S0022-3093(01)00706-2.

[22] D.S. Brauer, N. Karpukhina, R. V Law, R.G. Hill, Effect of TiO_2 addition on structure, solubility and crystallisation of phosphate invert glasses for biomedical applications, J. Non. Cryst. Solids. 356 (2010) 2626–2633. https://doi.org/https://doi.org/10.1016/j.jnoncrysol.2010.03.022.

[23] N. Kanwal, H. Toms, A.C. Hannon, F.A. Perras, D.L. Bryce, N. Karpukhina, I. Abrahams, Structure and solubility behaviour of zinc containing phosphate glasses, J. Mater. Chem. B. 3 (2015) 8842–8855. https://doi.org/10.1039/C4TB01504E.

[24] M.J. Dejneka, Transparent Oxyfluoride Glass Ceramics, MRS Bull. 23 (1998) 57–62. https://doi.org/10.1557/S0883769400031018.

[25] J.F. Philipps, T. Töpfer, H. Ebendorff-Heidepriem, D. Ehrt, R. Sauerbrey, Spectroscopic and lasing properties of Er^{3+}:Yb^{3+}-doped fluoride phosphate glasses, Appl. Phys. B. 72 (2001) 399–405. https://doi.org/10.1007/s003400100515.

[26] A.-. Obaton, J. Bernard, C. Parent, G. Le Flem, C. Labbe, P. Le Boulanger, G. Boulton, Synthesis and Spectroscopic Investigation of Yb^{3+}, Er^{3+} -Codoped $LaLiP_4O_{12}$Glasses Relevant for Laser Applications, in: CLEO/Europe Conf. Lasers Electro-Optics, 1998: p. 167. https://doi.org/10.1109/CLEOE.1998.719180.

[27] A.J. Kenyon, Recent developments in rare-earth doped materials for optoelectronics, Prog. Quantum Electron. 26 (2002) 225–284. https://doi.org/https://doi.org/10.1016/S0079-6727(02)00014-9.

[28] S. Taccheo, P. Laporta, S. Longhi, O. Svelto, C. Svelto, Diode-pumped bulk erbium-ytterbium lasers, Appl. Phys. B. 63 (1996) 425–436. https://doi.org/10.1007/BF01828937.

[29] P. Burns, J.M. Dawes, P. Wang, J.A. Piper, H. Zhang, L. Zhu, X. Meng, Energy transfer and investigation into laser performance in Er^{3+},Yb^{3+}:YCOB crystals at 1.5-1.6 μm, in: Adv. Solid-State Lasers, Optical Society of America, 2001: p. ME2. https://doi.org/10.1364/ASSL.2001.ME2.

[30] M. Yamane, Y. Asahara, Glasses for Photonics, 2000. https://doi.org/10.1017/cbo9780511541308.

[31] Y. Yan, A.J. Faber, H. de Waal, Luminescence quenching by OH groups in highly Er-doped phosphate glasses, J. Non. Cryst. Solids. 181 (1995) 283–290. https://doi.org/https://doi.org/10.1016/S0022-3093(94)00528-1.

[32] J. Dong, W. Gao, Q. Han, Y. Wang, J. Qi, X. Yan, M. Sun, Plasmon-enhanced upconversion photoluminescence: Mechanism and application, Rev. Phys. 4 (2019) 100026. https://doi.org/https://doi.org/10.1016/j.revip.2018.100026.

[33] D. Kumar, R.G. Ward, D.J. Williams, Effect of fluorides on silicates and phosphates, Discuss. Faraday Soc. 32 (1961) 147–154. https://doi.org/10.1039/DF9613200147.

[34] Y. Wang, J. Ohwaki, New transparent vitroceramics codoped with Er^{3+} and Yb^{3+} for

efficient frequency upconversion, Appl. Phys. Lett. 63 (1993) 3268–3270. https://doi.org/10.1063/1.110170.
[35] P.A. Tick, N.F. Borrelli, L.K. Cornelius, M.A. Newhouse, Transparent glass ceramics for 1300 nm amplifier applications, J. Appl. Phys. 78 (1995) 6367–6374. https://doi.org/10.1063/1.360518.
[36] G. Hai, Y. Min, Z. Weiping, Upconversion of Er^{3+} Ions in $LiKGdF_5$: Er^{3+} , Dy^{3+} Single Crystal Produced by Infrared and Green Laser, J. Rare Earths. 24 (2006) 740–744. https://doi.org/https://doi.org/10.1016/S1002-0721(07)60020-9.
[37] L.P. Naranjo, C.B. de Araújo, O.L. Malta, P.A.S. Cruz, L.R.P. Kassab, Enhancement of Pr^{3+} luminescence in $PbO–GeO_2$ glasses containing silver nanoparticles, Appl. Phys. Lett. 87 (2005) 241914. https://doi.org/10.1063/1.2143135.
[38] R. de Almeida, D.M. da Silva, L.R.P. Kassab, C.B. de Araújo, Eu^{3+} luminescence in tellurite glasses with gold nanostructures, Opt. Commun. 281 (2008) 108–112. https://doi.org/https://doi.org/10.1016/j.optcom.2007.08.072.
[39] A.P. Carmo, M.J. V Bell, V. Anjos, R. de Almeida, D.M. da Silva, L.R.P. Kassab, Thermo-optical properties of tellurite glasses doped with Eu^{3+} and Au nanoparticles, J. Phys. D. Appl. Phys. 42 (2009) 155404. https://doi.org/10.1088/0022-3727/42/15/155404.
[40] Y. Wu, X. Shen, S. Dai, Y. Xu, F. Chen, C. Lin, T. Xu, Q. Nie, Silver Nanoparticles Enhanced Upconversion Luminescence in Er^{3+} /Yb^{3+} Codoped Bismuth-Germanate Glasses, J. Phys. Chem. C. 115 (2011) 25040–25045. https://doi.org/10.1021/jp207035c.
[41] I. Soltani, S. Hraiech, K. Horchani-Naifer, M. Férid, Effects of silver nanoparticles on the enhancement of up conversion and infrared emission in Er^{3+}/Yb^{3+} co-doped phosphate glasses, Opt. Mater. (Amst). 77 (2018) 161–169. https://doi.org/https://doi.org/10.1016/j.optmat.2018.01.036.
[42] M. Eichelbaum, K. Rademann, Plasmonic Enhancement or Energy Transfer? On the Luminescence of Gold-, Silver-, and Lanthanide-Doped Silicate Glasses and Its Potential for Light-Emitting Devices, Adv. Funct. Mater. 19 (2009) 2045–2052. https://doi.org/10.1002/adfm.200801892.
[43] T. Aisaka, M. Fujii, S. Hayashi, Enhancement of upconversion luminescence of Er doped Al_2O_3 films by Ag island films, Appl. Phys. Lett. 92 (2008) 132105. https://doi.org/10.1063/1.2896303.
[44] L. Kuusela, A. Veber, N.G. Boetti, L. Petit, Impact of ZnO Addition on Er^{3+} Near-Infrared Emission, the Formation of Ag Nanoparticles, and the Crystallization of Sodium Fluorophosphate Glass, Materials (Basel). 13 (2020). https://doi.org/10.3390/ma13030527.
[45] M. Epifani, C. Giannini, L. Tapfer, L. Vasanelli, Sol–Gel Synthesis and Characterization of Ag and Au Nanoparticles in SiO_2, TiO_2, and ZrO_2 Thin Films, J. Am. Ceram. Soc. 83 (2000) 2385–2393. https://doi.org/10.1111/j.1151-2916.2000.tb01566.x.
[46] T. Hayakawa, S.T. Selvan, M. Nogami, Enhanced fluorescence from Eu^{3+} owing to surface plasma oscillation of silver particles in glass, J. Non. Cryst. Solids. 259 (1999) 16–22. https://doi.org/https://doi.org/10.1016/S0022-3093(99)00531-1.
[47] H. Granbohm, J. Larismaa, S. Ali, L.-S. Johansson, S.-P. Hannula, Control of the Size of Silver Nanoparticles and Release of Silver in Heat Treated SiO_2-Ag Composite Powders, Mater. (Basel, Switzerland). 11 (2018) 80. https://doi.org/10.3390/ma11010080.
[48] Z. Liu, H. Wang, H. Li, X. Wang, Red shift of plasmon resonance frequency due to the interacting Ag nanoparticles embedded in single crystal SiO_2 by implantation, Appl. Phys. Lett. 72 (1998) 1823–1825. https://doi.org/10.1063/1.121196.
[49] N. Perkas, G. Amirian, G. Applerot, E. Efendiev, Y. Kaganovskii, A.V. Ghule, B.-J. Chen, Y.-C. Ling, A. Gedanken, Depositing silver nanoparticles on/in a glass slide by the sonochemical method, Nanotechnology. 19 (2008) 435604. https://doi.org/10.1088/0957-4484/19/43/435604.

[50] O. Samson, T. Adeeko, E. Makama, Synthesis and Optical Characterization of Silver Nanoparticles (Ag-NPs) Thin Films (TFs) Prepared by Silar Technique, Int. J. Curr. Res. Acad. Rev. 5 (2017) 15–24. https://doi.org/10.20546/ijcrar.2017.512.003.

[51] M. Saad, W. Stambouli, S.A. Mohamed, H. Elhouichet, Ag nanoparticles induced luminescence enhancement of Eu^{3+} doped phosphate glasses, J. Alloys Compd. 705 (2017) 550–558. https://doi.org/https://doi.org/10.1016/j.jallcom.2016.12.410.

[52] M.C. Gonçalves, L.F. Santos, R.M. Almeida, Rare-earth-doped transparent glass ceramics, Comptes Rendus Chim. 5 (2002) 845–854. https://doi.org/https://doi.org/10.1016/S1631-0748(02)01457-1.

[53] A. de Pablos-Martín, A. Durán, M.J. Pascual, Nanocrystallisation in oxyfluoride systems: mechanisms of crystallisation and photonic properties, Int. Mater. Rev. 57 (2012) 165–186. https://doi.org/10.1179/1743280411Y.0000000004.

[54] X. Yu, L. Duan, L. Ni, Z. Wang, Fabrication and luminescence behavior of phosphate glass ceramics co-doped with Er^{3+} and Yb^{3+}, Opt. Commun. 285 (2012) 3805–3808. https://doi.org/https://doi.org/10.1016/j.optcom.2012.04.042.

[55] C. Yu, J. Zhang, L. Wen, Z. Jiang, New transparent Er^{3+}-doped oxyfluoride tellurite glass ceramic with improved near infrared and up-conversion fluorescence properties, Mater. Lett. 61 (2007) 3644–3646. https://doi.org/https://doi.org/10.1016/j.matlet.2006.12.006.

[56] S.D. Stookey, Method of making ceramics and products thereof, US Patent 2,920,971, 1960.

[57] X. Liu, J. Zhou, S. Zhou, Y. Yue, J. Qiu, Transparent glass-ceramics functionalized by dispersed crystals, Prog. Mater. Sci. 97 (2018) 38–96. https://doi.org/https://doi.org/10.1016/j.pmatsci.2018.02.006.

[58] T. Ozawa, Kinetic analysis of derivative curves in thermal analysis, J. Therm. Anal. 2 (1970) 301–324. https://doi.org/10.1007/BF01911411.

[59] H.E. Kissinger, Reaction Kinetics in Differential Thermal Analysis, Anal. Chem. 29 (1957) 1702–1706. https://doi.org/10.1021/ac60131a045.

[60] H.L. Friedman, Kinetics of thermal degradation of char-forming plastics from thermogravimetry. Application to a phenolic plastic, J. Polym. Sci. Part C Polym. Symp. 6 (1964) 183–195. https://doi.org/10.1002/polc.5070060121.

[61] N. Karpukhina, R.G. Hill, R. V Law, Crystallisation in oxide glasses – a tutorial review, Chem. Soc. Rev. 43 (2014) 2174–2186. https://doi.org/10.1039/C3CS60305A.

[62] D. Erdemir, A.Y. Lee, A.S. Myerson, Crystal Nucleation, in: A.S. Myerson, D. Erdemir, A.Y.E. Lee (Eds.), Handb. Ind. Cryst., 3rd ed., Cambridge University Press, 2019: pp. 76–114. https://doi.org/10.1017/9781139026949.003.

[63] P.G. Vekilov, Nucleation, Cryst. Growth Des. 10 (2010) 5007–5019. https://doi.org/10.1021/cg1011633.

[64] G.H. Beall, D.A. Duke, Transparent glass-ceramics, J. Mater. Sci. 4 (1969) 340–352. https://doi.org/10.1007/BF00550404.

[65] G.H. Beall, Design and Properties of Glass-Ceramics, Annu. Rev. Mater. Sci. 22 (1992) 91–119. https://doi.org/10.1146/annurev.ms.22.080192.000515.

[66] Q. Pan, Z. Cai, Y. Yang, D. Yang, S. Kang, Z. Chen, J. Qiu, Q. Zhan, G. Dong, Engineering Tunable Broadband Near-Infrared Emission in Transparent Rare-Earth Doped Nanocrystals-in-Glass Composites via a Bottom-Up Strategy, Adv. Opt. Mater. 7 (2019) 1801482. https://doi.org/10.1002/adom.201801482.

[67] X. Qiao, X. Fan, J. Wang, M. Wang, Luminescence behavior of Er^{3+} ions in glass–ceramics containing CaF_2 nanocrystals, J. Non. Cryst. Solids. 351 (2005) 357–363. https://doi.org/https://doi.org/10.1016/j.jnoncrysol.2004.11.021.

[68] Q.J. Chen, W.J. Zhang, X.Y. Huang, G.P. Dong, M.Y. Peng, Q.Y. Zhang, Efficient down- and up-conversion of Pr^{3+} –Yb^{3+} co-doped transparent oxyfluoride glass ceramics, J. Alloys Compd. 513 (2012) 139–144.

https://doi.org/https://doi.org/10.1016/j.jallcom.2011.10.007.
[69] J. Zhou, Y. Teng, S. Ye, G. Lin, J. Qiu, A discussion on spectral modification from visible to near-infrared based on energy transfer for silicon solar cells, Opt. Mater. (Amst). 34 (2012) 901–905. https://doi.org/https://doi.org/10.1016/j.optmat.2011.12.002.
[70] G. Gorni, A. Cosci, S. Pelli, L. Pascual, A. Durán, M.J. Pascual, Transparent Oxyfluoride Nano-Glass Ceramics Doped with Pr^{3+} and Pr^{3+} –Yb^{3+} for NIR Emission, Front. Mater. 3 (2017) 58. https://doi.org/10.3389/fmats.2016.00058.
[71] K. Hirao, K. Tanaka, M. Makita, N. Soga, Preparation and optical properties of transparent glass-ceramics containing β-PbF_2:Tm^{3+}, J. Appl. Phys. 78 (1995) 3445–3450. https://doi.org/10.1063/1.359975.
[72] K. Shioya, T. Komatsu, H.G. Kim, R. Sato, K. Matusita, Optical properties of transparent glass-ceramics in K_2O-Nb_2O_5-TeO_2 glasses, J. Non. Cryst. Solids. 189 (1995) 16–24. https://doi.org/https://doi.org/10.1016/0022-3093(95)00227-8.
[73] L.A. Bueno, P. Melnikov, Y. Messaddeq, S.J.L. Ribeiro, Er^{3+} and Eu^{3+} containing transparent glass ceramics in the system $PbGeO_3$–PbF_2–CdF_2, J. Non. Cryst. Solids. 247 (1999) 87–91. https://doi.org/https://doi.org/10.1016/S0022-3093(99)00067-8.
[74] H. Hayashi, S. Tanabe, T. Hanada, 1.4 μm band emission properties of Tm^{3+} ions in transparent glass ceramics containing PbF_2 nanocrystals for S-band amplifier, J. Appl. Phys. 89 (2001) 1041–1045. https://doi.org/10.1063/1.1335645.
[75] M. Mortier, F. Auzel, Rare-earth doped transparent glass-ceramics with high cross-sections, J. Non. Cryst. Solids. 256–257 (1999) 361–365. https://doi.org/https://doi.org/10.1016/S0022-3093(99)00475-5.
[76] M.A.P. Silva, Y. Messaddeq, V. Briois, M. Poulain, F. Villain, S.J.L. Ribeiro, Synthesis and structural investigations on TeO_2-PbF_2-CdF_2 glasses and transparent glass-ceramics, J. Phys. Chem. Solids. 63 (2002) 605–612. https://doi.org/https://doi.org/10.1016/S0022-3697(01)00200-1.
[77] S. Cui, J. Massera, M. Lastusaari, L. Hupa, L. Petit, Novel oxyfluorophosphate glasses and glass-ceramics, J. Non. Cryst. Solids. 445–446 (2016) 40–44. https://doi.org/10.1016/j.jnoncrysol.2016.05.005.
[78] A. Nommeots-Nomm, N.G. Boetti, T. Salminen, J. Massera, M. Hokka, L. Petit, Luminescence of Er^{3+} doped oxyfluoride phosphate glasses and glass-ceramics, J. Alloys Compd. 751 (2018) 224–230. https://doi.org/10.1016/j.jallcom.2018.04.101.
[79] A. Szczodra, A. Mardoukhi, M. Hokka, N.G. Boetti, L. Petit, Fluorine losses in Er^{3+} oxyfluoride phosphate glasses and glass-ceramics, J. Alloys Compd. 797 (2019) 797–803. https://doi.org/https://doi.org/10.1016/j.jallcom.2019.05.151.
[80] J. Zhao, X. Zheng, E.P. Schartner, P. Ionescu, R. Zhang, T.-L. Nguyen, D. Jin, H. Ebendorff-Heidepriem, Upconversion Nanocrystal-Doped Glass: A New Paradigm for Photonic Materials, Adv. Opt. Mater. 4 (2016) 1507–1517. https://doi.org/10.1002/adom.201600296.
[81] F. Liu, E. Ma, D. Chen, Y. Wang, Y. Yu, P. Huang, Infrared luminescence of transparent glass ceramic containing Er^{3+} :$NaYF_4$ nanocrystals, J. Alloys Compd. 467 (2009) 317–321. https://doi.org/https://doi.org/10.1016/j.jallcom.2007.11.109.
[82] Y. Gao, Y. Hu, D. Zhou, J. Qiu, Effect of heat treatment mechanism on upconversion luminescence in Er^{3+} /Yb^{3+} co-doped $NaYF_4$ oxyfluoride glass-ceramics, J. Alloys Compd. 699 (2017) 303–307. https://doi.org/https://doi.org/10.1016/j.jallcom.2016.12.437.
[83] G. Chen, C. Yang, P.N. Prasad, Nanophotonics and Nanochemistry: Controlling the Excitation Dynamics for Frequency Up- and Down-Conversion in Lanthanide-Doped Nanoparticles, Acc. Chem. Res. 46 (2013) 1474–1486. https://doi.org/10.1021/ar300270y.
[84] T. Laihinen, M. Lastusaari, L. Pihlgren, L.C. V Rodrigues, J. Hölsä, Thermal behaviour of the $NaYF_4$:Yb^{3+},R^{3+} materials, J. Therm. Anal. Calorim. 121 (2015) 37–43.

https://doi.org/10.1007/s10973-015-4609-x.
[85] J.A. Augis, J.E. Bennett, Calculation of the Avrami parameters for heterogeneous solid state reactions using a modification of the Kissinger method, J. Therm. Anal. 13 (1978) 283–292. https://doi.org/10.1007/BF01912301.
[86] J. Massera, J. Remond, J. Musgraves, M.J. Davis, S. Misture, L. Petit, K. Richardson, Nucleation and growth behavior of glasses in the TeO_2-Bi_2O_3-ZnO glass system, J. Non. Cryst. Solids. 356 (2010) 2947–2955. https://doi.org/10.1016/j.jnoncrysol.2010.03.045.
[87] A. Marotta, A. Buri, F. Branda, Nucleation in glass and differential thermal analysis, J. Mater. Sci. 16 (1981) 341–344. https://doi.org/10.1007/BF00738622.
[88] R.K. Brow, D.R. Tallant, W.L. Warren, A. McIntyre, D.E. Day, Spectroscopic studies of the structure of titanophosphate and calcium titanophosphate glasses, Phys. Chem. Glas. (1997).
[89] R.K. Brow, R.J. Kirkpatrick, G.L. Turner, Nature of Alumina in Phosphate Glass: II, Structure of Sodium Alurninophosphate Glass, J. Am. Ceram. Soc. (1993). https://doi.org/10.1111/j.1151-2916.1993.tb05316.x.
[90] S.I.S. Shaharuddin, I. Ahmed, D. Furniss, A.J. Parsons, C.D. Rudd, Investigation on the thermal properties, density and degradation of quaternary iron and titanium phosphate based glasses, in: IOP Conf. Ser. Mater. Sci. Eng., 2016. https://doi.org/10.1088/1757-899X/114/1/012124.
[91] M.H.M. Zaid, K.A. Matori, S.H. Abdul Aziz, A. Zakaria, M.S.M. Ghazali, Effect of ZnO on the physical properties and optical band gap of soda lime silicate glass, Int. J. Mol. Sci. (2012). https://doi.org/10.3390/ijms13067550.
[92] P. Lopez-Iscoa, L. Petit, J. Massera, D. Janner, N.G. Boetti, D. Pugliese, S. Fiorilli, C. Novara, F. Giorgis, D. Milanese, Effect of the addition of Al_2O_3, TiO_2 and ZnO on the thermal, structural and luminescence properties of Er^{3+}-doped phosphate glasses, J. Non. Cryst. Solids. 460 (2017) 161–168. https://doi.org/10.1016/J.JNONCRYSOL.2017.01.030.
[93] S. Toyoda, S. Fujino, K. Morinaga, Density, viscosity and surface tension of 50RO–50P_2O_5 (R: Mg, Ca, Sr, Ba, and Zn) glass melts, J. Non. Cryst. Solids. 321 (2003) 169–174. https://doi.org/https://doi.org/10.1016/S0022-3093(03)00174-1.
[94] M.T. Islam, N. Sharmin, G.A. Rance, J.J. Titman, A.J. Parsons, K.M.Z. Hossain, I. Ahmed, The effect of MgO/TiO_2 on structural and crystallization behavior of near invert phosphate-based glasses, J. Biomed. Mater. Res. Part B Appl. Biomater. (2020) 674–686. https://doi.org/10.1002/jbm.b.34421.
[95] H. Morikawa, S. Lee, T. Kasuga, D.S. Brauer, Effects of magnesium for calcium substitution in P_2O_5–CaO–TiO_2 glasses, J. Non. Cryst. Solids. 380 (2013) 53–59. https://doi.org/https://doi.org/10.1016/j.jnoncrysol.2013.08.029.
[96] A. Kiani, J. V. Hanna, S.P. King, G.J. Rees, M.E. Smith, N. Roohpour, V. Salih, J.C. Knowles, Structural characterization and physical properties of P_2O_5-CaO-Na_2O-TiO_2 glasses by Fourier transform infrared, Raman and solid-state magic angle spinning nuclear magnetic resonance spectroscopies, Acta Biomater. 8 (2012) 333–340. https://doi.org/10.1016/j.actbio.2011.08.025.
[97] H. Segawa, N. Akagi, T. Yano, S. Shibita, Properties and structures of TiO_2–ZnO–P_2O_5 glasses, J. Ceram. Soc. Japan. 118 (2010) 278–282. https://doi.org/10.2109/jcersj2.118.278.
[98] L.H.C. Andrade, S.M. Lima, A. Novatski, A.M. Neto, A.C. Bento, M.L. Baesso, F.C.G. Gandra, Y. Guyot, G. Boulon, Spectroscopic assignments of Ti^{3+} and Ti^{4+} in titanium-doped OH− free low-silica calcium aluminosilicate glass and role of structural defects on the observed long lifetime and high fluorescence of Ti^{3+} ions, Phys. Rev. B. 78 (2008) 224202. https://doi.org/10.1103/PhysRevB.78.224202.
[99] M.J. Starink, The determination of activation energy from linear heating rate experiments: a comparison of the accuracy of isoconversion methods, Thermochim. Acta. 404 (2003) 163–176. https://doi.org/https://doi.org/10.1016/S0040-6031(03)00144-8.

[100] C.S. Ray, D.E. Day, An Analysis of Nucleation-Rate Type of Curves in Glass as Determined by Differential Thermal Analysis, J. Am. Ceram. Soc. 80 (1997) 3100–3108. https://doi.org/10.1111/j.1151-2916.1997.tb03238.x.

[101] Y. Liu, D. Tu, H. Zhu, R. Li, W. Luo, X. Chen, A Strategy to Achieve Efficient Dual-Mode Luminescence of Eu^{3+} in Lanthanides Doped Multifunctional $NaGdF_4$ Nanocrystals, Adv. Mater. 22 (2010) 3266–3271. https://doi.org/10.1002/adma.201000128.

[102] J. Massera, M. Gaussiran, P. Głuchowski, M. Lastusaari, L. Petit, J. Hölsä, L. Hupa, Effect of the glass melting condition on the processing of phosphate-based glass–ceramics with persistent luminescence properties, Opt. Mater. (Amst). 52 (2016) 56–61. https://doi.org/https://doi.org/10.1016/j.optmat.2015.12.006.

[103] T. Aitasalo, J. Hölsä, H. Jungner, J.-C. Krupa, M. Lastusaari, J. Legendziewicz, J. Niittykoski, Effect of temperature on the luminescence processes of SrAl2O4:Eu^{2+}, Radiat. Meas. 38 (2004) 727–730. https://doi.org/https://doi.org/10.1016/j.radmeas.2004.01.031.

[104] J. Massera, M. Gaussiran, P. Gluchowski, M. Lastusaari, L. Hupa, L. Petit, Processing and characterization of phosphate glasses containing $CaAl_2O_4$:Eu^{2+} ,Nd^{3+} and $SrAl_2O_4$:Eu^{2+} ,Dy^{3+} microparticles, J. Eur. Ceram. Soc. 35 (2015) 3863–3871. https://doi.org/https://doi.org/10.1016/j.jeurceramsoc.2015.06.031.

[105] F. Auzel, Upconversion and Anti-Stokes Processes with f and d Ions in Solids, Chem. Rev. 104 (2004) 139–174. https://doi.org/10.1021/cr020357g.

[106] X. Lu, E.M. Arruda, W.W. Schultz, The effect of processing parameters on glass fiber birefringence development and relaxation, J. Nonnewton. Fluid Mech. 86 (1999) 89–104. https://doi.org/https://doi.org/10.1016/S0377-0257(98)00203-1.

[107] R. Gumenyuk, A. Poudel, T. Jouan, C. Boussard-Plédel, T. Niemi, L. Petit, Super-luminescence and spectral hole burning effect in ultra-short length Er/Yb-doped phosphate fiber, Opt. Mater. Express. 7 (2017) 4358–4366. https://doi.org/10.1364/OME.7.004358.

[108] D. Manikandan, S. Mohan, K.G.M. Nair, Absorption and luminescence of silver nanocomposite soda-lime glass formed by Ag^{+}–Na^{+} ion-exchange, Mater. Res. Bull. 38 (2003) 1545–1550. https://doi.org/https://doi.org/10.1016/S0025-5408(03)00165-X.

[109] Y. Dai, X. Hu, C. Wang, D. Chen, X. Jiang, C. Zhu, B. Yu, J. Qiu, Fluorescent Ag nanoclusters in glass induced by an infrared femtosecond laser, Chem. Phys. Lett. 439 (2007) 81–84. https://doi.org/https://doi.org/10.1016/j.cplett.2007.03.043.

[110] V.K. Tikhomirov, V.D. Rodríguez, A. Kuznetsov, D. Kirilenko, G. Van Tendeloo, V. V Moshchalkov, Preparation and luminescence of bulk oxyfluoride glasses doped with Ag nanoclusters, Opt. Express. 18 (2010) 22032–22040. https://doi.org/10.1364/OE.18.022032.

[111] J.A. Jiménez, M. Sendova, Catalyst role of Nd^{3+} ions for the precipitation of silver nanoparticles in phosphate glass, J. Alloys Compd. 691 (2017) 44–50. https://doi.org/https://doi.org/10.1016/j.jallcom.2016.08.231.

[112] L. Li, Y. Yang, D. Zhou, Z. Yang, X. Xu, J. Qiu, Influence of the Eu^{2+} on the Silver Aggregates Formation in Ag^{+}–Na^{+} Ion-Exchanged Eu^{3+}-Doped Sodium–Aluminosilicate Glasses, J. Am. Ceram. Soc. 97 (2014) 1110–1114. https://doi.org/10.1111/jace.12745.

[113] W.M. Pontuschka, J.M. Giehl, A.R. Miranda, Z.M. Da Costa, A.M. Alencar, Effect of the Al_2O_3 addition on the formation of silver nanoparticles in heat treated soda-lime silicate glasses, J. Non. Cryst. Solids. 453 (2016) 74–83. https://doi.org/https://doi.org/10.1016/j.jnoncrysol.2016.09.028.

[114] M. Ennouri, L. Kuusela, I. Jlassi, B. Gelloz, L. Petit, H. Elhouichet, Impact of Ag_2O Content on the Optical and Spectroscopic Properties of Fluoro-Phosphate Glasses, Materials (Basel). 12 (2019) 3516. https://doi.org/10.3390/ma12213516.

[115] V. Amendola, O.M. Bakr, F. Stellacci, A Study of the Surface Plasmon Resonance of Silver Nanoparticles by the Discrete Dipole Approximation Method: Effect of Shape, Size,

Structure, and Assembly, Plasmonics. 5 (2010) 85–97. https://doi.org/10.1007/s11468-009-9120-4.

[116] D. Yang, Q. Pan, S. Kang, G. Dong, J. Qiu, Weakening thermal quenching to enhance luminescence of Er^{3+} doped β-$NaYF_4$ nanocrystals via acid-treatment, J. Am. Ceram. Soc. 102 (2019) 6027–6037. https://doi.org/10.1111/jace.16490.

PUBLICATIONS

PUBLICATION I

Decomposition of persistent luminescent microparticles in corrosive phosphate glass melt

N. Ojha, H. Nguyen, T. Laihinen, T. Salminen, M. Lastusaari and L. Petit

Corrosion Science, Vol. 135, pp. 207-214
https://doi.org/10.1016/j.corsci.2018.02.050

Corrosion Science 135 (2018) 207–214

Contents lists available at ScienceDirect

Corrosion Science

journal homepage: www.elsevier.com/locate/corsci

Decomposition of persistent luminescent microparticles in corrosive phosphate glass melt

N. Ojha[a], H. Nguyen[a], T. Laihinen[b], T. Salminen[a], M. Lastusaari[b,c], L. Petit[a,*]

[a] Laboratory of Photonics, Tampere University of Technology, FI-33101 Tampere, Finland
[b] University of Turku, Department of Chemistry, FI-20014 Turku, Finland
[c] Turku University Centre for Materials and Surfaces (MatSurf), Turku, Finland

ARTICLE INFO

Keywords:
Phosphate glasses
$SrAl_2O_4:Eu^{2+},Dy^{3+}$ microparticles
Persistent luminescence
Corrosion
Decomposition

ABSTRACT

Findings on the decomposition of persistent luminescent (PeL) $SrAl_2O_4:Eu^{2+},Dy^{3+}$ microparticles (MPs) in phosphate glass melt under static condition are reported. PeL phosphate glasses with the composition ($50P_2O_5$-$10Na_2O$-40SrO) (in mol%) were prepared by adding the MPs in the glass melt. The decomposition of the MPs occurs during the preparation of the glass and leads to changes in the Eu^{2+} sites and to the formation of Eu^{3+} which decreases the PeL properties of the glasses. The decomposition of the MPs depends on the temperature at which the MPs are added in the melt and also on the time before casting the melts.

1. Introduction

There has been some interest during the past few years to process glass-ceramics (GCs) with persistent luminescence (PeL) properties as such GCs emit light for a long time (from seconds to hours) after the removal of the irradiation source [1]. These new materials can find applications as, for example, fluorescent light sources due to their high luminous efficiency, energy-saving, long lifetime and good features for protection of the environment [2].

PeL glass-ceramics were successfully obtained using the so called "Frozen sorbet method" developed by Nakanishi et al. [3]. This method was applied to the SrO-Al_2O_3-B_2O_3 glass system in which $SrAl_2O_4:Eu^{2+},Dy^{3+}$ crystals precipitate [4]. These crystal seeds, which grow into microparticles (MPs), are formed by the ions from the glass. In these $SrAl_2O_4:Eu^{2+},Dy^{3+}$ crystals, both Eu^{2+} and Dy^{3+} substitute for Sr^{2+}. The Eu^{2+} ions act as luminescent centers while the Dy^{3+} ions are used to increase the duration of the persistent luminescence as they increase the number of energy traps in the structure [5]. However, with this "Frozen sorbet method", the composition of the MPs depends on the composition of the glass matrix. Therefore, we developed an alternative route for the preparation of phosphate glasses with persistent luminescence properties [6]: PeL phosphate glasses were obtained by adding $SrAl_2O_4:Eu^{2+}$, Dy^{3+} microparticles (MPs) in glass batches prior to the glass melting. However, the MPs aggregate in the glasses leading to glasses with inhomogeneous persistent luminescence properties. Based on these results, our work has now been focused on the preparation of glasses with uniform persistent luminescence.

Recently, an alternative approach, the direct doping of particles into tellurite-based glass melts, was developed to prepare glasses with better dispersion of particles in the glass [7,8]. The first step consists of melting the glass batch. Then, the temperature is reduced to the doping temperature to increase the glass viscosity. The particles are, then, added at this doping temperature, mixed into the melt and finally cast after a short dwell time to allow dispersion of the particles. Recently, we showed, for the first time to our knowledge, that this direct doping method could be used to process phosphate glasses with upconversion (UC) while using a low amount of Er^{3+} and Yb^{3+} (0.01 at% of Er^{3+} and 0.06 at% of Yb^{3+}) [9]. Our study suggested that it is crucial to understand how the particles are corroded in the molten glass in order to control the dispersion and survival of the particles in the glass and so to prepare glasses with homogeneous luminescence properties.

Surprisingly, the works concerning the corrosion behavior of glass melts have been realized only since the late 1950s and on pure metals such as Pt [10] and Fe [11] just to cite a few. The behavior of pure metals immersed in molten glasses in terms of corrosion rates and corrosion layers was found to depend on the glass composition and melt temperature [12]. Therefore, the investigation of the corrosion of other materials in phosphate glass melt is of great interest and brings new knowledge on the corrosion behavior of the glass melts.

Here, $SrAl_2O_4:Eu^{2+},Dy^{3+}$ microparticle (MPs) were added in

* Corresponding author.
E-mail address: laeticia.petit@tut.fi (L. Petit).

https://doi.org/10.1016/j.corsci.2018.02.050
Received 30 August 2017; Received in revised form 15 February 2018; Accepted 21 February 2018
Available online 23 February 2018
0010-938X/

Table 1
Summary of the doping parameters used to prepare the glasses, sample codes and Standard deviation (SdtDev) of the pixel intensity from the analysis of the glass pictures (Fig. 1). The SdtDev was obtained using ImageJ, Java-based image processing program.

Melting condition			
Dwell time (t) (min)	Doping Temperature (T_{doping}) (°C)	Sample code (T_{doping}-t)	SdtDev
3	975	975 – 3	10
	1000	1000 – 3	11
	1025	1025 – 3	9
5	975	975 – 5	10
	1000	1000 – 5	8
	1025	1025 – 5	6
10	975	975 – 10	20
	1000	1000 – 10	12
	1025	1025 – 10	11

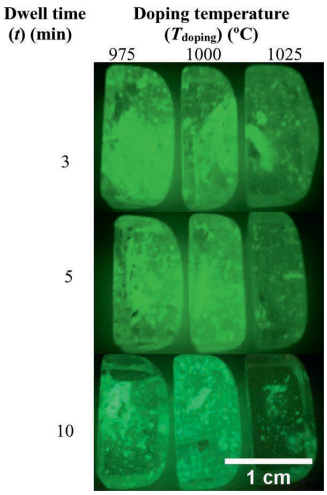

Fig. 1. Pictures of the glasses prepared using different (T_{doping}-t) parameters after stopping the UV irradiation.

phosphate glass melt after melting. The impact of different doping temperatures and dwell times on the corrosion of the MPs is discussed. In the context of this paper, corrosion can refer to the decomposition of the MPs in the glass. The decomposition of the MPs is correlated to the changes in the persistent luminescence properties of the glasses induced by the changes in the Eu^{2+} sites and to the formation of Eu^{3+} at the expense of Eu^{2+}.

2. Experimental procedure

2.1. Glass processing

Glasses with the composition $50P_2O_5$-$10Na_2O$-40SrO (mol%) were prepared using a standard melting method. $NaPO_3$, $SrCO_3$ and $(NH_4)_2HPO_4$ were used as the starting raw materials. $Sr(PO_3)_2$ precursors were first independently prepared from mixtures of the alkaline earth carbonates and $(NH_4)_2HPO_4$ using slow heating rate up to 900 °C. A 10 g batch glass was melted for 30 min at 1050 °C. After melting, 1 weight-% of commercial $SrAl_2O_4$: Eu^{2+},Dy^{3+} microparticles (MPs) (Jinan G.L. New Materials, China, BG-01) was added at a specific doping temperature (T_{doping} ranging between 975 and 1025 °C) and the glass was finally quenched after 3–5 min after adding the MPs (doping parameter called dwell time reported as t). Each glass was prepared from a specific batch and using specific (T_{doping} − t) doping parameters. Finally, the resulting glasses were annealed at 400 °C, which is 40 °C below the glass transition temperature, for 4 h in air. The different trials are summarized in Table 1.

2.2. Composition analysis

A scanning electron microscope (Carl Zeiss Crossbeam 540) equipped with Oxford Instruments X-Max^N 80 EDS detector was used to image and analyze the composition of the samples. The polished glasses were coated with a thin carbon layer before EDS mapping. As commonly performed when analyzing the composition of glasses, the at% were converted in mol%. The accuracy of the composition analysis was ± 1.5 mol%.

2.3. Luminescence

The persistent luminescence properties of the crushed microparticle-containing glasses were measured at room temperature using a Varian Cary Eclipse Fluorescence Spectrophotometer equipped with a Hamamatsu R928 photomultiplier (PMT). The conventional luminescence (λ_{exc}: 266 nm, Nd:YAG pulse laser, 8 ns, TII Lotis) was measured at room temperature using a CCD camera (Avantes, AvaSpec–2048 × 14). For persistent luminescence measurements, the samples were irradiated for 5 min at room temperature with a compact UV lamp (UVGL-25, 4 W, λ_{exc}: 254 nm). The persistent luminescence spectra were recorded 1 min after ceasing the irradiation with a 4 s data collection time.

3. Results and discussion

To succeed in doping the glasses homogenously with the MPs, it is crucial to identify a suitable temperature for doping and dispersing the MPs in the glass melt as explained in [8]. MPs were found to decompose in the investigated glass system when melting the glass at 1100 °C for 10 min while the MPs maintain their PeL properties in the glass when the glass is melted at 1000 °C for 10 min as reported in [13]. Therefore, 1100 °C is already an upper limit of the doping temperature. The lower limit of the doping temperature is determined by the glass melt viscosity; as the temperature decreases, the viscosity of the glass increases. As a result, there is a temperature at which the glass melt is too viscous for the MPs to disperse homogeneously as explained in [8]. Therefore, in this study, the MPs were added at 975, 1000 and 1025 °C after the melting to avoid the decomposition of MPs. As the doping temperatures are near the melting temperature, the viscosity of the glass does not change dramatically when the temperature of the melt is reduced between 975 and 1025 °C. This was confirmed by measuring the viscosity of the glass from 10^5 to 10^{11} Pa s using beam bending and parallel plate viscometers (not shown here) and by fitting the viscosity curve using the Vogel-Fulcher-Tamman equation to estimate the viscosity of the glass at the different doping temperatures. In addition to the doping temperature, the dwell time is another crucial parameter to identify in order to disperse homogeneously the MPs into the phosphate glass. As for the doping temperature, a better dispersion of the MPs can be

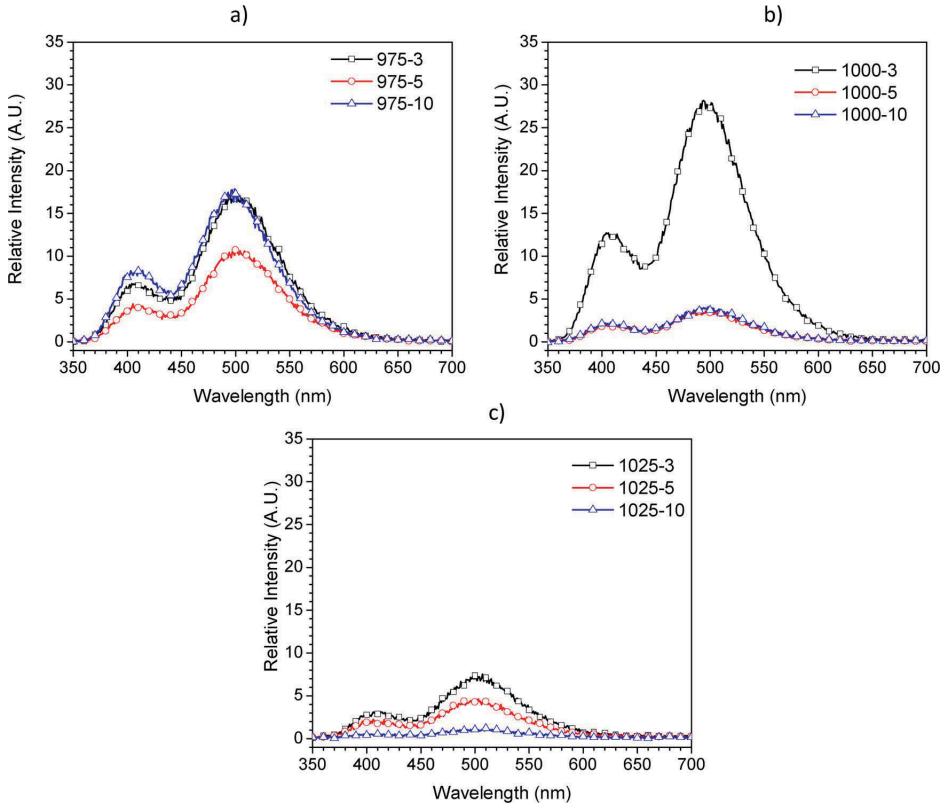

Fig. 2. Persistent luminescence spectra of the glasses prepared using a) (T_{doping} = 975 °C, *t*), b) (T_{doping} = 1000 °C, *t*) and c) (T_{doping} = 1025 °C, *t*) parameters.

obtained for prolonged dwell time but at the same time, it increases the risk of corroding the MPs in the glass melt; decomposition of the MPs inside the glass was observed when the glass was melted at 1000 °C for 30 min [13]. Therefore, the glasses of investigation were then quenched 3, 5 and 10 min after adding the MPs. The Table 1 summarizes the different trials as well as the sample codes used in this study.

Fig. 1 shows selected pictures of the investigated glasses after stopping the UV irradiation. All the glasses exhibit green persistent luminescence after ceasing the UV irradiation, which confirms the survival of the MPs in the glasses. Depending on the doping temperature and dwell time, some aggregated MPs can be observed in the glasses. In order to quantify and compare the dispersion of the MPs in the glasses, the pictures of the glasses were analyzed using ImageJ, Java-based image processing program. The standard deviation (StdDev) of the pixel intensity was measured for each glass and the data are summarized in Table 1. A high StdDev indicates large variation in the emission intensity within the glass, which can, then, be related to the distribution of MP aggregates. A smaller StdDev was measured for the glasses prepared using a 5 min dwell time than for the other glasses indicating that the dispersion of the MPs is insufficient if the dwell time (*t*) is too short (3 min) as suggested in [8]. However, the decomposition of the MPs is suspected to occur when the dwell time is too long (> 5 min) based on the lighter green emission of the (975/1000/1025 − 10) glasses compared to the other glasses.

To quantify the changes in the spectroscopic properties of the glasses, the bottom half of each sample was crushed into powder for the analysis of the spectroscopic properties of the glasses. The persistent luminescence (PeL) spectra of the glasses are shown in Fig. 2. The persistent luminescence spectra of the glasses exhibit two broad bands with a maximum at 410 and 490 nm which are attributed to the $4f^6 5d^1 \rightarrow 4f^7$ transition in Eu^{2+} located in two sites in the monoclinic $SrAl_2O_4$ structure [14,15]. As compared to the PeL spectrum of the MPs before being embedded in the glass which can be found in [13], the intensity of the band at 410 nm increases significantly as compared to the band at 490 nm when the MPs are embedded in the glasses. These changes in the persistent luminescence spectra of the glasses are a clear sign of the decomposition of the MPs during the glass preparation: diffusion of Eu, Al and/or Sr ions from the MPs into the glass is suspected to occur during the glass preparation which leads to changes in the Eu^{2+} environment and so to changes in the PeL properties. Furthermore, the 975 glasses exhibit larger PeL intensity than the 1000 and 1025 glasses, except for the (1000 − 3) glass, which exhibits the highest emission. This strong emission from the (1000 − 3) glass compared to the other glasses can be related to the aggregates of MPs that lead to inhomogeneity of the PeL in that glass. While the dwell time has no significant impact on the PeL intensity in the 975 glasses nor

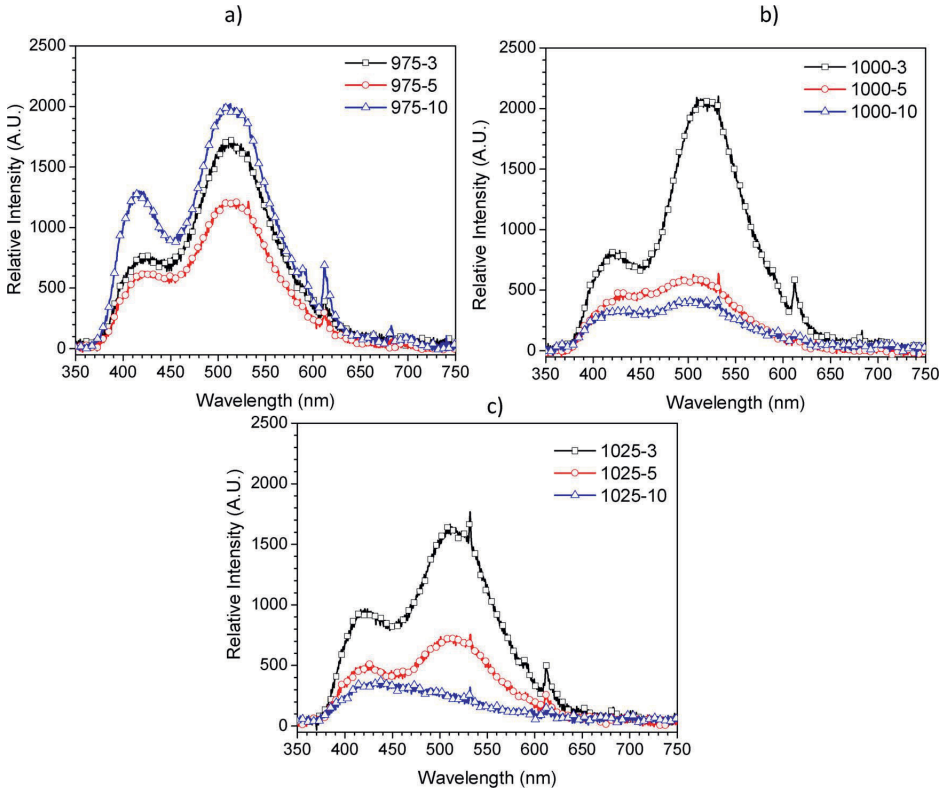

Fig. 3. Conventional luminescence spectra of the glasses prepared using a) (T_{doping} = 975 °C, *t*), b) (T_{doping} = 1000 °C, *t*) and c) (T_{doping} = 1025 °C, *t*) parameters.

most probably in the 1000 glasses, the progressive increase in the dwell time from 3 to 10 min decreases significantly the PeL intensity in the 1025 glasses confirming that 1025 °C is already an upper limit of the doping temperature.

The conventional luminescence spectra of the glasses are shown in Fig. 3. The spectra of all the investigated glasses exhibit a peak at 532 nm which is an harmonic of the 266 nm used for the excitation and also 3 bands at 590, 610 and 680 nm. The presence of these three bands in the spectra is a clear sign of the oxidation of some Eu^{2+} ions to Eu^{3+} ions, which is another sign of MPs decomposition [13]. An increase in the dwell time increases the intensity of these emission bands as compared to that of the main band at 525 nm. This confirms that for long dwell time, the risk of oxidizing Eu^{2+} into Eu^{3+} is high. The conventional luminescence spectra of the glasses exhibit also 2 bands at 400 and 525 nm which can be associated to the emission from Eu^{2+} located in two different cation sites in the $SrAl_2O_4$ structure according to [15]. For the 1000 and 1025 glasses, the band at 525 nm decreases in intensity compared to the band at 400 nm with increasing dwell time indicating that the concentration of Eu^{2+} in the site responsible for the 525 nm emission decreases with increasing dwell time. Therefore, the structure of the corroded MPs changes and may give new sites for Eu^{2+} [13], thus changing the crystal field around Eu^{2+}. This change can be observed by the broadening or the shifting of the emission peaks. It should be pointed out that less changes in the crystal field acting on the Eu^{2+} ions are expected to occur in the 975 glasses compared to the other glasses confirming that the doping temperature should be as low as possible to limit the decomposition of the MPs inside the glass. As shown in the normalized spectra presented in Fig. 4, with an increase in the dwell time, the site of the Eu^{2+} in the MPs is slightly modified when using a doping temperature of 975 °C whereas dramatic changes in the site occur when the doping temperature is 1025 °C. This confirms that decomposition of the MPs occurs when using a high doping temperature.

In order to confirm the decomposition of the MPs in the glasses, the morphology and the composition of the MPs were analyzed using a SEM/EDS. The SEM pictures of a MP found at the surface of the investigated glasses are shown in Fig. 5. Particles with an average size of 50 − 150 μm can be seen in the SEM images. As seen in the SEM picture of the MP in the (1025 − 10) glass, the morphology of the MPs looks different compared to the morphology of the MPs in other glasses. Crystals with needle like shape can, also, be seen around the MPs. From the SEM pictures, the size and number of these crystals are suspected to increase with the increases in the doping temperature and the dwell time. Fig. 6 shows the SEM images and EDS line profiles showing the elemental distribution across the MP diameter and interface with the (975 − 3), (1000 − 5) and (1025 − 10) glasses taken as examples. In all glasses, the composition of the glass matrix is in accordance with the theoretical one within the accuracy of the measurements (± 1.5 mol

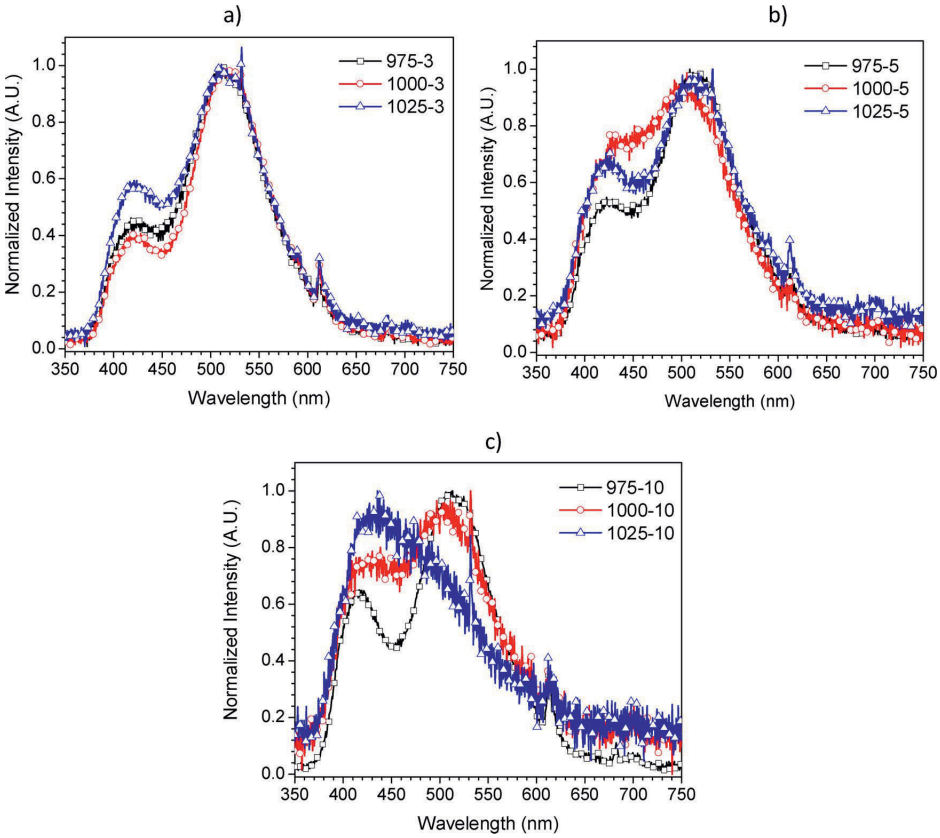

Fig. 4. Normalized conventional luminescence spectra of the glasses prepared using a) (T_{doping} = 975 °C, t), b) (T_{doping} = 1000 °C, t) and c) (T_{doping} = 1025 °C, t) parameters.

%). According to the composition analysis, the composition of the MPs in the (975 − 3) and (1000 − 5) glasses is $SrAl_2O_4$, indicating that the MPs maintain their compositional integrity in their center and so their PeL and CL properties as discussed in the previous section. However, the MP found in the (1025 − 10) glass does not maintain its compositional integrity and exhibits an Al_2O_3 rich outer layer at the interface with the glass as seen in [13], confirming the MP decomposition as suspected from the spectroscopic properties of the (1025 − 10) glass. The crystals precipitating around the MPs consist of Sr and P as those seen around the MPs when added in the batch prior to the melting [13]. The crystallization mechanism of the base glass can be found in [16] and suggested that $Sr(PO_3)_2$ and $NaSr(PO_3)_3$ are the two phases crystallizing upon heat treatment. However, based on the composition analysis of the crystals precipitating around the MPs, we suspect the crystals to be richer in Sr than the crystals forming upon heat treatment, most probably due to the diffusion of the Sr from the MPs during the decomposition of the MPs. Finally, a trace of Al_2O_3 in the glasses is also observed as seen when the MPs are added in the glass batch prior to the melting [13]. Fig. 7 shows the Al_2O_3 concentration profile at the MP-glass interface using the data from Fig. 6. In order to compare the Al_2O_3 diffusion in the glasses prepared using different doping parameters, the profiles were normalized to the glass-MP interface. An increase in the T_{doping} and the dwell time (t) is suspected to increase not only the concentration of Al_2O_3 in the MP-glass interface but also the thickness of the Al-rich outer layer. This layer becomes also richer in Al with an increase in the doping temperature and dwell time. Finally, it should be pointed out that the MP found in the (975 − 3) glass exhibits a thin Al-rich layer at the glass interface, indicating that the decomposition of the MPs in the glass melt already occurs when the glass is cast 3 min after adding the particles at 975 °C.

The impact of the doping temperature on the decomposition of the MPs was confirmed by investigating the corrosion process of an alumina tube in the glass melt as performed in [12]. An alumina rod with a 1.6 mm diameter from AdValue Technology was immersed in the glass batch at the 3 doping temperatures. After 6 h at the doping temperature, the rods were removed from the crucibles before quenching the glasses and embedded in epoxy prior to polishing. As shown in Fig. 8a–c, a small piece of glass could be seen at the surface of the rod immersed for 6 h at 975 °C whereas a thick layer of glass was attached at the surface of the rods immersed after 6 h at 1000 and 1025 °C. A small amount of Al_2O_3 (< 1mol%) was detected in the glasses quenched from the melts at 975 and 1000 °C. It increased to ~1mol% when the doping temperature was 1025 °C. This is in agreement with the decrease in the rod diameter to 1.2 mm when the doping temperature

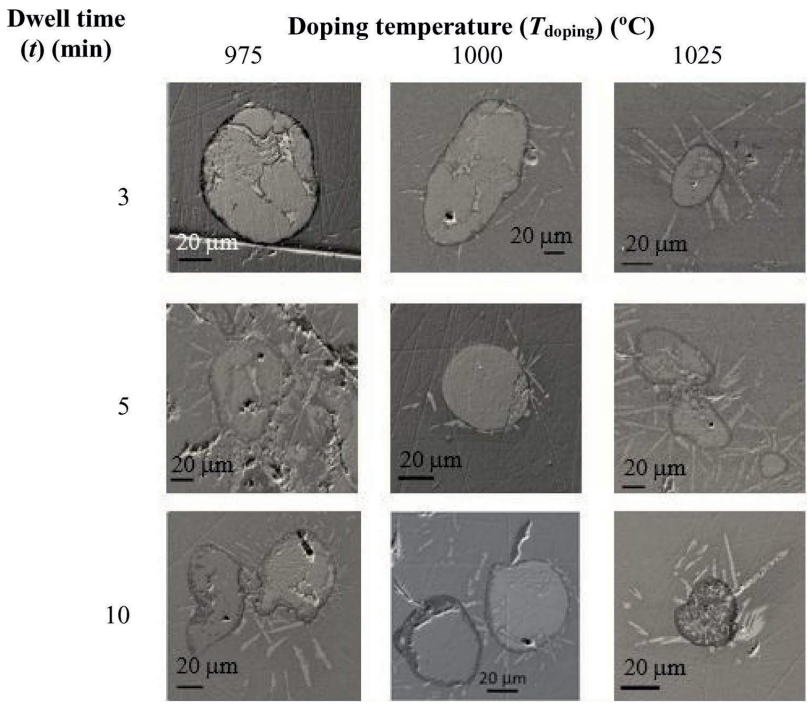

Fig. 5. SEM pictures of a MP found at the surface of the glasses prepared using the (T_{doping}-t) parameters.

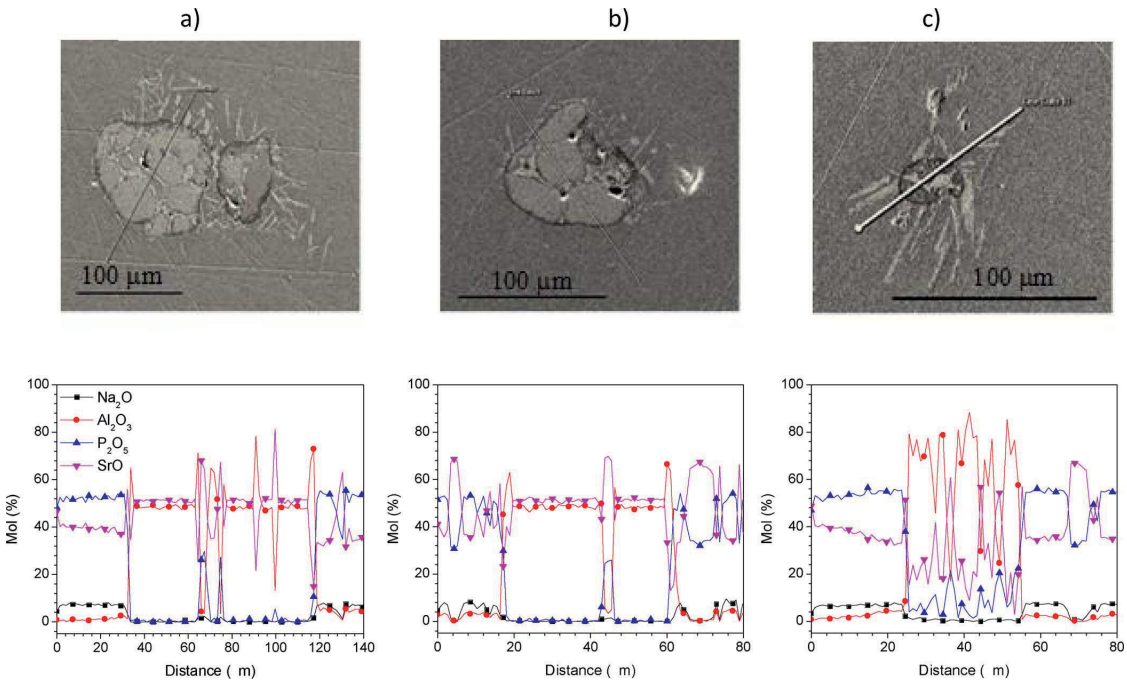

Fig. 6. SEM/EDS line profiles giving the elemental distribution across the MP diameter and interface with glasses prepared using (T_{doping} − t) parameters: a) (975 − 3), b) (1000 − 5) and c) (1025 − 10). The direction of scan starts at circle (corresponding to 0 µm).

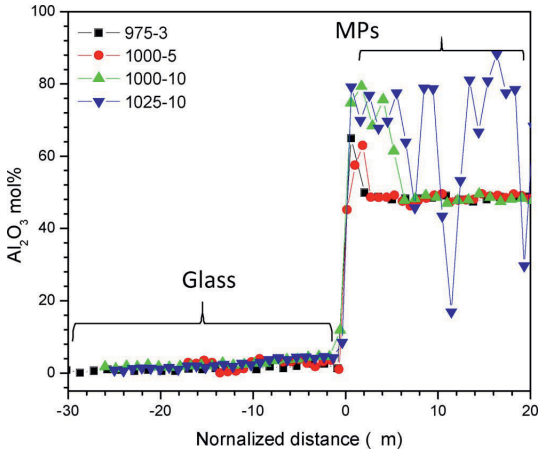

Fig. 7. Al_2O_3 concentration profile at the glass-MP interface. The glasses were prepared using (T_{doping} − t) parameters. Data are from Fig. 6 and are normalized to the glass-MP interface to compare the level of Al_2O_3 diffusion in the glasses.

was 1025 °C and to ~1.35 mm after immersion in the glass melts at 975 and 1000 °C. Therefore, with this corrosion test, we confirm that corrosion of the rod occurs already at 975 °C and is faster in glass melt with higher temperature in agreement with [10–12]. Finally, it is interesting to point out that Sr-rich phosphate crystals with a low amount of Na and Al were seen in the glasses quenched from the melts at 1000 and 1025 °C (Fig. 8d). It is possible to think that it is also the diffusion of the Al from the MPs in the glass, which induces the crystal formation.

4. Conclusion

In summary, the preparation and the characterization of phosphate glasses with uniform persistent luminescence was studied. The glasses were prepared by adding persistent luminescent microparticles with the composition $SrAl_2O_4:Eu^{2+},Dy^{3+}$ (MPs) in the melt under static condition. Using SEM and EDS, we found that the decomposition of the MPs occurs already when the glass is quenched 3 min after adding the MPs at 975 °C. The decomposition of the MPs in the glass melt leads to a decrease in the PeL properties due to changes in the Eu^{2+} site and also to the oxidation of Eu^{2+} to Eu^{3+}. A longer dwell time before casting the glass and a hotter doping temperature increase the MP decomposition, which leads to a significant reduction in the PeL properties of the phosphate glasses. The corrosive behavior of the glass melts was confirmed by investigating the corrosion process of an alumina tube in the glass melts: a reduction in the alumina tube diameter and the presence of Al_2O_3 contamination in the glasses were observed after immersing an alumina tube for 6 h in the glass melts.

Acknowledgment

LP would like to acknowledge the financial support of the Academy of Finland (Academy Project-308558).

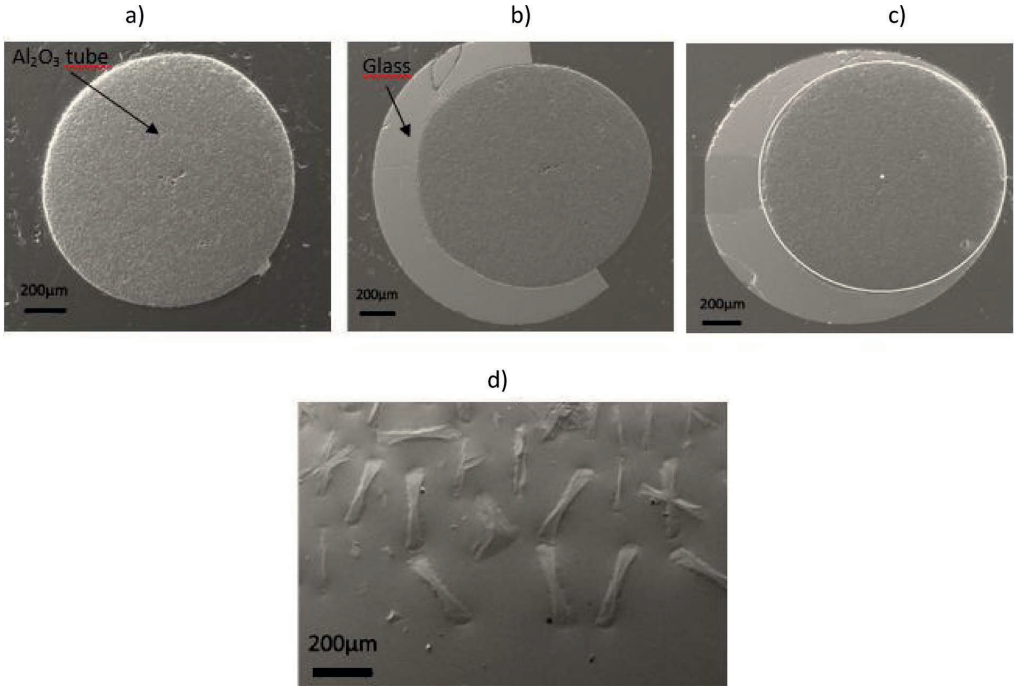

Fig. 8. SEM pictures of the alumina rods immersed for 6 h in the glass melt at 975 (a), 1000 (b) and 1025 °C (c) and of the crystals found in the glass quenched from the melt hold for 6 h at 1025 °C (d).

References

[1] T. Aitasalo, J. Hölsä, H. Jungner, M. Lastusaari, J. Niittykoski, Thermoluminescence study of persistent luminescence materials: eu^{2+}- and R^{3+}- doped calcium aluminates, $CaAl_2O_4:Eu^{2+}$, R^{3+}, J. Phys. Chem. B 110 (10) (2006) 4589–4598.

[2] C. Chang, Z. Yuan, D. Mao, Eu^{2+} activated long persistent strontium aluminate nano scaled phosphor prepared by precipitation method, J. Alloys Compd. 415 (2006) 220–224.

[3] T. Nakanishi, S. Tanabe, Preparation and luminescent properties of Eu^{2+}-activated glass ceramic phosphor precipitated with β-Ca_2SiO_4 and $Ca_3Si_2O_7$, Phys, Status Solidi A 206 (2009) 919–922.

[4] T. Nakanishi, Y. Katayama, J. Ueda, T. Honma, S. Tanabe, T. Komatsu, Fabrication of Eu:$SrAl_2O_4$ −based glass ceramics using Frozen sorbet method, J. Ceram. Soc. Jpn. 119 (2011) 609–615.

[5] T. Matsuzawa, Y. Aoki, N. Takeuchi, Y. Murayama, A new long phosphorescent phosphor with high brightness $SrAl_2O_4$: Eu^{2+}, Dy^{3+}, J. Electrochem. Soc. 143 (1996) 2670–2673.

[6] J. Massera, P. Głuchowski, M. Lastusaari, L.C.V. Rodrigues, L. Petit, J. Hölsä, L. Hupa, M. Hupa, New alternative route for the preparation of phosphate glasses with persistent luminescence properties, J. Eur. Ceram. Soc. 35 (2015) 1255–1261.

[7] H. Ebendorff-Heidepriem, Y. Ruan, H. Ji, A.D. Greentree, B.C. Gibson, T.M. Monro, Nanodiamond in tellurite glass Part I: Origin of loss in nanodiamond-doped glass, Opt. Mater. Express 4 (2014) 2608–2620.

[8] J. Zhao, X. Zheng, E.P. Schartner, P. Ionescu, R. Zhang, T.-L. Nguyen, D. Jin, H. Ebendorff-Heidepriem, Upconversion nanocrystals doped glass: a new paradigm for photonic materials, Adv. Opt. Mater. 4 (2016) 1507–1517.

[9] H. Nguyen, M. Tuomisto, J. Oksa, T. Salminen, M. Lastusaari, L. Petit, Upconversion in low rare-earth concentrated phosphate glasses using direct $NaYF_4$: Er^{3+} Yb^{3+} particles doping, Scr. Mater. 139 (2017) 130–133.

[10] J.K. Higgins, Studies of platinum and molybdenum electrodes in molten silicates, borates, and phosphates, J. Electrochem. Soc. 140 (1993) 3436–3448.

[11] J. Di Martino, C. Rapin, P. Berthod, R. Podor, P. Steinmetz, Corrosion of metals and alloys in molten glasses. Part 1: glass electrochemical properties and pure metal (Fe Co, Ni, Cr) behaviours, Corros. Sci. 46 (2004) 1849–1864.

[12] A. carton, C. Rapin, R. Podor, P. Berthod, Corrosion of Chromium in glass melts, J. Electrochem. Soc. 153 (2006) B121–B127.

[13] J. Massera, M. Gaussiran, P. Głuchowski, M. Lastusaari, L. Hupa, L. Petit, Processing and characterization of new phosphate glasses containing $CaAl_2O_4:Eu^{2+}$, Nd^{3+} and $SrAl_2O_4:Eu^{2+}$, Dy^{3+} microparticles, J. Eur. Ceram. Soc. 35 (14) (2015) 3863–3871.

[14] H. Yamamoto, T. Matsuzawa, Mechanism of long phosphorescence of $SrAl_2O_4:Eu^{2+}$ Dy^{3+} and $CaAl_2O_4:Eu^{2+}$, Nd^{3+}, J. Lumin. 72–74 (1997) 287–289.

[15] T. Aitasalo, J. Hölsä, H. Jungner, J.-C. Krupa, M. Lastusaari, J. Legendziewicz, J. Niittykoski, Effect of temperature on the luminescence processes of $SrAl_2O_4:Eu^{2+}$, Radiat. Meas. 38 (2004) 727–730.

[16] J. Massera, M. Mayran, J. Rocherulle, L. Hupa, Crystallization behavior of phosphate glasses and its impact on the glasses' bioactivity, J. Mater. Sci. 50 (2015) 3091–3102.

PUBLICATION II

Influence of the phosphate glass melt on the corrosion of functional particles occurring during the preparation of glass-ceramics

N. Ojha, T. Laihinen, T. Salminen, M. Lastusaari and L. Petit

Ceramics International, Vol. 44, Issue 10, pp.11807-11811
https://doi.org/10.1016/j.ceramint.2018.03.267

Ceramics International 44 (2018) 11807–11811

Contents lists available at ScienceDirect

Ceramics International

journal homepage: www.elsevier.com/locate/ceramint

Influence of the phosphate glass melt on the corrosion of functional particles occurring during the preparation of glass-ceramics

N. Ojha[a], T. Laihinen[b], T. Salminen[a], M. Lastusaari[b,c], L. Petit[a,*]

[a] Laboratory of Photonics, Tampere University of Technology, FI-33101 Tampere, Finland
[b] Department of Chemistry, University of Turku, FI-20014 Turku, Finland
[c] Turku University Centre for Materials and Surfaces (MatSurf), Turku, Finland

ARTICLE INFO

Keywords:
Phosphate glass-ceramics
Glass melt
$Sr_4Al_{14}O_{25}:Eu^{2+}$, Dy^{3+} microparticles
Corrosion
Direct doping method

ABSTRACT

We report our findings on the impact of the glass composition on the corrosion of microparticles occurring during the preparation of glass-ceramics using the direct doping method. Microparticles (MPs) with the composition $Sr_4Al_{14}O_{25}:Eu^{2+},Dy^{3+}$ with blue-green persistent luminescence were chosen as the changes in their spectroscopic properties can be related to the MPs' corrosion. The MPs were added in phosphate-based glasses with different compositions. When using the same doping parameters, the glass system with the composition $90NaPO_3$-$10Na_2O$ (mol%) was found to be the least corrosive on the MPs whereas the glass system with the composition $90NaPO_3$-10NaF (mol%) is the most corrosive on the MPs probably due to their different viscosity at 575 °C, the temperature at which the MPs are added in the glass melts.

1. Introduction

The corrosion behavior of glass melts has been studied since late 1950s [1] but the studies have been focused mainly on the behavior of pure metals in glass melts such as Pt [2] and Fe [3]. The behavior of pure metals immersed in molten glasses was found to depend on the glass composition and melt temperature [1]. One of the most important parameters when studying the corrosion behavior of glass melts was reported to be the glass temperature: while an increase in the glass temperature increases the fluidity of the glass, it also decreases the mechanical properties of the alloy and so its corrosion resistance [4]. The investigation of the corrosion of other materials in different glass melts is of great interest as it brings new knowledge on the corrosion behavior of glass melts.

Additionally, the study of the corrosion behavior of the glass melts could bring useful knowledge when preparing new glass-ceramics using direct doping method. Recently, we showed that although phosphate glasses have a large phonon energy, which is disadvantageous to the upconversion (UC) emission [5], UC was obtained from phosphate glasses within the glass system ($90NaPO_3$-(10-x)Na_2O-xNaF) (mol%) using a low amount of Er^{3+} and Yb^{3+} [6]. Such UC materials allow the conversion of longer wavelength radiation to shorter wavelength radiation due to the absorption of two or more photons [7]. These glasses were prepared by adding $NaYF_4:Yb^{3+}$, Er^{3+} nanoparticles (NPs) in the glass melt using the direct doping method. We explained that the fraction of NP's survival during the glass preparation can be augmented when replacing Na_2O with NaF in the glass. Therefore, to improve the spectroscopic properties of such glass-ceramics for UC application for example, it is crucial to study the corrosive behavior of the glass melt in order to limit the corrosion of the particles occurring during the glass preparation. Here, the corrosion of the particles refers to their decomposition in the glass.

In this paper, glass-ceramics with different compositions (and so with different melting temperatures) were prepared in order to investigate the impact of the glass composition on the corrosion of the particles. $Sr_4Al_{14}O_{25}:Eu^{2+},Dy^{3+}$ microparticles (MPs) were used for this study as they emit blue-green persistent luminescence after the removal of a UV excitation source [8]. This emission can last from seconds to hours after the light source is removed. Such persistent luminescent materials were reported for the first time in the mid 1990's [9]. In these MPs, Eu^{2+} is used as the luminescent center and Dy^{3+} as a co-dopant [10].

Here, we correlate the changes in the spectroscopic properties of the glass-ceramics to the corrosion of the particles occurring during the glass preparation. First, we explain how the direct doping method is optimized when preparing new glass-ceramic with the composition $50P_2O_5$-$10Na_2O$-40CaO (mol%). Then we compare the spectroscopic properties of the MPs when added in different phosphate-based glasses using the direct doping method. Finally, to confirm the corrosive behavior of the glass melts on the MPs, we investigate the corrosion

* Corresponding author.
E-mail address: laeticia.petit@tut.fi (L. Petit).

https://doi.org/10.1016/j.ceramint.2018.03.267
Received 9 January 2018; Received in revised form 22 March 2018; Accepted 29 March 2018
Available online 31 March 2018

process of an alumina rod in the different investigated glass melts.

2. Experimental procedure

The glass-ceramics with the composition $50P_2O_5$-$10Na_2O$-40CaO/SrO (mol%) (labeled as CaNaP and SrNaP, respectively) and ($90NaPO_3 - (10 - x)Na_2O - xNaF$) (mol%) (labeled as NaPF0 and NaPF10 respectively when x = 0 and 10) were prepared using direct doping method. $NaPO_3$ (Thermo Fisher Scientific, 99.0%), Na_2CO_3 (Sigma Aldrich, > 99.5%), $SrCO_3$ (Sigma Aldrich, 99.9%) $CaCO_3$ (Thermo Fisher Scientific, 99.0%), NaF (Sigma Aldrich, 99.99%) and $(NH_4)_2HPO_4$ (VWR, 98.0%) were used as the starting raw materials. $Ca(PO_3)_2$ and $Sr(PO_3)_2$ precursors were first independently prepared from mixtures of the $CaCO_3$ and $(NH_4)_2HPO_4$ and of the $SrCO_3$ and $(NH_4)_2HPO_4$, respectively. Prior to the melting, the NaPF0 glass was treated at 300 °C for 15 min to decompose Na_2CO_3 and evaporate CO_2. 1 wt% of commercial $Sr_4Al_{14}O_{25}:Eu^{2+},Dy^{3+}$ MPs (Jinan G.L. New Materials, China, BG-01) was added at a specific doping temperature (called doping temperature (T_{doping})) in the 10 g glass melted batches. The glass melts were, then, quenched after 3–10 min after adding the MPs (called dwell time) and after manual stirring to improve the dispersion of the MPs within the glass melts. Finally, all the MPs-containing glasses were annealed at 40 °C below their respective glass transition temperature for 8 h in air.

As explained in [6], the doping temperature and dwell time depend on the glass composition. The direct doping process of the glass-ceramics of the NaPF0 and NaPF10 can be found in [6] and of the SrNaP glass in [11]. The NaPF0 and NaPF10 glasses were melted at 750 °C for 5 min, then the MPs were added at 575 °C and finally the glass melts were quenched after a dwell time of 3 min. After melting the SrNaP glass at 1050 °C for 20 min, the MPs were added at 1000 °C and the glass melt was quenched after a dwell time of 5 min. The CaNaP glasses were melted at 1100 °C for 20 min. The MPs were added at 1000, 1025 and 1050 °C and the dwell time was varied between 3 and 10 min.

A scanning electron microscope (Carl Zeiss Crossbeam 540) equipped with Oxford Instruments X-Max^N 80 EDS detector was used to image and analyze the composition of the samples. The polished glass-ceramics were coated with a thin carbon layer before EDS mapping. The accuracy of the elemental analysis was ± 1.5 mol%.

The persistent luminescence properties of the crushed MPs-containing glasses were measured at room temperature using a Varian Cary Eclipse Fluorescence Spectrophotometer equipped with a Hamamatsu R928 photomultiplier (PMT). The samples were irradiated for 5 min at room temperature with a compact UV lamp (UVGL-25, 4 W, λ_{exc}: 254 nm). The persistent luminescence spectra were recorded 1 min after ceasing the irradiation with a 4 s data collection time. The conventional luminescence (λ_{exc}: 266 nm, Nd: YAG pulse laser, 8 ns, TII Lotis) was measured at room temperature using a CCD spectrometer (Avantes, AvaSpec-2048x14).

3. Results and discussion

Different phosphate glass-ceramics showing persistent luminescence (PeL) were prepared using direct doping method by adding commercial $Sr_4Al_{14}O_{25}:Eu^{2+},Dy^{3+}$ microparticles (MPs) in the glass melt prior to quenching. Such MPs exhibit a blue-green persistent emission after stopping UV irradiation. We compare here the spectroscopic properties of the glass-ceramics and we correlate them to the corrosion of the MPs occurring during the glass preparation. Before discussing the impact of the glass composition on the corrosion of the MPs, which leads to a degradation in the persistent luminescence of the different glass-ceramics, we first explain how the glass-ceramics were prepared using the direct doping method which has to be optimized for each glass system.

As explained in [12], the MPs need to be added in the glass batch at lower temperature than the melting temperature in order to balance the survival and dispersion of the MPs. The doping temperature (T_{doping}) and the dwell time prior to quenching the glass are the two main parameters to identify in order to optimize the direct doping process [6]. The T_{doping} and the dwell time were reported at 575 °C and 3 min for the NaPF0 and NaPF10 glasses [6] and at 1000 °C and 5 min for the SrNaP glass [11]. Here, we explain how these two doping parameters were optimized for the CaNaP glass system.

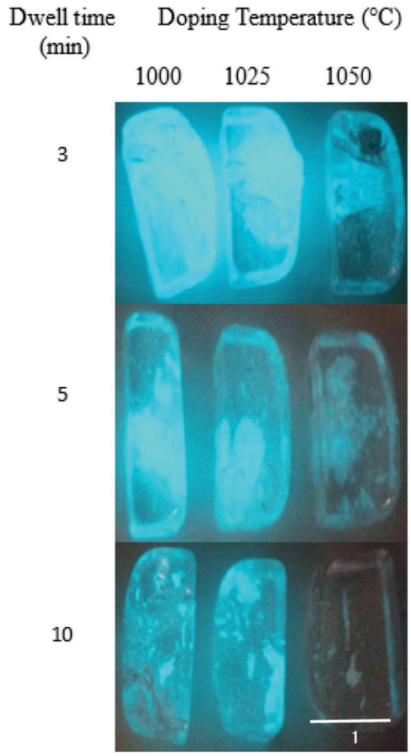

Fig. 1. Pictures of the PeL CaNaP glass-ceramics taken just after stopping the UV irradiation.

The afterglow pictures of the CaNaP glass-ceramics prepared using different T_{doping} and dwell time after stopping UV irradiation are depicted in Fig. 1. All CaNaP glass-ceramics exhibit blue-green persistent luminescence (PeL). As the MPs-free glass used in this study does not exhibit PeL, the PeL seen from the MPs-containing glasses is a clear sign of the survival of MPs in the glass-ceramics. One can notice that the PeL intensity depends on the direct doping parameters: the higher T_{doping} and the longer dwell time, the less intense emission from the glass-ceramics. Some aggregates of MPs can also be seen, the number and size of which depend on the direct doping parameters: the size of the MP aggregates decreases as the dwell time increases independently of the T_{doping}. Additionally, large aggregates of MPs can be seen when using T_{doping} of 1000 °C indicating that the glass melt at this temperature is too viscous for the MPs to disperse homogeneously.

The normalized conventional (PL) and persistent luminescence (PeL) properties of some glass-ceramics, taken as examples, are depicted respectively in Fig. 2a and b. The normalized PL spectra of the glass-ceramics, presented in Fig. 2a, exhibit two bands in the 350–575 nm range, the ratio of which depends on the melting conditions: an increase in the T_{doping} and dwell time decreases the intensity of the band at 488 nm as compared to that of the band at 425 nm. Those bands can be related to the luminescence of Eu^{2+} located in two different cation sites in the $Sr_4Al_{14}O_{25}$ structure [11,13]. Therefore, an increase in the T_{doping} and dwell time changes the sites of Eu^{2+} in the

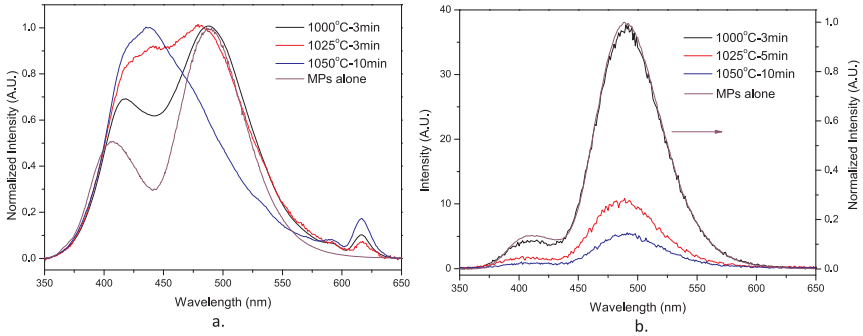

Fig. 2. Normalized conventional luminescence (PL) (a) and persistent luminescence (PeL) (b) spectra of the CaNaP glass-ceramics prepared using different (T_{doping} and dwell time) and of the MPs alone. In (b), the PeL spectrum of the MPs alone is normalized.

$Sr_4Al_{14}O_{25}$ structure. According to our previous studies [11,14,15], this change in the Eu^{2+} sites could be related to the diffusion of the MPs elements (Al, Sr, Eu and Dy) to the glass. The diffusion of Eu^{2+} to the glass is also suspected from the presence of the emission bands at ~ 590 and 615 nm, which are not present in the PL spectra of the MPs alone. These bands can be related to the emission from Eu^{3+} ions [15]. As explained in [11,14,15], the Eu^{2+} are suspected to be oxidized into Eu^{3+} when diffusing in the glass. One can notice that the intensity of the bands at ~ 590 and 615 nm is the largest in the spectrum of the (1050 °C-10 min) glass-ceramic indicating that an increase in the T_{doping} and dwell time increases the amount of Eu^{2+} oxidizing into Eu^{3+} in the glass. Although the glass should be melted or heated under a highly reduced atmosphere in order to reduce Eu^{3+} ions to Eu^{2+} ions [16], the coexistence of both Eu^{3+} and Eu^{2+} ions was found in some glasses melted in normal atmosphere [17,18]. Therefore, it is possible to consider that some Eu^{2+} remain in the glass. The PL emission in the region 400–450 nm could, then, come not only from the Eu^{2+} in the MPs but also from the Eu^{2+} present in the glass matrix due to the MPs decomposition.

The PeL spectra of the glass-ceramics exhibit a strong band centered at 490 nm and a weak one at 410 nm which are due to the $4f^65d^1 \rightarrow 4f^7$ transition of Eu^{2+} ions located in two different cation sites in the $Sr_4Al_{14}O_{25}$ structure [13]. The intensity of these bands decreases significantly with an increase in the T_{doping} and the dwell time in agreement with the afterglow picture of the glass-ceramics. However the ratio in intensity of the two PeL bands in the PeL of the glasses does not really change when the site of Eu^{2+} is modified, as the structure (defects and host matrix) needs to remain intact for the MPs to exhibit PeL. If other different kinds of environments are created for the sites of Eu^{2+}, it is most probable that there will not be suitable energy storage sites available for PeL in the vicinity.

SEM/EDS was used to image the morphology and to analyze the composition of the MPs. As seen in Fig. 3, an increase in T_{doping} and dwell time leads to MPs with different morphologies and compositions: the MPs retain their morphology and their compositional integrity when using a 1000 °C doping temperature and 3 min dwell time whereas they don't maintain their composition when using a 1050 °C T_{doping} and 10 min dwell time. As seen in our previous studies [14,15], the outermost layer of the MPs contain more Al and less Sr than the inner parts confirming the diffusion of the MPs' elements into the glass which leads to changes in the Eu^{2+} sites. Finally, we noticed that the MPs' size (and most probably the volume of the emitting particles) decreases with an increase in T_{doping} and dwell time confirming the corrosion of the MPs during the glass preparation. Therefore, it is clear that the PL spectra of the glass-ceramics can be used to check if corrosion of the MPs occurred during the glass melting process in agreement with [11]: a low intensity of the band at 488 nm compared to the band at 415 nm can be associated with the corrosion of MPs.

In summary, from the afterglow picture and the spectroscopic properties of the glass-ceramics, the CaNaP glass-ceramics should be prepared using a T_{doping} of 1025 °C and a 5 min dwell time to balance the survival and the dispersion of the MPs in the glass.

To understand the impact of the glass melts on the corrosion of the MPs occurring during the glass preparation, MPs were added in phosphate-based glasses with different compositions. The pictures of the MPs-containing glasses after stopping UV irradiation are shown in Fig. 4. As seen in Fig. 1, all the glass-ceramics exhibit a blue-green PeL, the intensity of which depends on the glass composition: intense PeL can be seen from the SrNaP and NaPF0 glass-ceramics whereas almost no PeL could be seen in the NaPF10 glass-ceramic. It is clear from this afterglow picture that the corrosion of the MPs is not related to the glass melt temperature as a T_{doping} of 575 °C was used to prepare the glass with x = 10 while a T_{doping} of 1000 °C was used to prepare the SrNaP glass. From Fig. 5a, we confirm that the SrNaP and NaPF0 glass-ceramics exhibit the strongest PeL while the NaPF10 glass-ceramic exhibits the least intense PeL. As seen in Fig. 5b, the intensity of the band at 488 nm is more intense than the band at 415 nm in the spectrum of the NaPF0 glass-ceramic indicating that small changes in the Eu^{2+} sites occur during the preparation of this glass. Therefore, the MPs are suspected to be the least corroded in this NaPF0 glass system. From the shape of the PL emission band, we suspect that some corrosion of the MPs occurs in the SrNaP and CaNaP glass systems whereas the MPs are suspected to be strongly corroded in NaPF10 glass system. It should be pointed out that the NaPF0 and NaPF10 glass-ceramics were prepared using the same T_{doping} (575 °C). However, the replacement of Na_2O by NaF is expected to lead to a decrease in the thermal properties (such as glass transition and crystallization temperatures as well as viscosity) according to [19]. Therefore, the viscosity of the melt at 575 °C is thought to be lower for the NaPF10 melt than for the NaPF0 melt, which probably enhances the corrosion of the MPs. Therefore, it is crucial to investigate the impact of the glass composition (the replacement of Na_2O by NaF) on the thermal properties of the glass and on the optimization of the direct particles doping process. This study is ongoing and will be published separately.

The impact of the glass composition on the corrosion of the MPs was also confirmed by investigating the corrosion process of an alumina rod in the glass melt as performed in [1,11]. An alumina rod with a 1.6 mm diameter from AdValue Technology was immersed in the 4 glass melts held at their respective doping temperature. After 6 h in the glass melts, the rods were removed from the crucibles. They were, then embedded in epoxy and finally polished for analyzing. The diameter of the alumina rod was found to decrease to 1.45, 1.35, 1.48, and 1.31 mm after immersion in SrNaP, CaNaP, NaPF0 and NaPF10 melts, respectively. The Al_2O_3 contamination from the rod at the glass-rod interface was quantified using EDS. As seen in Fig. 6, the level of Al_2O_3 at the glass-rod interface is the largest in the CaNaP and NaPF10 melts. Therefore,

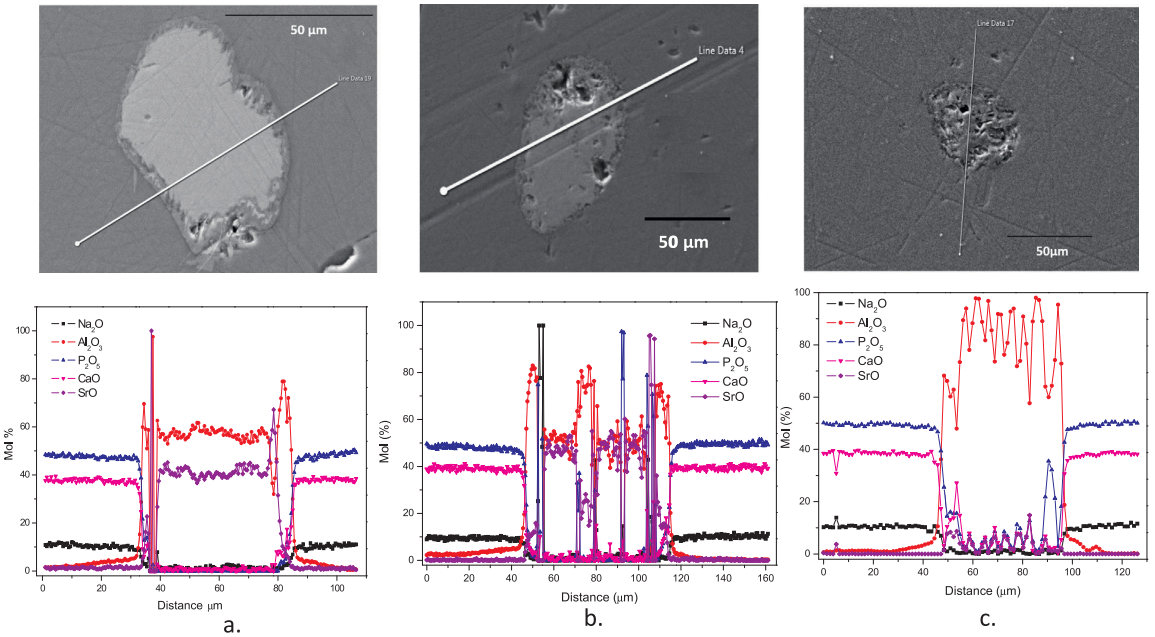

Fig. 3. SEM/EDS line profiles giving the elemental distribution along the diameter of a MP found at the surface of the glass-ceramics prepared using the T_{doping} and dwell time of 1000 °C-3 min (a), 1025 °C-5 min (b), 1050 °C-10 min (c).

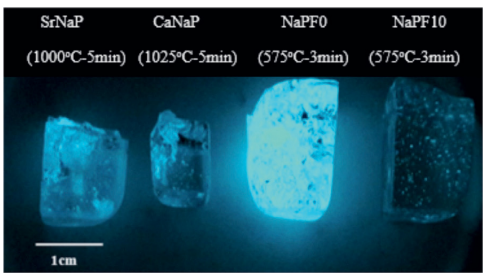

Fig. 4. Pictures of the investigated PeL glass-ceramics with the different compositions.

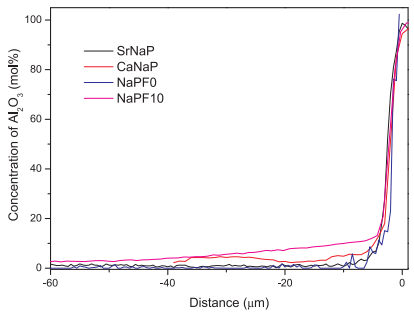

Fig. 6. Al_2O_3 concentration profile measured at the rod-glass interface after immersion of the alumina rod in the glass melts with different compositions.

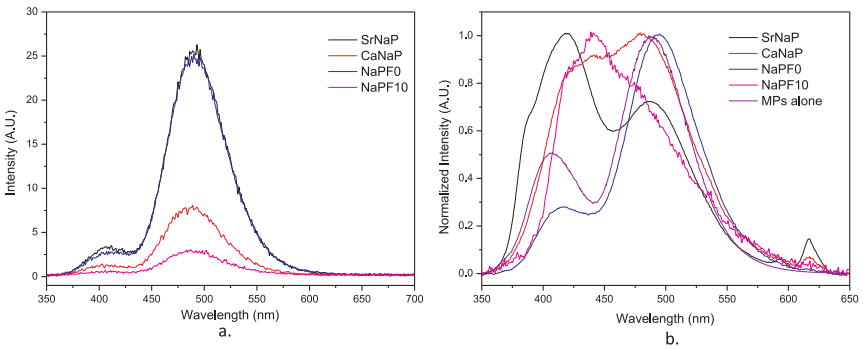

Fig. 5. Persistence luminescence (PeL) (a) and conventional luminescence (PL) (b) spectra of the PeL glass-ceramics with the different compositions.

the reduction of the alumina rod diameter can be related to the Al_2O_3 mol% found in the glass-rod interface. With this corrosion test, we confirm the strong corrosive behavior of the CaNaP and NaPF10 glass melts on the alumina rod, which is in agreement with the strong corrosion of the MPs observed when added in these glass melts. Therefore, this corrosion test could be used to estimate the level of MP corrosion in different glass melts, prior to the preparation of new glass-ceramics using the direct particles doping method.

4. Conclusion

In summary, the corrosion behavior of different phosphate-based glass melts on the microparticles with the composition $SrAl_2O_4:Eu^{2+},Dy^{3+}$ (MPs) was investigated. Corrosion of the MPs is suspected to depend not only on the temperature of the melt at which the MPs are added (T_{doping}) but also on the glass melt composition: the MPs were found to be the most corroded in the glass with the composition ($90NaPO_3$-10NaF) (mol%) and the least corroded in the glass with the composition ($90NaPO_3$-$10Na_2O$) (mol%) although these 2 glass-ceramics were prepared using the same T_{doping} of 575 °C. However, the viscosity of the melt at 575 °C is expected to be lower for the glass with the composition ($90NaPO_3$-10NaF) than for the glass with the composition ($90NaPO_3$-$10Na_2O$) which probably enhances the MP corrosion in the ($90NaPO_3$-10NaF) glass. Therefore, prior to comparing the MP decomposition in glasses, it is crucial first to optimize the direct doping process for each glass so the MP decomposition is limited while ensuring in the same time the MP dispersion in the glass.

We confirm that the conventional luminescence spectra can be used to check if corrosion of the MPs occurred during the glass melting. The corrosive behavior of the glass melts was confirmed by investigating the corrosion process of an alumina rod in the glass melts: a reduction of the alumina rod diameter and the presence of Al_2O_3 contamination in the glasses were observed after immersing an alumina rod for 6 h in the glass melts held at their respective doping temperature.

Surprisingly, in our previous study [6], we showed that $NaYF_4$:Yb,Er particles are less corroded when added in the $90NaPO_3$-10NaF glass than in the $90NaPO_3$-$10Na_2O$ glass. Therefore, our study suggests that the corrosion of particles in glass melts also depends on the composition of the particles.

Acknowledgment

LP would like to acknowledge the financial support of the Academy of Finland (Academy Project-308558).

References

[1] A. Carton, C. Rapin, R. Podor, P. Berthod, Corrosion of chromium in glass melts, J. Electrochem. Soc. 153 (2006) B121–B127.
[2] J.K. Higgins, Studies of platinum and molybdenum electrodes in molten silicates, borates, and phosphates, J. Electrochem. Soc. 140 (1993) 3436–3448.
[3] J. Di Martino, C. Rapin, P. Berthod, R. Podor, P. Steinmetz, Corrosion of metals and alloys in molten glasses. Part 1: glass electrochemical properties and pure metal (Fe, Co, Ni, Cr) behaviours, Corros. Sci. 46 (2004) 1849–1864.
[4] S. Michon, P. Berthod, L. Aranda, C. Rapin, R. Podor, P. Steinmetz, Application of thermodynamic calculations to study high temperature behavior of TaC-strengthened Co-base superalloys, CALPHAD: Comput. Coupling Phase Diagr. Thermochem. 27 (2003) 289.
[5] C. Ming, F. Song, H. Liu, Intense blue up-conversion emission in Tm^{3+}/Yb^{3+} co-doped phosphate glass, J. Non-Cryst. Solids 360 (2013) 1–3.
[6] H. Nguyen, M. Tuomisto, J. Oksa, T. Salminen, M. Lastusaari, L. Petit, Upconversion in low rare-earth concentrated phosphate glasses using direct $NaYF_4:Er^{3+},Yb^{3+}$ particles doping, Scr. Mater. 139 (2017) 130–133.
[7] F. Auzel, Upconversion and anti-Stokes processes with f and d ions in solids, Chem. Rev. 104 (2004) 139–173.
[8] T. Aitasalo, J. Hölsä, H. Jungner, M. Lastusaari, J. Niittykoski, Thermoluminescence study of persistent luminescence materials: Eu^{2+}- and R^{3+}-doped calcium aluminates, $CaAl_2O_4:Eu^{2+},R^{3+}$, J. Phys. Chem. B 110 (10) (2006) 4589–4598.
[9] S. Shionoya, W.M. Yen (Eds.), Phosphor Handbook, CRC Press, Boca Raton, FL, USA, 1999, p. 651.
[10] T. Matsuzawa, Y. Aoki, N. Takeuchi, Y. Murayama, A new long phosphorescent phosphor with high brightness, $SrAl_2O_4:Eu^{2+},Dy^{3+}$, J. Electrochem. Soc. 143 (1996) 2670–2673.
[11] N. Ojha, H. Nguyen, T. Laihinen, T. Salminen, M. Lastusaari, L. Petit, Decomposition of persistent luminescent microparticles in corrosive phosphate glass melt, Corros. Sci. 135 (2018) 207–214.
[12] J. Zhao, X. Zheng, E.P. Schartner, P. Ionescu, R. Zhang, T.-L. Nguyen, D. Jin, H. Ebendorff-Heidepriem, Upconversion nanocrystals doped glass: a new paradigm for photonic Materials, Adv. Opt. Mater. 4 (2016) 1507–1517.
[13] E. Nakazawa, Y. Murazaki, S. Saito, Mechanism of the persistent phosphorescence in $Sr_4Al_{14}O_{25}$:Eu and $SrAl_2O_4$:Eu codoped with rare earth ions, J. Appl. Phys. 100 (2006) 113113.
[14] J. Massera, P. Głuchowski, M. Lastusaari, L.C.V. Rodrigues, L. Petit, J. Hölsä, L. Hupa, M. Hupa, New alternative route for the preparation of phosphate glasses with persistent luminescence properties, J. Eur. Ceram. Soc. 35 (2015) 1255–1261.
[15] J. Massera, M. Gaussiran, P. Głuchowski, M. Lastusaari, L.C.V. Rodrigues, L. Petit, J. Hölsä, L. Hupa, Effect of the glass melting condition on the processing of phosphate-based glass-ceramics with persistent luminescence properties, Opt. Mater. 52 (2016) 56–61.
[16] K. Fujita, K. Hirao, N. Soga, Room-temperature persistent spectral hole burning of Eu^{3+} in sodium aluminosilicate glasses, Opt. Lett. 23 (1998) 543.
[17] M. Nogami, T. Kawaguchi, A. Yasumori, Spectral hole burning of Eu^{3+} doped Al_2O_3-SiO_2 glass prepared by melt quenching, Opt. Commun. 193 (2001) 237.
[18] Q. Zeng, Z. Pei, S. Wang, Q. Su, The reduction of Eu^{3+} in SrB_6O_{10} prepared in air and the luminescence of SrB_6O_{10}:Eu, J. Alloy. Compd. 275–277 (1998) 238.
[19] S. Cui, J. Massera, M. Lastusaari, L. Hupa, L. Petit, Novel oxyfluorophosphate glasses and glass-ceramics, J. Non-Cryst. Solids 445 (2016) 40–44.

PUBLICATION III

Upconversion from fluorophosphate glasses prepared with $NaYF_4$: Er^{3+}, Yb^{3+} nanocrystals

N. Ojha, M. Tuomisto, M. Lastusaari and L. Petit

RSC Advances, Vol. 8, Issue 34, pp. 19226-19236
https://doi.org/10.1039/C8RA03298J

RSC Advances

PAPER

View Article Online
View Journal | View Issue

Cite this: *RSC Adv.*, 2018, **8**, 19226

Upconversion from fluorophosphate glasses prepared with $NaYF_4:Er^{3+},Yb^{3+}$ nanocrystals

N. Ojha,[a] M. Tuomisto,[b] M. Lastusaari[bc] and L. Petit*[a]

Received 17th April 2018
Accepted 17th May 2018

DOI: 10.1039/c8ra03298j

rsc.li/rsc-advances

The direct doping method was applied to fabricate upconverter fluorophosphate glasses in the system $(90NaPO_3\text{-}(10\text{-}x)Na_2O\text{-}x NaF)$ (mol%) by adding $NaYF_4:Er^{3+},Yb^{3+}$ nanocrystals. An increase in the network connectivity, a red shift of the optical band gap and a decrease in the thermal properties occur when Na_2O is progressively replaced by NaF. To ensure the survival and the dispersion of the nanocrystals in the glasses with $x = 0$ and 10, three doping temperatures (T_{doping}) (525, 550 and 575 °C) at which the nanocrystals were added in the glass melt after melting and 2 dwell times (3 and 5 minutes) before quenching the glasses were tested. Using 5 wt% of the $NaYF_4:Er^{3+},Yb^{3+}$ nanocrystals, green emission from the $NaYF_4:Er^{3+},Yb^{3+}$ nanocrystals-containing glasses was observed using a 980 nm pumping, the intensity of which depends on the glass composition and on the direct doping parameters (T_{doping} and dwell time). The strongest upconversion was obtained from the glass with $x = 10$ prepared using a T_{doping} of 550 °C and a 3 min dwell time. Finally, we showed that the upconversion, the emission at 1.5 μm and of the transmittance spectra of the nanocrystals-containing glasses could be measured to verify if decomposition of the nanocrystals occurred in glass melts during the preparation of the glasses.

Introduction

Upconversion (UC) luminescent materials have been intensively investigated in recent decades as they can find applications in various fields such as solar cells, color displays, solid-state lasers, bioassays, biological imaging and remote photoactivation just to cite a few.[1–10] The codoping with Er^{3+} and Yb^{3+} allows the conversion of NIR radiation usually to green and red emissions due to the absorption of two or more photons. As Yb^{3+} ion possesses a high absorption cross-section and also a broad absorption band between 850 and 1080 nm compared to the weak absorption of Er^{3+} ions, it absorbs the pump energy which is then transferred to the Er^{3+} ion as ref. 4.

A suitable host glass should be carefully chosen in order to achieve highly efficient upconversion emission.[5] Due to their high phonon energies, oxide glasses such as silicate and borate glasses exhibit low upconversion. In such glasses, the relaxation occurs through multi-phonon relaxation. Oxyfluoride glass-ceramics (GCs) appear to be ideal for upconversion luminescence because they possess the advantages of both the fluorides and the oxides: low-phonon-energy of fluoride crystals and the desirable chemical and mechanical properties of oxide glasses.[11,12] The GCs are polycrystalline materials with one or more crystalline phases embedded in a glass phase. They are obtained from the heat treatment of the parent glass. The GCs possess negligible or even zero porosity. Compared to sintered ceramics, they possess a large number of advantages: superior uniformity and reproducibility, possibility of fabricating complex shapes.[13] In order to observe an enhancement of the upconversion in the oxyfluoride GCs as compared to the parent glasses, the heat treatment should lead to the formation of rare-earth containing fluoride crystals embedded in the glass.

Studies have been focused on the fabrication of glass-ceramics containing $NaYF_4$ as this crystal is one of the most efficient fluoride crystals. This crystal possesses low phonon energies (<350 cm^{-1}) reducing the energy losses at the intermediate states of lanthanide ions.[14] $NaYF_4$ nanocrystals are generally synthesized *via* routes such as molten salt, solvothermal, sol–gel and hydrothermal methods.[15] $NaYF_4$ nanocrystals were also found to precipitate in glasses within the glass system SiO_2–Al_2O_3–Na_2O–NaF–YF_3–ErF_3–YbF_3 after heat-treatment.[16,17] However, it was found recently, that the crystal growth of $NaYF_4$ in this glass system is limited by the duration of the heat treatment. Crystal size was reported to be between 9 and 12 nm when heat treating the glass at 560 °C.[18] It is known that the structure of the glass has a significant impact on the crystallization species, crystal size, crystal shapes and the distance among the particles. However, there is no report, to the best of our knowledge, on the precipitation of $NaYF_4$ nanocrystals in phosphate glass upon heat treatment.

Recently, we reported in[19] our latest achievement on the preparation of $NaYF_4:Er^{3+},Yb^{3+}$ nanocrystals containing phosphate glasses within the $NaPO_3$–Na_2O glass system. Because of

[a]*Laboratory of Photonics, Tampere University of Technology FI-33101 Tampere, Finland. E-mail: laeticia.petit@tut.fi*

[b]*University of Turku, Department of Chemistry, FI-20014 Turku, Finland*

[c]*Turku University Centre for Materials and Surfaces (MatSurf), Turku, Finland*

the low dissolution point (750 °C) of the nanocrystals, the glasses could be only obtained using direct particles doping method.[20] The concept of this method is based on using glass matrices with lower melting temperatures than those of the admixed nanoparticles. Using this method, we found that it is possible to increase the upconversion intensity from the $NaYF_4$:Er^{3+},Yb^{3+} nanocrystals containing phosphate glasses by replacing Na_2O by NaF in the glass matrix.

In this paper, more information about the choice of the glass matrix are provided. We explain how the direct particles doping method can be optimized to further enhance the upconversion properties of phosphate glasses with the composition ($90NaPO_3$-$(10\text{-}x)Na_2O$-xNaF) (mol%).

Experiment

The glasses with the composition ($90NaPO_3$-$(10\text{-}x)Na_2O$-xNaF) (mol%) with x varying from 0 to 10 were prepared using a standard melting process in a quartz crucible using $Na_6O_{18}P_6$ (Alfa-Aesar, technical grade), Na_2CO_3 (Sigma-Aldrich, >99.5%) and NaF (Sigma-Aldrich, 99.99%). Prior to the melting, the glass with $x = 0$ was treated at 300 °C for 30 min to decompose Na_2CO_3 and evaporate CO_2. The nanocrystals-free glasses were melted at 750 °C for 5 min. The nanocrystals-containing glasses were prepared by adding, after melting the glasses at 750 °C, 5 weight-% of $NaYF_4$:Er^{3+}, Yb^{3+} at a lower temperature (T_{doping}). After 3 or 5 min (dwell time) and manual stirring to improve the dispersion of the MPs within the glass melts, the glasses were poured onto a brass mold. The glasses are labelled as (T_{doping}-dwell time). All the glasses were annealed at 40 °C below their respective glass transition temperature for 8 h in air. The nanocrystals (NCs) under investigation were $NaYF_4$:Er^{3+},Yb^{3+}, the synthesis of which can be found in.[21] The nanocrystals were synthetized with 3 at% Er^{3+} and 17 at% Yb^{3+}.

The density was measured by utilizing Archimedes principle, using ethanol as the immersion liquid. The accuracy of the measurement is ± 0.02 g cm^{-3}.

Differential Thermal Analysis of all the glasses was done using DTA, Netzch Jupiter F1 at a heating rate of 10 °C min^{-1}. The analysis was carried out in Pt crucibles with 50 ml min^{-1} flow of N_2. The glass transition temperature T_g was calculated as the inflection point of the endotherm obtained as the first derivative of the DTA curve. The onset of crystallization temperature T_x and the crystallization temperature T_p were ascertained from the beginning of the crystallization feature, and peak of the exotherm, respectively. All the temperatures were obtained with an accuracy of $\pm$ 3 °C. The hot processing window ΔT was obtained as the difference between T_x and T_g.

A beam-bending viscometer (BBV) was used to measure the viscosity in the (log 11–log 13 Pa s) range. The measurement was conducted under the test protocol ASTM C-1351M. The glasses were cut in 4 × 5 × 50 mm bars. The glass viscosity in the softening range (log 5–log 8 Pa s) was measured using a parallel-plate viscometer, Model PPV-1000 following the test protocol ASTM C-1351M. In this test, the glasses were prepared in disk with a diameter of 10 mm and a thickness of 5 mm.

The IR spectra of the glasses were analyzed using Perkin Elmer Spectrum One FTIR Spectrophotometer in Attenuated Total Reflectance (ATR) mode in the range of 600–1600 cm^{-1}. The spectra are normalized to the band having maximum intensity. All presented spectra are an average of 8 scans and have a resolution of 1 cm^{-1}.

The Raman spectra were recorded using a 532 nm wavelength laser (Cobolt Samba) and measured with a 300 mm spectrograph (Andor Shamrock 303) and a cooled CCD camera for data collection (Andor Newton 940P). All spectra are normalized to the band showing the maximum intensity.

The absorption and transmission spectra were recorded from polished glasses in the range of 200–1600 nm at room temperature, using a UV-3600 Plus UV-VIS-NIR Spectrophotometer Shimadzu.

The up-conversion photoluminescence spectra were measured at room temperature using a monochromator (Digikrom, DK480) and a lock-in amplifier (Stanford Research Systems, SR830) equipped with a TEC-cooled silicon photodiode. The materials were excited using a TEC-cooled fiber-coupled multimode laser (II-VI Laser Enterprise, λ_{exc} ~980 nm, incident power on sample 23.5 mW). The up-converted light emission was collimated, collected and directed to the monochromator through a short-pass filter with a cutoff at 800 nm (Thorlabs, FES800). The smallest excitation spot size is estimated to be ~100 μm in diameter.

The up-conversion luminescence lifetimes were measured at room temperature with a Newport 5060 laser driver and Optical Fiber Systems IFC-975-008 laser (6 W; $\lambda_{exc} = 974$ nm). A long-pass filter (Newport 10LWF-850-B) was used between the excitation and the sample. A short-pass filter (Newport 10SWF-850-B) was used between the sample and a photomultiplier tube (Hamamatsu R1465). The optical path had a 90° angle between the excitation and detection. The emission was collected at 544 nm (Thorlabs band-pass filter FL543.5- 10) and at 650 nm (Thorlabs band-pass filter FB650-10). A current amplifier FEMTO DHPCA-100 was used. The excitation power used were 1000–9000 mV. The excitation pulse duration was 50 ms and after each pulse there were a 50 ms delay before the next excitation pulse. The number of pulse–delay cycles in one measurement was 1000.

Results and discussion

We successfully prepared phosphate glasses, which contain $NaYF_4$:Er^{3+},Yb^{3+} nanocrystals, using the direct particles doping method.[19] In this method, the nanocrystals need to be added in the glass melts after melting but prior to quenching to ensure the survival of the nanocrystals. First, a host glass in which the nanocrystals can be dispersed without being decomposed, needs to be identified. As explained in,[20] two parameters need to be optimized when preparing a nanocrystals-containing glass using the direct particles doping method: the doping temperature (T_{doping}) at which the nanocrystals are added in the glass batch and the dwell time before quenching the glass after adding the nanocrystals. The doping temperature should be lower than the nanocrystals' dissolution points, which was

Table 1 Density and thermal properties of the investigated glasses

x	T_g (°C) ±3 °C	T_x (°C) ±3 °C	$\Delta T = T_x - T_g$ (°C) ±3 °C	T_p (°C) ±3 °C	Density (g cm^{-3}) ±0.02 g cm^{-3}
0	284	374	90	414	2.47
2.5	272	378	106	415	2.47
5	264	374	110	403	2.47
7.5	255	368	113	395	2.46
10	246	356	110	402	2.45

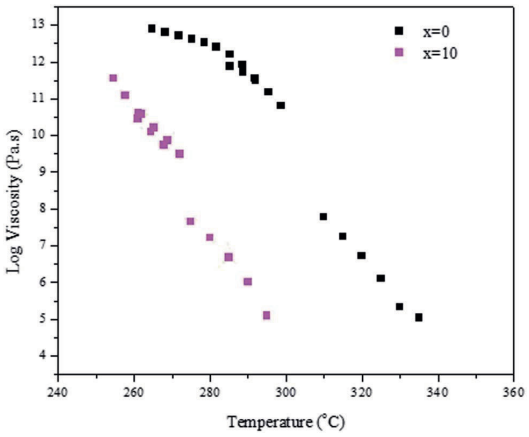

Fig. 1 Viscosity curves of the glasses with $x = 0$ and 10.

reported to be 750 °C.[21] Furthermore, to avoid crystallization when adding the nanocrystals, the host glass must be stable against crystallization as checked by its ΔT ($\Delta T = T_x - T_g$), which needs to be greater than 100 °C.

Because of these requirements, we tested glasses with the composition (90NaPO$_3$-(10-x)Na$_2$O-xNaF) (mol%) because of their low melting temperature (750 °C). The density and the thermal properties of the glasses are reported in Table 1. When increasing x, the glass transition (T_g), the onset of crystallization (T_x) and the peak of crystallization (T_p) temperatures decrease in agreement with the shift of the viscosity of the glasses to lower temperature (Fig. 1). One can notice that an increase in x increases ΔT indicating that the F-containing glasses are stable against crystallization and so are good candidates for the direct doping method. Finally, whereas the changes in the glass composition has no significant impact on the glasses' density, the structure of the glasses changes as shown in Fig. 2a and b, which present the IR and Raman spectra of the glasses, respectively. The spectra are obviously relevant to the metaphosphate structure according to.[22] The glasses are expected to be free of Q^3 groups as there is no IR and Raman band at >1300 cm^{-1}, where the ν(P═O) of Q^3 groups usually appear. The attribution of the IR and Raman bands can be found in Table 2.[23–31] The replacement of Na$_2$O by NaF increases the number of Q^2 units at the expense of Q^1 units as seen by the increase in intensity of the shoulders in the 980–1050 cm^{-1} range and of the bands at 1080 cm^{-1} and at 1240 cm^{-1} and the decrease in intensity of the band at 1140 cm^{-1} with an increase in x (Fig. 2a). These changes in the structure induced by the increase in x can also be suspected from the shift of the Raman band at 1150 cm^{-1} to higher wavenumbers (Fig. 2b).[26] The shortening of linear metaphosphate chains occurring when Na$_2$O is replaced by NaF is evidenced by the small increase in intensity of the IR shoulder at 950 cm^{-1} and the decrease in intensity of the Raman band at 700 and 1250 cm^{-1} with an increase in x.[28] The increase in the intensity of the IR shoulder at 1010 cm^{-1} can reveal an increase in the (PO_3F) bonds as suggested in.[27] The shift in the position of the IR bands to longer wavenumbers with an increase in x indicates the formation of F–P–F bonds when NaF replaces Na$_2$O as suggested in.[26] The increase in the

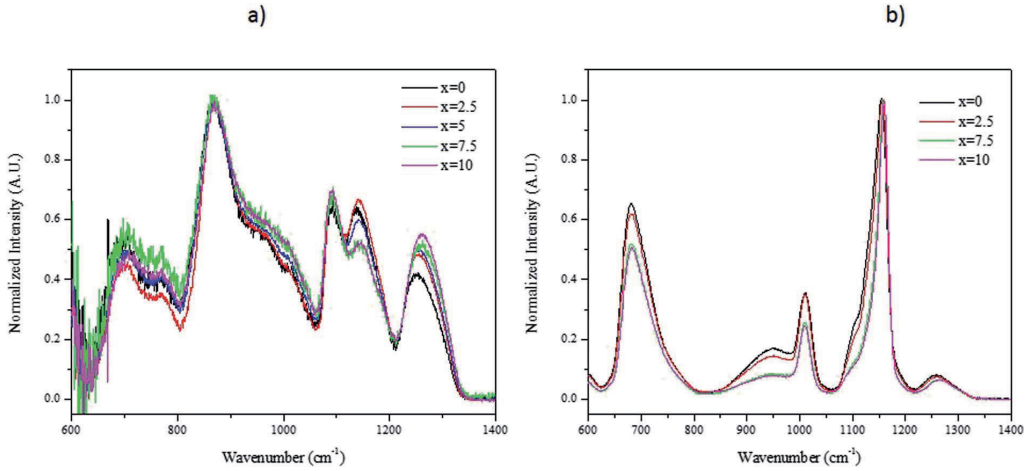

Fig. 2 IR (a) and Raman (b) spectra of the investigated glasses.

Table 2 Bands assignment in Raman and IR spectra

Wavenumber (cm^{-1})	Raman Shift	FTIR
700	ν_s(P–O–P) of Q^2 and Q^1 units[23]	
770		ν_s(P–O–P) of Q^2 units[23]
880		ν_{as}(P–O–P) of Q^2 units[23]
950		ν_{as}(P–O–P) of Q^2 units in small rings[25]
980	$\nu_s(PO_4)^{3-}$ in Q^0 units[28]	$\nu_s(PO_3^{2-})$ in Q^1 units
1010	ν_s(P–O) of terminal Q^1 units[26]	$\nu_s(PO_3F)$ bonds[27]
1030		ν_{as}(P–O–P) of Q^2 units in large rings[25]
1080		$\nu_{as}(PO_3)^{2-}$ in Q^1 units[28]
1150	$\nu_s(PO_2)$ of Q^2 groups.[29–31]	$\nu_s(PO_3^{2-})$ in Q^2 units [24]
1240	$\nu_{as}(PO_2)$ of Q^2 groups.[29–31]	$\nu_{as}(PO_2)$ of Q^2 units[23]

amount of the Q^2 units at the expense of the Q^1 units, the formation of P–F bonds and to the reduction in non-bridging terminal groups are also supported by the shift of the optical band gap to a lower wavelengths (Fig. 3) as suggested by Venkateswara Rao.[32] In summary, these changes in the glass structure lead to a decrease in the thermal properties of the glass when Na_2O is replaced by NaF (Table 1 and Fig. 1). Therefore, the glass with $x = 10$ was selected for this study due to its low T_g and viscosity as compared to the glass with $x = 0$ and also due to its high ΔT. For comparison, the glass with $x = 0$ was also included in the study.

In the next stage, $NaYF_4$:Er^{3+},Yb^{3+} nanocrystals were added in the glasses. In the doping process, one can identify four main factors that will influence the up-conversion behavior of the final products: (1) the thermal stability of the bare $NaYF_4$:-Er^{3+},Yb^{3+} nanocrystals, (2) the temperature of glass melt when adding the $NaYF_4$:Er^{3+},Yb^{3+} nanocrystals, (3) the viscosity of the glass matrix, and (4) the homogeneity of the dispersion of the nanocrystals in the glass. Inhomogeneities in the dispersion of the nanocrystals will have rather straightforward effects on the up-conversion intensity observed at different parts of the glasses and thus this must be considered when comparing the intensities from different samples. The factors associated with points (1)–(3) are discussed in more detail below.

(1) It is known that the hexagonal $NaRF_4$ (R = rare earth) structure will transform irreversibly to the high-temperature cubic structure at high temperature.[33] The exact temperature will depend on the composition of the material,[21] but for the present composition, it has been reported to be at 660 °C.[34] This change in structure is driven by a gradual change in stoichiometry due to the loss of NaF from the $NaRF_4$ matrix. The high-temperature cubic structure has only one site for the Er^{3+} ions, whereas the hexagonal one has three.[33] Therefore, the shape of the spectra will be somewhat different for these two forms. Furthermore, the average R–R distances are longer in the cubic form than in the hexagonal one (cubic: 3.88 Å, hexagonal: 3.50 to 3.65 Å[33]). This results in less efficient energy transfer between Yb^{3+} and Er^{3+} lowering the intensity of the up-conversion

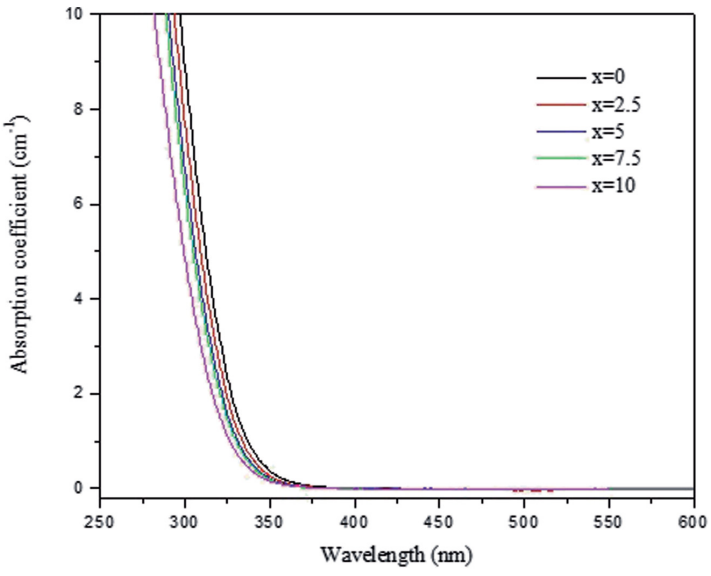

Fig. 3 Absorption spectra of the investigated glasses.

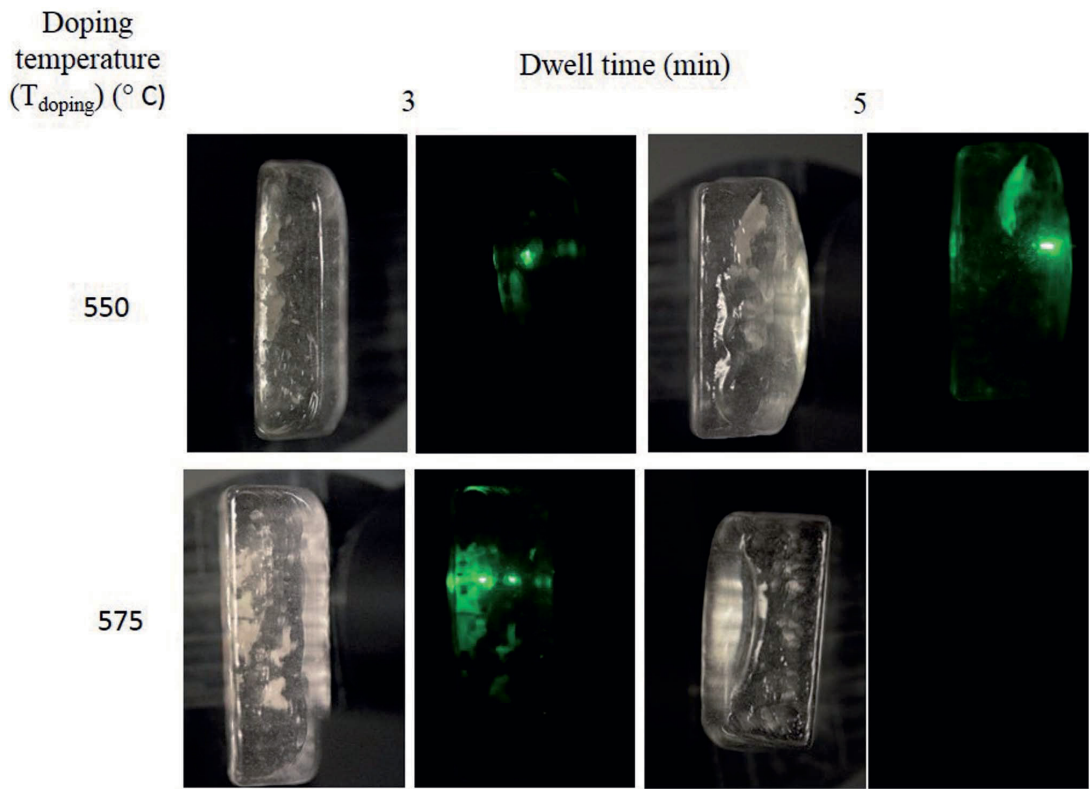

Fig. 4 Pictures of the $NaYF_4:Er^{3+},Yb^{3+}$ nanocrystals-containing glasses with $x = 0$ in daylight and under pumping at 980 nm. The glasses were prepared using different doping temperatures and dwell times.

emission. The cubic structure is also more centrosymmetric than the hexagonal one and thus it has less allowed transitions and hence lower emission intensity[35] and one can expect longer emission lifetimes. It is also expected that the cross-relaxation mechanisms, which are an important de-excitation route for the green emission but do not affect the red one,[36] will become less effective and thus the lifetime of the green emission would increase when the structure of the nanocrystals changes from hexagonal to cubic.[37] On the other hand, it has been reported that the lifetime of the red up-conversion emission of Er^{3+} is shorter in the cubic than in the hexagonal form.[38] It should be also noted that in bulk $NaRF_4$ materials, the structural form can be easily identified with X-ray powder diffraction measurements, but in the present work the concentration of the $NaYF_4:Er^{3+},Yb^{3+}$ nanocrystals is too small to allow such identification.

(2) The heating of the glass matrix may decrease the structural transition temperature of the $NaYF_4:Er^{3+},Yb^{3+}$ nanocrystals and thus the structure can be partially or completely transformed to the high-temperature cubic phase in the process. The heating may also induce the corrosion of the nanocrystals either uniformly or a change in their composition. In the case of uniform corrosion, the relative concentrations of the R^{3+} would remain the same, but the particle size would decrease. Generally, a decrease in particle size leads to lower up-conversion intensity and shorter emission lifetimes.[37] This can be associated with *e.g.* the increase in surface/volume ratio and subsequent increased surface-related quenching. If the composition changes due to corrosion, then it is expected that the up-conversion intensity decreases but the lifetimes increase for both the green[37] and red[39] emissions. In the present case, it is possible to also have the effect of NaF, which is present in the $x = 10$ glass and not on the $x = 0$ glass. Based on the discussion above, one would expect that the presence of NaF will make the hexagonal to cubic phase transition less probable and thus lessen its possible effects on the up-conversion properties.

(3) The glass matrix will affect the up-conversion properties. This is related to non-radiative quenching through the surface of the nanocrystals with the probability for such relaxation increasing with decreasing crystallite size. In this glass matrix, the surface quenching is likely to proceed *via* multiphonon de-excitation due to the fundamental vibrations of the phosphate Q^2 units at around 1200 cm^{-1}.[40] Then, it takes only three such phonons to relax from the red-emitting $^4F_{9/2}$ level to the NIR level $^4I_{9/2}$ *ca.* 3000 cm^{-1} below. The green-emitting $^4S_{3/2}$ also needs only three such phonons (*ca.* 3000 cm^{-1}) to relax to the red-emitting $^4F_{9/2}$ level and then three more to go to NIR. In phosphate glasses, the multiphonon decay rate for 3000 cm^{-1}

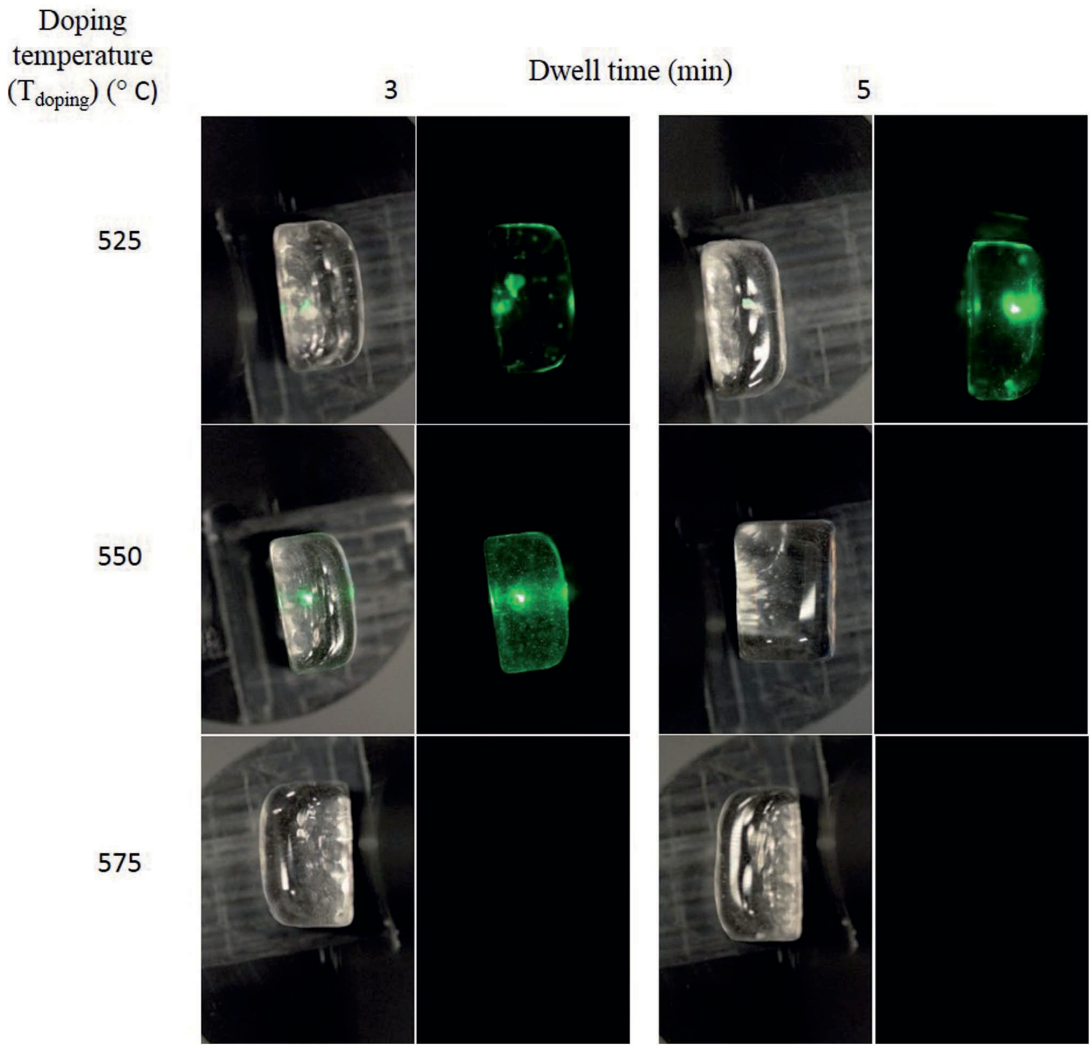

Fig. 5 Pictures of the $NaYF_4$:Er^{3+},Yb^{3+} nanocrystals-containing glasses with $x = 10$ in daylight and under pumping at 980 nm. The glasses were prepared using different doping temperatures and dwell times.

energy gaps has been reported to be *ca.* 10^7 s^{-1},[40] which is very high when compared to the millisecond range lifetimes associated with the up-conversion in Yb^{3+},Er^{3+} co-doped systems. Increased multiphonon relaxation is commonly associated with decreased up-conversion lifetimes.[41]

5 wt% of $NaYF_4$:Er^{3+},Yb^{3+} nanocrystals were added in the glasses with $x = 0$ and 10 at T_{doping} varying from 525 and 575 °C and the glasses were quenched after 3 and 5 min (dwell time) after adding the nanocrystals. It should be pointed out that the glass with $x = 0$ could not be quenched when using a T_{doping} of 525 °C due to high viscosity. The glasses are labelled as (T_{doping}-dwell time). As a first test, pictures of the glasses were taken in daylight and under pumping using 980 nm and are presented in Fig. 4 and 5, respectively for the glasses with $x = 0$ and 10. Under pumping at 980 nm, some glasses exhibit green emission which is a clear indication of the survival of the $NaYF_4$:Er^{3+},Yb^{3+} nanocrystals in the glasses. While green emission can be seen from the (575-3) glass with $x = 0$, no green emission could be seen from the glass $x = 10$ when prepared using the same T_{doping} of 575 °C. The T_{doping} needed to be reduced to 550 °C to observe the green emission from the glass with $x = 10$. The reduction in the T_{doping} from 575 to 550 °C when x increases from 0 to 10 to ensure the survival of the nanocrystals is in agreement with the changes in the thermal properties of the glasses when Na_2O is replaced by NaF discussed in the previous paragraph. Since the beam size of the 980 nm laser is much smaller (*ca.* 2 mm in diameter) than the glass pieces, it is not possible to evaluate the dispersion of the nanocrystals based on

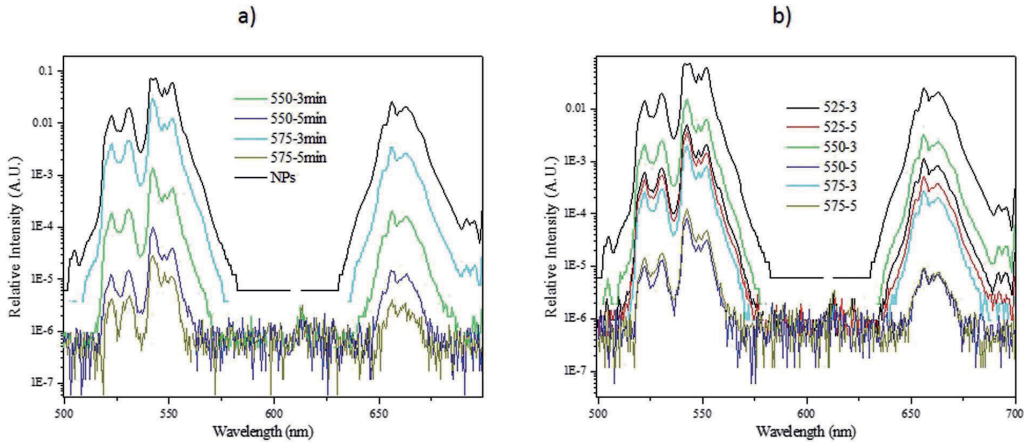

Fig. 6 Upconversion spectra of the $NaYF_4:Er^{3+},Yb^{3+}$ nanocrystals-containing glasses with $x = 0$ (a) and 10 (b) using a 980 nm excitation. Note the logarithmic intensity scales.

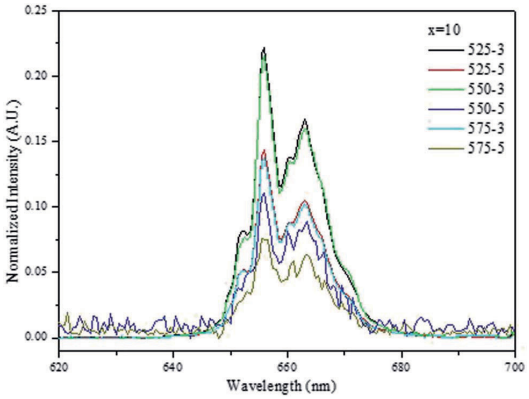

Fig. 7 Red emission band when the upconversion spectra of the $NaYF_4:Er^{3+},Yb^{3+}$ nanocrystals-containing glasses with $x = 10$ are normalized to the green emission.

emission intensity. However, under daylight, agglomerates of nanocrystals can be seen in some glasses. The (550-3) glass with $x = 10$ appears to be agglomerate-free. In both glass systems, the visually observed intensity of the green emission decreases with increasing T_{doping} and longer dwell time.

The upconversion spectra of the glasses, crushed into powder for the analysis, were measured using 980 nm pumping and the spectra are presented in Fig. 6. The spectra exhibit green ($^2H_{11/2}$–$^4I_{15/2}$ and $^4S_{3/2}$–$^4I_{15/2}$) and red ($^4F_{9/2}$–$^4I_{15/2}$) emission, which are typical emissions for Er^{3+}.[9] The upconversion spectra of the nanocrystals-containing glasses exhibit distinct fine structure, which is a characteristic of Er^{3+} ions coordinated in crystalline sites confirming the presence of $NaYF_4:Er^{3+},Yb^{3+}$ nanocrystals in the glasses. As a general observation and in agreement with the pictures presented in Fig. 4 and 5, the glasses with $x = 10$ exhibit stronger upconversion than the glasses with $x = 0$, which is also in agreement with our previous study.[19] Additionally, an increase in T_{doping} and in dwell time leads to a reduction in the intensity of the green and red emission. As discussed above, this may be due to the increase of the concentration of the cubic $NaYF_4$ structure initiated by heating at a higher temperature or for a longer time. We also confirm that the (550-3) glass with $x = 10$ exhibits a strong intensity of upconversion. Compared to our previous study,[19] we showed that the upconversion from the investigated fluorophosphate glasses can be further enhanced if the T_{doping} is reduced to 550 °C.

Furthermore, one can notice that the (575-3) glass with $x = 0$ exhibits a higher intensity of upconversion compared to the other glasses. Based on Fig. 4 and 5, this strong upconversion is suspected to come from the agglomerates of nanocrystals seen in the glass. However, the agglomerates of nanocrystals in the glasses are reducing the amount of nanocrystals dispersed in the glass, which in turn results in a lower upconversion than expected. This is the case for the (525-3) glass with $x = 10$ which exhibits a lower upconversion than the (550-5) glass with $x = 10$. Therefore, it is crucial to compare the upconversion spectra of the glasses with the pictures of the glasses under pumping when optimizing the direct particles doping method.

Fig. 7 exhibit the red up-conversion emission band of the glasses with $x = 10$ when normalizing to the green emission. An increase in the T_{doping} and the dwell time decreases the intensity of the red emission as compared to the green emission. These results indicate that the quenching of the red emission becomes more effective than that of the green one probably due to the decrease of the relative concentration of Er^{3+} in the nanocrystals which may be either due to the leakage of the Er^{3+} ions from the crystal to the glass, as reported previously by us,[19,42,43] or due to the increase of the amount of the cubic phase as discussed above.

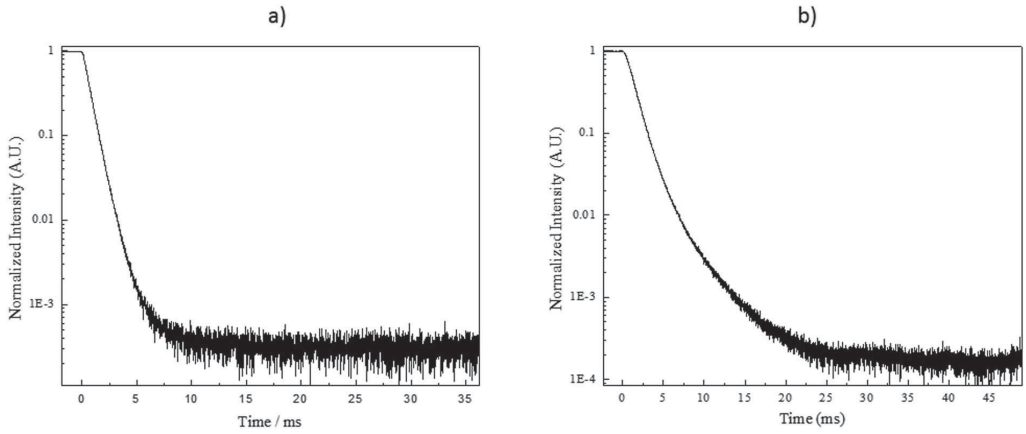

Fig. 8 Decay curves of the $NaYF_4$:Yb^{3+},Er^{3+} particles for green (a) and red (b) emissions.

To gain further information on the processes affecting the $NaYF_4$:Yb^{3+},Er^{3+} nanocrystals, the up-conversion decay curves were measured for the green and red emissions. The data were then fitted with a two-term exponential function as illustrated in Fig. 8. The results related to the green and red emission are summarized in Fig. 9a and b, respectively. It should be pointed out that the estimated decay times are not the actual decay times of the emitting states of the Er^{3+} but they are the apparent decay times for the detected emissions, which result from the complex excitation and emission system between Yb^{3+} and Er^{3+} ions.

For the green emission (Fig. 9a), the lifetimes are slightly longer in the $x = 0$ glasses while the lifetimes are clearly longer in the $x = 10$ glasses than for the bare NCs. When comparing the effect of the doping parameters on the lifetimes of the green emission, we notice that for the $x = 0$ glasses, the lifetime decreases when the T_{doping} and dwell time increase suggesting that homogeneous corrosion of the NCs occurs in these glasses. For the $x = 10$ glasses, the lifetime increases when the T_{doping} increases from 525 to 550 °C while using 3 min dwell time indicating that the Er^{3+} concentration in the nanocrystals decreases after embedding the nanocrystals in the glass. However, when preparing the glasses using higher T_{doping} and longer dwell times, the lifetimes decrease suggesting a homogeneous corrosion of the NCs. The marked difference between the lifetimes in the $x = 0$ and $x = 10$ glasses is probably due to the effect of NaF in the latter. We propose that NaF acts as a diluting agent for the NCs thus decreasing the Er^{3+} concentration and increasing the green emission lifetimes.

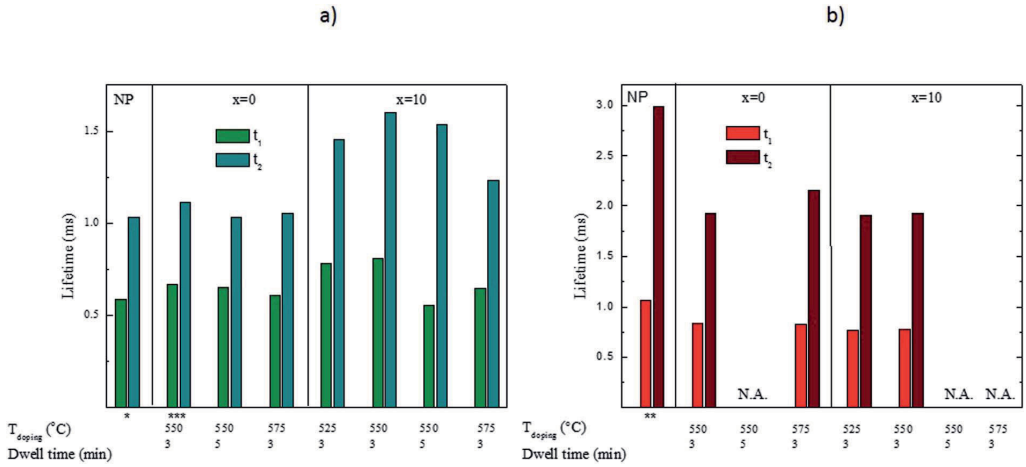

Fig. 9 Lifetimes of the green (a) and red (b) up-conversion emissions in the NCs alone and in the investigated glasses. All were excited at 975 nm with a 0.9 V voltage except *0.1 V, **0.2 V and ***0.5 V. The voltage is expected to have only a small impact on the lifetimes as reported in ref 45. In the cases marked with N.A., the lifetimes could not be measured due to a too low signal intensity.

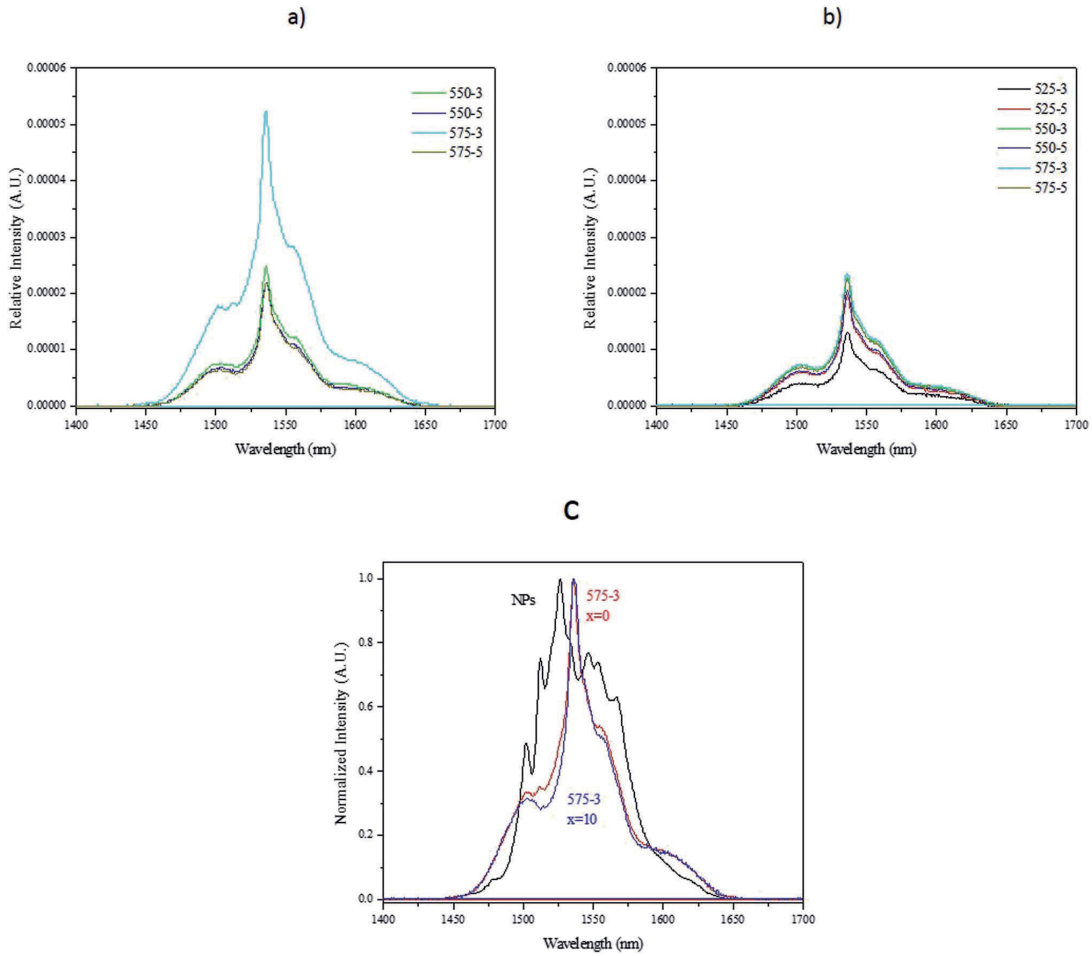

Fig. 10 Emission spectra of the $NaYF_4:Er^{3+},Yb^{3+}$ nanocrystals-containing glasses with $x = 0$ (a) and 10 (b). Normalized emission spectrum of the $NaYF_4:Er^{3+},Yb^{3+}$ nanocrystals compared with those of the 575-3 samples (c).

For the red emission (Fig. 9b), our results show that incorporating the nanocrystals into the glass matrices decreases the lifetimes probably due to an increase in the multiphonon de-excitation when the NCs are embedded into the glass.[41] It is also possible that the crystallite size of the NCs decreases during the glass processing, decreasing further the lifetimes.[37] As explained in the previous paragraph, the increase in the green lifetime can indicate that the concentration of the rare-earth decreases in the nanocrystals according to.[37,39] However, we are left with the question of why the red lifetimes do not increase. We propose that it is because the red emission may be considered as a three-photon pile-up[36] whereas the green is a two-photon one. Therefore, the red emission would be more drastically affected by the surface quenching caused by the glass matrix than the green one. Finally, the evolution of the red lifetimes as a function of the T_{doping} and dwell time is more difficult to explain than that of the green lifetimes. It seems as if there is no impact at all from changes in temperature or time. At the moment, it is impossible to suggest why that is, other than a complex interplay of the effects described above.

The down-shifting emission spectra of the nanocrystals-containing glasses with $x = 0$ and 10 using a 980 nm pumping spectra are depicted in Fig. 10a and b, respectively. They exhibit a broad emission band which is different from the emission spectra of the nanocrystals alone (Fig. 10c) confirming the changes in the Er^{3+} sites after embedding the nanocrystals in the glasses. We propose that the spectrum is an overlay of the emission of Er^{3+} in the NCs as well as those leaked to the glass matrix, probably having mostly emission from latter ones. The rounded shapes of the peaks suggest that Er^{3+} has multiple sites with close to similar symmetries as is typical for glasses. Because the up-conversion spectra revealed no differences between the bare NCs and those embedded into the glass, we can deduce that only the Er^{3+} ions in the NCs show up-

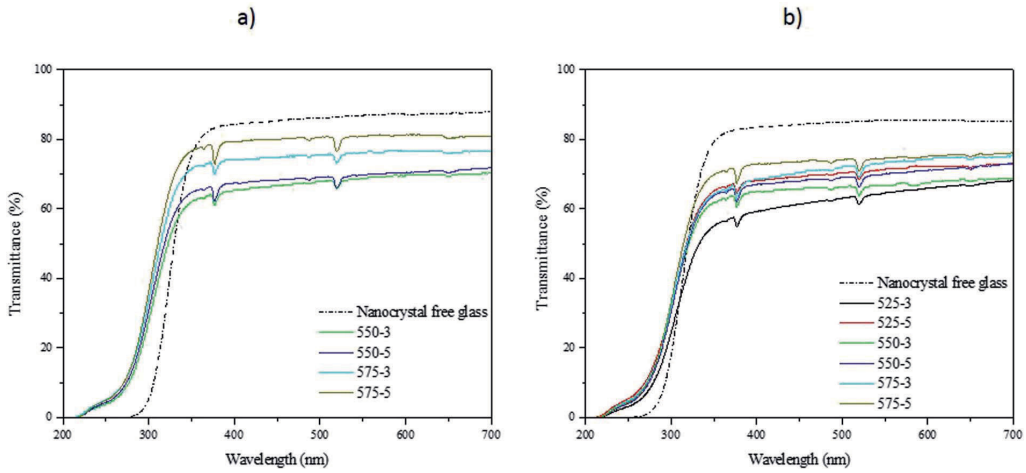

Fig. 11 Transmittance spectra of the $NaYF_4:Er^{3+},Yb^{3+}$ nanocrystals-free and containing glasses with $x = 0$ (a) and 10 (b).

conversion emission. One can notice that the glasses exhibit similar intensity of emission at 1.5 μm except for the (575-3) glass with $x = 0$ which exhibits a high intensity of emission. This can be associated with the highest amount of Er^{3+} ions leaked to the glass matrix at this highest T_{doping}. For the $x = 10$ glasses, such drastic increase is not observed because the NaF present probably slows down the corrosion of the nanocrystals.

Although a transmission electron microscope (TEM) can be used to characterize the nanocrystals embedded in the glasses as in,[44] it is extremely challenging to perform the analysis due to the small volume fraction of the NCs when compared to the glass and also due to the small size of the NCs as reported in.[20] Therefore, it is shown here that simple measurement as upconversion spectra measurement can be used to check if decomposition of the nanocrystals occurs during the glass melting. Therefore, based on Fig. 10, we confirm that 550 °C is an appropriate T_{doping} when preparing the glass with $x = 10$. This T_{doping} allows the dispersion of the nanocrystals in the glass while limiting their decomposition. As the (575-3) glass exhibits a more intense red emission than the (550-5) glass, we suspect the dwell time to have a stronger impact than the T_{doping} on the decomposition of the nanocrystals. Therefore, the dwell time needs to be controlled to limit the decomposition: the 5 min dwell time before quenching the glass after adding the nanocrystals at 550 °C seems to be already long enough to lead to the decomposition of the nanocrystals.

In order to verify the decomposition of the nanocrystals during the preparation of the glass, the transmittance spectra of the glasses were measured and they are presented in Fig. 11. As seen previously,[19] the nanocrystals-containing glasses exhibit a lower transmittance than the nanocrystals-free glasses due to the presence of nanocrystals as explained in.[20] One can notice that an increase in T_{doping} and dwell time increases the transmittance of the glasses confirming the decomposition of the nanocrystals in the glasses.

Conclusion

Upconverter fluorophosphate glasses were prepared by adding in the glass melt $NaYF_4:Er^{3+},Yb^{3+}$ nanocrystals using the direct particles doping method. First we investigated the effect of NaF addition at the expense of Na_2O on the thermal, physical, optical and structural properties of glasses in the system $(90NaPO_3\text{-}(10\text{-}x)Na_2O\text{-}xNaF)$ (mol%). Using IR and Raman spectroscopies, we found that an increase in the NaF content (x) leads to an increase in the number of Q^2 units at the expense of the Q^1 units, a shift of the optical band gap to lower wavelengths and so to a decrease in the thermal properties of the glasses. As compared to our previous work,[15] the upconversion from the glasses can be further enhanced by optimizing the direct particles doping method: a strong and homogeneous upconversion can be obtained by adding at 550 °C the $NaYF_4:Er^{3+},Yb^{3+}$ nanocrystals in the glass melt with $x = 10$. The glass should be quenched 3 minutes after adding the nanocrystals to ensure the survival and the dispersion of the nanocrystals in the glass while limiting their decomposition in the glass melts. Finally, we demonstrated that the measurement of the upconversion, upconversion emission lifetimes, the emission at 1.5 μm and of the transmittance spectra of the nanocrystals-containing glasses allows one to verify if decomposition of the nanocrystals occurred in glass melts.

These results provide important new information on the preparation of nanocrystals-containing fluorophosphates glasses using direct particles doping method. This method offers the possibility of preparing a variety of new glasses by introducing nanocrystals of various chemical compositions.

Conflicts of interest

The authors declare no conflict of interest. The funding sponsors had no role in the design of the study; in the collection,

analyses, or interpretation of data; in the writing of the manuscript and in the decision to publish the results.

Acknowledgements

The authors would like to acknowledge Hoang Nguyen (from Tampere University of Technology, Finland) for preparing the nanocrystals-free glasses, Dr Salminen (from Tampere University of Technology, Finland) for measuring the Raman spectra of the glasses and also Prof. Delia Brauer and Thilo Grammes (from Friedrich Schiller University, Germany) for performing the viscosity measurement. LP would like to acknowledge the financial support of the Academy of Finland (Academy Project-308558) and MT the financial support from the Magnus Ehrnrooth foundation (Finland).

References

1 W. S. Tsang, W. M. Yu, C. L. Mak, W. L. Tsui, K. H. Wong and H. K. Hui, *J. Appl. Phys.*, 2002, **91**, 1871.
2 G. S. Qin, W. P. Qin, C. F. Wu, S. H. Huang, J. S. Zhang, S. Z. Lu, D. Zhao and H. Q. Liu, *J. Appl. Phys.*, 2003, **93**, 4328.
3 S. Sanders, R. G. Waarts, D. G. Mehuys and D. F. Wetch, *Appl. Phys. Lett.*, 1995, **67**, 1815–1817.
4 J. Zhang, S. Dai, G. Wang, L. Zhang, H. Sun and L. Hu, *Phys. Lett. A*, 2005, **345**, 409–414.
5 H. Lin, E. Y. B. Pun and X. R. Liu, *J. Non-Cryst. Solids*, 2001, **283**, 27.
6 N. M. Idris, M. K. G. Jayakumar, A. Bansal and Y. Zhang, *Chem. Soc. Rev.*, 2015, **44**, 1449–1478.
7 W. Zheng, P. Huang, D. Tu, E. Ma, H. Zhu and X. Chen, *Chem. Soc. Rev.*, 2015, **44**, 1379–1415.
8 Y. I. Park, K. T. Lee, Y. D. Suh and T. Hyeon, *Chem. Soc. Rev.*, 2015, **44**, 1302–1317.
9 F. Auzel, *Chem. Rev.*, 2004, **104**, 139–173.
10 J. Ruan, Z. Yang, A. Huang, H. Zhang, J. Qiu and Z. Song, *ACS Appl. Mater. Interfaces*, 2018, **10**, 14941–14947.
11 Y. Wang and J. Ohwaki, *Appl. Phys. Lett.*, 1993, **63**, 3268.
12 P. A. Tick, N. F. Borrelli, L. K. Cornelius and M. A. Newhouse, *J. Appl. Phys.*, 1995, **78**, 6367.
13 T. Berthier, V. M. Fokin and E. D. Zanotto, *J. Non-Cryst. Solids*, 2008, **354**, 1721–1730.
14 G. Y. Chen, C. H. Yang and P. N. Prasad, *Acc. Chem. Res.*, 2013, **46**, 1474–1486.
15 B. S. Cao, Y. Y. He, L. Zhang and B. Dong, *J. Lumin.*, 2013, **135**, 128–132.
16 Y. Gao, Y. Hu, D. Zhou and J. Qiu, *J. Alloys Compd.*, 2017, **699**, 303–307.
17 F. Liu, E. Ma, D. Chen, Y. Wang, Y. Yu and P. Huang, *J. Alloys Compd.*, 2009, **467**, 317–321.
18 A. de Pablos-Martín, J. Méndez-Ramos, J. del-Castillo, A. Durán, V. D. Rodriguez and M. J. Pascual, *J. Eur. Ceram. Soc.*, 2015, **35**, 1831–1840.
19 H. Nguyen, M. Tuomisto, J. Oksa, T. Salminen, M. Lastusaari and L. Petit, *Scr. Mater.*, 2017, **139**, 130–133.
20 J. Zhao, X. Zheng, E. P. Schartner, P. Ionescu, R. Zhang, T.-L. Nguyen, D. Jin and H. Ebendorff-Heidepriem, *Adv. Opt. Mater.*, 2016, DOI: 10.1002/adom.201600296.
21 T. Laihinen, M. Lastusaari, L. Pihlgren, L. C. V. Rodrigues and J. Hölsä, *J. Therm. Anal. Calorim.*, 2015, **121**, 37–43.
22 K. Meyer, *J. Non-Cryst. Solids*, 1997, **209**, 227–239.
23 I. Konidakis, C.-P. E. Varsamis, E. I. Kamitsos, D. Möncke and D. Ehrt, *J. Phys. Chem.*, 2010, **114**, 9125–9138.
24 K. Griebenow, C. B. Bragatto, E. I. Kamitsos and L. Wondraczek, *J. Non-Cryst. Solids*, 2018, **481**, 447–456.
25 J. A. Wilder and J. E. Shelby, *J. Am. Ceram. Soc.*, 1984, **67**, 438–444.
26 S. Cui, J. Massera, M. Lastusaari, L. Hupa and L. Petit, *J. Non-Cryst. Solids*, 2016, **445**, 40–44.
27 M. K. Murthy, *J. Am. Ceram. Soc.*, 1963, **46**, 558–559.
28 R. K. Brow, *J. Non-Cryst. Solids*, 2000, **263**, 1–28.
29 S. Lee, A. Obata and T. Kasuga, *J. Ceram. Soc. Jpn.*, 2009, **117**, 935–938.
30 M. A. Karakassides, A. Saranti and I. Koutselas, *J. Non-Cryst. Solids*, 2004, **347**, 69–79.
31 A. G. Kalampounias, *J. Phys. Chem. Solids*, 2012, **73**, 148–153.
32 G. Venkateswara Rao and H. D. Shashikala, *J. Adv. Ceram.*, 2014, **3**, 109–116.
33 E. Harju, I. Hyppänen, J. Hölsä, J. Kankare, M. Lahtinen, M. Lastusaari, L. Pihlgren and T. Soukka, *Z. Kristallogr. Proc.*, 2011, **1**, 381–387.
34 I. Hyppänen, J. Hölsä, J. Kankare, M. Lastusaari, L. Pihlgren and T. Soukka, *Terrae Rarae*, 2009, **16**, 1–6.
35 A. Noculak and A. Podhorodecki, *Nanotechnology*, 2017, **28**, 175706.
36 M. T. Berry and P. S. May, *J. Phys. Chem. A*, 2015, **119**, 9805–9811.
37 A. Kar, S. Kundu and A. Patra, *ChemPhysChem*, 2015, **16**, 505–521.
38 E. Palo, L. Pihlgren, M. Tuomisto, T. Laihinen, I. Hyppänen, J. Kankare, M. Lastusaari, T. Soukka, H. Swart and J. Hölsä, *Opt. Mater.*, 2016, **59**, 49–54.
39 S. Georgescu, V. Lupei, A. Lupei, V. I. Zhekov, T. M. Murina and M. I. Studenikin, *Opt. Commun.*, 1991, **81**, 186–192.
40 C. B. Layne, W. H. Lowdermilk and M. J. Weber, *Phys. Rev. B*, 1977, **16**, 10–21.
41 I. Hyppänen, N. Höysniemi, R. Arppe, M. Schäferling and T. Soukka, *J. Phys. Chem. C*, 2017, **121**, 6924–6929.
42 J. Massera, P. Głuchowski, M. Lastusaari, L. C. V. Rodrigues, L. Petit, J. Hölsä, L. Hupa and M. Hupa, *J. Eur. Ceram. Soc.*, 2015, **35**, 1255–1261.
43 J. Massera, M. Gaussiran, P. Głuchowski, M. Lastusaari, L. C. V. Rodrigues, L. Petit, J. Hölsä and L. Hupa, *Opt. Mater.*, 2016, **52**, 56–61.
44 J. Zhao, Z. Yang, C. Yu, J. Qiu and Z. Song, *Chem. Eng. J.*, 2018, **341**, 175–186.
45 X. Xue, M. Thitsa, T. Cheng, W. Gao, D. Deng, T. Suzuki and Y. Ohishi, *Opt. Express*, 2016, **24**, 26307.

PUBLICATION IV

Effect of heat treatment on the upconversion of $NaYF_4:Yb^{3+}$, Er^{3+} nanocrystals containing silver phosphate glass

N. Ojha, M. Bogdan, R. Galatus and L. Petit

Journal of Non-Crystalline Solids, Vol. 544, p. 120243
https://doi.org/10.1016/j.jnoncrysol.2020.120243

Journal of Non-Crystalline Solids 544 (2020) 120243

Contents lists available at ScienceDirect

Journal of Non-Crystalline Solids

journal homepage: www.elsevier.com/locate/jnoncrysol

Effect of heat-treatment on the upconversion of $NaYF_4:Yb^{3+}$, Er^{3+} nanocrystals containing silver phosphate glass

N. Ojha[a,*], M. Bogdan[b], R. Galatus[b], L. Petit[a]

[a] Photonics Laboratory, Tampere University, Korkeakoulunkatu 3, FI-33720Tampere, Finland
[b] Faculty of Electronics, Telecommunication and Information Technology, Technical University of Cluj Napoca, Memorandumului 28 street, Cluj-Napoca, 400114, Romania

ARTICLE INFO

Keywords:
$NaYF_4:Yb^{3+}$, Er^{3+} nanocrystals
Silver nanoparticles
Phosphate glass
Absorption
Luminescence

ABSTRACT

Novel $NaYF_4:Yb^{3+}$, Er^{3+} nanocrystals containing phosphate glass with composition $83.25NaPO_3$–9.25NaF-5ZnO-$2.5Ag_2O$ (in mol%) was prepared by adding the $NaYF_4:Yb^{3+}$, Er^{3+} nanocrystals in the glass using the direct doping method. The optical and luminescence properties of this new glass are presented and discussed. The newly developed glass exhibits visible emission under 980 nm pumping with high intensity confirming the presence of the $NaYF_4:Yb^{3+}$, Er^{3+} nanocrystals in the glass. From the absorption spectrum of the as-prepared glass, it is showed that the as-prepared glasses contains already Ag nanoparticles which are thought to precipitate due to the decomposition of some of the $NaYF_4:Yb^{3+}$, Er^{3+} nanocrystals occurring during the glass preparation. A heat treatment of the glass was found to lead to the migration of Ag species at the surface of the glass as evidenced using SEM and to a decrease of the intensity of the upconversion mostly due to an increase of the inter defects in the $NaYF_4:Yb^{3+}$, Er^{3+} nanocrystals due to the heat treatment.

1. Introduction

There has been significant research in the development of rare-earth (RE) doped glasses as these glasses can find potential applications in solar cells, color displays, high resolution sensing, biomedical imaging and bio-label to name few examples [1–6]. Unlike silica glass which possesses a 3D network, phosphate glasses can dissolve considerable amounts of alkaline earth, transition metal and rare earth ions due to their 2D network [7]. Additionally, phosphate glasses can be engineered with excellent transparency, low viscosity, high ultraviolet (UV) transmission and thermal stability [8]. However, some phosphate glasses possess low chemical durability and thermal stability which can be improved by adding elements such as MgO or ZnO as reported in [9,10].

Among the RE ions, Er^{3+} ions are one of the most studied RE ions since Er^{3+} ions can provide infrared-to-visible upconversion emissions as well as a C-broadband in the telecommunication range, supreme importance to fabricate optical fibers and amplifiers[11]. An enhancement of the emission properties due to Ag nanoparticles (NPs) was reported in Er^{3+} doped glasses and was related to an increase in the local incident field close to the optical center, an increase of intrinsic radiative decay rate and/or to fluorophore-metal resonance energy transfer[12]. Therefore, RE-doped glasses containing metallic NPs have gained attraction for the few past decades. Several methods to grow metallic NPs inside glass matrices have been intensively investigated, such as sol-gel[13], heat treatment [14–16], direct metal-ion implantation[17], sonochemical method[18], SILAR (successive ionic layer adsorption and reaction) technique[19] just to cite a few; the heat treatment method being the most used method due to its simplicity and cost effectiveness. Basically, in the heat treatment method, the formation of Ag NPs consists of two-steps: first the metal ions are added inside the glass matrix and secondly post heat treatment is performed to form metal clusters aided by nucleation and growth.

Recently, Ag nanoparticles were successfully formed in glasses with the composition $(87.3\text{-}x)NaPO_3$-(9.7-x)NaF-xZnO-$2.5Ag_2O$-$0.5Er_2O_3$ with $x = 0$, 1.25, 2.5, and 5 (in mol%)[20]. The addition of ZnO was found to promote the silver ions clustering ability when heat treating the glass leading to an increase in the intensity of the emission at 1.5 μm. However, we showed that the temperature of the heat treatment should be optimized to avoid the formation of an excessive amount of the Ag aggregates to avoid a decrease in the intensity of the emission at 1.5 μm due to the energy transfer from the exited states of Er^{3+} to the silver NPs, as suggested in [21].

$NaYF_4$ crystal is considered to be one of the most efficient host lattices with low phonon energies (<350 cm^{-1}) to minimize energy losses at the intermediate states of lanthanide ions [22]. $NaYF_4:Yb^{3+}$,

* Corresponding author.
E-mail address: nirajan.ojha@tuni.fi (N. Ojha).

https://doi.org/10.1016/j.jnoncrysol.2020.120243
Received 25 March 2020; Received in revised form 25 May 2020; Accepted 8 June 2020

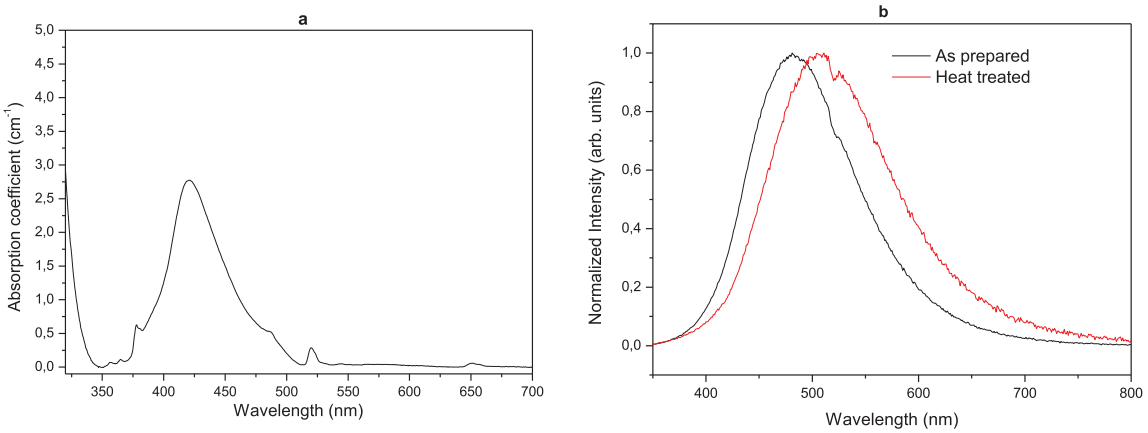

Fig. 1.. Absorption spectra of the as-prepared 2.5Ag glass a) and emission spectra of the 2.5Ag glass prior to and after heat treatment at (T_g + 10 °C) for 4 h (λ_{exc} = 320 nm) b).

Er^{3+} nanocrystals containing phosphate glasses with the composition $90NaPO_3$-xNaF-(10-x)Na_2O with $x = 0$ and 10 (in mol%) were successfully prepared using the direct particles doping method [23]. The direct doping parameters such as the doping temperature (T_{doping}) and dwell time were optimized to balance the survival and dispersion of the nanocrystals in the glass. The strongest upconversion was obtained from the glass with $x = 10$ prepared using a T_{doping} of 550 °C and a 3 min dwell time[24].

In this paper, new $NaYF_4$:Yb^{3+}, Er^{3+} nanocrystals containing glass with the $83.25NaPO_3$–$9.25NaF$-$5ZnO$-$2.5Ag_2O$ (in mol%) was prepared using the direct doping method and was heat treated to precipitate Ag nanoparticles in the glass in order to prepare new glasses with strong upconversion under 980 nm pumping. At first, we present the optical and luminescence properties of the newly developed glass and discuss the impact of the direct doping process on the survival of $NaYF_4$:Yb^{3+}, Er^{3+} nanocrystals and on the formation of Ag nanoparticles in the as-prepared glass. Then, we discuss the impact of the heat treatment on the precipitation of Ag nanoparticles in the glass and on the intensity of the upconversion from the glass.

2. Experimental

Glasses with the composition $90NaPO_3$–10NaF (in mol%) (label as 0Ag) and $83.25NaPO_3$–$9.25NaF$-$5ZnO$-$2.5Ag_2O$ (in mol%) (labeled as 2.5Ag) were prepared with $NaYF_4$:Yb^{3+}, Er^{3+} nanocrystals using the direct doping method. The raw materials were $Na_6O_{18}P_6$ (Alfa-Aesar, technical grade), NaF (Sigma-Aldrich, 99.99%), ZnO (Sigma-Aldrich, 99.50%) and Ag_2SO_4 (Sigma Aldrich, 99.99%). The preparation of the Ag0 glass can be found in [24]. The Ag2.5 glass was melted at 875 °C for 5 min in a quartz crucible and the temperature of the glass melt was reduced to 550 °C prior to adding the $NaYF_4$:Yb^{3+}, Er^{3+} nanocrystals. The glass was quenched 3 min after adding the $NaYF_4$:Yb^{3+}, Er^{3+} nanocrystals and finally annealed at 40 °C below its glass transition temperature in air for 8 h. The $NaYF_4$:Yb^{3+}, Er^{3+} nanocrystal were prepared by using the method described by Hyppänen et al.[25].

The glass transition temperature (T_g) was determined by differential thermal analysis (DTA) (TA instruments SDT Q600) using heating rate of 10 °C/min and platinum pans in N_2atmosphere. The glass transition temperature was taken at the inflection point of the endotherm, as obtained by taking the minima of first derivative of the DTA curve. The accuracy of measurement was ± 3 °C.

The absorption spectra were measured in a polished sample of thickness 2 mm using a UV–Vis-NIR spectrophotometer (UV-3600 Plus, Shimadzu) from 200 to 1800 nm with 0.5 nm interval.

The upconversion spectra were measured using a Spectro 320 optical spectrum analyzer (Instrument Systems Optische Messtechnik GmbH, Germany) at room temperature. The center emission wavelength (λ_{exc}) of the laser was ~975 nm and its incident power at the sample surface was ~23.5 mW. The upconversion spectra of the investigated samples were collected from polished glasses with the same thickness (2 mm) to allow the comparison of the emission intensity.

A FLS1000 Photoluminescence Spectrometer equipped with a xenon arc lamp and a PMT-900 detector was also used for the measurement of the emission spectra obtained using an excitation at 320 nm.

A scanning electron microscope (Crossbeam 540, Carl Zeiss, Oberkochen, Germany) and an EDS detector (X-MaxN 80, Oxford Instruments, Abingdon-on-Thames, UK) was used to image and analyze the composition of the samples.

3. Results and discussion

The glass with the composition $90NaPO_3$–10NaF (in mol%) (labeled 0Ag) was successfully prepared with $NaYF_4$:Yb^{3+}, Er^{3+} nanocrystals using the direct doping method as explained in [23,26]. Due to the presence of the $NaYF_4$:Yb^{3+}, Er^{3+} nanocrystals in the glass matrix, the glass exhibits upconversion with high intensity under 975 nm excitation. In order to increase the intensity of the upconversion, Ag_2O was added in the glass as in[12]. ZnO was also added in the glass to promote the formation of Ag nanoparticles as in our previous study[20]. Therefore, the glass with the composition $83.25NaPO_3$–$9.25NaF$-$5ZnO$-$2.5Ag_2O$ (in mol%) (labeled 2.5Ag) was prepared with $NaYF_4$:Yb^{3+}, Er^{3+} nanocrystals (5 wt%) using the direct doping method as in[23,24]. Although the melting temperature was increased from 750 to 875 °C due to the change in the glass composition, the 2.5Ag glass could be prepared using the same doping parameters than the ones used to prepare the 0Ag glass: T_{doping} was 550 °C and dwell time was 3 min. No visible agglomerates of the $NaYF_4$:Yb^{3+}, Er^{3+} nanocrystals could be seen in the 2.5Ag glass with naked eyes indicating the good dispersion of the $NaYF_4$:Yb^{3+}, Er^{3+} nanocrystals. However, the 2.5Ag glass exhibits a yellowish color after quenching. As depicted in Fig. 1a, the color of the glass can be related to the presence of an absorption band centered at ~430 nm. One should point out the presence of other bands with small intensity which can be related to the 4f-4f transition of Er^{3+} ions. The band centered at 430 nm can be associated to the surface plasmon resonance (SPR) band of Ag nanoparticles (NPs) according to [15]. This SPR band is asymmetric indicating that the average distance

between Ag particles may be larger than their sizes as suggested in[27]. From the position of this SPR absorption band, the size of the Ag NPs is suspected to be larger than 40 nm. The emission spectrum of the 2.5Ag is presented in Fig. 1b. Upon 320 nm excitation, the emission band is broad and can be formed by bands located at ~480 nm, ~540 nm and ~620 nm. These bands can be related to Ag^+ species, Ag^+ - Ag^+ species and Ag_3^{2+} species, respectively according to [28,29]. An absorption band relative to Er^{3+} ions can be seen in superposition of the broad emission band of Ag species.

Silver NPs are typically formed in the glass using a 2 step process: (i) the inclusion of metal ions into the glass matrix and (ii) the formation of clusters upon a post-treatment[14–16]. Here, we showed that our as-prepared glass can be processed with Ag NPs without additional heat treatment. Similar generation of Au nanoparticles without heat treatment was reported in silicate glass in which selenium oxide and carbon were used as additives [30].

In order to understand the formation of the Ag NPs in the 2.5Ag glass, nanocrystals free 2.5Ag glasses were prepared using standard melting process (melting and quenching at 875 °C) and also using the melting process used for the preparation of the nanocrystals containing glass (melting at 875 °C and quenching at 550 °C). After quenching, both glasses were colorless with low or few Ag NPs based on their absorption spectra (see Fig. 2a) indicating that the precipitation of the Ag NPs does not occur due to the low quenching temperature. Therefore, it is the presence of the $NaYF_4$:Yb^{3+}, Er^{3+} nanocrystals in the glass which is thought to lead to the precipitation of the Ag NPs. Glasses were prepared with different amount of $NaYF_4$:Yb^{3+}, Er^{3+} nanocrystals and as shown in Fig. 2b, the intensity of the absorption band centered at 430 nm increases as the wt% of the $NaYF_4$:Yb^{3+}, Er^{3+} nanocrystals increases. As explained in [26,31], although the direct doping method is optimized to balance the survival and dispersion of the particles, decomposition of some of the $NaYF_4$:Yb^{3+}, Er^{3+} nanocrystals is expected to occur during the glass preparation. The decomposition of the nanocrystals leads to the diffusion of the elements from the nanocrystals (Na, Y, F, Er and Yb) to the glass. One should point out that fluorine component is usually added in the glass to promote the precipitation of Ag nanoclusters[32] and RE ions were reported to have also a catalyst role on the formation of Ag nanoparticles glass [33,34]. Therefore, Na, Y, F, Er and Yb from the $NaYF_4$:Yb^{3+}, Er^{3+} nanocrystals might act as reducing agents leading to the precipitation of Ag NPs during the preparation of the glass. It is also possible that the Ag NPs form due to the presence of negative charges in the glass network. Indeed, the

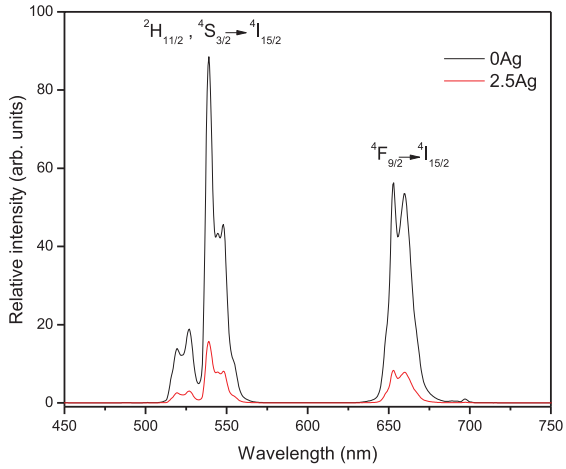

Fig. 3.. Upconversion spectra of the investigated glasses (λ_{exc} = 975 nm).

absorption band centered at 430 nm can also be related to phosphorus oxygen hole center (POHC) which has an unpaired electron shared by two nonbridging oxygen atoms bonded to the same phosphorus [35]. As reported in[20], the addition of ZnO and Ag_2O in the 90$NaPO_3$–10NaF glass leads to an increase in the Q_1 units at the expense of Q_2 units and so to a greater number of non-bridging oxygens (NBOs). Therefore, it is also possible that the other source of the negative charges available to the matrix assisted reduction of the Ag^+ ions in this system is provided by the NBOs in agreement with[36].

The survival of the $NaYF_4$:Yb^{3+}, Er^{3+} in the 2.5Ag was confirmed by observing upconversion when pumping the glass at 975 nm (see Fig. 3). The upconversion spectrum exhibits the typical green ($^2H_{11/2}$–$^4I_{15/2}$ and $^4S_{3/2}$–$^4I_{15/2}$) and red ($^4F_{9/2}$–$^4I_{15/2}$) typical emissions of Er^{3+} [37]. Also shown in Fig. 3 is the upconversion spectrum of the 0Ag glass. Although the glasses were prepared with the same amount of $NaYF_4$:Yb^{3+}, Er^{3+} nanocrystals (5 wt%), the intensity of the upconversion from the 2.5Ag glass is lower than from the 0Ag glass. The low intensity of the upconversion of the 2.5Ag glass as compared to the 0Ag glass might be related to a lower amount of the $NaYF_4$:Yb^{3+}, Er^{3+}

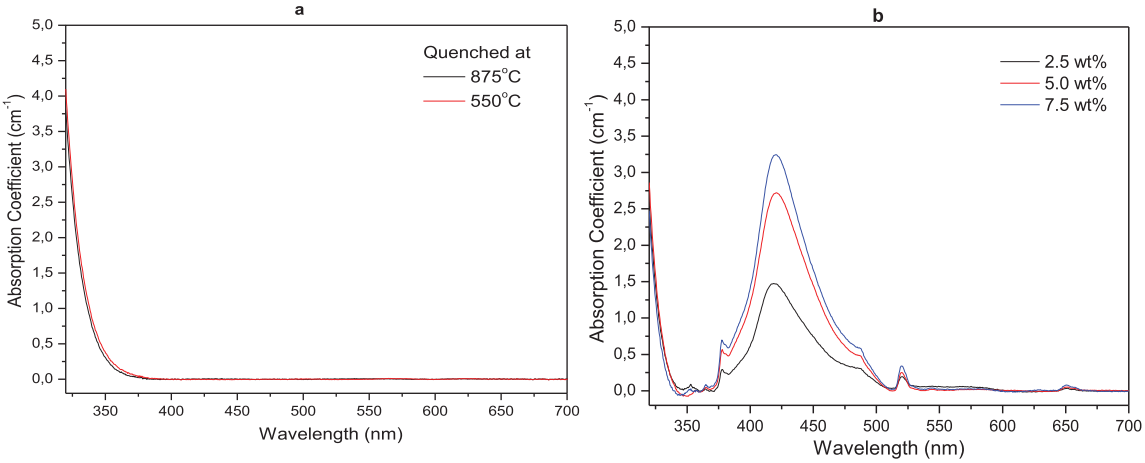

Fig. 2.. Absorption spectra of the nanocrystals free 2.5AgO glasses melted at 875 °C and quenched at 875 and 550 °C a) and of the nanocrystals containing 2.5Ag glasses prepared with different wt% of $NaYF_4$:Yb^{3+}, Er^{3+} nanocrystals b).

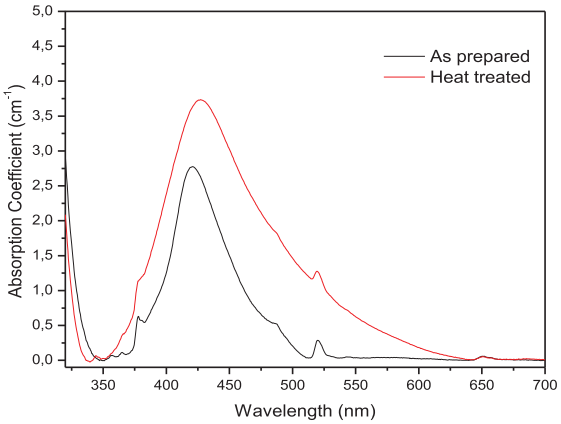

Fig. 4.. Absorption spectra of the 2.5Ag glass prior to and after heat treatment at (T_g + 10 °C) for 4 h.

nanocrystals surviving the melting process of the 2.5Ag glass maybe due to the stronger corrosive behavior of the 2.5Ag glass melt as compared to that of 0Ag glass melt . The low intensity of the upconversion from the 2.5Ag glass can also be related to the energy transfer from the exited states of Er^{3+} to the silver NPs as seen in [20].

The 2.5Ag glass was heat treated for 4 h at (T_g + 10 °C) in order to grow Ag NPs as performed in [20,38](T_g measured at (276 ± 3)°C). The absorption spectrum of the heat treated 2.5Ag glass is presented in Fig. 4. The heat treatment leads to an increase in the intensity and in the bandwidth of the absorption band centered at ~430 nm which also shifts to longer wavelength. These changes indicate that the heat treatment increases the number of the Ag NPs, which are also suspected to increase in size [39]. Indeed, as shown in Fig. 1b, the emission band shifts to longer wavelength after heat treatment confirming the formation of molecule-like Ag nanoclusters (ML-Ag NCs) with large sizes during the heat treatment. As depicted in the SEM image of the cross-section of the 2.5Ag glass prior to and after heat treatment (Fig. 5a and b), the heat treatment leads to the migration of the Ag species to the surface forming a layer of Ag species of ~2 μm at the surface of the glass (see Fig. 5c). Similar results were reported by Ennouri et al.[38].

As shown in Fig. 6a, the intensity of the upconversion is reduced by ~60% after heat treatment, probably due to the energy transfer from the exited states of Er^{3+} to the silver NPs as discussed earlier. As shown in Fig. 6b, a heat treatment of the as-prepared $NaYF_4$:Yb^{3+}, Er^{3+} nanocrystals at the same temperature (285 °C) for 4 h also leads to a similar decrease in the intensity of the upconversion. An increase in the heat treatment temperature and duration further reduces the intensity of the upconversion. Similar decrease in the intensity of the upconversion during heat treatment was reported recently in[40] and was related to the thermal activation of the deleterious thermal phonons from host lattice, internal/surface crystalline defects and surface chemical bonds. Therefore, it is the increase of the inter defects in the $NaYF_4$:Yb^{3+}, Er^{3+} nanocrystals which is thought to cause the intensity of the upconversion to decrease after heat treatment of the 2.5Ag glass.

4. Conclusion

Fluorophosphate glass with the composition 83.25$NaPO_3$–9.25NaF-5ZnO-2.5Ag_2O (in mol%) was prepared by adding $NaYF_4$:Yb^{3+}, Er^{3+} nanocrystals in the glass melt using the direct doping method. This glass exhibits upconversion confirming the survival of the nanocrystals during the glass preparation. However, compared to the glass with the composition 90$NaPO_3$–10NaF (in mol%) prepared with the same amount of nanocrystals and same method, the intensity of upconversion from the newly developed glass is lower indicating that the amount of the $NaYF_4$:Yb^{3+}, Er^{3+} nanocrystals surviving the melting process is probably lower in the newly developed glass than in the glass with the composition 90$NaPO_3$–10NaF. The low upconversion intensity of the newly developed glass could be also related to energy transfer from the exited states of Er^{3+} to the Ag nanoparticles already present in the as-prepared glasses, as evidenced from the optical and spectroscopic properties of the glass. The precipitation of the Ag nanoparticles in the as-prepared glass is thought to be due mainly to the decomposition of some $NaYF_4$:Yb^{3+}, Er^{3+} nanocrystals during the glass preparation. A heat treatment of the glass near its glass transition temperature leads to the formation of a large number of Ag nanoparticles which migrate to the surface as evidenced using SEM and also to a decrease in the intensity of the upconversion due to an increase in the inter defects in the $NaYF_4$:Yb^{3+}, Er^{3+} nanocrystals occuring durnig the heat treatment

Credit author statement

L.P. and R.G. conceived and designed this work. N.O. prepared the nanocrystals containing glass. N.O. and M.B. both carried out the optical and spectroscopic measurements. All the authors discussed and analyzed the results, contributed to writing and approved the final manuscript.

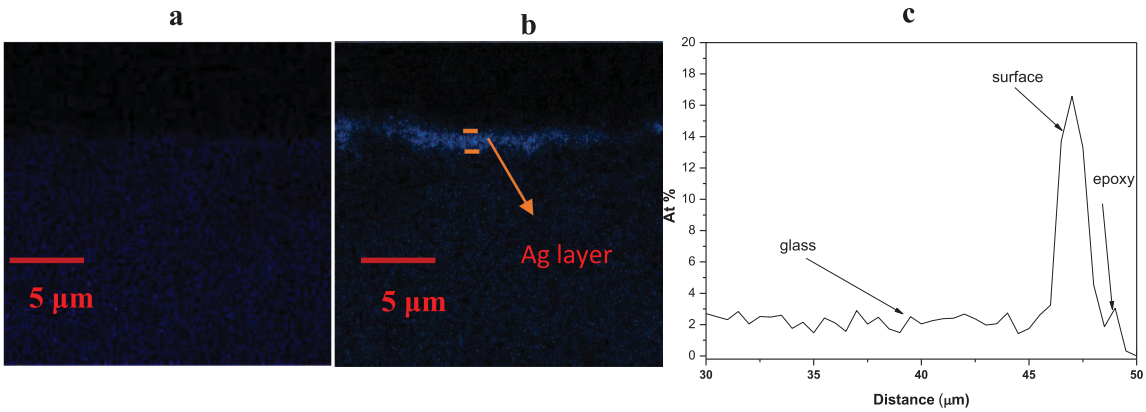

Fig. 5.. Ag color mapping measured at the cross-section of the 2.5Ag glass prior to a) and after heat treatment at (T_g + 10 °C) for 4 h b) (the gradient of the blue color being related to the Ag content) and Ag concentration profile measured from the surface of the heat-treated glasses c).

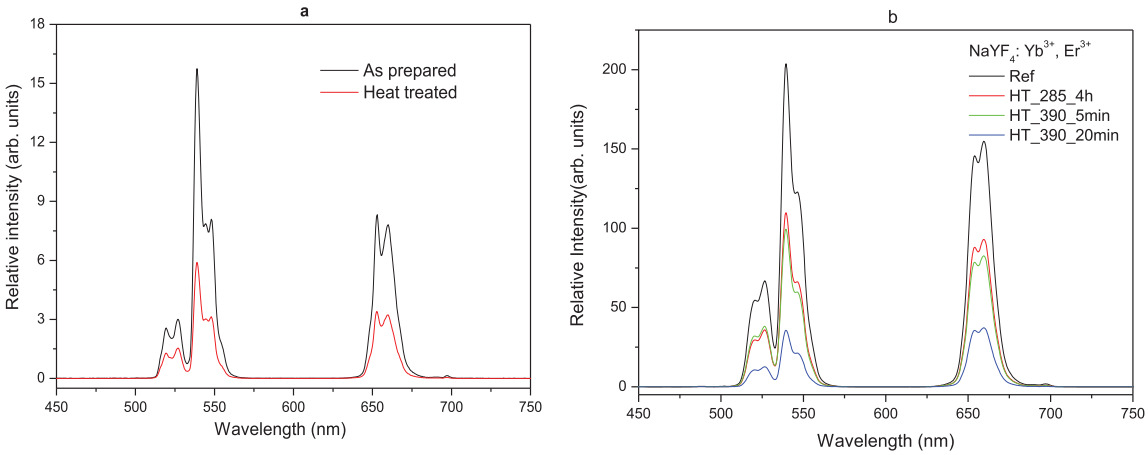

Fig. 6.. Upconversion spectra of the 2.5Ag glass prior to and after heat treatment at ($T_g + 10$ °C) for 4 h.a) and upconversion spectra of the NCs alone prior to and after heat treatment at different temperatures and durations b) ($\lambda_{exc} = 975$ nm).

Declaration of Competing Interest

The authors declare that they have no known competing financial interests or personal relationships that could have appeared to influence the work reported in this paper.

Acknowledgement

Academy of Finland (Flagship Programme, Photonics Research and Innovation PREIN-320165 and Academy Project −326418) is greatly acknowledged for the financial support. This work made use of Tampere Microscopy Center facilities at Tampere University. Dr. Mika Lastusaari from Turku University (Finland) is also acknowledged for providing the $NaYF_4:Yb^{3+}$, Er^{3+} nanocrystals.

References

[1] W.S. Tsang, W.M. Yu, C.L. Mak, W.L. Tsui, K.H. Wong, H.K. Hui, Evidence of the influence of phonon density on Tm^{3+} upconversion luminescence in tellurite and germanate glasses, J. Appl. Phys. 91 (2002) 1871–1874, https://doi.org/10.1063/1.1429762.

[2] H. Lin, E.Y.B. Pun, B.J. Chen, Y.Y. Zhang, Rare-earth ion doped lead- and cadmium-free bismuthate glasses, J. Appl. Phys. 103 (2008) 56103, https://doi.org/10.1063/1.2891252.

[3] Y. Il Park, K.T. Lee, Y.D. Suh, T. Hyeon, Upconverting nanoparticles: a versatile platform for wide-field two-photon microscopy and multi-modal in vivo imaging, Chem. Soc. Rev. 44 (2015) 1302–1317, https://doi.org/10.1039/C4CS00173G.

[4] N.M. Idris, M.K.G. Jayakumar, A. Bansal, Y. Zhang, Upconversion nanoparticles as versatile light nanotransducers for photoactivation applications, Chem. Soc. Rev. 44 (2015) 1449–1478, https://doi.org/10.1039/C4CS00158C.

[5] D. Auzel, Pecile F., D. Morin, Rare Earth Doped Vitroceramics, New, Efficient, Blue and Green Emitting Materials for Infrared Up-Conversion, J. Electrochem. Soc. 122 (1975) 101–107.

[6] J. Ruan, Z. Yang, A. Huang, H. Zhang, J. Qiu, Z. Song, Thermomchromic Reaction-Induced Reversible Upconversion Emission Modulation for Switching Devices and Tunable Upconversion Emission Based on Defect Engineering of WO_3:yb^{3+},Er^{3+} Phosphor, ACS Appl. Mater. Interfaces 10 (2018) 14941–14947, https://doi.org/10.1021/acsami.8b03616.

[7] R.J. Amjad, M.R. Sahar, S.K. Ghoshal, M.R. Dousti, S. Riaz, B.A. Tahir, Enhanced infrared to visible upconversion emission in Er^{3+} doped phosphate glass: role of silver nanoparticles, J. Lumin. 132 (2012) 2714–2718, https://doi.org/10.1016/j.jlumin.2012.05.008.

[8] M. Saad, W. Stambouli, S.A. Mohamed, H. Elhouichet, Ag nanoparticles induced luminescence enhancement of Eu^{3+} doped phosphate glasses, J. Alloys Compd. 705 (2017) 550–558, https://doi.org/10.1016/j.jallcom.2016.12.410.

[9] D.S. Brauer, N. Karpukhina, R.V. L.aw, R.G. Hill, Effect of TiO_2 addition on structure, solubility and crystallisation of phosphate invert glasses for biomedical applications, J. Non Cryst. Solids 356 (2010) 2626–2633, https://doi.org/10.1016/j.jnoncrysol.2010.03.022.

[10] N. Kanwal, H. Toms, A.C. Hannon, F.A. Perras, D.L. Bryce, N. Karpukhina, I. Abrahams, Structure and solubility behaviour of zinc containing phosphate glasses, J. Mater. Chem. B. 3 (2015) 8842–8855, https://doi.org/10.1039/C4TB01504E.

[11] H. Zheng, D. Gao, Z. Fu, E. Wang, Y. Lei, Y. Tuan, M. Cui, Fluorescence enhancement of Ln^{3+} doped nanoparticles, J. Lumin. 131 (2011) 423–428, https://doi.org/10.1016/j.jlumin.2010.09.026.

[12] C.D. Geddes, J.R. Lakowicz, Editorial: metal-Enhanced Fluorescence, J. Fluoresc. 12 (2002) 121–129, https://doi.org/10.1023/A:1016875709579.

[13] M. Epifani, C. Giannini, L. Tapfer, L. Vasanelli, Sol–Gel Synthesis and Characterization of Ag and Au Nanoparticles in SiO_2, TiO_2, and ZrO_2 Thin Films, J. Am. Ceram. Soc. 83 (2000) 2385–2393, https://doi.org/10.1111/j.1151-2916.2000.tb01566.x.

[14] R. de Almeida, D.M. da Silva, L.R.P. Kassab, C.B. de Araújo, Eu^{3+} luminescence in tellurite glasses with gold nanostructures, Opt. Commun. 281 (2008) 108–112, https://doi.org/10.1016/j.optcom.2007.08.072.

[15] T. Hayakawa, S.T. Selvan, M. Nogami, Enhanced fluorescence from Eu^{3+} owing to surface plasma oscillation of silver particles in glass, J. Non. Cryst. Solids 259 (1999) 16–22, https://doi.org/10.1016/S0022-3093(99)00531-1.

[16] H. Granbohm, J. Larismaa, S. Ali, L.-.S. Johansson, S.-.P. Hannula, Control of the Size of Silver Nanoparticles and Release of Silver in Heat Treated SiO_2-Ag Composite Powders, Mater. (Basel, Switzerland) 11 (2018) 80, https://doi.org/10.3390/ma11010080.

[17] Z. Liu, H. Wang, H. Li, X. Wang, Red shift of plasmon resonance frequency due to the interacting Ag nanoparticles embedded in single crystal SiO_2 by implantation, Appl. Phys. Lett. 72 (1998) 1823–1825, https://doi.org/10.1063/1.121196.

[18] N. Perkas, G. Amirian, G. Applerot, E. Efendiev, Y. Kaganovskii, A.V. Ghule, B.-.J. Chen, Y.-.C. Ling, A. Gedanken, Depositing silver nanoparticles on/in a glass slide by the sonochemical method, Nanotechnology 19 (2008) 435604, , https://doi.org/10.1088/0957-4484/19/43/435604.

[19] O. Samson, T. Adeeko, E. Makama, Synthesis and Optical Characterization of Silver Nanoparticles (Ag-NPs) Thin Films (TFs) Prepared by Silar Technique, Int. J. Curr. Res. Acad. Rev. 5 (2017) 15–24, https://doi.org/10.20546/ijcrar.2017.512.003.

[20] L. Kuusela, A. Veber, N.G. Boetti, L. Petit, Impact of ZnO Addition on Er^{3+} Near-Infrared Emission, the Formation of Ag Nanoparticles, and the Crystallization of Sodium Fluorophosphate Glass, Materials (Basel) (2020) 13, https://doi.org/10.3390/ma13030527.

[21] H. Fares, H. Elhouichet, B. Gelloz, M. Férid, Surface plasmon resonance induced Er3+ photoluminescence enhancement in tellurite glass, J. Appl. Phys. 117 (2015) 193102, , https://doi.org/10.1063/1.4921436.

[22] G. Chen, C. Yang, P.N. Prasad, Nanophotonics and Nanochemistry: controlling the Excitation Dynamics for Frequency Up- and Down-Conversion in Lanthanide-Doped Nanoparticles, Acc. Chem. Res. 46 (2013) 1474–1486, https://doi.org/10.1021/ar300270y.

[23] H. Nguyen, M. Tuomisto, J. Oksa, T. Salminen, M. Lastusaari, L. Petit, Upconversion in low rare-earth concentrated phosphate glasses using direct $NaYF_4$:er^{3+}, Yb^{3+} nanoparticles doping, Scr. Mater. 139 (2017) 130–133, https://doi.org/10.1016/j.scriptamat.2017.06.050.

[24] N. Ojha, M. Tuomisto, M. Lastusaari, L. Petit, Upconversion from fluorophosphate glasses prepared with $NaYF_4$:er^{3+},Yb^{3+} nanocrystals, RSC Adv. 8 (2018) 19226–19236, https://doi.org/10.1039/C8RA03298J.

[25] I. Hyppänen, J. Hölsä, J. Kankare, M. Lastusaari, L. Pihlgren, T. Soukka, Preparation and Up-Conversion Luminescence Properties of $NaYF_4$:yb^{3+},Er^{3+} Nanomaterials, Terrae Rarae 16 (2009) 1–6.

[26] N. Ojha, H. Nguyen, T. Laihinen, T. Salminen, M. Lastusaari, L. Petit, Decomposition of persistent luminescent microparticles in corrosive phosphate glass melt, Corros. Sci. 135 (2018) 207–214, https://doi.org/10.1016/j.corsci.

2018.02.050.
[27] O.L. Malta, P.A. Santa-Cruz, G.F. De Sá, F. Auzel, Fluorescence enhancement induced by the presence of small silver particles in Eu^{3+} doped materials, J. Lumin. 33 (1985) 261–272, https://doi.org/10.1016/0022-2313(85)90003-1.
[28] D. Manikandan, S. Mohan, K.G.M. Nair, Absorption and luminescence of silver nanocomposite soda-lime glass formed by Ag^{+}–Na^{+} ion-exchange, Mater. Res. Bull. 38 (2003) 1545–1550, https://doi.org/10.1016/S0025-5408(03)00165-X.
[29] Y. Dai, X. Hu, C. Wang, D. Chen, X. Jiang, C. Zhu, B. Yu, J. Qiu, Fluorescent Ag nanoclusters in glass induced by an infrared femtosecond laser, Chem. Phys. Lett. 439 (2007) 81–84, https://doi.org/10.1016/j.cplett.2007.03.043.
[30] T. Jitwatcharakomol, E. Meechoowa, M. Jiarawattananon, S. Jiemsirilers, Kinetic Investigation on the Color Striking of Gold Ruby Glass, Procedia Eng. 32 (2012) 584–589, https://doi.org/10.1016/j.proeng.2012.01.1312.
[31] N. Ojha, T. Laihinen, T. Salminen, M. Lastusaari, L. Petit, Influence of the phosphate glass melt on the corrosion of functional particles occurring during the preparation of glass-ceramics, Ceram. Int. 44 (2018) 11807–11811, https://doi.org/10.1016/j.ceramint.2018.03.267.
[32] V.K. Tikhomirov, V.D. Rodríguez, A. Kuznetsov, D. Kirilenko, G. Van Tendeloo, V.V. M.oshchalkov, Preparation and luminescence of bulk oxyfluoride glasses doped with Ag nanoclusters, Opt. Express 18 (2010) 22032–22040, https://doi.org/10.1364/OE.18.022032.
[33] J.A. Jiménez, M. Sendova, Catalyst role of Nd^{3+} ions for the precipitation of silver nanoparticles in phosphate glass, J. Alloys Compd. 691 (2017) 44–50, https://doi.org/10.1016/j.jallcom.2016.08.231.
[34] L. Li, Y. Yang, D. Zhou, Z. Yang, X. Xu, J. Qiu, Influence of the Eu^{2+} on the Silver Aggregates Formation in Ag^{+}–Na^{+} Ion-Exchanged Eu^{3+}-Doped Sodium–Aluminosilicate Glasses, J. Am. Ceram. Soc. 97 (2014) 1110–1114, https://doi.org/10.1111/jace.12745.
[35] P. Ebeling, D. Ehrt, M. Friedrich, X-ray induced effects in phosphate glasses, Opt. Mater. (Amst). 20 (2002) 101–111, https://doi.org/10.1016/S0925-3467(02)00052-6.
[36] W.M. Pontuschka, J.M. Giehl, A.R. Miranda, Z.M. Da Costa, A.M. Alencar, Effect of the Al_2O_3 addition on the formation of silver nanoparticles in heat treated soda-lime silicate glasses, J. Non. Cryst. Solids 453 (2016) 74–83, https://doi.org/10.1016/j.jnoncrysol.2016.09.028.
[37] F. Auzel, Upconversion and Anti-Stokes Processes with f and d Ions in Solids, Chem. Rev. 104 (2004) 139–174, https://doi.org/10.1021/cr020357g.
[38] M. Ennouri, L. Kuusela, I. Jlassi, B. Gelloz, L. Petit, H. Elhouichet, Impact of Ag_2O Content on the Optical and Spectroscopic Properties of Fluoro-Phosphate Glasses, Materials (Basel) 12 (2019) 3516, https://doi.org/10.3390/ma12213516.
[39] V. Amendola, O.M. Bakr, F. Stellacci, A Study of the Surface Plasmon Resonance of Silver Nanoparticles by the Discrete Dipole Approximation Method: effect of Shape, Size, Structure, and Assembly, Plasmonics 5 (2010) 85–97, https://doi.org/10.1007/s11468-009-9120-4.
[40] D. Yang, Q. Pan, S. Kang, G. Dong, J. Qiu, Weakening thermal quenching to enhance luminescence of Er^{3+} doped β-$NaYF_4$ nanocrystals via acid-treatment, J. Am. Ceram. Soc. 102 (2019) 6027–6037, https://doi.org/10.1111/jace.16490.

PUBLICATION V

Nucleation and growth behavior of Er^{3+} doped oxyfluorophosphate glasses

N. Ojha, A. Szczodra, N. G. Boetti, J. Massera and L. Petit

RSC Advances, Vol. 10, Issue 43, pp. 25703-25716
https://doi.org/10.1039/D0RA04681G

RSC Advances

PAPER

Cite this: *RSC Adv.*, 2020, **10**, 25703

Nucleation and growth behavior of Er^{3+} doped oxyfluorophosphate glasses

N. Ojha, *[a] A. Szczodra,[a] N. G. Boetti,[b] J. Massera[c] and L. Petit[a]

Received 27th May 2020
Accepted 1st July 2020

DOI: 10.1039/d0ra04681g

rsc.li/rsc-advances

The nucleation and growth behavior of glasses with the composition (75 $NaPO_3$-25 $CaF_2)_{100-x}$–$(TiO_2/ZnO/MgO)_x$, with $x = 0$ and $x = 1.5$ (in mol%) is investigated. The glasses possess similar activation energy for crystallization and Johnson–Mehl–Avrami exponent, with value 2 confirming bulk crystallization of crystals with needle like shape. The Ti and Mg glasses exhibit broader nucleation curve and higher $T_{n\ max}$ than the $x = 0$ and Zn glasses due to their stronger field strength. The crystal growth rates were determined and validated using SEM. Finally, we showed that the nucleation and growth of glasses can be controlled due to the large difference between onset of crystallization and maximum nucleation temperature which is crucial when preparing novel transparent glass-ceramics.

Introduction

Addition of rare-earth (RE) ions in glasses has been of great interest for a wide range of applications in the field of telecommunications, light detection and ranging (LIDAR), solar panels, color sensing, biomedical diagnostics, just to name a few.[1–3] Among the rare earth ions, Er^{3+} ions have been in the limelight due to their large number of energy levels and especially due to the transition from $^4I_{13/2}$ to $^4I_{15/2}$ levels which corresponds to the emission at 1530 nm that makes Er^{3+} doped glasses useful for eye-safe laser and optical telecommunications of the third window.[4,5] Oxyfluorophosphate glasses in particular are promising glasses for the fabrication of new lasing glasses as these glasses combine the properties of both oxides and fluorides. These glasses possess good chemical durability, thermal stability, mechanical strength and high rare earth ion solubility.[6] Additionally, these oxyfluorophosphate glasses can be engineered with low melting point and so they can be prepared quite easily as compared to their silica counterparts.

Nowadays, glass-ceramics (GCs) are gaining much more attention due to their widespread applications in optical, laser and biomedical fields to name a few.[7] Stookey discovered the first GCs in 1960 where he defined them as special glasses that contains nucleating agent and controlled crystallization.[8] Transparent RE doped GCs which contain crystals homogeneously distributed in the volume of the glass matrix are considered promising materials for a variety of additional applications such as optical amplifiers, optical electronic chips, luminescence labels and 3D displays.[9] Indeed, these glass-ceramics exhibit larger absorption and emission cross-sections and energy transfer rates compared to their glassy counterparts when the desirable crystalline phases are generated around the rare earth ions or transition metal ions.[10,11] Auzel *et al.*[12] successfully prepared a partially crystalline material having luminescence efficiency double than that of LaF_3:Er^{3+}, Yb^{3+} phosphor using lead fluoride and several glass forming oxides. However, those materials lacked transparency due to the presence of large crystals (~10 μm). For the GCs to be transparent, the crystals need to have a size smaller than the incident light wavelength.[13] Therefore, the size and size distribution of the crystals as well as the refractive index difference between the crystals and the glass should be tailored in order to minimize light scattering. One of the first transparent glass-ceramics was successfully prepared with crystalline Pb_xCd_{1-x}-F_2 cubic fluoride phase doped with Er^{3+} and Yb^{3+} ions in ref. 14. Since this achievement, great effort has been made on the preparation of novel transparent GCs within different glass systems such as silicate,[15–19] tellurite,[20–23] germanate[24–27] and phosphate,[28–31] just to cite few examples.

When developing novel GCs, it is therefore crucial to understand the formation of crystals inside the glass matrix in order to control their size and size distribution in the amorphous network. The GCs are usually fabricated using a three (3) step process: at first, a glass is obtained. Then, the glass is heat treated at a specific temperature called the nucleation temperature to form the nuclei and finally heat treated at higher temperature in order to grow the nuclei into crystals. This process can result in a glass having crystals that are relatively uniform in size and dispersed homogeneously within the glassy matrix.[32] The crystallization is typically defined by the activation energy for crystallization, which is related to the temperature dependence of the crystallization process and by the Johnson–

[a]*Photonics Laboratory, Tampere University, Korkeakoulunkatu 3, FI-33720 Tampere, Finland. E-mail: nirajan.ojha@tuni.fi*

[b]*Fondazione LINKS – Leading Innovation & Knowledge for Society, Via P. C. Boggio 61, 10138 Torino, Italy*

[c]*Faculty of Medicine and Health Technology, Tampere University, Korkeakoulunkatu 3, FI-33720 Tampere, Finland*

Mehl–Avrami (JMA) exponent, which provides the information on the crystal growth dimensionality.[33–35] It is also important to estimate the growth rate of the crystals as a function of the heat treatment temperature, in order to fabricate transparent GCs.

In our previous study,[36] Er^{3+} doped glasses with the composition $(75NaPO_3–(25 - x)CaO–xCaF_2)$ were prepared and heat treated. We showed that the transparent GC can be obtained from the glass with $x = 25$. CaF_2 crystals were found in the volume of the glass and doped with Er^{3+}.[37]

In this study, we present a complete study on the nucleation and growth behavior of the glass with $x = 25$. We also investigate the impact of the addition of TiO_2, MgO and ZnO in this glass on the precipitation of the Er^{3+} doped CaF_2 crystals in the volume of the glass during heat treatment. We report first the study of the impact of the glass composition on the thermal, optical, structural and luminescence properties of the newly developed glasses. The activation energy for crystallization, the Johnson–Mehl–Avrami exponent, the nucleation-like curves and the growth rates of the glasses are presented and discussed as a function of the glass composition.

Experimental

Oxyfluorophosphate glasses with the composition $(100\text{-}x\text{-}0.25)(75NaPO_3–25CaF_2) – x(TiO_2/ZnO/MgO)$ (in mol%), doped with 0.25 mol% Er_2O_3, with $x = 0$ and $x = 1.5$ were prepared using standard melting procedure in air using platinum crucible. The glass with $x = 0$ is labelled as Ref and the glasses prepared with 1.5 mol% TiO_2 as Ti glass, with 1.5 mol% ZnO as Zn glass and with 1.5 mol% MgO as Mg glass. The chemicals used for the glass preparation were $NaPO_3$ (Alfa-Aesar, technical grade), CaF_2 (Honeywell-Fluka, 99%), Er_2O_3 (Sigma-Aldrich, 99.9%), MgO (Honeywell, ≥99%), TiO_2 (Sigma-Aldrich, 99.8%) and ZnO (Sigma-Aldrich, 99.99%). The glasses were melted for 5 minutes between 900 and 1025 °C depending on the composition of the glass. After melting, the glasses were quenched and annealed for 6 h at 40 °C below their respective glass transition temperature to release the stress from the quench. The glasses were polished and finally heat treated for 17 h at 20 °C above their glass transition temperature T_g and then at $\sim T_p$ for upto 6 hours.

The glass transition temperature (T_g) as well as the onset of the crystallization (T_x) and the crystallization temperature (T_p) of the glasses were determined by differential thermal analysis (DTA) (TA instruments SDT Q600) using various heating rates (5°, 10°, 15°, and 20 °C min^{-1}) using glasses crushed into powder with a 125–250 μm particles size. The measurements were performed using platinum pans in N_2 atmosphere. The glass transition temperature was taken at the inflection point of the endotherm, as obtained by taking the minima of first derivative of the DTA curve. T_p was taken at the maximum of the exothermic peak and T_x at the onset of the crystallization peak. All measurements were performed with an accuracy of ±3 °C.

Electron Probe MicroAnalyzer (EPMA) (CAMECA, SX100) equipped with 5 wavelength dispersive X-ray analyzers (WDX) was used to determine the fluorine content with an accuracy of ±0.1 at%. The EPMA was operated at 15 keV and 40 nA. Quantitative analyses were performed using the Cameca QUANTITOOL analytical programme, calibrated with ErF_3 reference standard, applying a PAP matrix correction. A scanning electron microscope (Carl Zeiss Crossbeam 540) equipped with Oxford Instruments X-MaxN 80 EDS detector was used to image and analyse the composition of the crystals. The error of composition is ±1.5 mol%. For the EPMA and SEM analysis, the glasses and GCs were polished and coated with a carbon layer to prevent charging.

The activation energy for crystallization (E_c) was determined by measuring T_p at different heating rates of powdered sample of size 125–250 μm and then applying the Kissinger equation:[34]

$$\ln\left(\frac{\beta}{T_p^2}\right) = -\frac{E_c}{RT_p} + \text{constant} \quad (1)$$

where ß is the heating rate, T_p is the maximum of the crystallization peak measured with heating rates of 5°, 10°, 15°, and 20 °C min^{-1}, and R is the gas constant. The accuracy of the measurement was ±30 kJ mol^{-1}.

To verify the Kissinger equation, E_c was also determined using the Friedman method using the equation:[35]

$$\ln\left(\frac{d\alpha_i}{dt}\right) = -\frac{E_{c\alpha}}{RT_i} + \text{constant} \quad (2)$$

where $d\alpha_i$ is the transformation rate at a temperature T_i.

The Johnson–Mehl–Avrami (JMA) exponent, which is related to the dimensionality of the crystallization (surface *vs.* bulk crystallization), was determined using the equation proposed by Augis and Bennett:[38]

$$n = \frac{2.5}{\Delta T_{FWHM}} \frac{T_p^2}{\frac{E_c}{R}} \quad (3)$$

where n is the JMA exponent, ΔT_{FWHM} is the full width at half maximum of the DTA peak, E_c is the activation energy for crystallization, and R is the gas constant. The accuracy of the measurement was found to be ±0.1.

n was also obtained using the Ozawa method from the fraction of glass crystallized at various heating rates at a constant temperature using the following equation:[33]

$$\left[\frac{d(\ln(-\ln(1-\alpha)))}{d(\ln(\beta))}\right]_T = -n \quad (4)$$

where ß is the heating rate and α volume fraction of glass crystallized at a fixed temperature T. Based on this equation, the plot $\ln(-\ln(1-\alpha)) = f(\ln(\beta))$ yields a straight line with a slope equals to $-n$. The accuracy of the measurement using this method was ±0.5.

The temperature of maximum nucleation ($T_{n\ max}$) was determined from the nucleation-like curve using the method described by Marotta *et al.*[39] In this method, the glass powder was subjected to an isothermal hold, inside the DTA, at various temperatures T (between T_g and T_x) near the suspected temperature of the maximum nucleation ($T_{n\ max}$). The temperature was then reduced to 200 °C and finally increased to a temperature T, above the crystallization temperature. The nucleation like curve was obtained from the plot of

Table 1 Density and thermal properties of the investigated glasses. Also included is the F quantification using EPMA

	Quantification using EPMA/WDX							
Glass label	Expected F at%	Measured F at% (±0.1 at%)	T_m (°C)	ρ ± 0.02 (g cm^{-3})	T_g ± 3 (°C)	T_x ± 3 (°C)	T_p ± 3 (°C)	ΔT ± 6 (°C)
Ref	11.1	9.2	900	2.63	269	323	338	54
Ti	11.0	8.9	1025	2.65	286	350	370	64
Mg		9.4	900	2.66	279	345	365	66
Zn		9.1	1000	2.65	276	334	350	58

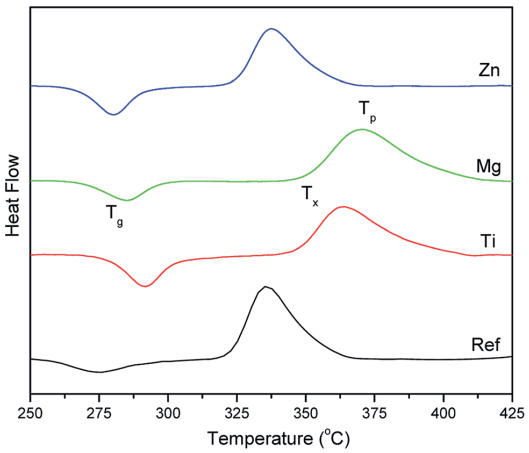

Fig. 1 DTA thermogram of the investigated glasses.

$(1/T_p^{\circ} - 1/T_p) = f(T)$, (where T_p and T_p° are the maximum of the exothermal peak with and without the nucleation thermal hold). The maximum of the obtained curve gives $T_{n\ max}$.

The phases present in the heat treated glasses were analyzed using the Panalytical EMPYREAN multipurpose X-ray Diffractometer (XRD) using nickel filtered copper K-Alpha radiation. The spectra were obtained using the Bragg–Brentano geometry and by rotating the sample holder around the Phi-axis at a constant speed of 16 revolutions per minute.

The absorption spectra were measured using a UV-Vis-NIR spectrophotometer (UV-3600 Plus, Shimadzu) from 200 to 1800 nm with 0.5 nm interval. Samples were polished and their thickness were measured using a digital caliper with an accuracy of ±0.05 mm. The absorption cross-section σ (in cm^2) was calculated using the following equation:

$$\sigma(\lambda) = \frac{2.303}{NL}\log\left(\frac{I_o}{I}\right) \quad (5)$$

where N is the number of ions per cm^3 absorbing at the specific wavelength (λ), I/I_o is the absorbance and L is the thickness of the sample (in cm). The accuracy of the measurement is ±10%.

The glass samples, crushed into powder, were excited using a TEC-cooled fiber-coupled multimode laser (II–VI Laser Enterprise). The center emission wavelength (λ_{exc}) of the laser was ~975 nm and its incident power at the sample surface was ~23.5 mW. The resulting normal photoluminescence (PL) and up-conversion spectra were measured using a Spectro 320 optical spectrum analyzer (Instrument Systems Optische Messtechnik GmbH, Germany) at room temperature. The spectrum analyzer was equipped with a photomultiplier tube capable of measuring wavelengths between 350 and 850 nm and an InGaAs detector for wavelengths ranging from 800 to 1700 nm. The luminescence light was collected from the samples to the spectrum analyzer using a lens and a liquid light guide.

The lifetime of the Er^{3+}:$^4I_{13/2}$ energy level was measured using a fiber pigtailed laser diode at 976 nm. The signal was recorded using a digital oscilloscope (Tektronix TDS350) and the decay traces were fitted using single exponential. The detector used for this measurement was a Thorlabs PDA10CS-EC. The accuracy of the measurement was ±0.20 ms.

The IR spectra of the powder glasses were measured using a Perkin Elmer Spectrum FTIR2000 spectrometer with Attenuated Total Reflection (ATR) mode between 600 and 2000 cm^{-1} with a resolution of 2 cm^{-1} and 8 scan accumulation.

Results and discussion

The thermal and physical properties of the glasses are shown in Table 1. DTA thermogram of the investigated glasses can be

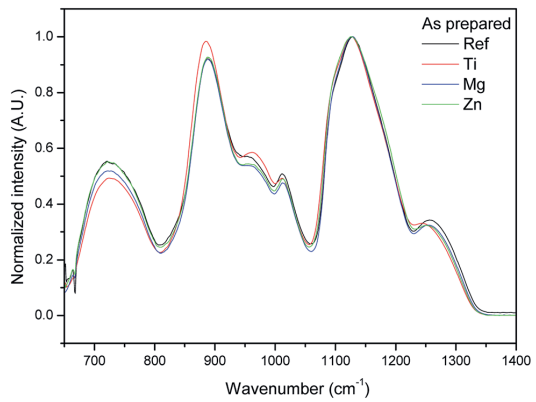

Fig. 2 Normalized IR spectra of the investigated glasses.

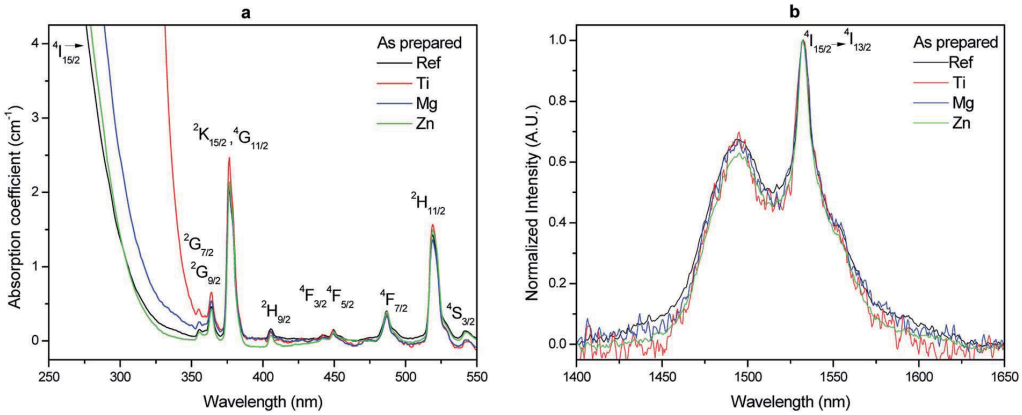

Fig. 3 Absorption spectra (a) and normalized absorption band at 1500 nm (b) of the investigated glasses.

Table 2 Absorption coefficients and cross-sections of the investigated glasses

Glass label	Er^{3+} ions/ cm^3 (10^{19}) ± 5%	α_{abs} at 975 nm (cm^{-1})	σ_{Abs} at 975 nm (10^{-21} cm^2) ± 10%	α_{abs} at 1532 nm (cm^{-1})	σ_{Abs} at 1532 nm (10^{-21} cm^2) ± 10%
Ref	8.19	0.16	2.01	0.52	6.32
Ti	8.27	0.19	2.34	0.52	6.23
Mg	8.35	0.15	1.82	0.47	5.61
Zn	8.27	0.18	2.16	0.53	6.41

seen in Fig. 1. The changes in the glass composition leads to a slight increase in the density, T_g, T_x and T_p, the addition of TiO_2 being the most effective in these changes. As seen in Table 1, the increase in the melting temperature decreases the F at% in the glass as measured using EPMA in agreement with our previous study.[19] Therefore, the increase in T_g may be related to the different F at% in the glasses but it may also indicate that the changes in the glass composition increases the strength of the network and the bond strength as reported in ref. 40. The changes in the glass composition increases slightly ΔT ($\Delta T = T_x - T_g$) confirming that the addition Ti, Mg or Zn can be used to increase slightly the resistance of the glass towards crystallization. However, one should point out the ΔT of the investigated glasses still remains lower than 90 °C.

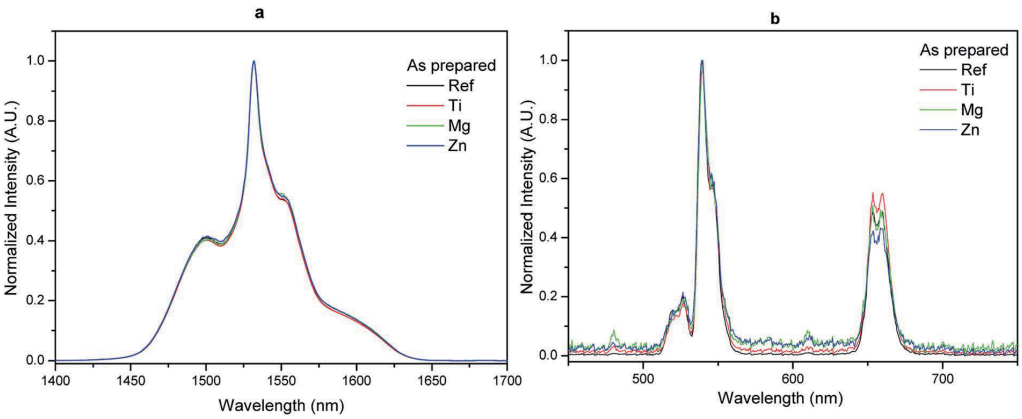

Fig. 4 Normalized emission spectra centered at 1.5 μm (a) and normalized upconversion spectra (b) of the investigated glasses ($\lambda_{exc} = 975$ nm).

Table 3 Er^{3+}:$^4I_{13/2}$ Lifetime values of the investigated glasses before and after heat treatment at (T_g + 20 °C) for 17 h and at T_p for 1 to 6 hours

Glass label	As-prepared glasses	Duration of the heat treatment at T_p for		
		1 h	3 h	6 h
Ref	8.2	8.9	8.9	8.8
Ti	8.4	8.7	8.6	8.9
Mg	8.2	8.7	8.6	8.7
Zn	8.3	8.6	8.8	8.7

The IR spectra of the glasses are presented in Fig. 2. They are normalized to the main band at ~1130 cm^{-1}. Consequently, the intensity changes are expressed relatively to the main band. The IR spectra of the new glasses are similar to those reported in ref. 36 where a detailed attribution of the bands can be found. The addition of ZnO and MgO leads to a small decrease in intensity of the bands at about 700, 950, ~1000 and 1250 cm^{-1} and to a slight increase in the intensity of the shoulder at 1100 cm^{-1} as compared to the main band whereas the addition of TiO_2 increases the intensity of the bands at around 880 and 950 cm^{-1} and decreases the intensity of the band at 1250 cm^{-1}. One can also notice that the position of the bands at 880 and 1250 cm^{-1} shifts towards smaller wavenumbers when adding TiO_2 due to the strong field strength of the Ti ions. These changes in the IR spectra can be related to a decrease in the Q^2 units and to an increase in Q^1 units as expected from the change in the O/P ratio when adding ZnO, MgO and TiO_2.[41] In agreement with,[42] Mg, Ti and Zn are expected to cross-link the phosphate chains by creating P–O–Mg/Ti/Zn bonds at the expense of P–O–P bonds associated with a reduction in the number of Q^2 units.[41,43] Therefore, the addition of ZnO, MgO and TiO_2 is suspected to cause distortion of the glass network which is in agreement with the increase in T_g seen in Table 1. Similar results were reported in ref. 44. Due to the higher field strength of Mg compared to Zn,[45] the changes in the IR spectra are more visible when adding MgO than ZnO in the network.

The absorption spectra and the normalized absorption spectra are shown in Fig. 3a and b respectively. As seen in Fig. 3a, the addition of TiO_2 leads to a shift of the band gap to longer wavelength most probably due to the presence of Ti^{3+} according to ref. 46. The change in the position of the band gap can also be related to the formation of Ti–O–P bonds as discussed earlier. Due to the decrease in the connectivity of the phosphate network, the bandgap is shifted to longer wavelengths when adding MgO and ZnO, the shift being more visible when adding MgO. The shape of the absorption band centered at ~1532 nm is similar in all glasses (Fig. 3b).

The absorption coefficients and the absorption cross-sections at 975 and 1532 nm are presented in Table 2. Within the accuracy of the measurement, the changes in the glass composition have no impact on the absorption cross-sections at

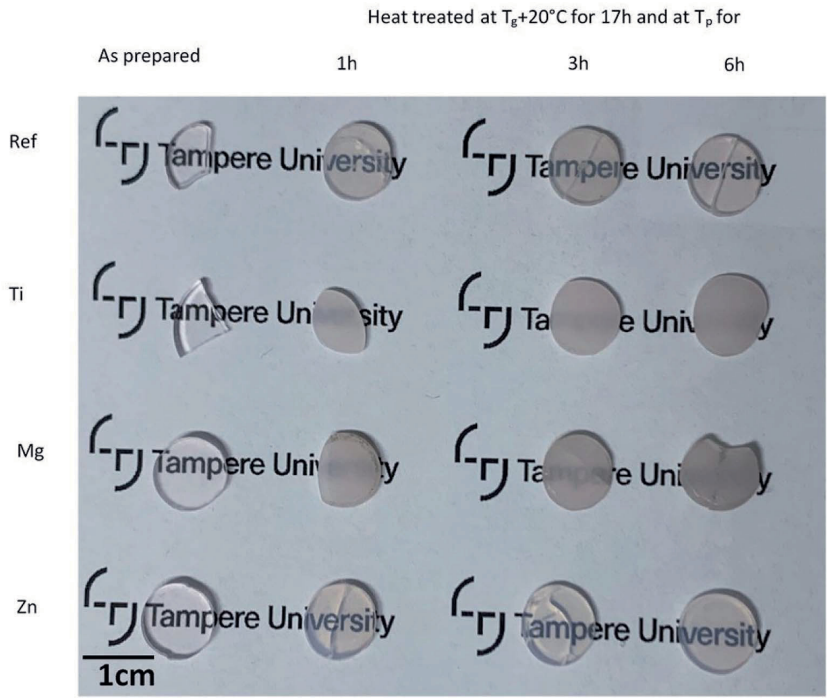

Fig. 5 Pictures of the glasses heat treated at T_g + 20 °C for 17 h and at T_p for 1, 3 and 6 hours.

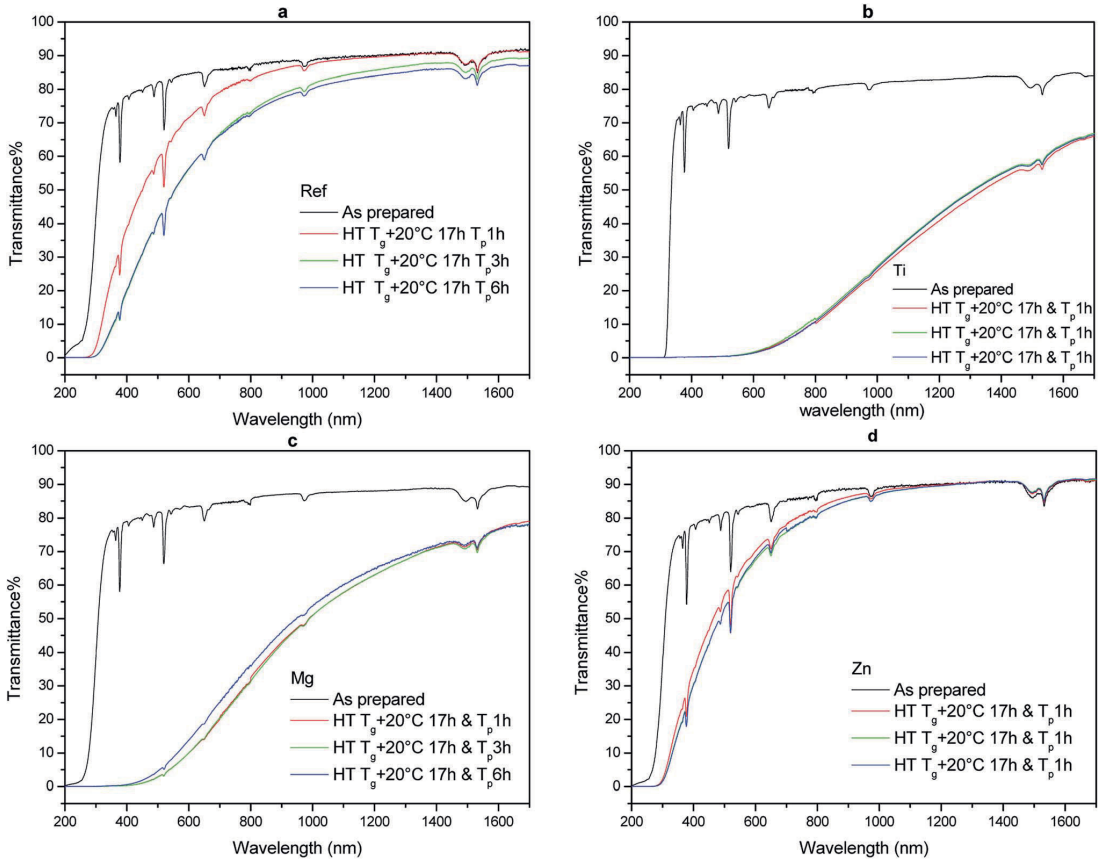

Fig. 6 Transmittance spectra of the Ref (a), Ti (b), Mg (c) and Zn (d) glasses heat treated at T_g + 20 °C for 17 h and at T_p for 1, 3 and 6 hours (thickness of the glasses was ~1mm).

those wavelengths. Therefore, the site of the Er^{3+} ions is suspected not to be strongly impacted by the changes in the glass composition; Ti, Mg and Zn are not suspected to participate to the second coordination shell around Er^{3+}.

The spectra presented in Fig. 4a exhibit the typical broadband Er^{3+} emission ($^4I_{13/2} \rightarrow {}^4I_{15/2}$) in glasses.[3] The glasses exhibit similar intensity (within ± 10%) and shape of the emission centered at 1.5 μm confirming that Ti, Mg and Zn have no noticeable impact on the site of the Er^{3+} ions. Similarly, the relative intensity of the upconversion was found not to be affected by the change in the composition (within 10%). As seen in Fig. 4b, the upconversion spectra exhibit the typical green and red emissions from Er^{3+} ions in amorphous site after pumping at 975 nm. These green and red emissions correspond to $^2H_{11/2}$ (525 nm) $^4S_{3/2}$ (550 nm) $\rightarrow {}^4I_{15/2}$ and $^4F_{9/2} \rightarrow {}^4I_{15/2}$ transitions of Er^{3+}, respectively.[47] No noticeable changes can be seen in the shape of the emission band at 550 nm, which can be associated to a hypersensitive transition[48] with the changes in the glass composition confirming that the site of the Er^{3+} ions is not strongly modified by the addition of TiO_2, MgO and ZnO. The addition of ZnO has no impact on the ratio of the intensity of the green to red emissions while the intensity of the red emission increases slightly as compared to the green emission when adding TiO_2 and MgO probably due to their strong field strength.

The lifetime values of the Er^{3+}:$^4I_{13/2}$ level in the investigated glasses are listed in Table 3. Within the accuracy of the measurement, the change in the glass composition has no impact on the lifetime value confirming that the sites of Er^{3+} ions are similar in the glasses. One should point out that the lifetime values are similar to those reported in ref. 37 but longer than the lifetime values reported inref. 36 although the Er_2O_3 concentration is larger in the investigated glasses than in ref. 36. It is possible that the glasses used in ref. 36 contain a larger amount of OH groups, known as quenchers of Er^{3+} ions luminescence,[49,50] than the glasses used in this study and in ref. 37.

As performed in ref. 36 and 37, the glasses were heat treated at T_g + 20 °C for 17 h and then at T_p for 1 to 6 h. The glasses were polished prior to the heat treatment and were heat treated in air on a Pt foil to avoid contamination from the sample holder. The pictures of the glasses prior to and after heat treatment are presented in Fig. 5. All the investigated glasses exhibit bulk

crystallization. The Ref and the Zn glasses are still transparent while the Ti and Mg glasses become opaque after 6 h at T_p.

The transmittance spectra of the glasses prior to and after heat treatment are presented in Fig. 6. They clearly show losses in the transparency of the glasses after heat treatment especially for the Ti and Mg glasses. The large decrease in the transmittance of the Ti and Mg glasses can be related to the presence of a larger amount of crystals and/or larger crystals inside these glass matrices than in the Ref and Zn glass matrices causing stronger scattering.[51]

The XRD pattern of these HT glass were measured to verify if CaF_2 crystals precipitate in all glasses during heat treatment. The XRD pattern of the glasses prior to and after heat treatment are shown in Fig. 7.

The XRD pattern of the as-prepared glasses exhibit a broad band confirming that the as-prepared glasses are amorphous prior to the heat treatment. The XRD patterns of the heat treated glasses show sharp peaks which correspond to the precipitation of CaF_2 (ICDD PDF #00-035-0816) indicating that the change in the glass composition has no impact on the crystal phase

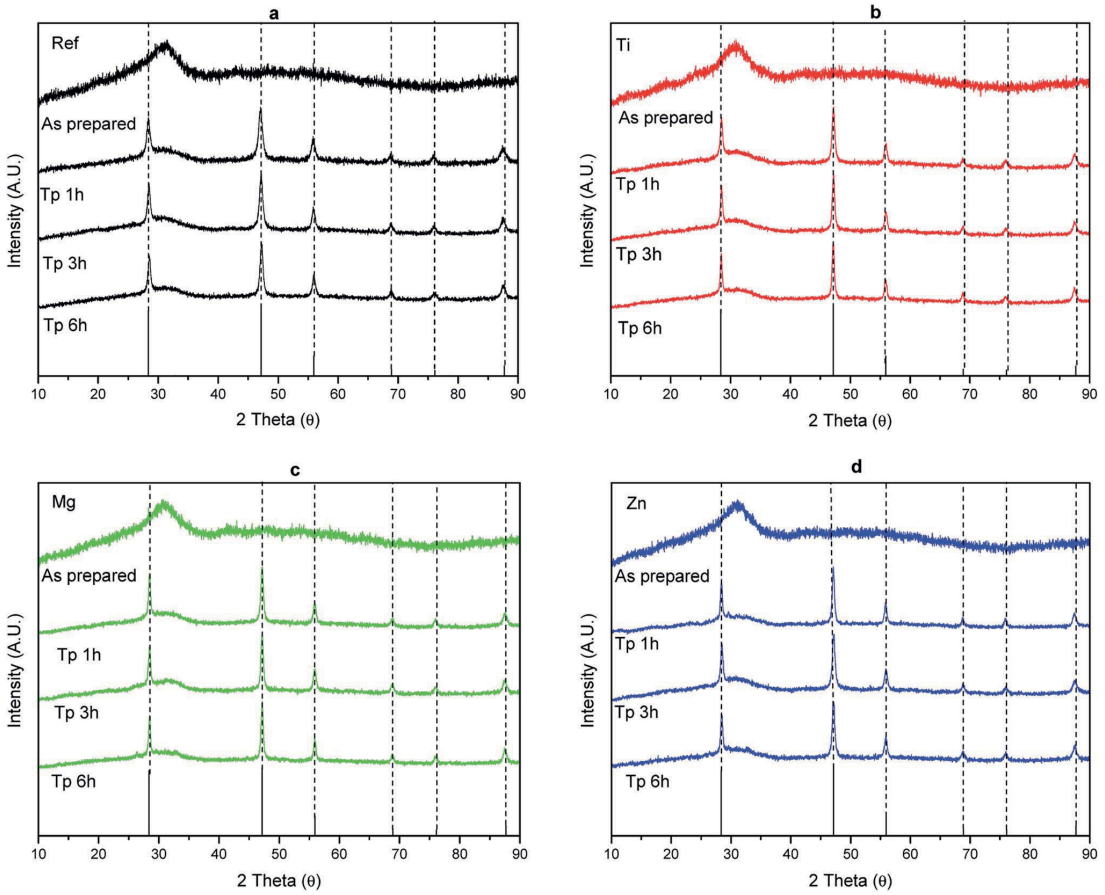

Fig. 7 XRD patterns of the Ref (a), Ti (b), Mg (c) and Zn (d) glasses prior to and after heat treatment T_g + 20 °C for 17 h and at T_p for 1, 3 and 6 hours.

Table 4 Estimation of the mean crystalline sizes (nm) of CaF_2 crystals in the glasses heat treated at T_g + 20 °C for 17 h and then at T_p for 1 to 6 h

Glass label	Heat treated at T_g + 20 °C for 17 h and then at T_p for 1 h	Heat treated at T_g + 20 °C for 17 h and then at T_p for 3 h	Heat treated at T_g + 20 °C for 17 h and then at T_p for 6 h
Ref	17	19	19
Ti	24	31	56
Mg	24	24	38
Zn	14	17	20

precipitating in the glass. The size of the CaF_2 crystallites can be estimated from the XRD pattern using the Scherrer's equation:[52]

$$D = K\lambda/\beta \cos\theta \quad (6)$$

where $K = 0.9$ is the numerical factor, $\lambda = 0.154056$ nm represents the wavelength of the X-ray (Cu K_α) radiation, β is the full width at half maximum of the X-ray diffraction peak in radians and θ is the Bragg angle. Here, the strongest diffraction peak at $2\theta = 47°$, which corresponds to the (220) crystal plane, was used for the calculation.

The Table 4 summarizes the mean crystalline sizes of CaF_2 crystals in the heat treated glasses.

As seen in Table 4, the large decrease in the transmittance observed in the Ti and Mg glasses (Fig. 6) is probably due to the presence of large crystals of CaF_2 in the glasses. It is interesting to point out that the mean crystalline size of the CaF_2 crystals in the Ti and Mg glasses seems to be highly dependent on the duration of the heat treatment while the CaF_2 crystals are expected to grow slower in the Ref and Zn glasses when heat treated at their respective T_p. The crystal volume fraction was estimated by calculating the ratio of integrating area of the peaks to total integrated area of the XRD patterns as in ref. 15, 53 and was found to be about $(3.4 \pm 0.1)\%$, independently of the glass composition. One should point out that this crystal volume fraction is small compared to other glass-ceramics.[15]

Similar to previous report,[36] a decrease in the intensity of the emission centered at 1.5 μm and an increase in the intensity of the upconversion and in the lifetime values of the Er^{3+}:$^4I_{13/2}$ level (Table 3) were observed after heat treating all the investigated glasses. We also noticed for all the investigated glasses that the shape of the emission centered at 1.5 μm and of the green emission, known to be a hypersensitive transition and so sensitive to changes in the environment of Er^{3+} ions, changed post heat treatment (Fig. 8 and 9) confirming that the CaF_2 crystals precipitating in all the investigated glasses contain Er^{3+}

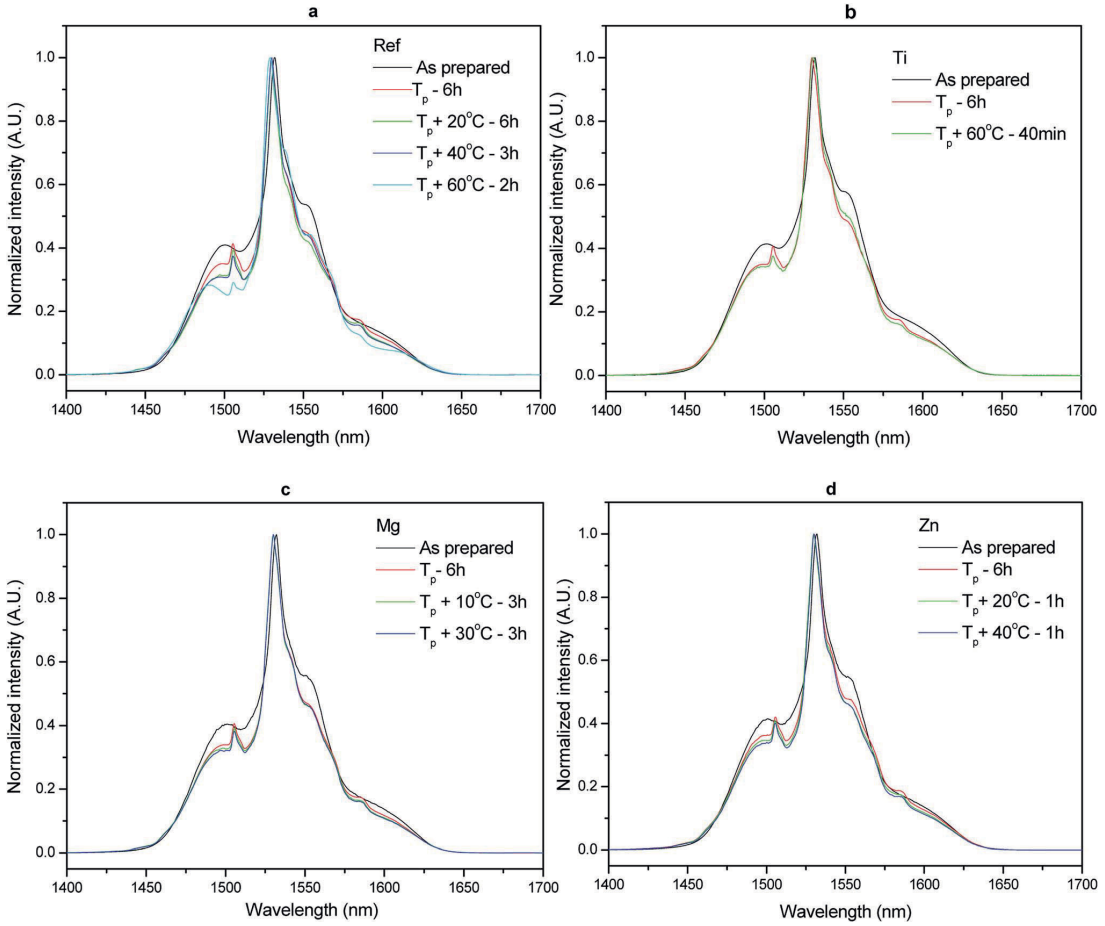

Fig. 8 Normalized emission spectra of the Ref (a), Ti (b), Mg (c), and Zn (d) glasses prior to and after heat treatment at (T_g + 20 °C) for 17 h and then at different temperatures and durations. Spectra were obtained using $\lambda_{exc} = 975$ nm.

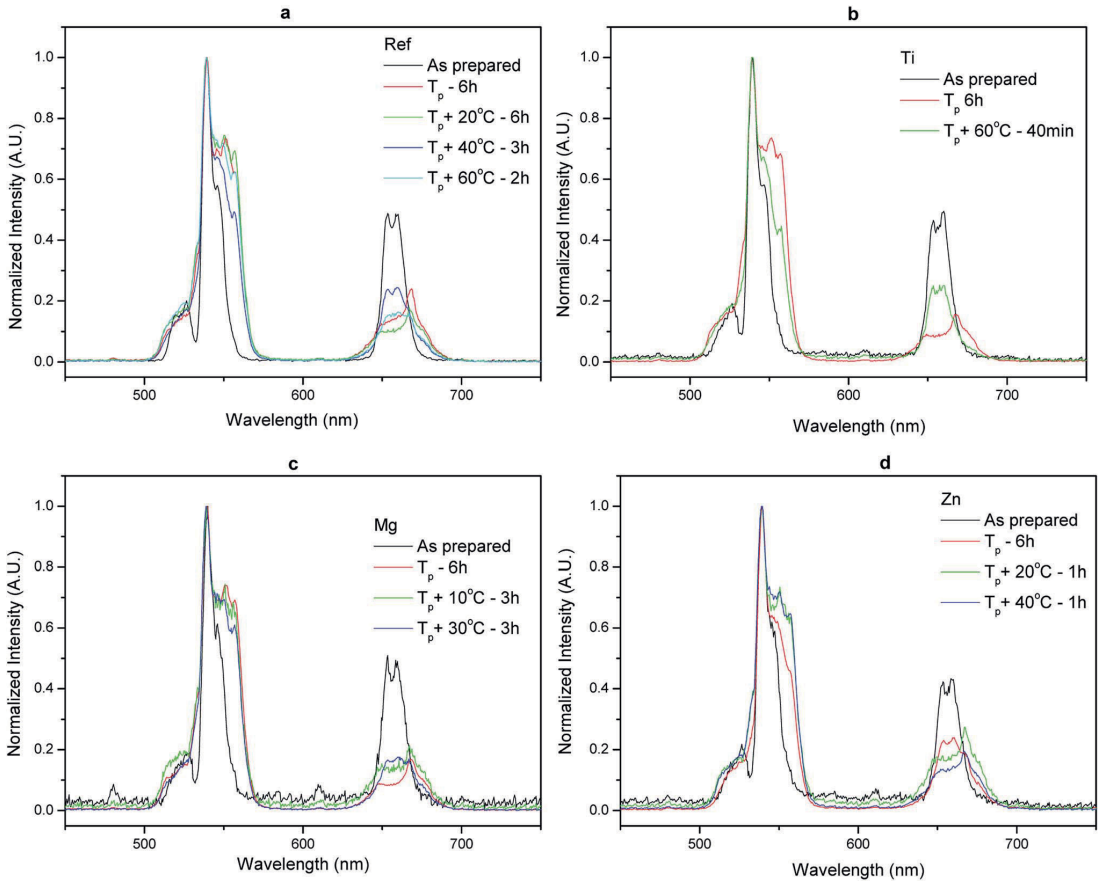

Fig. 9 Normalized upconversion spectra of the Ref (a), Ti (b), Mg (c), and Zn (d) glasses prior to and after heat treatment at (T_g +20 °C) for 17 h and then at different temperatures and durations. Spectra were obtained using $\lambda_{exc} = 975$ nm.

ions. One should point out that no noticeable impact of the glass composition on the reduction of the intensity of the emission at 1.5 μm and on the increase of the upconversion intensity (within ± 10%) was seen indicating that the glass composition has no significant impact on the sites of the Er^{3+} ions; Er^{3+} ions are suspected to be located in similar (amorphous and CaF_2) sites in the investigated glasses.

In order to better understand the impact of the glass composition on the crystallization process, the activation energy for crystallization (E_c), JMA exponent nucleation curve and crystal growth rate of the glasses were calculated. The activation energy for crystallization of the glasses was calculated using two methods and the E_c's are listed in Table 5. The activation energies reported using the Kissinger method appeared

Table 5 Activation energy for crystallization, nucleation temperature and JMA exponent of the investigated glasses

	Activation energy (E_c)		JMA exponent (n)			
Glass label	Kissinger method ±30 kJ mol^{-1}	Friedman method kJ mol^{-1}	Augis–Benett method (±0.1)	Ozawa–Chen method	Maximum nucleation temperature $T_{n\ max}$ (°C)	$T_x - T_{n\ max}$ (°C)
Ref	190	182 ± 10	2.1	2.0 ± 0.5	276 ± 5	47 ± 8
Ti	185	226 ± 20	1.7	1.5 ± 0.4	295 ± 5	55 ± 8
Mg	158	186 ± 11	1.8	1.6 ± 0.4	285 ± 15	60 ± 23
Zn	206	199 ± 6	1.9	1.9 ± 0.5	280 ± 5	54 ± 8

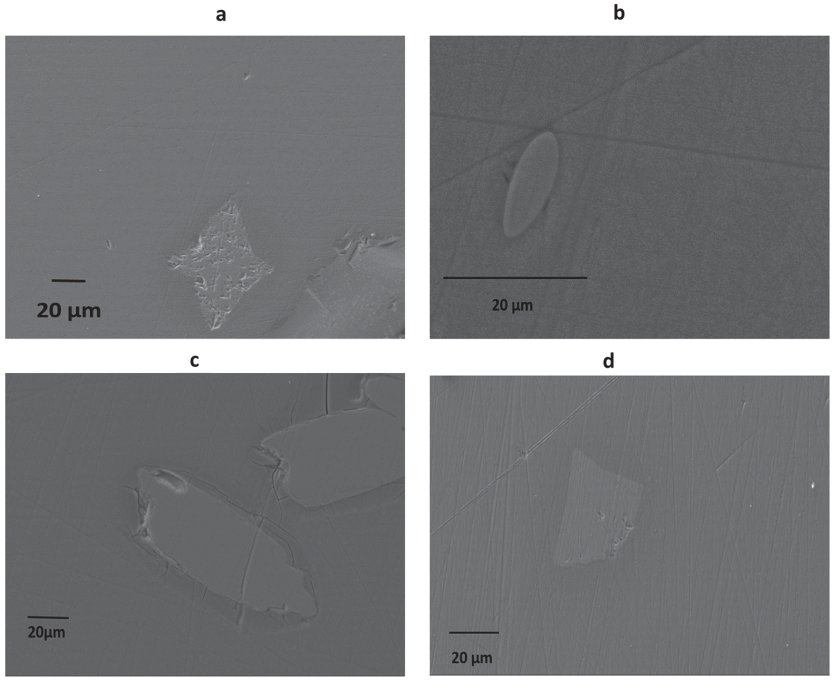

Fig. 10 SEM image of CaF_2 crystals found in the glasses heat treated at T_g + 20 °C for 17 h and then at (T_p + 60 °C) for 2 h for the Ref glass (a), at T_p for 2.5 h for Ti glass (b), at (T_p + 30 °C) for 3 h for the Mg glass (c), and (T_p + 40 °C) for 4 h for the Zn glass.

to be similar regardless of the glass composition. The standard deviation in E_c calculated using the Friedman method, for each glass composition, is less than 10% indicating that only one crystallization mechanism is involved throughout the entire crystallization process. The low standard deviation also validates the Kissinger method which is often used to further calculate the JMA exponent. The similarity in E_c between glasses and the low standard deviation measured for each E_c using the Friedman technique tend to indicate that the crystallization process is nucleation and growth and the primary crystal field is similar in all the investigated glasses.[34,54]

The JMA exponent of the glasses was calculated using two methods (Augis–Bennett and Ozawa–Chen) and the n values can be found in Table 5. The n values from both techniques are in close agreement. The crystal growth dimensionality in the glasses is ~2 within the accuracy of the measurement indicating that the glasses, independently of their composition, have a dominant bulk crystallization with needle like crystals when subjected to heat treatment.[55] The shape of the crystal was checked using SEM (Fig. 10) and their composition was

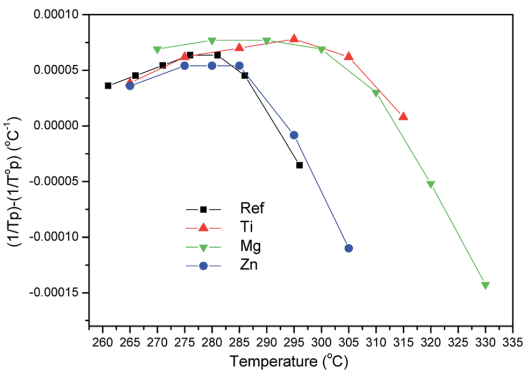

Fig. 11 Nucleation curve of the investigated glasses.

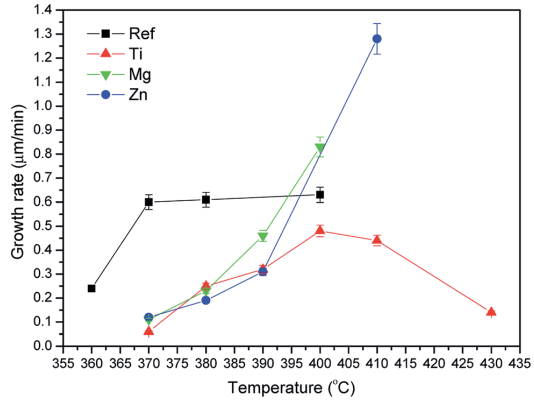

Fig. 12 Crystal growth rate as a function of temperature.

confirmed to be CaF_2 using EDS. The crystals exhibit similar shape than needle like shape: they grow preferentially in one direction.

The nucleation like curve were determined using the method proposed by Ray *et al.*[56] and Marrota *et al.*[39] The nucleation curve of the glasses is shown in Fig. 11. The maximum nucleation temperature ($T_{n\ max}$) was taken from the maximum of the nucleation-like curve.

The maximum nucleation temperature varies between 276 °C to 295 °C depending on the glass composition. The $T_{n\ max}$ of the glasses is summarized in Table 5. The Mg and Ti glasses exhibit similar nucleation like curve, which is shifted to higher temperature and is broader than that of the Ref and Zn glasses. Therefore, the formation of nuclei occurs at higher temperature and is less dependent on the temperature when adding ions with strong field strength in the phosphate

Table 6 Comparison of the crystal size expected from the crystal growth rate curve and from the SEM images

Glass Label	Heat treatment at T_g + 20 °C for 17 h and	Expected crystal size from the growth curve (μm)	Measured crystal size from SEM images (Fig. 10) (μm) ±5 μm
Ref	T_p + 60 °C (400 °C) – 2 h	72	86
Ti	T_p (370 °C) – 2.5 h	11	16
Mg	T_p + 30 °C (395 °C) – 3 h	117	125
Zn	T_p + 40 °C (390 °C) – 4 h	72	50

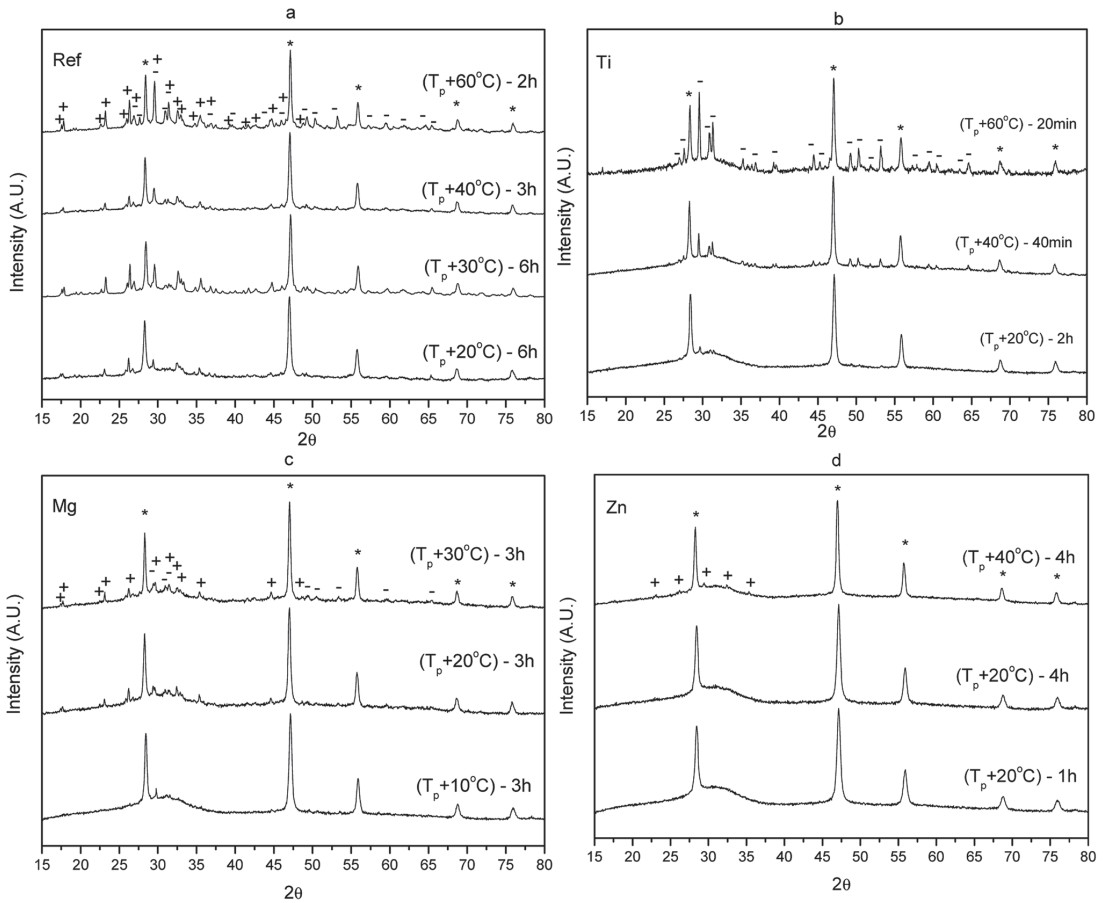

Fig. 13 XRD patterns of the Ref (a), Ti (b), Mg (c), and Zn (d) glasses prior to and after heat treatment at (T_g + 20 °C) for 17 h and then at different temperatures and durations [peaks correspond to *CaF_2, +$NaPO_3$, and −$Na_2Ca_2(P_2O_7)F_2$].

network. Also shown in Table 5 is the temperature difference between onset of crystallization (T_x) and maximum nucleation temperature ($T_{n\ max}$) of the glasses indicating that the nucleation and growth can be controlled in the investigated glasses and so a heat treatment using tailored temperature and duration can be used for the fabrication of transparent GCs with small crystal size distribution.

The crystal growth rate curves were calculated from the slope of measured crystal size as a function of duration of heat treatment performed at different temperatures. The crystal growth rates as a function of temperature are shown in Fig. 12.

The maximum growth rate increases from (385 ± 15) °C (Ref glass) to (400 ± 10) °C when adding TiO_2 and to above 400 °C when adding MgO and ZnO probably due to the changes in the glass network as discussed earlier. It should be pointed out that the Mg and Zn glasses could not be heat treated above 410 °C due to excessive viscous flow. The crystal growth rate curves are in agreement with the transparency of the heat treated glasses. Indeed, according to Fig. 12, the crystals are expected to be ~3, 4, 21 and 21 μm in the Ref, Zn, Mg and Ti glasses, respectively, after heat treatment at T_g + 20 °C for 17 h and then at T_p for 6 h indicating that larger crystals are present in the Mg and Ti glasses after such heat treatment. This is in agreement with the losses in the transparency of the Mg and Ti glasses after heat treatment seen in Fig. 5. The sizes of the crystals depicted in the SEM images (Fig. 10) are in agreement with the sizes estimated from the crystal growth rate curves (Fig. 12) as shown in Table 6.

Finally, the XRD spectra of the glasses heat treated at temperatures higher than T_p are shown in Fig. 13. All the XRD spectra exhibit the peaks associated with CaF_2 (ICDD PDF #04-035-0816) but new peaks appear in the XRD pattern of the glasses heat treated at higher temperatures. In the XRD pattern of the Ref and Mg glasses, these peaks can be related to $NaPO_3$ (ICDD PDF#04-011-3120). When the temperature increases, $Na_2Ca_2P_2O_7F_2$ (ICDD PDF#04-012-1844) precipitate in the Ref and Mg glasses. The additional peaks found in the XRD pattern of the Ti glass could be related only to $Na_2Ca_2P_2O_7F_2$ (ICDD PDF#04-012-1844). $NaPO_3$ (ICDD PDF#04-011-3120) is suspected to precipitate in the Zn glass. Therefore, although the change in the glass composition has no impact on the precipitation of CaF_2 at T_p, it leads to the precipitation of different crystals when heat treating the glasses at higher temperatures. One should mention that the $NaPO_3$ and $Na_2Ca_2P_5O_7F_2$ crystals could not be seen using SEM probably due to their small size and/or low number. One should also mention that the precipitation of these different crystals has no impact on the intensity and shape of the emission at 1.5 μm (Fig. 8) and of the upconversion (Fig. 9) confirming that the Er^{3+} ions are thought to be mainly located in the CaF_2 crystals.

Conclusion

Novel oxyfluorophosphate glass with composition (100-*x*-0.25) (75$NaPO_3$-25 CaF_2) doped with 0.25 mol% of Er_2O_3 were prepared by adding TiO_2, MgO and ZnO. The change in the glass composition increases the glass transition and crystallization temperatures and increases the number of Q^1 units at the expense of Q^2 units leading to a shift of the bandgap to longer wavelength. We suspect also the formation P–O–Ti/Mg/Zn bonds at the expense of P–O–P bonds. The change in the glass composition has no impact on the crystallization of the glasses when heat treated at their respective T_p; volume precipitation of Er^{3+} doped CaF_2 crystals occurs in all the glasses after nucleation at T_g + 20 °C for 17 h and then crystal growth at T_p for 1 to 6 h leading to an increase in the intensity of the upconversion. However, multiple crystals, the composition of which depends on the glass composition, were found to precipitate in the glasses when heat treated at higher temperature than T_p.

The calculation of the activation energy for crystallization using two methods allowed one to confirm that the crystallization process is a nucleation and growth process in all the glasses. All glasses exhibit similar E_c and JMA exponent which was found to be ~2 confirming the bulk crystallization of crystals with needle like shape. The Ti and Mg glasses exhibit a broader nucleation curve and higher $T_{n\ max}$ than the Ref and Zn glasses due to their strong field strength. A large difference between T_g and $T_{n\ max}$ was found for all the glasses confirming that it is possible to control the size and size distribution of the crystals during heat treatment which is crucial for the preparation of transparent glass-ceramics. The crystal growth rate of the glasses was determined and was in agreement with the size of the crystals found in heat treated glasses measured using SEM.

Conflicts of interest

There are no conflicts to declare.

Acknowledgements

Academy of Finland (Flagship Programme, Photonics Research and Innovation PREIN-320165 and Academy Project -326418) is greatly acknowledged for the financial support. This work made use of Tampere Microscopy Center facilities at Tampere University. We are also thankful to Dr Alexander Veber for fruitful discussions.

References

1 M. J. Dejneka, Transparent Oxyfluoride Glass Ceramics, *MRS Bull.*, 1998, **23**, 57–62, DOI: 10.1557/S0883769400031018.

2 J. F. Philipps, T. Töpfer, H. Ebendorff-Heidepriem, D. Ehrt and R. Sauerbrey, Spectroscopic and lasing properties of Er^{3+}:Yb^{3+}-doped fluoride phosphate glasses, *Appl. Phys. B*, 2001, **72**, 399–405, DOI: 10.1007/s003400100515.

3 A. Obaton, J. Bernard, C. Parent, G. Le Flem, C. Labbe, P. Le Boulanger and G. Boulton, Synthesis and Spectroscopic Investigation of Yb^{3+}, Er^{3+} -Codoped $LaLiP_4O_{12}$Glasses Relevant for Laser Applications, in *CLEO/Europe Conf*, Lasers Electro-Optics, 1998, p. 167, DOI: 10.1109/CLEOE.1998.719180.

4 S. Taccheo, P. Laporta, S. Longhi, O. Svelto and C. Svelto, Diode-pumped bulk erbium-ytterbium lasers, *Appl. Phys. B*, 1996, **63**, 425–436, DOI: 10.1007/BF01828937.

5 P. Burns, J. M. Dawes, P. Wang, J. A. Piper, H. Zhang, L. Zhu and X. Meng, Energy transfer and investigation into laser performance in Er^{3+},Yb^{3+}:YCOB crystals at 1.5-1.6 μm, in *Adv. Solid-State Lasers*, Optical Society of America, 2001, p. ME2, DOI: 10.1364/ASSL.2001.ME2.

6 S. Cui, J. Massera, M. Lastusaari, L. Hupa and L. Petit, Novel oxyfluorophosphate glasses and glass-ceramics, *J. Non-Cryst. Solids*, 2016, **445–446**, 40–44, DOI: 10.1016/j.jnoncrysol.2016.05.005.

7 E. D. Zanotto, A bright future for glass-ceramics, *Am. Ceram. Soc. Bull.*, 2010, **89**, 19–27.

8 S. D. Stookey, Method of making ceramics and products thereof, *US Pat.*, 2,920,971, 1960.

9 D. Ehrt, Photoactive glasses and glass ceramics, *IOP Conf. Ser.: Mater. Sci. Eng.*, 2011, **21**, 012001, DOI: 10.1088/1757-899X/21/1/012001.

10 M. C. Gonçalves, L. F. Santos and R. M. Almeida, Rare-earth-doped transparent glass ceramics, *C. R. Chim.*, 2002, **5**, 845–854, DOI: 10.1016/S1631-0748(02)01457-1.

11 A. de Pablos-Martín, A. Durán and M. J. Pascual, Nanocrystallisation in oxyfluoride systems: mechanisms of crystallisation and photonic properties, *Int. Mater. Rev.*, 2012, **57**, 165–186, DOI: 10.1179/1743280411Y.0000000004.

12 D. Auzel, F. Pecile and D. Morin, Rare Earth Doped Vitroceramics: New, Efficient, Blue and Green Emitting Materials for Infrared Up-Conversion, *J. Electrochem. Soc.*, 1975, **122**, 101–107.

13 G. H. Beall and D. A. Duke, Transparent glass-ceramics, *J. Mater. Sci.*, 1969, **4**, 340–352, DOI: 10.1007/BF00550404.

14 Y. Wang and J. Ohwaki, New transparent vitroceramics codoped with Er^{3+} and Yb^{3+} for efficient frequency upconversion, *Appl. Phys. Lett.*, 1993, **63**, 3268–3270, DOI: 10.1063/1.110170.

15 X. Li, D. Xu, X. Liu and H. Guo, Dual valence Eu-doped phospho-alumino-silicate glass-ceramics containing $Ba_3AlO_3PO_4$ nanocrystals for W-LEDs, *RSC Adv.*, 2017, **7**, 53839–53845, DOI: 10.1039/C7RA11261K.

16 P. A. Tick, N. F. Borrelli, L. K. Cornelius and M. A. Newhouse, Transparent glass ceramics for 1300 nm amplifier applications, *J. Appl. Phys.*, 1995, **78**, 6367–6374, DOI: 10.1063/1.360518.

17 V. K. Tikhomirov, A. B. Seddon, M. Ferrari, M. Montagna, L. F. Santos and R. M. Almeida, The structure of Er^{3+}-doped oxy-fluoride transparent glass-ceramics studied by Raman scattering, *Europhys. Lett.*, 2003, **64**, 529–535, DOI: 10.1209/epl/i2003-00106-9.

18 Y. Jiang, J. Fan, B. Jiang, X. Mao, C. Zhou and L. Zhang, Structure and optical properties of transparent Er^{3+}-doped CaF_2–silica glass ceramic prepared by controllable sol–gel method, *Ceram. Int.*, 2016, **42**, 9571–9576, DOI: 10.1016/j.ceramint.2016.03.039.

19 X. Miao, Z. Bai, X. Huo, M. Guo, F. Cheng and M. Zhang, Controllable preparation of CaF_2 transparent glass ceramics: Dependence of the light transmittance mechanism on the glass crystallization behaviour, *Ceram. Int.*, 2019, **45**, 8510–8517, DOI: 10.1016/j.ceramint.2019.01.164.

20 K. Shioya, T. Komatsu, H. G. Kim, R. Sato and K. Matusita, Optical properties of transparent glass-ceramics in K_2O-Nb_2O_5-TeO_2 glasses, *J. Non-Cryst. Solids*, 1995, **189**, 16–24, DOI: 10.1016/0022-3093(95)00227-8.

21 M. A. P. Silva, Y. Messaddeq, V. Briois, M. Poulain, F. Villain and S. J. L. Ribeiro, Synthesis and structural investigations on TeO_2-PbF_2-CdF_2 glasses and transparent glass-ceramics, *J. Phys. Chem. Solids*, 2002, **63**, 605–612, DOI: 10.1016/S0022-3697(01)00200-1.

22 C. Yu, J. Zhang, L. Wen and Z. Jiang, New transparent Er^{3+}-doped oxyfluoride tellurite glass ceramic with improved near infrared and up-conversion fluorescence properties, *Mater. Lett.*, 2007, **61**, 3644–3646, DOI: 10.1016/j.matlet.2006.12.006.

23 Y. Zhang, H. Lei, G. Li, L. Zeng and J. Tang, Yb^{3+}/Er^{3+} co-doped transparent tellurite glass-ceramic for enhanced upconversion luminescence, *Opt. Mater.*, 2020, **99**, 109552, DOI: 10.1016/j.optmat.2019.109552.

24 H. Hayashi, S. Tanabe and T. Hanada, 1.4 μm band emission properties of Tm^{3+} ions in transparent glass ceramics containing PbF_2 nanocrystals for S-band amplifier, *J. Appl. Phys.*, 2001, **89**, 1041–1045, DOI: 10.1063/1.1335645.

25 M. Mortier and F. Auzel, Rare-earth doped transparent glass-ceramics with high cross-sections, *J. Non-Cryst. Solids*, 1999, **256–257**, 361–365, DOI: 10.1016/S0022-3093(99)00475-5.

26 K. Hirao, K. Tanaka, M. Makita and N. Soga, Preparation and optical properties of transparent glass-ceramics containing β-PbF_2:Tm^{3+}, *J. Appl. Phys.*, 1995, **78**, 3445–3450, DOI: 10.1063/1.359975.

27 J. Zhao, L. Huang, S. Zhao and S. Xu, Enhanced luminescence in Tb^{3+}-doped germanate glass ceramic scintillators containing CaF_2 nanocrystals, *J. Am. Ceram. Soc.*, 2019, **102**, 1720–1725, DOI: 10.1111/jace.16095.

28 X. Yu, F. Song, W. Wang, L. Luo, C. Ming, Z. Cheng, L. Han, T. Sun, H. Yu and J. Tian, Effects of Ce^{3+} on the spectroscopic properties of transparent phosphate glass ceramics co-doped with Er^{3+}/Yb^{3+}, *Opt. Commun.*, 2009, **282**, 2045–2048, DOI: 10.1016/j.optcom.2009.02.024.

29 Y. Ledemi, A.-A. Trudel, V. A. G. Rivera, S. Chenu, E. Véron, L. A. Nunes, M. Allix and Y. Messaddeq, White light and multicolor emission tuning in triply doped Yb^{3+}/Tm^{3+}/Er^{3+} novel fluoro-phosphate transparent glass-ceramics, *J. Mater. Chem. C*, 2014, **2**, 5046–5056, DOI: 10.1039/C4TC00455H.

30 Y. Ledemi, M. El Amraoui, J. L. Ferrari, P.-L. Fortin, S. J. L. Ribeiro and Y. Messaddeq, Infrared to Visible Up-Conversion Emission in Er^{3+}/Yb^{3+} Codoped Fluoro–Phosphate Glass–Ceramics, *J. Am. Ceram. Soc.*, 2013, **96**, 825–832, DOI: 10.1111/jace.12109.

31 Y. Chen, G. H. Chen, X. Y. Liu and T. Yang, Enhanced up-conversion luminescence and optical thermometry characteristics of Er^{3+}/Yb^{3+} co-doped transparent phosphate glass-ceramics, *J. Lumin.*, 2018, **195**, 314–320, DOI: 10.1016/j.jlumin.2017.11.049.

32 P. G. Vekilov, *Cryst. Growth Des.*, 2010, **10**, 5007–5019, DOI: 10.1021/cg1011633.

33 T. Ozawa, Kinetic analysis of derivative curves in thermal analysis, *J. Therm. Anal.*, 1970, **2**, 301–324, DOI: 10.1007/BF01911411.

34 H. E. Kissinger, Reaction Kinetics in Differential Thermal Analysis, *Anal. Chem.*, 1957, **29**, 1702–1706, DOI: 10.1021/ac60131a045.

35 H. L. Friedman, Kinetics of thermal degradation of char-forming plastics from thermogravimetry. Application to a phenolic plastic, *J. Polym. Sci., Part C: Polym. Symp.*, 1964, **6**, 183–195, DOI: 10.1002/polc.5070060121.

36 A. Nommeots-Nomm, N. G. Boetti, T. Salminen, J. Massera, M. Hokka and L. Petit, Luminescence of Er^{3+} doped oxyfluoride phosphate glasses and glass-ceramics, *J. Alloys Compd.*, 2018, **751**, 224–230, DOI: 10.1016/j.jallcom.2018.04.101.

37 A. Szczodra, A. Mardoukhi, M. Hokka, N. G. Boetti and L. Petit, Fluorine losses in Er^{3+} oxyfluoride phosphate glasses and glass-ceramics, *J. Alloys Compd.*, 2019, **797**, 797–803, DOI: 10.1016/j.jallcom.2019.05.151.

38 J. A. Augis and J. E. Bennett, Calculation of the Avrami parameters for heterogeneous solid state reactions using a modification of the Kissinger method, *J. Therm. Anal.*, 1978, **13**, 283–292, DOI: 10.1007/BF01912301.

39 A. Marotta, A. Buri and F. Branda, Nucleation in glass and differential thermal analysis, *J. Mater. Sci.*, 1981, **16**, 341–344, DOI: 10.1007/BF00738622.

40 P. Lopez-Iscoa, L. Petit, J. Massera, D. Janner, N. G. Boetti, D. Pugliese, S. Fiorilli, C. Novara, F. Giorgis and D. Milanese, Effect of the addition of Al_2O_3, TiO_2 and ZnO on the thermal, structural and luminescence properties of Er^{3+}-doped phosphate glasses, *J. Non-Cryst. Solids*, 2017, **460**, 161–168, DOI: 10.1016/J.JNONCRYSOL.2017.01.030.

41 M. T. Islam, N. Sharmin, G. A. Rance, J. J. Titman, A. J. Parsons, K. M. Z. Hossain and I. Ahmed, The effect of MgO/TiO_2 on structural and crystallization behavior of near invert phosphate-based glasses, *J. Biomed. Mater. Res., Part B*, 2020, 674–686, DOI: 10.1002/jbm.b.34421.

42 H. Morikawa, S. Lee, T. Kasuga and D. S. Brauer, Effects of magnesium for calcium substitution in P_2O_5–CaO–TiO_2 glasses, *J. Non-Cryst. Solids*, 2013, **380**, 53–59, DOI: 10.1016/j.jnoncrysol.2013.08.029.

43 A. Kiani, J. V. Hanna, S. P. King, G. J. Rees, M. E. Smith, N. Roohpour, V. Salih and J. C. Knowles, Structural characterization and physical properties of P_2O_5-CaO-Na_2O-TiO_2 glasses by Fourier transform infrared, Raman and solid-state magic angle spinning nuclear magnetic resonance spectroscopies, *Acta Biomater.*, 2012, **8**, 333–340, DOI: 10.1016/j.actbio.2011.08.025.

44 H. Segawa, N. Akagi, T. Yano and S. Shibita, Properties and structures of TiO_2–ZnO–P_2O_5 glasses, *J. Ceram. Soc. Jpn.*, 2010, **118**, 278–282, DOI: 10.2109/jcersj2.118.278.

45 S. Toyoda, S. Fujino and K. Morinaga, Density, viscosity and surface tension of 50RO–50P_2O_5 (R: Mg, Ca, Sr, Ba, and Zn) glass melts, *J. Non-Cryst. Solids*, 2003, **321**, 169–174, DOI: 10.1016/S0022-3093(03)00174-1.

46 L. H. C. Andrade, S. M. Lima, A. Novatski, A. M. Neto, A. C. Bento, M. L. Baesso, F. C. G. Gandra, Y. Guyot and G. Boulon, Spectroscopic assignments of Ti^{3+} and Ti^{4+} in titanium-doped OH− free low-silica calcium aluminosilicate glass and role of structural defects on the observed long lifetime and high fluorescence of Ti^{3+} ions, *Phys. Rev. B*, 2008, **78**, 224202, DOI: 10.1103/PhysRevB.78.224202.

47 F. Auzel, Upconversion and Anti-Stokes Processes with f and d Ions in Solids, *Chem. Rev.*, 2004, **104**, 139–174, DOI: 10.1021/cr020357g.

48 T. Li, C. Guo, S. Zhou, C. Duan and M. Yin, Highly Sensitive Optical Thermometry of Yb^{3+}-Er^{3+} Codoped AgLa(MoO4)2 Green Upconversion Phosphor, *J. Am. Ceram. Soc.*, 2015, **98**, 2812–2816, DOI: 10.1111/jace.13698.

49 Y. Yan, A. J. Faber and H. de Waal, Luminescence quenching by OH groups in highly Er-doped phosphate glasses, *J. Non-Cryst. Solids*, 1995, **181**, 283–290, DOI: 10.1016/S0022-3093(94)00528-1.

50 H. Desirena, E. De la Rosa, L. A. Díaz-Torres and G. A. Kumar, Concentration effect of Er^{3+} ion on the spectroscopic properties of Er^{3+} and Yb^{3+}/Er^{3+} co-doped phosphate glasses, *Opt. Mater.*, 2006, **28**, 560–568, DOI: 10.1016/j.optmat.2005.04.002.

51 X. Liu, J. Zhou, S. Zhou, Y. Yue and J. Qiu, Transparent glass-ceramics functionalized by dispersed crystals, *Prog. Mater. Sci.*, 2018, **97**, 38–96, DOI: 10.1016/j.pmatsci.2018.02.006.

52 U. Holzwarth and N. Gibson, The Scherrer equation versus the "Debye-Scherrer equation, *Nat. Nanotechnol.*, 2011, **6**, 534, DOI: 10.1038/nnano.2011.145.

53 I. C. Madsen, N. V. Y. Scarlett and A. Kern, Description and survey of methodologies for the determination of amorphous content via X-ray powder diffraction, *Z. Kristallogr.*, 2011, **226**, 944, DOI: 10.1524/zkri.2011.1437.

54 M. J. Starink, The determination of activation energy from linear heating rate experiments: a comparison of the accuracy of isoconversion methods, *Thermochim. Acta*, 2003, **404**, 163–176, DOI: 10.1016/S0040-6031(03)00144-8.

55 J. Massera, J. Remond, J. Musgraves, M. J. Davis, S. Misture, L. Petit and K. Richardson, Nucleation and growth behavior of glasses in the TeO_2-Bi_2O_3-ZnO glass system, *J. Non-Cryst. Solids*, 2010, **356**, 2947–2955, DOI: 10.1016/j.jnoncrysol.2010.03.045.

56 C. S. Ray and D. E. Day, An Analysis of Nucleation-Rate Type of Curves in Glass as Determined by Differential Thermal Analysis, *J. Am. Ceram. Soc.*, 1997, **80**, 3100–3108, DOI: 10.1111/j.1151-2916.1997.tb03238.x.